THE DEVELOPMENT OF WERNER-TYPE COBALT COMPLEXES IN ENANTIOSELECTIVE HYDROGEN BOND MEDIATED CATALYSIS

A Dissertation

by

KYLE GENE LEWIS

Submitted to the Office of Graduate and Professional Studies of
Texas A&M University
in partial fulfillment of the requirements for the degree of

DOCTOR OF PHILOSOPHY

Chair of Committee,	John Gladysz
Committee Members,	Donald Darensbourg
	Karen Wooley
	A. Paul Schwab
Head of Department,	David Russell

December 2013

Major Subject: Chemistry

ABSTRACT

Chiral-at-metal Werner complexes of the type (Λ/Δ)-$[Co(1,2\text{-diamine})_3]^{3+}$ $3X^-$ have long been a cornerstone of coordination chemistry. However, despite being inexpensive and readily available in enantiopure form, they have had no applications in enantioselective organic synthesis. This derives from their poor solubility in organic solvents and the fact that the chelating ligands are non-labile, preventing metal based substrate activation. However, it was conceived that the abundant nitrogen-hydrogen bonds of the diamine ligands could activate Lewis basic substrates towards nucleophilic addition *via* hydrogen bonding.

Towards this end, the diastereomeric trications Λ-$[Co((S,S)\text{-dpen})_3]^{3+}$ and Δ-$[Co((S,S)\text{-dpen})_3]^{3+}$ (dpen = diphenyl ethylenediamine) were prepared by stereoselective syntheses. Incorporation of the lipophilic BAr_f^- ($B(3,5\text{-}CF_3\text{-}C_6H_3)_4^-$) anion, among others, afforded the organic-soluble mixed salts Λ-$[Co((S,S)\text{-dpen})_3]^{3+}$ $2X^-$ BAr_f^- and Δ-$[Co((S,S)\text{-dpen})_3]^{3+}$ $2X^-$ BAr_f^- ($X = Cl^-$, BF_4^-, PF_6^-). These Werner complexes were then applied as hydrogen bond mediating catalysts for enantioselective Michael additions of dialkyl malonates to nitroolefins.

The catalyzed Michael addition of dimethyl malonate (**15a**) to *trans*-β-nitrostyrene was optimized with respect to solvent, temperature, and catalyst counteranion and then extended to a range of nitroolefin substrates. Under optimized conditions, Λ-(*S*,*S*)-$\mathbf{3}^{3+}$ $2BF_4^-$ BAr_f^- (10 mol%) catalyzes the Michael addition of **15a** to 2-benzyloxy-*trans*-β-nitrostyrene in acetone at 0 °C in the presence of Et_3N (1.0 equiv) to afford dimethyl 2-(2-nitro-1-(2-benzyloxyphenyl)ethyl)malonate in 95% isolated yield and 96% ee.

This work marks the first time that a Werner-type complex has been applied as a catalyst for organic transformations with high enantioselectivities. The unique stereochemistry of the Werner complex, which features a chiral metal center, is primarily responsible for the stereoselectivity of the catalyzed reactions.

DEDICATION

I dedicate this dissertation to my wife, Jamie, who was crazy enough to marry an organic chemist while still in grad school. She has been my number one support through years of late nights and weekends at the lab. Her help, patience, and love cannot possibly be measured.

ACKNOWLEDGEMENTS

I would like to thank my research advisor, Dr. John Gladysz, for the opportunity to work in his group. He has always allowed me the intellectual freedom to pursue research of my own interest and trusted me to steer my project in the directions that I found the most rewarding. He has been instrumental in the organizing and editing of this dissertation. I would also like to thank my committee members, Dr. Don Darensbourg, Dr. Karen Wooley, Dr. Paul Schwab, and Dr. Steven Wheeler for taking their time to review this dissertation. It has been a pleasure working with Dr. Nattamai Bhuvanesh, who is a very skilled and helpful crystallographer.

The entire Gladysz group has also been immensely helpful and each member has played a role in keeping the lab running smoothly. Specifically, I would like to thank Subrata Ghosh and Tathagata Mukherjee for all of our many discussions about our related chemistry projects. Additionally, I thank Jan Breitenfeld, Melissa Clough, Alex Estrada, Sebastien Gauthier, Juan Guerrero-Leal, Yoshi Kobayashi, Georgette Lang, and Paul Zeits for their personal friendship, both inside and outside of the lab.

From the real world, I especially want to thank Tim Herrman and Pete England, who on separate occasions kept me sane and encouraged me to stick with grad school.

Thanks to Kelly Frasure, for many kind words of encouragement, bags of coffee and sacks of peanuts over the years. Finally, I would like to thank my parents, Cathy and Everett Lewis, for their encouragement, love, and support throughout my 22 years of formal education and for instilling in me the importance of discipline and pride in my work.

TABLE OF CONTENTS

LIST OF FIGURES

FIGURE Page

FIGURE Page

FIGURE Page

FIGURE Page

FIGURE Page

FIGURE Page

LIST OF SCHEMES

SCHEME Page

SCHEME Page

LIST OF TABLES

TABLE Page

NOMENCLATURE

δ	chemical shift in ppm
ε	molar extinction coefficient
ν	stretching mode (IR)
σ	sigma Hammett constant
$\{^1H\}$	proton decoupled
Å	Angstrom
Anal.	analysis
Ar	aryl
aq	aqueous
Bn	benzyl
br	broad
Bz	benzoyl
Bu	butyl
Calcd.	calculated
cat	catalyst
CD	circular dichroism
chxn	1,2-cyclohexanediamine
COD	cyclooctadiene
conv	conversion
d	doublet (NMR), days
DABCO	1,4-diazabicyclo[2.2.2]octane
DBU	diazabicycloundecene
dec	decomposition
DMAP	dimethylamino pyridine
dr	diastereomer ratio
DMSO	dimethylsulfoxide

dnen	dinaphthyl ethylenediamine
dpen	diphenyl ethylenediamine
ee	enantiomeric excess
en	ethylenediamine
er	enantiomer ratio
Et	ethyl
Et_3N	triethylamine
EtOAc	ethyl acetate
equiv	equivalent
fac	facial
h	hour
HPLC	high pressure liquid chromatography
Hz	hertz
i	*ipso*, iso
$^{i}J_{jk}$	scalar coupling constant for coupling of nucleus j with nucleus k through i bonds
IR	infrared
kcal	kilocalorie
kJ	kilojoule
lel	parallel to the C_3 axis
M	metal, mol/Liter, mega
m	multiplet (NMR), medium (IR)
m	*meta*
Me	methyl
MeOH	methanol
mer	meridional
mg	milligram
min	minutes
mol	mole

mmol	millimole
mp	melting point
NMM	N-methyl morpholine
NMR	nuclear magnetic resonance
o	*ortho*
OAc	acetate
ob	oblique to the C_3 axis
OBz	benzoate
ORD	optical rotary dispersion
OTf	triflate
p	*para*
Ph	phenyl
pn	propylenediamine
ppm	parts per million
Pr	propyl
q	quartet
R	organic group
rac	racemic
rt	room temperature
s	singlet (NMR), strong (IR)
t	triplet
t	tertiary
TADDOL	α,α,α,α-tetraaryl-1,3-dioxolane-4,5-dimethanol
TBME	*t*-butyl methyl ether
TBS	*t*-butyldimethylsilyl
TBSCl	*t*-butyldimethylsilyl chloride
temp	temperature
TFAA	trifluoroacetic acid
TLC	thin layer chromatography

UV	ultraviolet
v/v	volume/volume
vis	visible
vs	very strong
w	weak

CHAPTER I

INTRODUCTION:

HYDROGEN BOND MEDIATED CATALYSIS

1.1 Could a transition metal complex also be an organocatalyst?

The synthesis of enantiomerically pure organic molecules is of vital importance in pharmaceutical and agricultural chemistry.[1] Asymmetric synthesis with a substoichiometric amount of a chiral catalyst represents an extremely powerful and atom economic approach[2] to this task. Traditionally, concepts in enantioselective catalysis have focused on two classes of catalysts: (1) transition metal complexes containing chiral ligands and (2) biologically available enzymes. In 1990, Seebach predicted that "new synthetic methods are most likely to be encountered in the fields of biological and organometallic chemistry".[3] Even as late as 1996, Nicolau and Sorensen, in their authoritative textbook, "Classics in Total Synthesis", reduced the pool of enantiomerically pure catalysts to "enzyme(s) or synthetic, soluble transition metal complex(es)".[4]

However, one of the most important storylines in asymmetric synthesis over the first part of the 21st century has been the conceptualization and maturation of a new mode of catalysis in which relatively small *organic* molecules serve as the catalytic entity. Originally, this phenomenon was commonly referred to as "metal-free catalysis" so as to distinctly separate catalysis promoted by organic molecules from catalysis promoted by organometallic complexes.[5] The term "organocatalysis", first introduced by MacMillan in 1998,[6] is now the universally recognized name for this field.

As a result of the tremendous expansion of organocatalysis in asymmetric synthesis, several review articles, books, and a special topic highlight have been written on the subject.[5,7] Many of these continue to define the term "organocatalyst" in such a way as to completely exclude metals from the structure of the catalyst. For instance, Berkessel and Gröger define organocatalysts as "purely 'organic' molecules, i.e. composed of (mainly) carbon, hydrogen, nitrogen, oxygen, sulfur, and phosphorous."[5] Such a narrow definition excludes the possibility that an organocatalyst could contain a metal atom in any capacity, regardless of its role in catalysis. Perhaps a more thoughtful definition is offered by List, who describes organocatalysis as "catalysis with small organic molecules, where an inorganic element is not part of the active principle".[7d] This allows for a transition metal to be incorporated into an organocatalyst as a structural motif, provided that it was not directly involved in bond-making or bond-breaking processes in the reaction.

An example of such a catalyst is Fu's ferrocene DMAP derivative (**I**), which has been employed as a chiral nucleophile in several enantioselective transformations.[8] One such application, featured in Scheme 1.1, involves the asymmetric synthesis of a β-lactam by a formal [2 + 2] addition of a ketene with an imine.[8b] The orientation of the ligands above and below the central iron atom establishes "planar chirality" in the catalyst, but the metal itself is not directly involved in the activation of the organic substrates. Rather, the ketene is activated by nucleophilic addition of the pyridine nitrogen atom. Although it is clearly an organometallic compound, **I** is widely considered to be an organocatalyst because the organic fragment is the catalytically "active site".[5] Therefore, in deciding whether a particular molecule should belong to the family of "organocatalysts", the mode of substrate activation should be considered with greater weight than the absolute atom constitution of the catalyst.

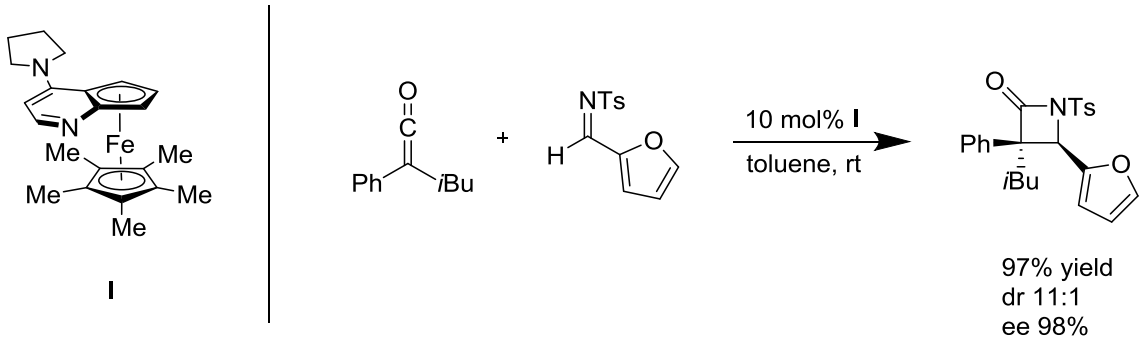

Scheme 1.1. Enantioselective synthesis of a β-lactam with a metal containing organocatalyst.

Provided with the otherwise vastly unexplored regions of "transition metal containing organocatalysts", the Gladysz research group has recently pursued several inorganic and organometallic structures that utilize transition metals as structural motifs, yet activate substrates solely through the organic ligands. Transition metal complexes with ligands capable of forming hydrogen bonds with substrate molecules have been of particular interest. As a means of introduction, a brief summary of the current state of the art in hydrogen bond mediated catalysis with traditional organocatalysts is provided.

1.2 Small molecule hydrogen bond donors in catalysis

1.2.1 Molecular recognition and reaction rate acceleration with achiral hydrogen bond donors

As part of the proliferation of organocatalysts in asymmetric synthesis, hydrogen bond mediation with chiral, organic molecules has garnered specific interest as a general mode of substrate activation. At the root, hydrogen bonding catalysis with synthetic organic molecules is inspired by the action of biological enzymes such as the serine

proteases. These enzymes possess a highly conserved active site containing two specific hydrogen bond donors located in the glycine-193 and serine-195 residues (Scheme 1.2).[9] These hydrogen bond donors establish an "oxyanion hole" that activates the amide carbonyl group and stabilizes the resulting tetrahedral adduct after nucleophilic alcoholysis.

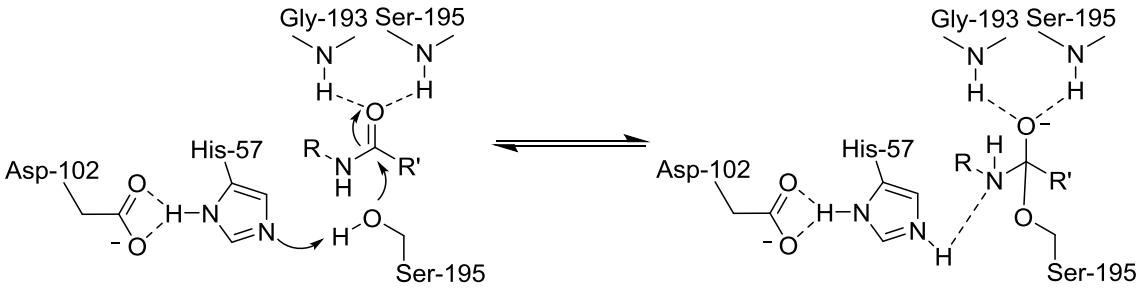

Scheme 1.2. The role of hydrogen bonding in the active site of the serine protease enzymes.

The dual hydrogen bonding nature of the serine proteases can be mimicked in many synthetic organic molecules. For example, Etter has demonstrated hydrogen bond driven molecular recognition between diarylureas and various oxygen containing guest molecules in the solid state.[10] A representative crystal structure is given in Figure 1.1. The cocrystal structure reveals a 1:1 ratio between the hydrogen bond donating urea and the nitroaryl acceptor. Both oxygen atoms of the nitro group are simultaneously engaged in hydrogen bonding with the urea.

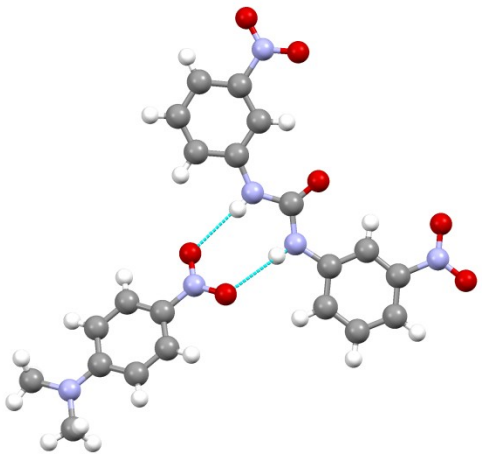

Figure 1.1. The 1:1 complex of 1,2-bis(*m*-nitrophenyl)urea and *N*,*N*-dimethyl-*p*-nitroaniline featuring hydrogen bonding.[11]

Subsequently, synthetic urea compounds were used in substoichiometric amounts to accelerate organic reactions. Scheme 1.3 shows the Claisen rearrangement of 6-methoxy allyl vinyl ether in the presence of various amounts of diarylurea **II**.[12] Due to the intrinsic low solubility of ureas in non-polar organic solvents, a long aliphatic chain was incorporated into the catalyst to ensure solution homogeniety. Catalyst loadings as low as 10 mol% **II** were applied, resulting in a nearly 3-fold rate increase compared to the background reaction.

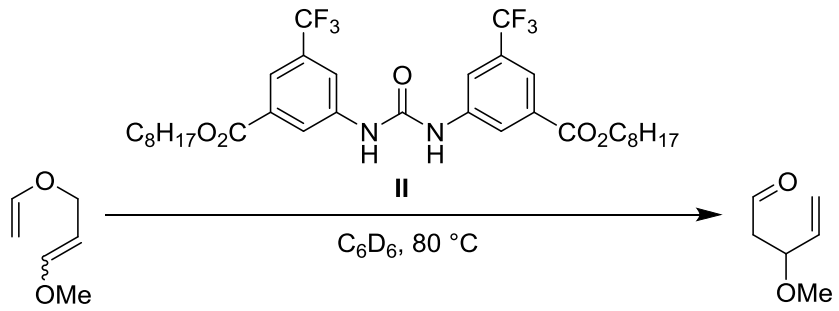

mol% **II**	k_{rel}
0	1
10	2.7
40	5
100	22.4

Scheme 1.3. Accelerated Claisen rearrangement in the presence of urea **II**.

Diarylthioureas have higher solubilities in organic solvents than the corresponding diarylureas. Therefore, Schreiner was able to prepare thiourea **III** with additional electron withdrawing CF_3 groups on the aryl ring.[13] In general, electron withdrawing groups will render a molecule a stronger hydrogen bond donor. This compound served as an efficient catalyst for Diels-Alder reactions. Scheme 1.4 shows that the rate of a Diels-Alder cycloaddition between an enone and cyclopentadiene was increased 8-fold in the presence of only 1 mol% **III**.

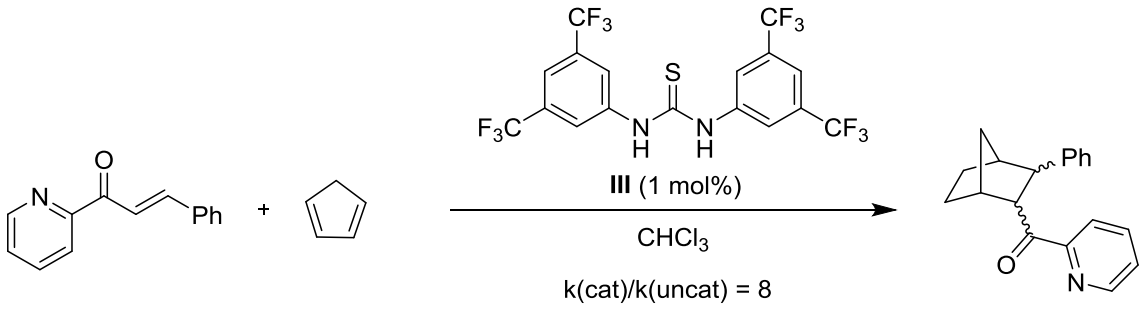

Scheme 1.4. Accelerated Diels-Alder reaction in the presence of thiourea **III**.

Compounds with other kinds of hydrogen bond donating functional groups also demonstrate strong molecular recognition with organic molecules containing Lewis basic groups. Hine discovered that the biphenylenediol **IV**, which contains two coplanar

carbon-OH (carbon-hydroxyl) bonds, would cocrystallize with phosphoramide, pyridone, and pyrone containing molecules.[14] In each case, the two hydroxyl groups formed hydrogen bonds with the same oxygen atom in the guest molecule. A representative example is shown in Figure 1.2.

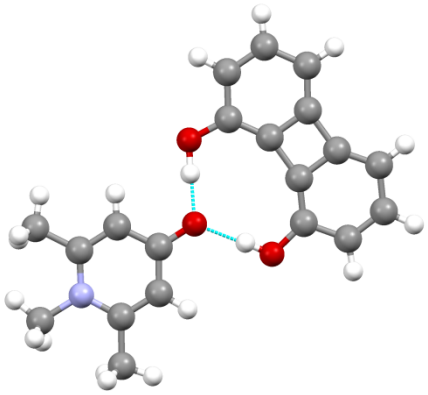

Figure 1.2. The 1:1 complex of biphenylenediol **IV** and 1,2,6-trimethyl-4-pyridone featuring hydrogen bonding.[15]

The same molecule promoted epoxide ring openings with the nucleophile ethylamine, as depicted in Scheme 1.5.[16] The rate acceleration afforded by biphenylenediol **IV** was significantly higher than that of the structurally related, single hydrogen bond donor, phenol. This emphasizes the importance of the dual hydrogen bond system.

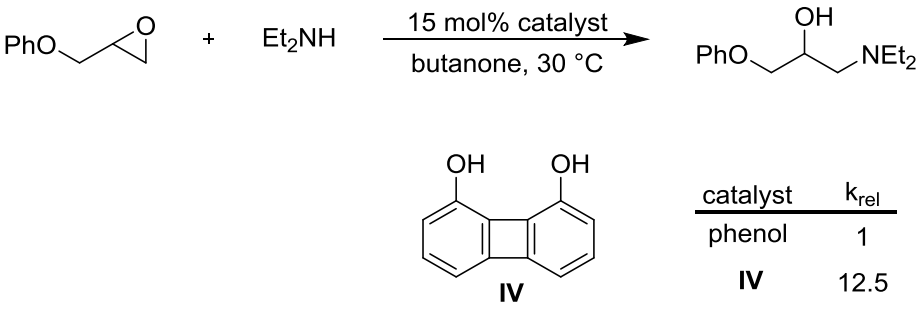

Scheme 1.5. Accelerated epoxide ring opening in the presence of biphenylenediol **IV**.

1.2.2 Enantioselective catalysis with chiral hydrogen bond donors

Building on the success of achiral hydrogen bond donors in accelerating organic transformations, researchers began to explore enantioselective reactions mediated by chiral, enantiopure hydrogen bond donors. The first application was provided by Jacobsen, who discovered that chiral thiourea **V** catalyzed an enantioselective Strecker reaction in up to 91% ee, as shown in Scheme 1.6.[17] Detailed mechanistic investigations revealed that the thiourea N-H units were solely responsible for the activation of the imine, despite the presence of the acidic phenolic hydrogen.[18]

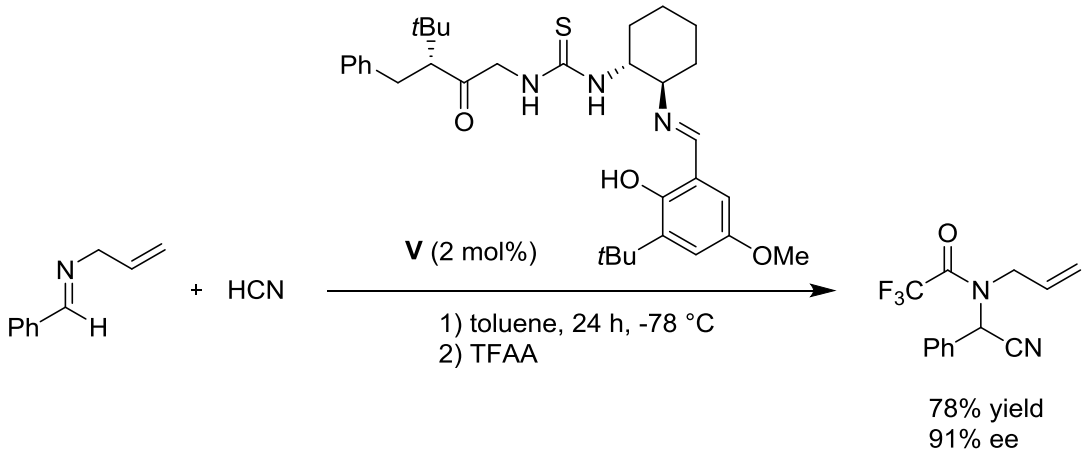

Scheme 1.6. Enantioselective Strecker reaction catalyzed by Jacobsen's chiral thiourea **V**.

Since this seminal report, the field of asymmetric catalysis with synthetic organic hydrogen bond donors has flourished, and the progress in this area has been summarized in several reviews and textbooks.[9,19] Part of this success is due to the virtually unlimited array of unique chiral hydrogen bond donors that can be synthesized in the laboratory. Besides thioureas, other hydrogen bond donating units including alcohols, amines, amides, guanidines, carboxylic acids, and phosphoric acids have been elaborated with chiral structural features and applied to enantioselective catalysis. Additionally, hydrogen bonding catalysis is a very general mode of activation and organic molecules containing a variety of Lewis basic functional groups have been promoted toward asymmetric transformations.

1.2.2.1 Design elements in chiral hydrogen bond donors

In surveying the current pool of chiral, hydrogen bond donors, it is apparent that there exist two main strategies in the design of enantioselective catalysts. Both strategies

rest on the principle that the hydrogen bonded electrophile is held in a fixed position and maintains close contact with the catalyst. The chiral parameters of the catalyst then dictate the approach of the nucleophile by allowing access to only one prochiral face of the activated electrophile.

The first strategy accomplishes this by strictly steric means and often incorporates bulky organic groups to control access of the nucleophile to the catalytic active site. This approach is termed here as *monofunctional catalysis*, because such catalysts contain only hydrogen bond donating functional groups. The prefix "mono" is not related to the total number of functional groups. In fact, most monofunctional catalysts employ at least two hydrogen bond donors to facilitate the previously described dual hydrogen bond activation. Representative examples of this class of catalysts are shown in Figure 1.3.

The compounds **VI-X** in Figure 1.3 comprise a diverse set of chiral platforms and hydrogen bonding functional groups, which are highlighted in red.[20-24] Each catalyst has been applied to a separate asymmetric organic reaction with excellent enantioselectivity. One unifying theme is the high number of bulky aromatic rings that surround the hydrogen bonding functional groups. These bulky groups establish a chiral atmosphere around the catalytic active site. Catalyst **VI**, which is derived from L-tartaric acid, belongs to the TADDOL family of chiral ligands. Originally, these ligands were designed for asymmetric catalysis with titanium Lewis acids,[25] but they have proven to be highly enantioselective metal-free catalysts in their own right. Catalysts **VII-IX** do not contain a stereogenic center, but rather possess "axial chirality" deriving from the hindered rotation around the biaryl single bond. Whereas catalysts **VI-IX** display C_2 symmetry, catalyst **X** is unique in that it features an unusual "helical chirality" motif. The shown catalyst exists in a right-handed helix. Racemization would require the

nitrogen heterocycle to pass under a terminal C_6H_4 moiety, which would be prohibitive in strain.

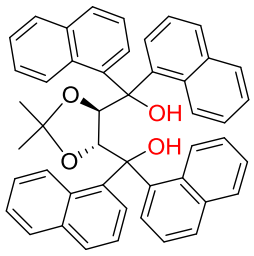

VI

Hetero-Diels-Alder reaction

up to 98% ee

(ref. 20)

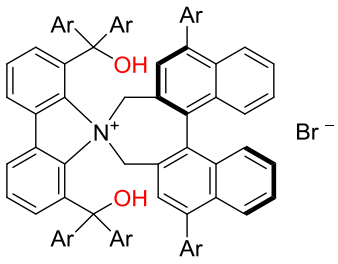

VII

Ar = 3,5-bis(phenyl)phenyl

Phase-transfer epoxidation of unsaturatred ketones

up to 99% ee

(ref. 21)

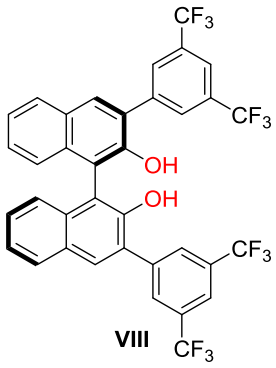

VIII

requires Et_3P cocatalyst

Baylis-Hillman reaction

up to 96% ee

(ref. 22)

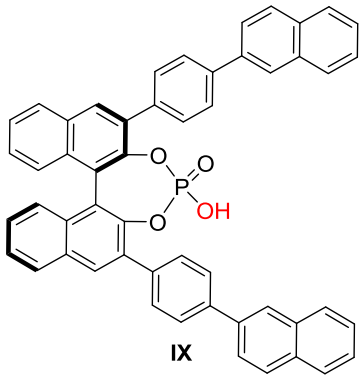

IX

Mannich reaction of malonates to imines

up to 98% ee

(ref. 23)

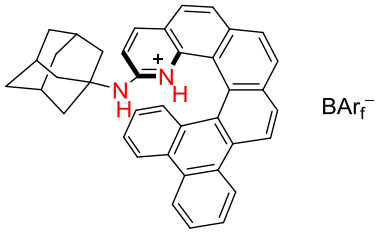

X

Friedel-Crafts addition of dihydroindoles to nitroolefins

up to 96% ee

(ref. 24)

Figure 1.3. Representative examples of monofunctional hydrogen bond donors in asymmetric catalysis.

In contrast, *bifunctional catalysts* incorporate an additional Lewis basic functional group to compliment the role of the hydrogen bond donors. In this strategy,

the nucleophile is activated by the Lewis base by deprotonation at the same time that the electrophile is activated by hydrogen bonding. With a well-designed bifunctional catalyst, the spatial organization of the simultaneously activated organic substrates resembles the geometry of the catalytic transition state. Highly organized transition states often result in high stereoselectivity and increased reaction rates. Representative examples of bifunctional catalysts are shown in Figure 1.4.

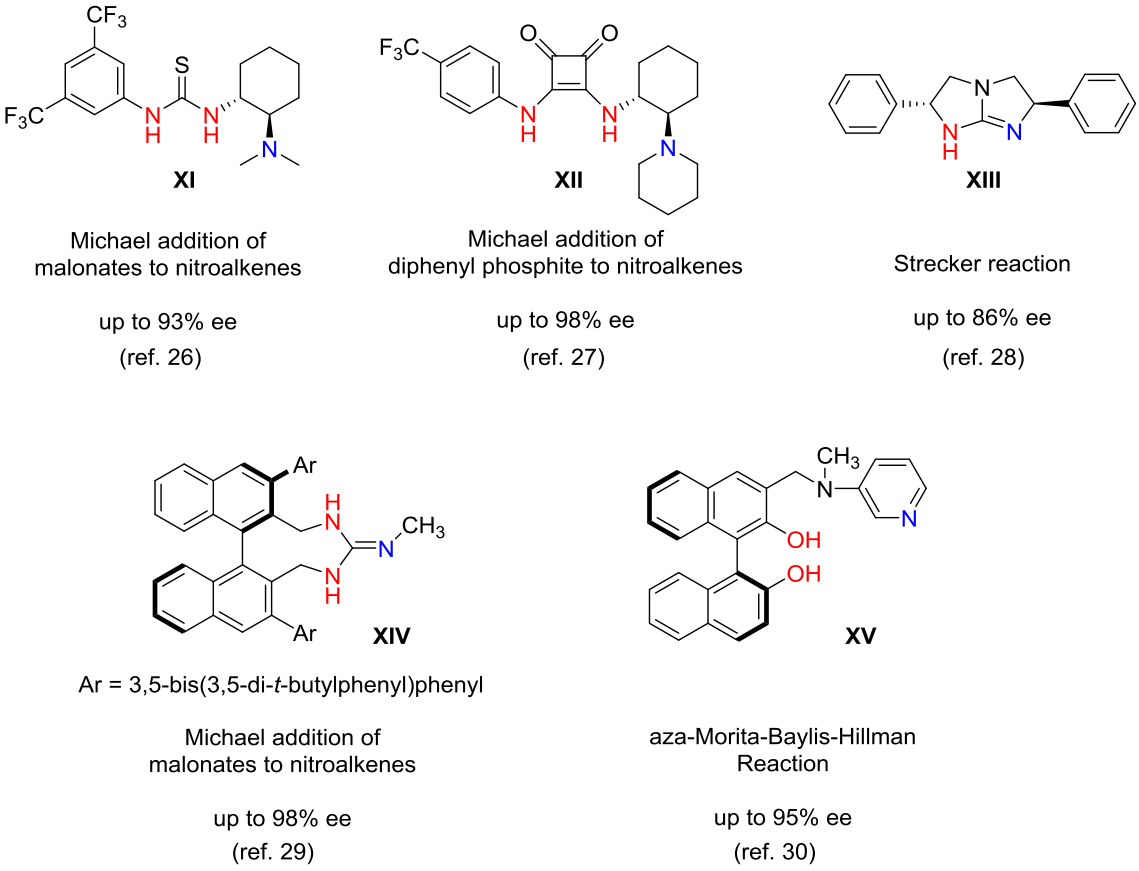

Figure 1.4. Representative examples of bifunctional hydrogen bond donors in asymmetric catalysis.

Catalysts **XI-XV** utilize a diverse set of hydrogen bond donating functional groups, highlighted in red, along with an auxiliary nitrogen base, highlighted in blue.[26-

[30] The chirality of the bifunctional thiourea catalyst **XI** is introduced in the *trans*-cyclohexanediamine (*trans*-chxn) side-arm containing the basic tertiary amine. Catalyst **XII** utilizes a similar chiral base motif, but in this case the dual hydrogen bond donor is established with a squaramide functional group. Both catalysts **XIII** and **XIV** incorporate a bifunctional guanidine functional group that contains a hydrogen bond donating N-H unit and a basic nitrogen. The structure of the axially chiral catalyst **XV** resembles that of the monofunctional catalyst **VIII** (Figure 1.3) except that the pendant pyridine arm has replaced the need for an external Et_3P cocatalyst for the Morita-Baylis-Hillman reaction.

Catalyst **XI** is used in the enantioselective Michael addition of diethyl malonate to *trans*-β-nitrostyrene.[26] The enantioenriched product is isolated with the *R* enantiomer predominating. The proposed transition state model is shown in Scheme 1.7. The nitroolefin is held by dual hydrogen bonds to the thiourea functional group so that the phenyl ring points away from the *trans*-chxn arm. Diethyl malonate is then deprotonated by the tertiary amine and must attack the nitroolefin from the top, pro-*R* face. This restriction is followed because the malonate presumably remains in close contact with the nitrogen base between deprotonation and nucleophilic addition by means of hydrogen bonding and ionic interactions.

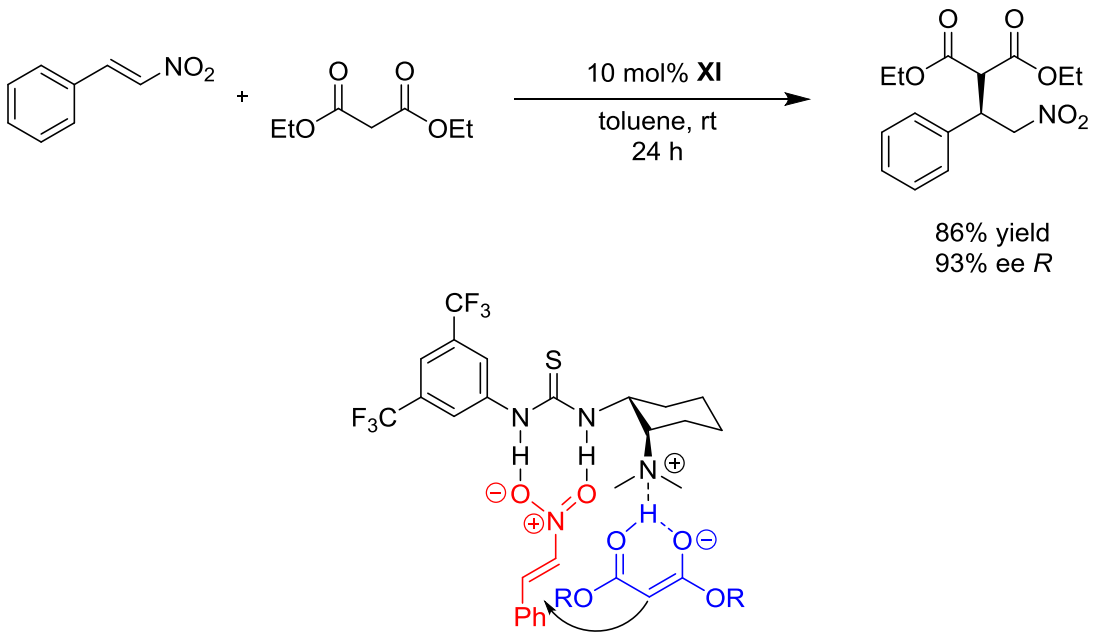

Scheme 1.7. The enantioselective Michael addition catalyzed by thiourea **XI**.

CHAPTER II

THE STEREOCHEMISTRY OF WERNER COMPLEXES CONTAINING 1,2-DIAMINES

2.1 Overview

Werner complexes with 1,2-chelating diamines have a long history in the development of structural inorganic chemistry and stereochemistry.[31] In this chapter, a comprehensive analysis of the stereochemical features of substituted tris(1,2-ethylenediamine) metal complexes is presented. The focus will be on complexes containing Co(III), which is by far the most studied, but by no means the exclusive central metal. This chapter is believed to be comprehensive in terms of stereochemical possibilities, but only illustrative literature examples are provided.

Toward this end, the first section describes the configurational stereoisomers that can form with unsubstituted tris(1,2-ethylenediamine) Co(III) complexes. Various stereochemical patterns with carbon-substituted 1,2-diamines are then covered in subsequent sections.

Although there exists a relatively small collection of literature pertaining to N-substituted 1,2-diamine Co(III) complexes, these do not represent the central theme of Werner complex chemistry. Some tetramethyl ethylenediamine (TMEDA) complexes with Co(III) have been reported, but these are far less stable and have radically different physical properties than complexes with primary amine ligands.[32] Chelating 1,2-diamines with single N-substitutions create additional stereocenters upon coordination,[33] generating further complications to the stereochemical analysis of Werner complexes and are not reviewed here.

2.2 Werner complexes with unsubstituted 1,2-ethylenediamine ligands

2.2.1 The configuration of the metal center

A "Werner complex" has recently been defined as a transition metal complex that does not contain a single carbon metal bond.[34] It is named in honor of Alfred Werner, who was the first to demonstrate the octahedral coordination geometry of inorganic molecules. In a key conceptual breakthrough, Werner proposed that the tris(1,2-ethylenediamine) Co(III) tricationic species $[Co(en)_3]^{3+}$, when confined to an octahedral configuration, should exist as two enantiomeric isomers. In 1912, Werner proved this postulate by successfully separating the two enantiomers, now conventionally labeled as Λ and Δ, by fractional crystallization of the diastereomeric tartrate salts. Chloride anion exchange then afforded the resolved enantiomers of Λ and Δ-$[Co(en)_3]^{3+}$ $3Cl^-$.[35] The related metal complexes $[M(en)_3]^{3+}$ (M = Cr, Rh, Ir) and the tetracation $[Pt(en)_3]^{4+}$ where similarly resolved with various chiral anions.[31a,36-41]

The chirality of the $[Co(en)_3]^{3+}$ trication derives from the arrangement of the chelating diamine ligands around the central metal atom. Before analyzing the individual enantiomers, it is worth noting that the trication possesses an idealized D_3 symmetry. This means that there is one C_3 axis and three C_2 axes in a plane perpendicular to the C_3 axis. It is sometimes forgotten that chiral molecules can have symmetry elements.

Figure 2.1 shows three different representations of the Λ and Δ enantiomers of the $[Co(en)_3]^{3+}$ trication. The conventional system to distinguish the Λ and Δ isomers relates them to left and right-handed helices.[42] A view down the C_3 rotation axis, best seen as the center of the top triangular face in Figure 2.1c, reveals that the Λ isomer

conforms to a left-handed or counter-clockwise helix. A similar treatment of the Δ isomer reveals a right-handed or clockwise helical configuration.

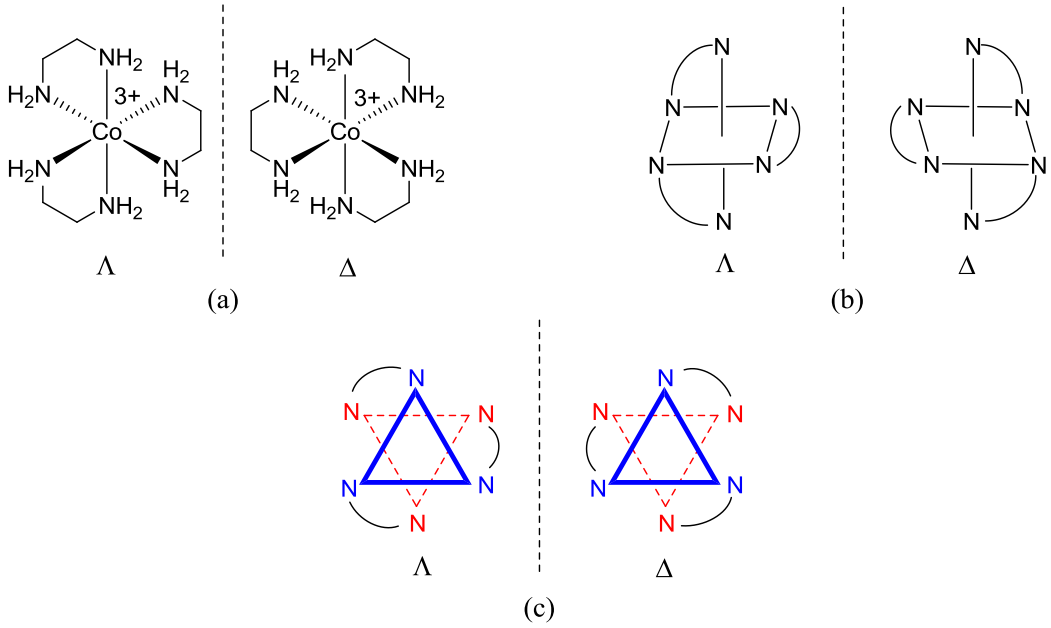

Figure 2.1. Three-dimensional views of the Λ and Δ-$[Co(en)_3]^{3+}$ trication represented by a) modern wedges and dashes, b) Werner's original 1912 depiction, and c) staggered triangles.

The resolved Λ and Δ isomers of the $[Co(en)_3]^{3+}$ trication are considered kinetically non-labile or substitution inert because they are extremely stable against ligand dissociation and racemization under ambient conditions. The estimated half-lives for hydrolysis and racemization in 0.1 M NaOH at 25 °C for $[Co(en)_3]^{3+}$ $3Cl^-$ is 3.2 years and >3.2 years, respectively.[32,43] The activation energy required for hydrolysis was determined to be 159 kJ mol^{-1} (38 kcal mol^{-1}).[43] Other anecdotal reports confirm that no racemization occurs in aqueous solutions of enantiopure $[Co(en)_3]^{3+}$ $3Cl^-$ during a) 3 months at room temperature, b) 15 hours at reflux in HCl, or c) 75 minutes at 85 °C

in the presence of 100 equivalents of $NaNO_2$.[44] However, when activated charcoal is introduced as a catalyst, racemization takes place within two minutes at 90 °C.[45]

2.2.2 The conformation of the 1,2-ethylenediamine chelating ligand

In addition to the chirality of the metal center, each diamine chelate must adopt one of two enantiomeric gauche conformations. Figure 2.2 shows the geometry of the two enantiomeric chelates, which are conventionally labeled with the lower case Greek letters λ and δ. The Newman projections in Figure 2.2 (top) look down the C–C bond of ethylenediamine. The two chelate conformations are also related to a left-handed helix (λ) and a right-handed helix (δ).

Like the chair conformations of cyclohexane, the λ and δ conformations of the ethylenediamine chelates rapidly interconvert through a low energy barrier transition state. This renders it impossible to separate them. However, in the absence of disorder, the chelates will crystallize in one conformation or the other.

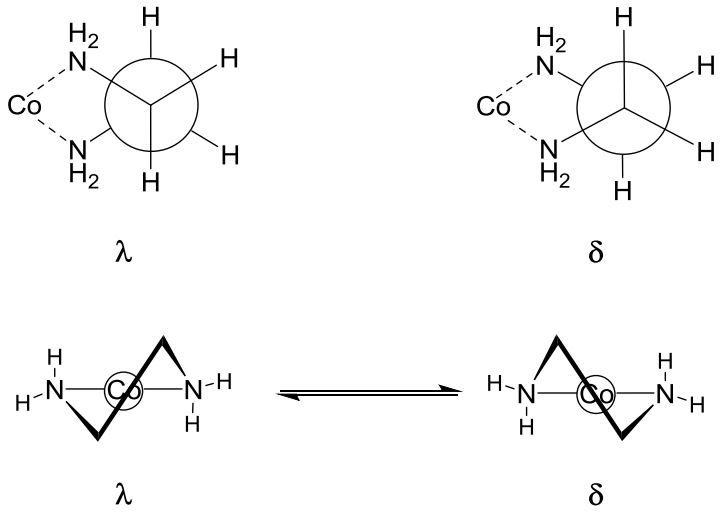

Figure 2.2. Diamine chelate conformations of 1,2-ethylenediamine.

As illustrated in Figure 2.3 and 2.4, the conformation of the ethylenediamine chelate also affects the relative orientation of the C–C bond and the C_3 rotational axis of the $[Co(en)_3]^{3+}$ trication. For Δ-$[Co(en)_3]^{3+}$, the λ chelate adopts the *lel* conformation, so named because the C–C bond is paral*lel* to the C_3 axis.[46] Alternatively, the δ chelate adopts the *ob* conformation, because the C–C bond is *ob*lique to the C_3 rotational axis. Structures of the Δ-$[Co(en)_3]^{3+}$ trication in which all three chelates adopt the *lel* and *ob* conformations are shown in Figure 2.3.

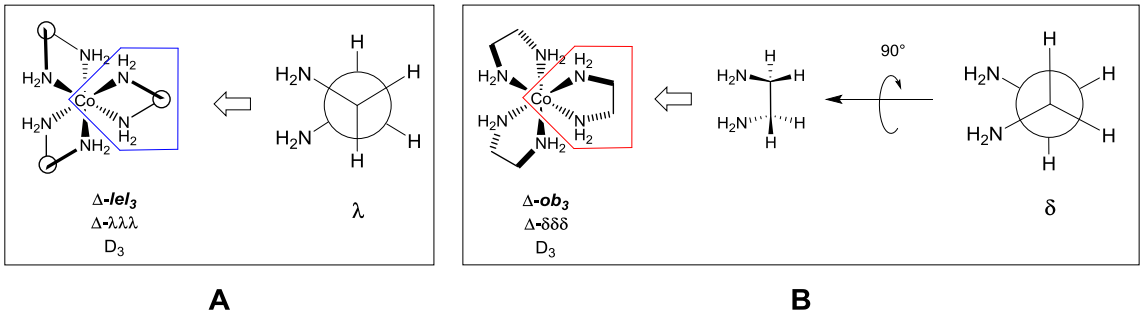

Figure 2.3. Accommodation of ethylenediamine ligands with three λ or three δ conformations in the coordination sphere of an octahedral cobalt atom with the Δ configuration.

In Figure 2.3, an effort has been made to relate the Newman projections in Figure 2.2 to the structures of the Δ-$[Co(en)_3]^{3+}$ trications, which are viewed down the C_3 rotational axes. Specifically, the ready fit of the λ diamine conformation into two octahedral binding sites is depicted in panel A. The other two chelates can dock similarly. As shown in panel B, the δ diamine conformation must first be rotated by 90° about a horizontal vector passing through the midpoint of the C–C bond. This allows the cobalt to accommodate three diamines while maintaining a Δ configuration.

For the Λ-$[Co(en)_3]^{3+}$ trication, these relationships are reversed. The λ chelate gives the *ob* conformation while the δ chelate adopts the *lel* conformation. In any case,

each of the three ethylenediamine ligands can independently adopt either of the two chelate conformations. Therefore, for a complex with a fixed metal chirality, up to four diastereomers may exist. Figure 2.4 shows the four possible isomers of both Λ-$[Co(en)_3]^{3+}$ (top row) and Δ-$[Co(en)_3]^{3+}$ (bottom row).

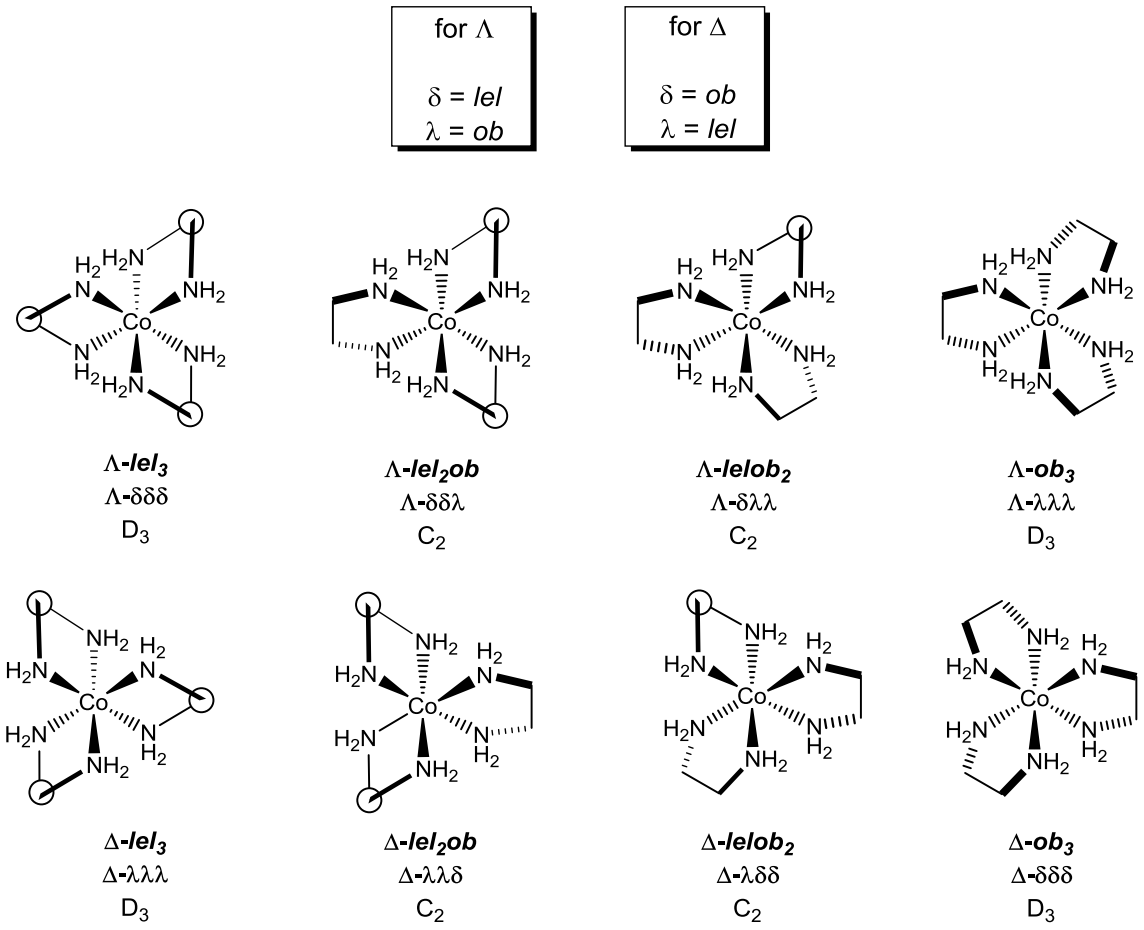

Figure 2.4. All possible stereoisomers of the $[Co(en)_3]^{3+}$ trication.

Admittedly, the intricacies of the conventional stereochemical nomenclature concerning Werner complexes can be overwhelming for the first time reader. One point that deserves clarification here is that complexes with Λ-lel_3 and Δ-lel_3 stereochemistry

are *enantiomers*. It would be an easy trap for a chemist to interpret Λ-lel$_3$ and Δ-ob$_3$ as describing enantiomers. In fact, these two labels describe diastereomers that are epimeric at the metal center.

In practice, the rapidly interconverting conformations of the ethylenediamine chelates are not considered when determining the absolute enantiopurity of a Werner complex. Only the Λ and Δ metal configurations are considered, with the understanding that each "pure" enantiomer may actually exist in a number of conformations at any one time. However, this type of isomerism is very relevant to the analysis of crystal structures, as the $[Co(en)_3]^{3+}$ trication can crystallize in any of the motifs in shown in Figure 2.4 (Chapter 3).

In addition to 1,2-ethylenediamine, tris-chelating Co(III) complexes of 1,3-diaminopropane[47] and 1,4-diaminobutane[48] have also been reported. As is easily conceptualized from Figures 2.1b and 2.1c, these systems also give Λ and Δ configurations at the metal center. However, the additional bonds required to form the six and seven member chelating rings result in a higher number of possible conformations. To date, there is no report of an analogous system containing tris-chelating 1,5-diaminopentane ligands.

2.3 Werner complexes with monosubstituted 1,2-ethylenediamine ligands

The simplest case of a monosubstituted diamine ligand is 1,2-propylenediamine (pn). The substituted diamine exists as two enantiomers: (*R*)-1,2-propylenediamine ((*R*)-pn) and (*S*)-1,2-propylenediamine ((*S*)-pn). The illustrative discussion here will mainly focus on tris-chelating Co(III) complexes with homochiral ligands.[49]

2.3.1 The configuration of the metal center

The chelation of three pn ligands around Co(III) produces Λ and Δ configurations at the metal center. However, the methyl group of the pn ligand also allows for *fac*ial (*fac*) and *mer*idional (*mer*) geometries leading to additional stereoisomers. For example, a complex with the Λ configuration must also adopt either a *fac* or *mer* configuration. Figure 2.5 illustrates the four possible isomers with homochiral *R*-pn ligands with consideration only for the Λ/Δ and *fac*/*mer* stereochemical descriptors.

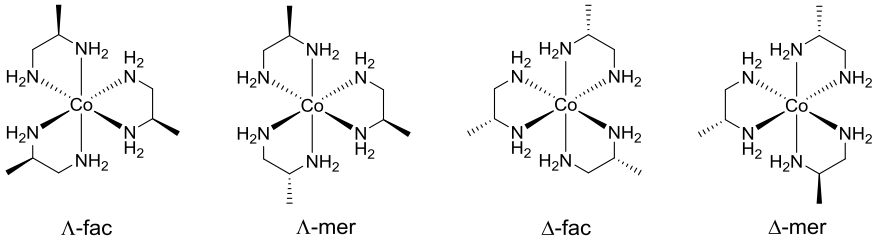

Figure 2.5. The *fac*/*mer* isomers of the $[Co((R)\text{-pn})_3]^{3+}$ trication.

2.3.2 The conformation of the 1,2-propylenediamine chelating ligand

The conformation of the 5-membered chelate ring plays a more significant role for substituted diamines than for unsubstituted ethylenediamine. For 1,2-propylenediamine, the chelate will prefer the conformation that places the methyl group in a pseudo-equatorial position. Figure 2.6 shows the conformational possibilities for (*R*)-pn and (*S*)-pn ligands.

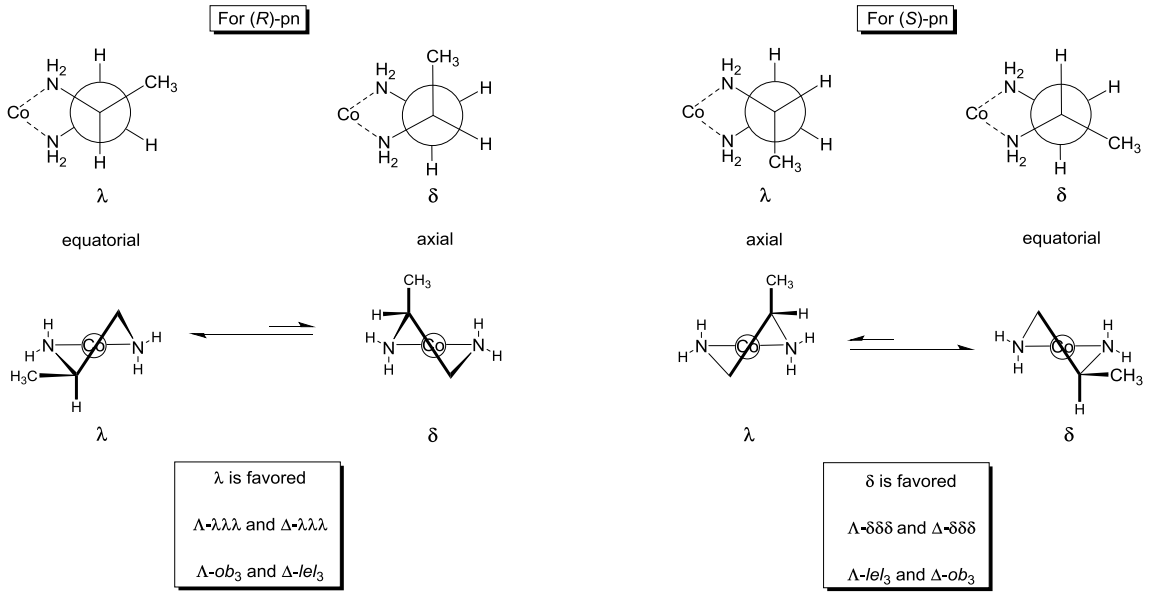

Figure 2.6. Diamine chelate conformations of pn ligands.

For (*R*)-pn, the Newman projection shows that the λ conformation of the ligand places the methyl group in the equatorial position. A ring flip to the δ conformation is unfavorable because it places the methyl group in the less stable axial position. It follows then that the tris-chelating $[Co((R)\text{-pn})_3]^{3+}$ should preferentially adopt either the Λ-λλλ conformation or the Δ-λλλ conformation. With reference to the previous discussion with unsubstituted 1,2-ethylenediamine, this means that if the Λ configuration is adopted, the chelating ligands will all be oblique to the C_3 rotational axis (Λ-*ob*$_3$). Likewise, the Δ complex will have ligands aligned parallel to the C_3 rotational axis (Δ-*lel*$_3$). In contrast, the *S*-pn ligand will preferentially occupy the δ conformation, thus giving rise to the possible product conformations of Λ-*lel*$_3$ and Δ-*ob*$_3$. Figure 2.7 shows the four possible isomers of the $[Co((R)\text{-pn})_3]^{3+}$ trication considering contributions for the metal configuration, chelate conformation, and *fac*/*mer* orientation.

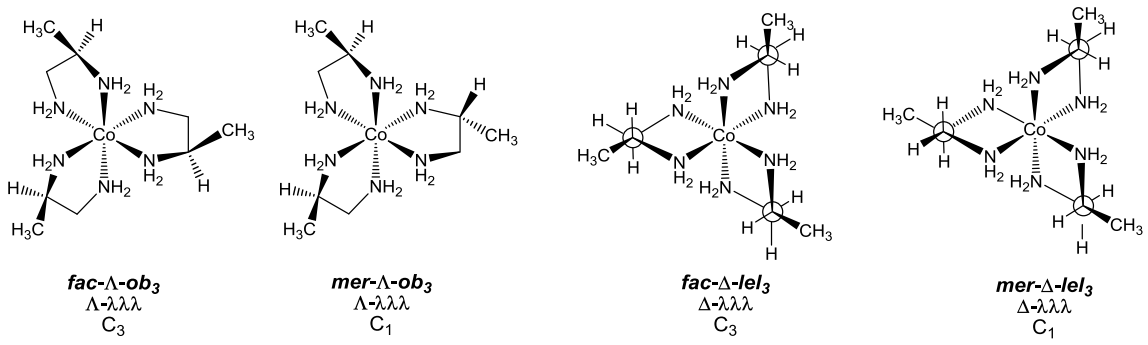

Figure 2.7. Significant configurational stereoisomers of the $[Co((R)\text{-pn})_3]^{3+}$ trication.

Complexes with racemic pn (*rac*-pn) ligands also give chiral structures. In this case, a complex may contain a heterochiral mixture of (*R*)-pn and (*S*)-pn diamine ligands. All such isomers are listed in Table 2.1.

Table 2.1. Stereoisomers of the $[Co(pn)_3]^{3+}$ trication (gray shading is for enantiopure (*R*)-pn).

Conformation	Configurational isomers	Geometrical isomers relating to methyl group	Number of stereoisomers
lel$_3$	Λ(δδδ) = Λ(*SSS*)	*fac* (1), *mer* (1)	2
	Δ(λλλ) = Δ(*RRR*)	*fac* (1), *mer* (1)	2
lel$_2$*ob*	Λ(δδλ) = Λ(*SSR*)	*fac* (1), *mer* (3)	4
	Δ(λλδ) = Λ(*RRS*)	*fac* (1), *mer* (3)	4
lelob$_2$	Λ(δλλ) = Λ(*SRR*)	*fac* (1), *mer* (3)	4
	Δ(λδδ) = Δ(*RSS*)	*fac* (1), *mer* (3)	4
ob$_3$	Λ(λλλ) = Λ(*RRR*)	*fac* (1), *mer* (1)	2
	Δ(δδδ) = Δ(*SSS*)	*fac* (1), *mer* (1)	2
Total number of isomers			24

2.4 Werner complexes with symmetrically disubstituted 1,2-ethylenediamine ligands

There are several examples of Werner complexes comprised of ethylenediamine ligands with two identical substituents. These include 2,3-butanediamine,[50] 1,2-

cyclohexanediamine (chxn),[51] and 1,2-diphenylethylenediamine (dpen).[52] Examples with chxn have been the most studied and the stereochemical possibilities are treated here first. Although there has been less attention given to dpen ligands, these will then be treated in equal detail as these complexes are the focus of later chapters.

Diamine ligands with two identical substituents have two stereocenters and, therefore, three stereoisomers are possible. As an example, 1,2-chxn exists as two enantiomeric *trans*-isomers ((*R*,*R*)-chxn and (*S*,*S*)-chxn) as well as the meso, *cis*-isomer ((*R*,*S*)-chxn). The three possible isomers are shown in Figure 2.8.

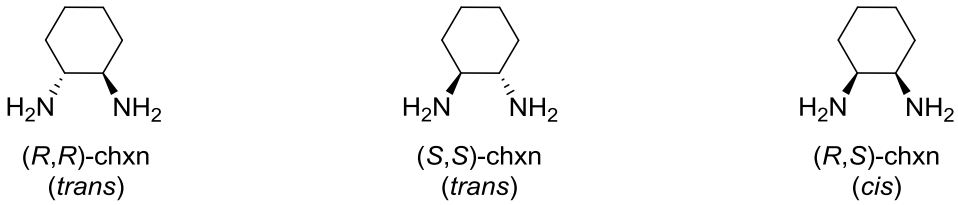

Figure 2.8. Configurational stereoisomers of 1,2-cyclohexanediamine.

2.4.1 The configuration of the metal center

The chelation of three chxn ligands around Co(III) produces Λ and Δ configurations at the metal center. As a general rule, disubstituted ethylenediamine ligands that have C_2 symmetry, such as the *trans*-chxn ligands, do not produce additional *fac*/*mer* isomers. For *cis* (*R*,*S*)-chxn, which is not C_2 symmetric, additional *fac* and *mer* isomers must be considered.

2.4.2 The conformations of the 1,2-cyclohexanediamine chelating ligand

The conformational properties of *trans*-chxn and *cis*-chxn are naturally different and must be treated separately. For the *trans*-isomers, the diamine will form a chelate in such a way that the cyclohexanediamine ring will occupy two equatorial positions, as shown in Figure 2.9. For (*R*,*R*)-chxn, this is restricted to the λ chelate conformer. Considering the tris-chelate $[Co((R,R)\text{-chxn})_3]^{3+}$, only the Λ-λλλ (Λ-$ob_3$) and Δ-λλλ (Δ-$lel_3$) isomers are possible. In contrast, the (*S*,*S*)-chxn tris-chelate is restricted to the δ conformer and the $[Co((S,S)\text{-chxn})_3]^{3+}$ trication will only exist in the Λ-δδδ (Λ-lel_3) or Δ-δδδ (Δ-ob_3) conformations. Figure 2.9 also shows the possible configurational stereoisomers of the $[Co(trans\text{-chxn})_3]^{3+}$ trication with only homochiral ligands.

Unlike (*R*)-pn, which prefers the λ conformation over the δ conformation in an equilibrium distribution, (*R*,*R*)-chxn is fixed into the λ conformation. Because of the cyclic nature of the diamine backbone, it is impossible to simultaneously flip the chair conformation of the cyclohexane ring and maintain chelation to the metal because the amino groups would then be in the *trans*-diaxial orientation.

It is also conceivable to prepare tris-chelating Co(III) complexes from a racemic mixture of *trans*-chxn ligands. In this case, octahedral complexes containing heterochiral combinations of (*R*,*R*)-chxn and (*S*,*S*)-chxn would also be possible. Figure 2.10 shows each of the eight possible isomers.

When the meso compound *cis*-chxn (Figure 2.7) forms a chelate, one C-C bond of the cyclohexane ring will occupy an equatorial position while the other C-C bond is forced into an axial position, as shown in Figure 2.11 (insert). This is true for both the λ and δ chelate conformations. Therefore, for (*R*,*S*)-chxn, there is no preferential conformation for an individual chelate ring and interconversion between λ and δ

conformations is possible (Figure 2.11, insert). Figure 2.11 also shows the possible configurational stereoisomers of the $[Co(\textit{cis}\text{-chxn})_3]^{3+}$ trication with respect to metal configuration, chelate conformation, and *fac*/*mer* orientation.

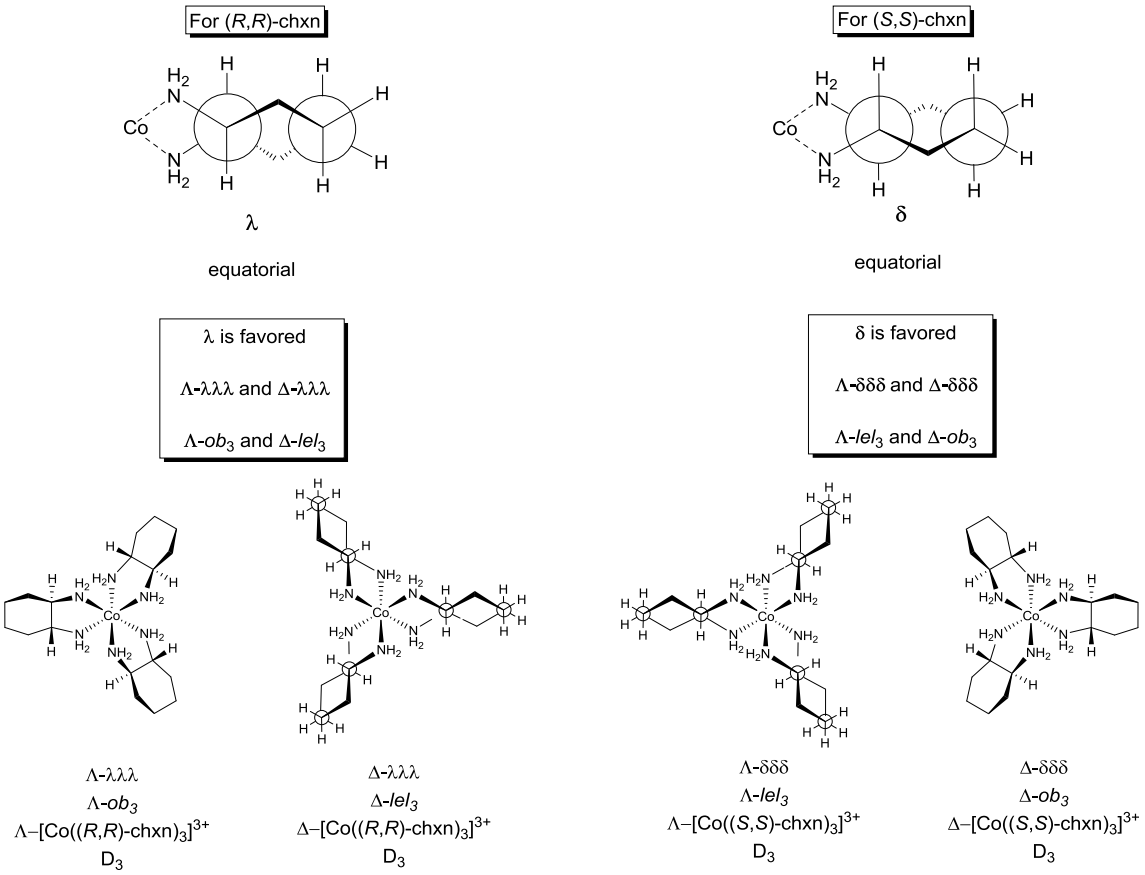

Figure 2.9. Diamine chelate conformations and significant configurational stereoisomers of the $[Co(\textit{trans}\text{-chxn})_3]^{3+}$ trication with homochiral ligands.

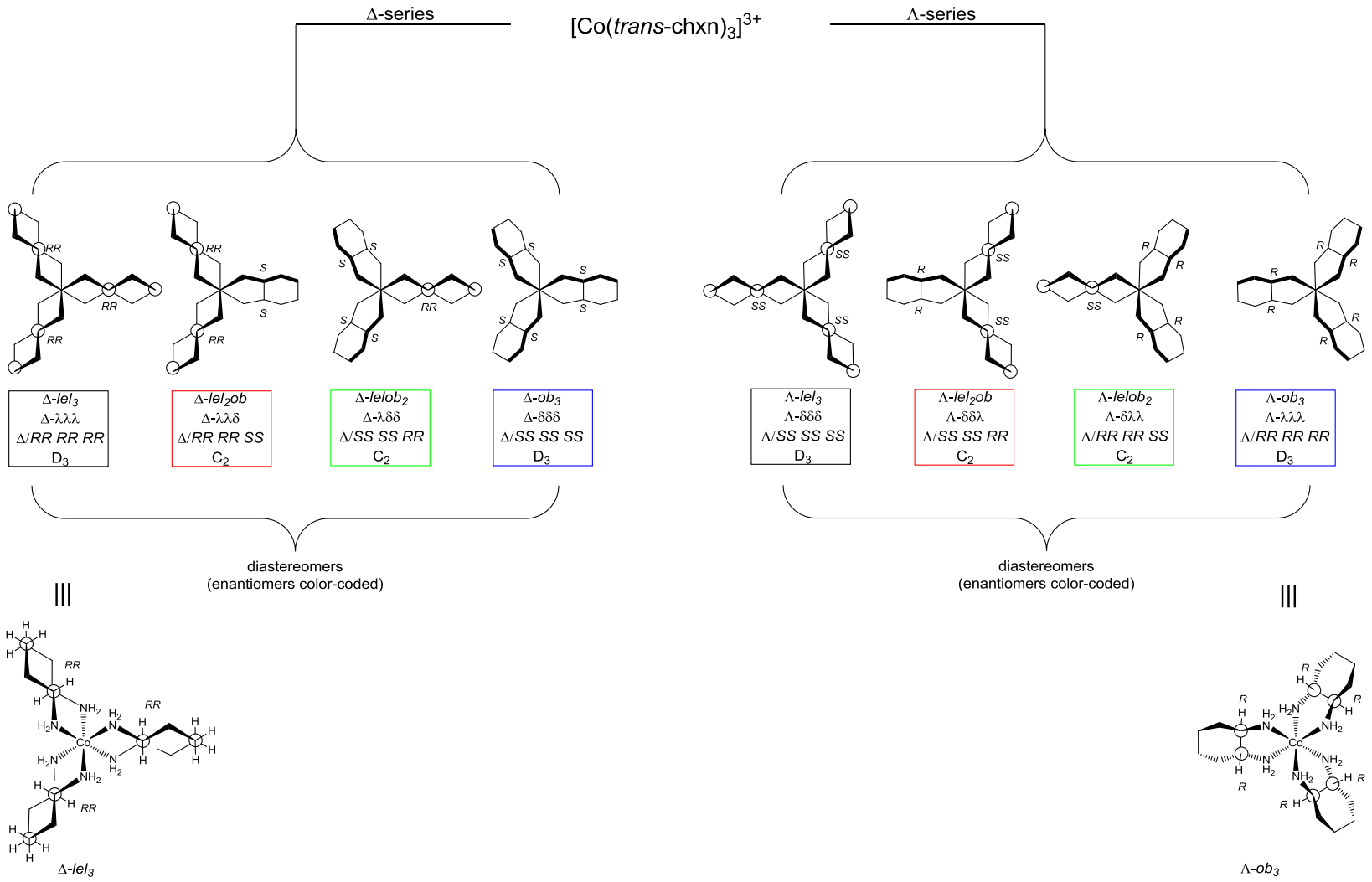

Figure 2.10. Significant configurational stereoisomers of the $[Co(\textit{trans}\text{-chxn})_3]^{3+}$ trication with mixed (*R*,*R*)-chxn and (*S*,*S*)-chxn ligands.

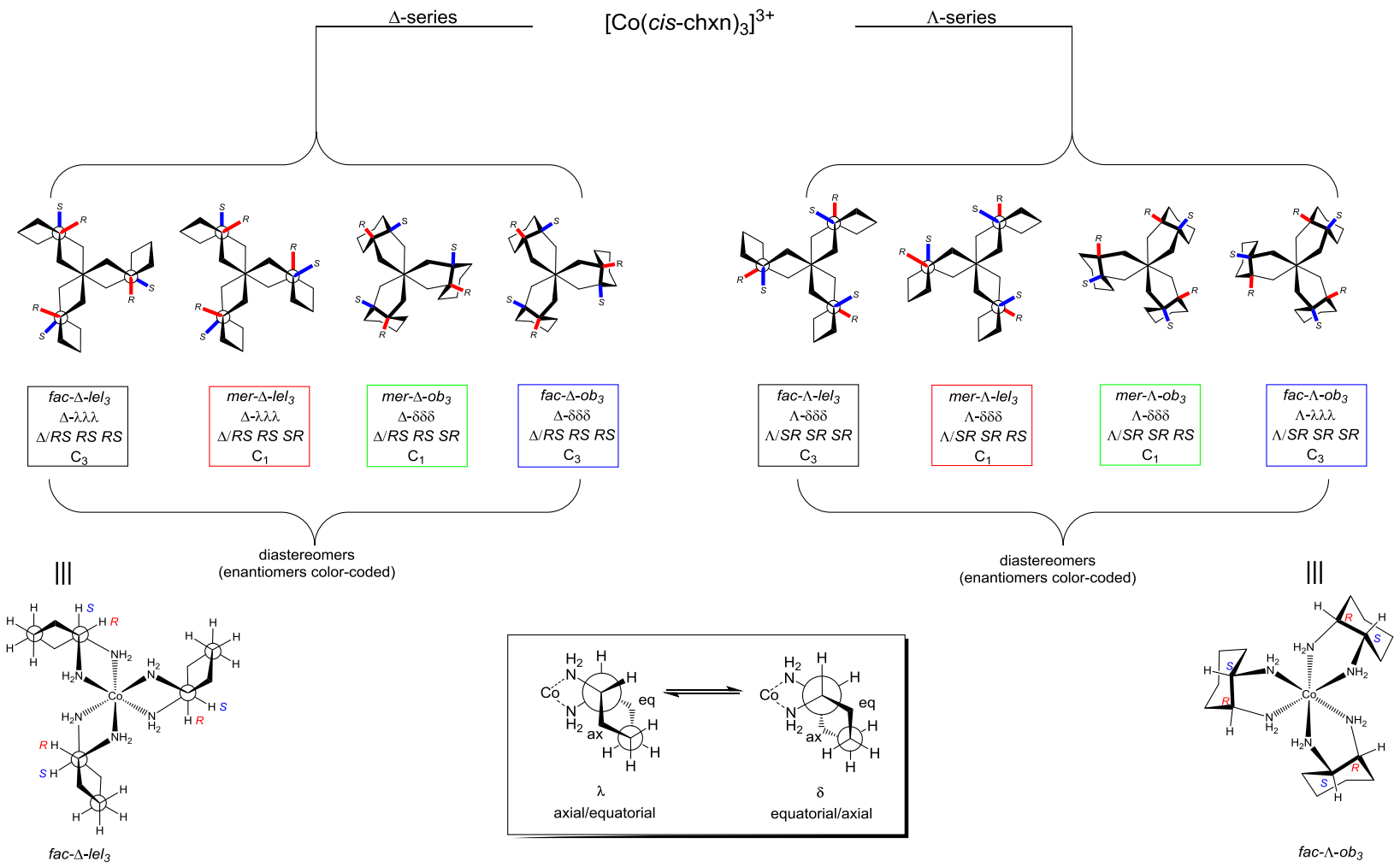

Figure 2.11. Diamine chelate conformations and significant configurational stereoisomers of the $[Co(cis\text{-chxn})_3]^{3+}$ trication.

2.4.3 The conformations of the 1,2-diphenylethylenediamine chelating ligand

The conformational behavior of *trans*-dpen and *cis*-dpen also must be treated separately. For the *trans*-isomers, (*R*,*R*)-dpen and (*S*,*S*)-dpen, the diamine will form a chelate in such a way that the bulky phenyl groups both occupy the pseudo-equatorial positions, as shown in Figure 2.12. The (*R*,*R*)-dpen chelate prefers the λ conformation. For tris-chelating $[Co((R,R)\text{-dpen})_3]^{3+}$, the Λ-λλλ (Λ-$ob_3$) and Δ-λλλ (Δ-$lel_3$) isomers are favorable. In contrast, the (*S*,*S*)-dpen chelate prefers the δ conformation, and $[Co((S,S)\text{-dpen})_3]^{3+}$ will preferentially exist in the Λ-δδδ (Λ-lel_3) or Δ-δδδ (Δ-ob_3) conformations. Figure 2.12 also shows the possible configurational stereoisomers of the $[Co(trans\text{-chxn})_3]^{3+}$ trication with homochiral ligands.

In principal, it is also possible to prepare tris-chelating Co(III) complexes from a racemic mixture of *trans*-dpen ligands. In this case, octahedral complexes containing heterochiral combinations of (*R*,*R*)-dpen and (*S*,*S*)-dpen would also be possible. Figure 2.13 shows each of the eight possible configurational stereoisomers.

A chelate formed with *cis*-dpen is intrinsically less stable than a chelate formed with either enantiomer of *trans*-dpen. In this case, one phenyl group must occupy an axial position while the other occupies the equatorial position, as shown in Figure 2.14 (insert). This is true for both the λ and δ chelate conformations, and therefore neither is preferred to the other. Interconversion between the two chelate conformations is possible. Figure 2.14 also shows the possible configurational stereoisomers of $[Co(cis\text{-dpen})_3]^{3+}$ with respect to metal configuration, chelate conformation, and *fac*/*mer* orientation.

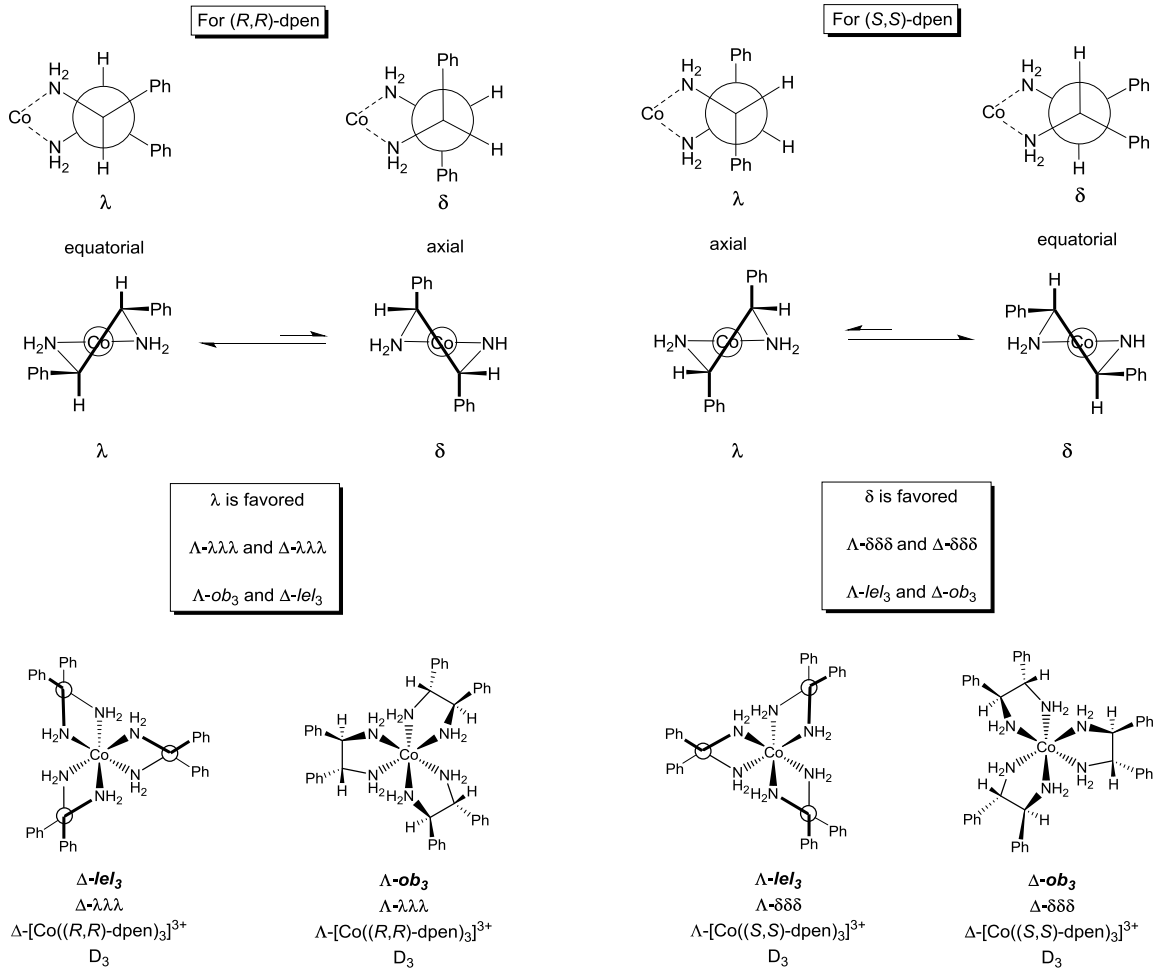

Figure 2.12. Diamine chelate conformations and significant configurational stereoisomers of the [Co(*trans*-dpen)$_3$]$^{3+}$ trication with homochiral ligands.

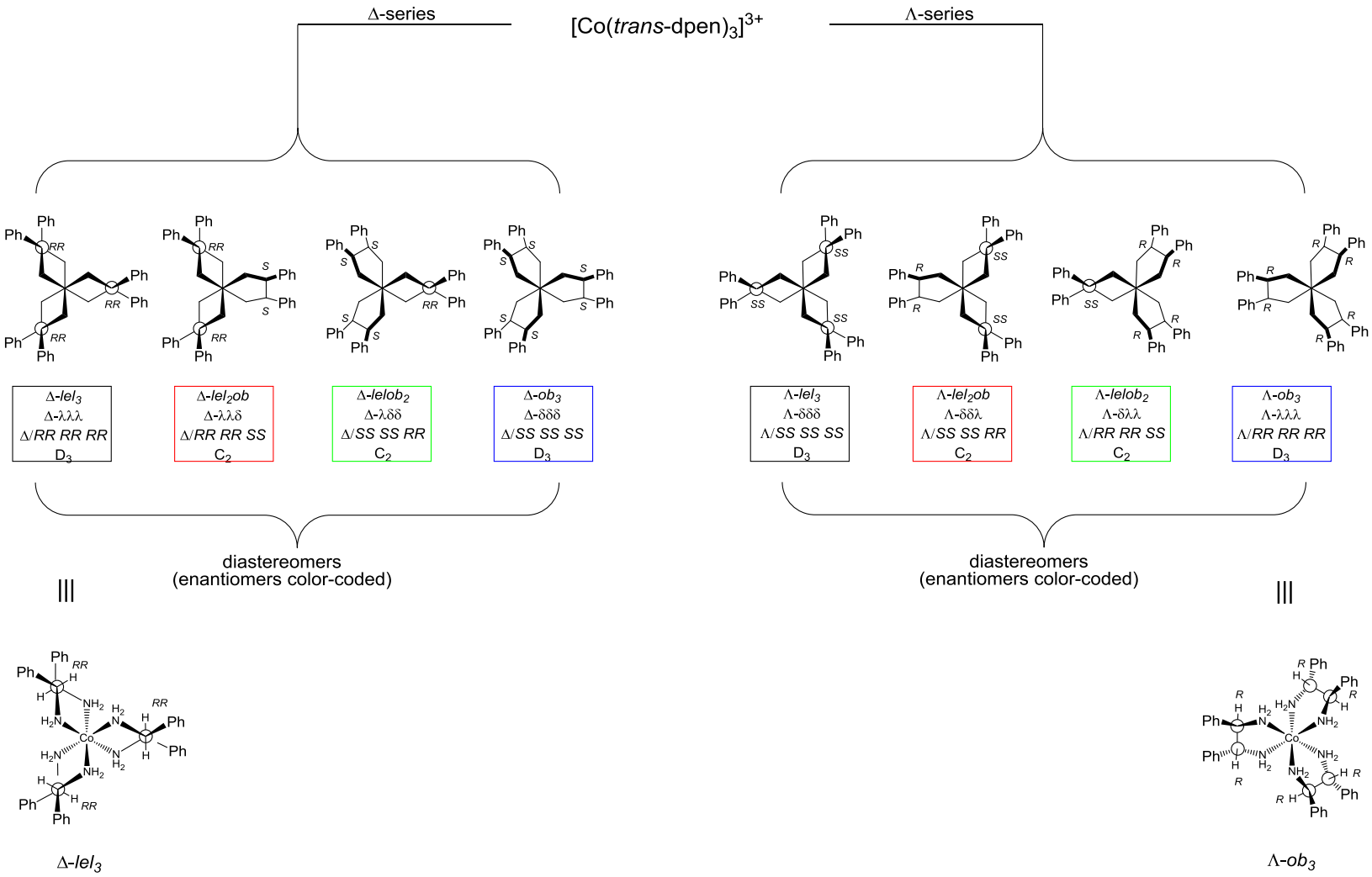

Figure 2.13. Significant configurational stereoisomers of the $[Co(trans\text{-dpen})_3]^{3+}$ trication with mixed (*R*,*R*)-dpen and (*S*,*S*)-dpen ligands.

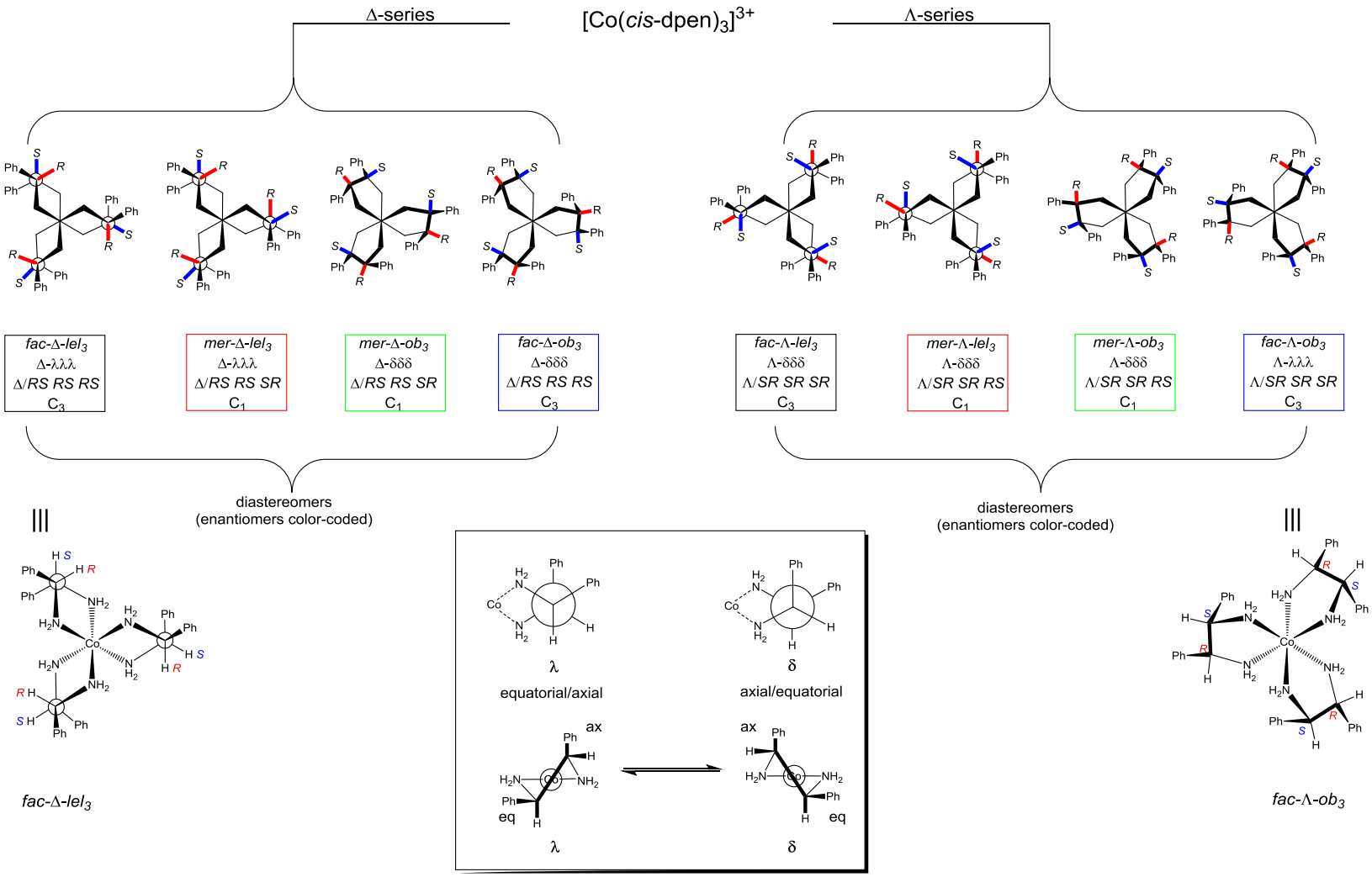

Figure 2.14. Diamine chelate conformations and significant configurational stereoisomers of the $[Co(cis\text{-dpen})_3]^{3+}$ trication.

2.5 Stabilities of *lel* and *ob* conformations

Two chiral Werner complexes with the same metal configuration and opposite diamine chelate conformations are diastereomers and should have different energies. In the case of the $[Co(en)_3]^{3+}$ trication, the energy difference between the *lel* or *ob* conformation of a single ethylenediamine chelate makes little difference with respect to the overall stability. However, the additive effect of three ethylenediamine ligands, considering spatial interactions between the atoms of the three chelates, makes one set of conformations slightly more preferred than the others. For the Δ isomer, Corey and Bailar calculated Δ-lel_3-$[Co(en)_3]^{3+}$ to be more stable than Δ-ob_3-$[Co(en)_3]^{3+}$ by 7.5 kJ mol^{-1} (1.8 kcal mol^{-1}), based solely on intramolecular C–H and H–H interactions.[46] The Δ-lel_2ob and Δ-$lelob_2$ conformers occupy an undefined intermediate space between these two extremes. The authors freely admit that the calculated energy difference in this complicated stereochemical case is only a rough approximation and should only be treated qualitatively.

Harnung performed thermodynamic equilibration studies with $[Co(trans\text{-}chxn)_3]^{3+}$ trications.[51] An aqueous solution of racemic lel_3-$[Co(chxn)_3]^{3+}$ $3Cl^-$ was refluxed over charcoal in the presence of uncoordinated racemic chxn (*rac*-chxn) for 30 minutes (Scheme 2.1). The equilibrium distribution of the isolated products showed a strong preference for complexes in the lel_3 conformation.

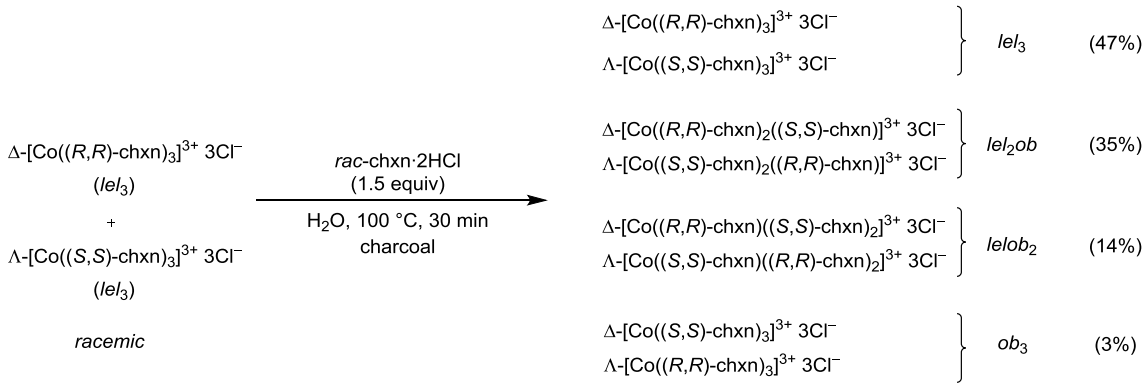

Scheme 2.1. Thermal equilibration of racemic lel_3-$[Co(chxn)_3]^{3+}$ $3Cl^-$.

In a follow up experiment,[51] an aqueous solution of enantiopure Δ-lel_3-$[Co((R,R)\text{-dpen})_3]^{3+}$ $3Cl^-$ was refluxed over charcoal in the presence of enantiopure (*R*,*R*)-chxn for 30 minutes (Scheme 2.2). After this equilibration time, only 7% of the pure material had isomerized from the lel_3 to ob_3 conformation.

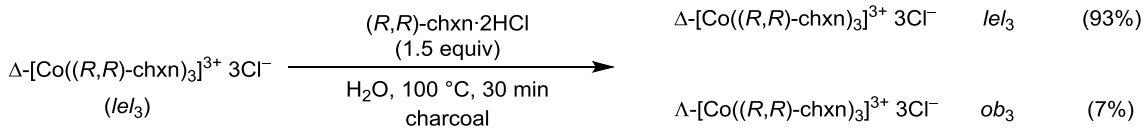

Scheme 2.2: Thermal equilibration of enantiopure Δ-lel_3-$[Co((R,R)\text{-dpen})_3]^{3+}$ $3Cl^-$.

Though a clear bias for the lel_3 conformation is observed under these experimental conditions, it should be noted that the equilibration in each case was performed on complexes already in the lel_3 conformation. Even though refluxing conditions over charcoal have been used in other cases to facilitate the isomerization of Werner-type complexes,[45] it was not clear from this report how the authors established the equilibration time. Perhaps longer reaction times could have shifted the equilibrium

more toward the ob_3 conformation. Furthermore, the counteranion in each case was Cl^-, which may form preferential associations with complexes of one conformation over the other. In the next chapter, the influence of outer-sphere interactions between Werner cations and their counteranions will be examined in more detail.

CHAPTER III

HYDROGEN BONDING WITH WERNER COMPLEXES

3.1 Overview

A survey of the Cambridge Crystallographic Data Centre (May 2013) revealed 350+ hits for unsubstituted and substituted tris(1,2-ethylenediamine) Co(III) complexes. Dozens of these structures have been inspected in detail and all exhibit hydrogen bonding between the N-H units of the coordinated amines and their corresponding counteranions or cocrystallized solvent molecules. Examination of the intricate hydrogen bonding networks of Werner complexes in the solid state can provide insight into the kinds of intermolecular interactions that are possible between chiral Werner-type tricationic species and Lewis basic substrates.

3.2 The N-H hydrogen bond donors of Werner complexes

The $[Co(1,2\text{-diamine})_3]^{3+}$ trication possesses 12 N-H bonds. Due to the idealized D_3 symmetry of the trication, there exist two distinct classes of hydrogen bonding units. The first class constitutes a triangular face on the C_3 rotational axis. There are three N-H units per C_3 face and two C_3 faces per complex, resulting in 6 N-H units in the C_3 class. The N-H units of the second class are symmetrically disposed across the C_2 rotational axis. There are two N-H units on this C_2 face and three such C_2 faces per complex, resulting in 6 N-H units in the C_2 class. The structures in Figure 3.1 show views of the C_3 and C_2 N-H units of both *lel*$_3$ and *ob*$_3$ Λ-$[Co(en)_3]^{3+}$ trications, as determined crystallographically.[53,54]

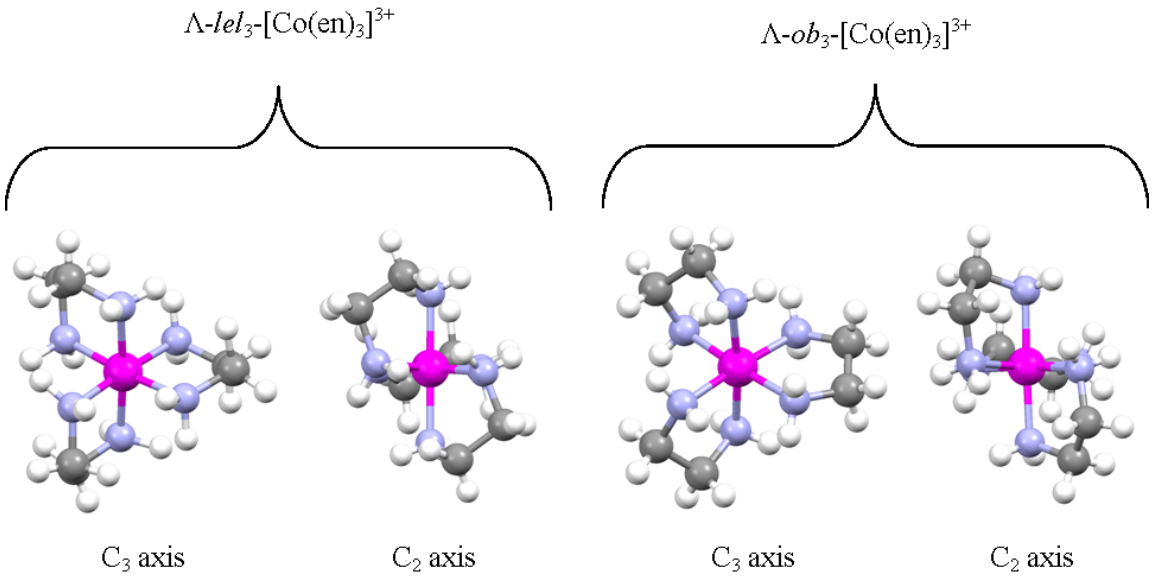

Figure 3.1. Views of the isomeric Λ-*lel*$_3$-[Co(en)$_3$]$^{3+}$ and Λ-*ob*$_3$-[Co(en)$_3$]$^{3+}$ tricationsfrom the C_3 and C_2 axes.[55]

The *lel*/*ob* conformations of the diamine chelate rings have a profound influence on the positions and angles of the N-H bonds. In addition to the structures in Figure 3.1, both the *lel*$_3$ and *ob*$_3$ isomers of [Co(pn)$_3$]$^{3+}$,[56,57] [Co(chxn)$_3$]$^{3+}$,[58,59] and [Co(dpen)$_3$]$^{3+}$ [60] have been crystallographically characterized. I have measured the distance between each adjacent N-*H* atom within a particular class (C_2 or C_3). The average values are given in Table 3.1.

Table 3.1. The effect of the *lel*/*ob* conformations on the position of N-H bonds.

entry	trication	*conformation*	average N*H*···*H*N distances (Å)		average HN···NH dihedral angles (°)	
			C_3[a]	C_2[b]	C_3[c]	C_2[d]
1	Λ-$[Co(en)_3]^{3+}$	lel_3	2.45(.28)[e]	1.75(.03)[e]	15.9(12.5)[e]	38.2(0.7)[e]
2	Λ-$[Co(en)_3]^{3+}$	ob_3	2.63(.07)	2.59(.18)	49.5(5.1)	79.8(12.1)
3	Δ-$[Co((R)\text{-pn})_3]^{3+}$	lel_3	2.36(.09)	2.40(.00)	2.9(0.6)	39.0(0.0)
4	Λ-$[Co((R)\text{-pn})_3]^{3+}$	ob_3	2.74(.08)	2.83(.17)	53.7(7.5)	78.0(11.3)
5	Δ-$[Co((R,R)\text{-chxn})_3]^{3+}$	lel_3	2.41(.04)	2.429(.002)	11.5(9.3)	29.9(0.1)
6	Λ-$[Co((R,R)\text{-chxn})_3]^{3+}$	ob_3	2.65(.02)	2.86(.01)	65.5(0.9)	90.4(2.0)
7	Λ-$[Co((S,S)\text{-dpen})_3]^{3+}$	lel_3	2.40(.13)	2.26(.07)	7.6(5.9)	29.6(5.2)
8	Δ-$[Co((S,S)\text{-dpen})_3]^{3+}$	ob_3	2.63(.07)	2.61(.10)	48.5(4.7)	81.4(5.8)

[a]Average of six distances. [b]Average of three distances. [c]Average of six torsion angles. [d]Average of three torsion angles. [e]Standard deviation from the mean (not an esd value)

For each trication, the N-H units are positioned more closely together in the lel_3 conformation compared to the analogous ob_3 conformation. This is true in each case for the three N-H units of the C_3 face and the two N-H units of the C_2 face.

The average H-N···N-H dihedral angles are calculated for each adjacent pairing of N-H units in the same class and are also given in Table 3.1. These data reflect the degree to which two adjacent N-H bonds are oriented in the same direction. A dihedral angle of 0° means that two N-H bonds are parallel, point in the same direction, and are thereby well-suited for forming dual hydrogen bonds with a suitable acceptor molecule.

The dihedral angles of adjacent C_3 N-H units in the lel_3 conformation are relatively small (2-16°), meaning that the N-H bonds are roughly parallel. By comparison, the dihedral angles of the C_3 N-H units in the ob_3 conformation are

significantly skewed (49-65°). The same pattern is found with the C_2 N-H units, but in this case all angles are considerably more skewed than those of the C_3 N-H units.

In effect, the *lel*$_3$ conformation forces the N-H units closer together and orients them in roughly the same direction. As was seen in Figure 3.3, the three C_3 N-H units also appear to converge slightly inward towards the C_3 axis. Because the three C_3 N-H units are roughly parallel, they are in a position to form triple hydrogen bonds with a single acceptor molecule. By comparison, the *ob*$_3$ conformation forces the hydrogen atoms further apart and orients adjacent N-H units in different directions. Figure 3.3 also demonstrates that these three C_3 N-H units are slightly skewed away from the C_3 axis.

The orientation of the N-H bonds resulting from the *lel*/*ob* conformations of the diamine chelate have a significant effect on the hydrogen bonding interactions between Werner trications and corresponding counteranions. Ogino determined the outer-sphere association constants between various anions and cobalt trications by measuring the variation in the UV/visible extinction coefficients at various anion concentrations.[61] For each anion tested, the association constants were greater for Δ-*lel*$_3$-[Co((*R*)-pn)$_3$]$^{3+}$ trications than for diastereomeric Λ-*ob*$_3$-[Co((*R*)-pn)$_3$]$^{3+}$ trications, as shown in Table 3.2. Although the two trications analyzed are epimeric at the metal center, the *lel*$_3$ diastereomer displayed stronger associations with both enantiomers of the tartrate anions.

Table 3.2. Association constants (M^{-1}) of Λ and Δ-[Co((*R*)-pn)$_3$]$^{3+}$ trications with various anions with an ionic strength of 0.1 in H_2O at 25 °C.

Entry	trication	*conformation*	(*R*,*R*)-tartrate^{2-}	(*S*,*S*)-tartrate^{2-}	SO_4^{2-}
1	Δ-[Co(*R*-pn)$_3$]$^{3+}$	*lel*$_3$	30	28	70
2	Λ-[Co(*R*-pn)$_3$]$^{3+}$	*ob*$_3$	7	16	43

Cation exchange chromatography on SP-Sephadex resins with aqueous solutions of various salts has been used to separate isomers of $[Co(1,2\text{-diamine})_3]^{3+}$ salts. The separation of the isomers depends on the differential outer-sphere recognition between the cobalt trication and the eluent anion. The isomer with the strongest association with the anions will elute fastest. Cation exchange chromatography with the salts Na_3PO_4 and Na_2SO_4, which feature a tetrahedral trianion and dianion, respectively, both elute Δ-*lel*$_3$-$[Co(R\text{-pn})_3]^{3+}$ faster than Λ-*ob*$_3$-$[Co(R\text{-pn})_3]^{3+}$.[49,62] Likewise, Δ-*lel*$_3$-$[Co((R,R)\text{-chxn})_3]^{3+}$ is eluted more rapidly than Λ-*ob*$_3$-$[Co((R,R)\text{-chxn})_3]^{3+}$ with Na_3PO_4 as eluent.[51] These results have been attributed to the fact that the C_3 N-H groups of the *lel*$_3$ isomers are almost parallel and more predisposed to form triple, linear hydrogen bonds with anions.[49,62] Because the N-H units of the *ob*$_3$ isomers point in different directions and are skewed outward from the C_3 axis, the corresponding hydrogen bonds are bent and ultimately weaker.[63]

The structures of two well-known hydrogen bond mediating catalysts containing thiourea and squaramide hydrogen bond donors have been reported (Figure 3.2).[64,65] I computed the N*H*···*H*N distances and HN···NH dihedral angles of these structures. For the Werner complexes analyzed in Table 3.2, nearly all bond distances are intermediate between Takemoto's thiourea organocatalyst[64] and Rawal's squaramide organocatalyst.[65] The dihedral angles of Werner complexes are generally greater than those of the organic catalysts, but in some cases, complexes with *lel*$_3$ conformations have narrower dihedral angles than the squaramide catalyst.

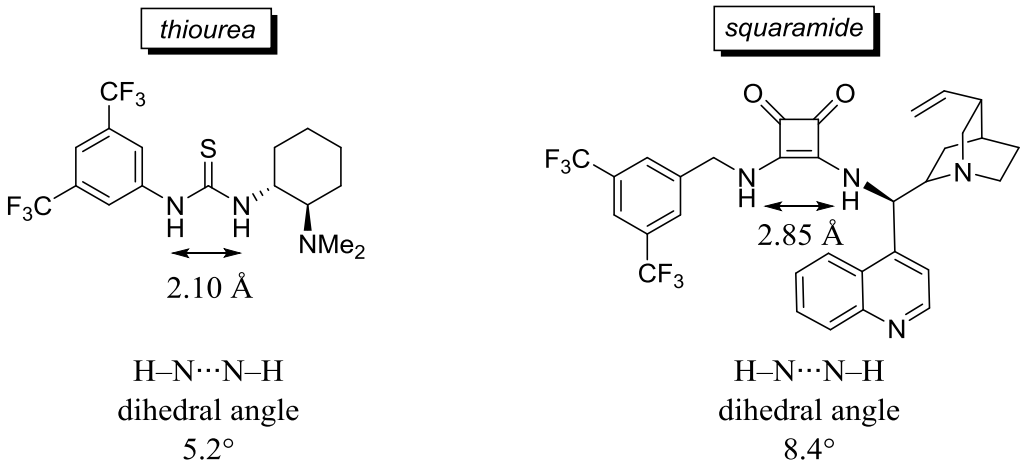

Figure 3.2. N-*H*···*H*-N distances and dihedral angles for two established metal-free organocatalysts.

3.3 Hydrogen bonding interactions between Werner trications and anions/solvent

Werner trications exhibit diverse hydrogen bonding networks with anions and solvent molecules. Even in a single crystal structure, different kinds of interactions can be observed with the same hydrogen bond acceptor. For instance, one Cl^- anion might be found to form a single hydrogen bond with a C_3 N-H unit while another forms a hydrogen bond with two C_2 N-H units. The situation becomes even more complicated with an anion that has multiple hydrogen bond accepting atoms.

3.3.1 Nomenclature to describe hydrogen bonding in Werner complexes

To aid and orient the reader, a systematic categorization has been invented to describe all of the hydrogen bonding contacts in a particular crystal structure at a glance. In Table 3.3, possible hydrogen bonding scenarios are described, followed by the new shorthand nomenclature.

Table 3.3. Nomenclature for hydrogen bonding interactions observed with $[Co(1,2\text{-diamine})_3]^{3+}$ trications and anions (X^{n-}) or solvent molecules.

Description of hydrogen bond	C_2 N-H	C_3 N-H	Interligand C_2,C_3 N-H	Intraligand (C_2/C_3) N-H
One NH binds to X at a single atom	[C_2][1]	[C_3][1]	---	---
Two NH bind to X at a single atom	[C_2,C_2][1]	[C_3,C_3][1]	[C_2,C_3][1]	[(C_2/C_3)][1]
Three NH bind to X at a single atom	---	[C_3,C_3,C_3][1]	[C_2,C_3,C_3][1] or [C_2,C_2,C_3][1]	[(C_2/C_3),C_3][1] or [C_2,(C_2/C_3)][1]
One NH binds to X at two different atoms	[C_2][2]	[C_3][2]	---	---
Two NH bind to X at two different atoms	[C_2,C_2][2]	[C_3,C_3][2]	[C_2,C_3][2]	[(C_2/C_3)][2]
Three NH bind to X at two different atoms	---	[C_3,C_3,C_3][2]	[C_2,C_3,C_3][2] or [C_2,C_2,C_3][2]	[(C_2/C_3),C_3][2] or [C_2,(C_2/C_3)][2]
One NH binds to X at three different atoms	[C_2][3]	[C_3][3]	---	---
Two NH bind to X at three different atoms	[C_2,C_2][3]	[C_3,C_3][3]	[C_2,C_3][3]	[(C_2/C_3)][3]
Three NH bind to X at three different atoms	---	[C_3,C_3,C_3][3]	[C_2,C_3,C_3][3] or [C_2,C_2,C_3][3]	[(C_2/C_3),C_3][3] or [C_2,(C_2/C_3)][3]

$[C_w^x][YZ]$

W = symmetry label of the N-H hydrogen bond donor
X = number of H-bond accepting atoms engaged by a single N-H hydrogen bond donor (default = 1)
Y = total number of H-bond accepting atoms engaged
Z = type of atom that is accepting a hydrogen bond (only included if ambiguous)

A hydrogen bonding pair is labeled with the symmetry of the N-H donor ([C_2] or [C_3]) followed by the number of engaged atoms in the hydrogen bond acceptor in a separate bracket. For instance, a single hydrogen bond between a Cl^- anion and a C_3 N-H is labeled as [C_3][1]. For molecules that accept multiple hydrogen bonds at the same atom, the hydrogen bond donors are listed in succession. Therefore, for a Cl^- anion, the label [C_3,C_3][1] indicates that the anion simultaneously accepts hydrogen bonds from two different C_3 N-H units.

When a molecule has multiple Lewis basic atoms, such as the NO_3^- anion, multiple oxygen atoms can be engaged by the same Werner trication. As an example, if two C_2 N-H units form hydrogen bonds with two different oxygen atoms, the interaction would be labeled [C_2,C_2][2].

In rare cases, a single N-H unit will simultaneously form hydrogen bonds with two or more atoms of the same acceptor molecule. In this situation, a superscript is added to indicate the number of acceptor atoms that are engaged. Returning to the previous example with the NO_3^- anion, the label [C_2^2,C_2][2] would indicate that one C_2 N-H unit simultaneously bonded to two oxygen atoms while the second C_2 N-H unit bonded to only one oxygen atom.

In most cases, synergistic hydrogen bonding involving two or more N-H units involves two or more diamine ligands. No examples have been found in which one hydrogen bond accepting molecule simultaneously binds both C_3 N-H units or both C_2 N-H units of the same diamine ligand. However, this technically could be possible with large or oligomeric hydrogen bond acceptors that can wrap around the Werner trication.

In some cases, the hydrogen bond acceptor will simultaneously bind both a C_2 and C_3 N-H unit. Most commonly this involves two different diamine ligands (Interligand C_2,C_3 N-H; Table 3.3). However, there are occasions when the hydrogen

bond acceptor binds to a C_2 and C_3 N-H unit of the same diamine ligand or, more precisely, the same nitrogen atom (Intraligand (C_2/C_3) N-H; Table 3.3). This rare case deserves a separate descriptor. The contributing donors are separated by a forward slash and confined within parentheses. For example, the interaction between a Cl^- anion that simultaneously engages both N-H units of the same nitrogen atom is described as [(C_2/C_3)][1].

When a hydrogen bond acceptor contains more than one kind of Lewis basic atom, there is some ambiguity as to which atom is engaged in the hydrogen bond. For example, the thiocyanate anion (NCS^-) could accept a hydrogen bond at either the nitrogen or sulfur atom. In this case, the atom is listed after the number of hydrogen bond acceptors. The label [C_3][1N] indicates that NCS^- forms a hydrogen bond with a single C_3 N-H unit at the nitrogen atom.

The preceding rules of nomenclature are believed to be concise, yet adequately descriptive, for each hydrogen bonding scenario. Over time, new kinds of hydrogen bonding interactions with Werner trications could be discovered, requiring amendments to this original list.

3.3.2 Case studies of hydrogen bonding interactions

Selected examples from the pool of 350+ Werner complexes obtained from the Cambridge Crystallographic Data Centre were examined in greater detail. The ball and stick representations have been refined to include all hydrogen bonding contacts available to a single $[Co(1,2\text{-diamine})_3]^{3+}$ trication. Each unique hydrogen bond acceptor is described with the previously explained nomenclature to delineate the nature

of the hydrogen bonding interactions. It should be kept in mind that a given anion or solvent molecule can hydrogen bond to more than one trication in the unit cell.

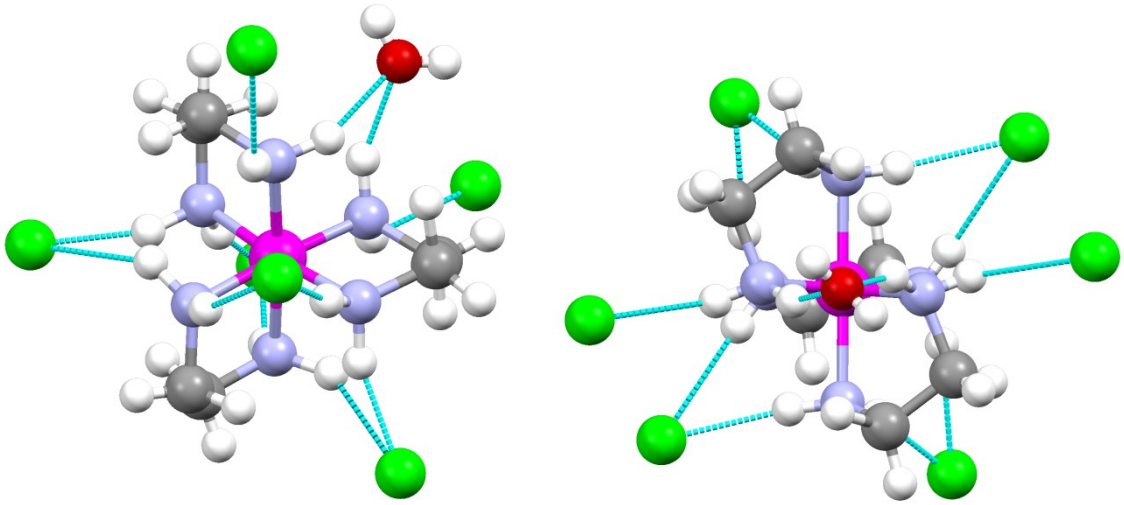

Λ-*lel*$_3$-$[Co(en)_3]^{3+}$ $3Cl^- \cdot H_2O$		
H-bond acceptor (X)	Type of H-Bond	Total number of similar interactions
Cl^-	$[C_3,C_3][1]$	2
Cl^-	$[C_3][1]$	2
Cl^-	$[C_2,C_2][1]$	2
H_2O	$[C_2,C_2][1]$	1

Figure 3.3. Hydrogen bonding interactions in the crystal structure of Λ-*lel*$_3$-$[Co(en)_3]^{3+}$ $3Cl^- \cdot H_2O$ viewed from a C_3 axis (left) and a C_2 axis (right).

The structure and hydrogen bonding interactions of the monohydrated trichloride salt, Λ-*lel*$_3$-$[Co(en)_3]^{3+}$ $3Cl^- \cdot H_2O$, are shown in Figure 3.3.[53] Each Werner trication forms hydrogen bonds with a total of six Cl^- anions and one H_2O molecule. All twelve

N-H units are engaged in hydrogen bonding. A mixture of single and double hydrogen bonds to Cl^- are observed for C_3 N-H units while C_2 units give only double hydrogen bonds. The H_2O molecule is engaged by two C_2 N-H units. To accommodate the dual hydrogen bond with the C_2 N-H units, the H_2O molecule is rotated 38.1° from the horizontal CoN_4 plane.

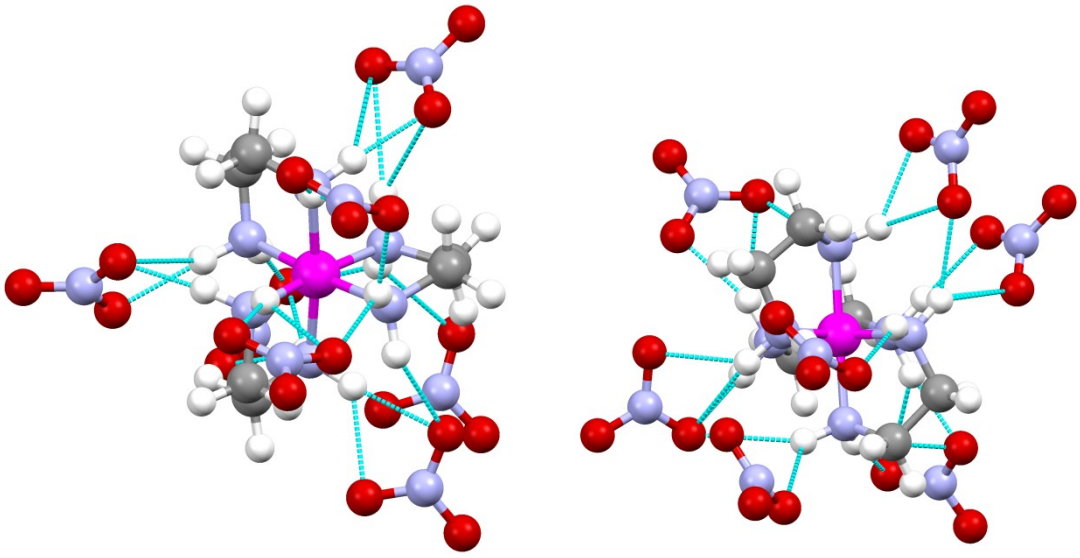

Λ-*lel*$_3$-$[Co(en)_3]^{3+}$ $3NO_3^-$		
H-bond acceptor (X)	Type of H-Bond	Total number of similar interactions
NO_3^-	$[C_3^2,C_3][2]$	2
NO_3^-	$[C_3^2,C_3,C_3][2]$	1
NO_3^-	$[C_3][1]$	1
NO_3^-	$[C_2^2,C_2^2][2]$	1
NO_3^-	$[C_2^2,C_2][2]$	2

Figure 3.4. Hydrogen bonding interactions in the crystal structure of Λ-*lel*$_3$-$[Co(en)_3]^{3+}$ $3NO_3^-$ viewed from the from a C_3 axis (left) and a C_2 axis (right).

The structure and hydrogen bonding interactions of the nitrate salt, Λ-*lel*$_3$-$[Co(en)_3]^{3+}$ $3NO_3^-$, are shown in Figure 3.4.[66] There are no coordinated H_2O molecules, despite being crystallized from an aqueous solution. All twelve N-H units are engaged in hydrogen bonding to NO_3^- anions. Interestingly, there is enough space at each C_3 face to engage two separate NO_3^- anions simultaneously. The C_3 N-H units display single, double, and triple hydrogen bonding to the NO_3^- anions. The C_2 N-H units all give double hydrogen bonding to two oxygen atoms of the NO_3^- anions.

The crystal structure of the tetrahydrated mixed carbonate/iodide salt, Λ-*lel*$_2$*ob*-$[Co(en)_3]_3^{+}$ CO_3^{2-} $I^-\cdot 4H_2O$, is shown in Figure 3.5.[67] Two ethylenediamine chelates adopt the *lel* conformation and one adopts the *ob* conformation. Each Werner trication hydrogen bonds to a total of three CO_3^{2-} dianions, two I^- anions, and three H_2O molecules. At both C_3 faces, two C_3 N-H units bind to separate oxygen atoms of a CO_3^{2-} dianion. The third C_3 N-H unit on each face binds to H_2O. There is also hydrogen bonding between this H_2O molecule and the CO_3^{2-} dianion. One CO_3^{2-} dianion also binds at a C_2 face. In order to engage both C_2 N-H units simultaneously, the dianion must rotate 44.6° from the horizontal CoN_4 plane (Figure 3.5, right).

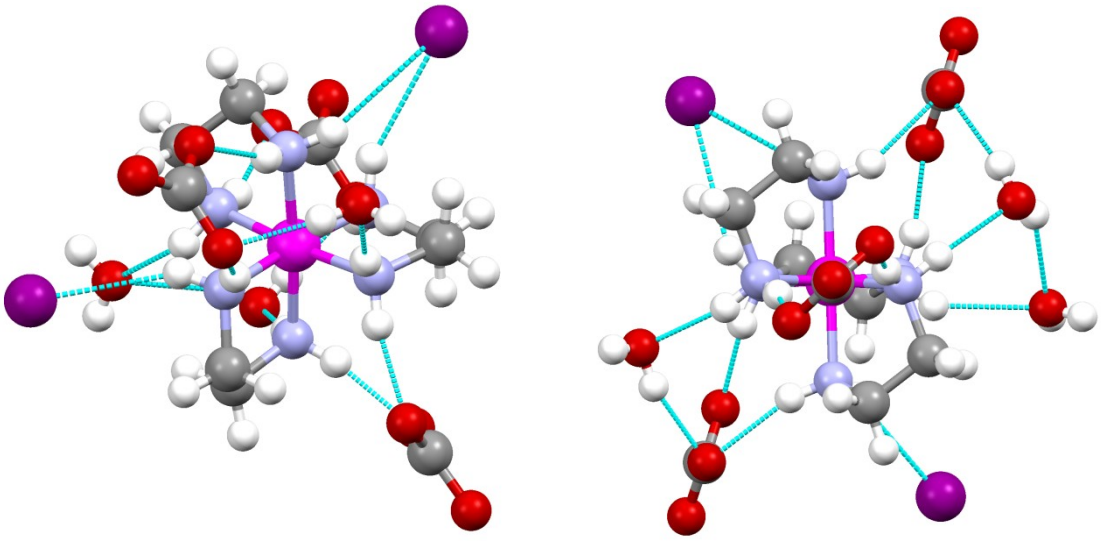

Λ-*lel*$_2$*ob*-[Co(en)$_3$]$^{3+}$ CO_3^{2-} I^-·4H_2O		
H-bond acceptor (X)	Type of H-Bond	Total number of similar interactions
CO_3^{2-}	[C_2,C_2][2]	1
CO_3^{2-}	[C_3,C_3][2]	2
I^-	[C_2,C_2][1]	1
I^-	[C_2][1]	1
H_2O	[C_3][1]	2
H_2O	[C_2][1]	1

Figure 3.5. Hydrogen bonding interactions in the crystal structure of Λ-*lel*$_2$*ob*-[Co(en)$_3$]$_3^+$ CO_3^{2-} I^-·4H_2O viewed from a C_3 axis (left) and a C_2 axis (right).

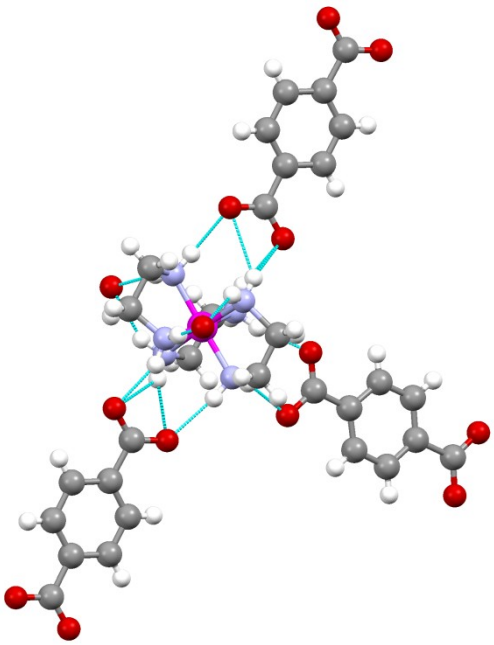

$2\{\Lambda\text{-}lel_3\text{-}[Co(en)_3]^{3+}\}\ 3(terephthalate)^{2-}\cdot 10H_2O$		
H-bond acceptor (X)	Type of H-Bond	Total number of similar interactions
$Ar\text{-}CO_2^{2-}$	$[C_3^2,C_3,C_3][2]$	2
$Ar\text{-}CO_2^{2-}$	$[C_2,C_2][2]$	1
H_2O	$[C_2][1]$	2

Figure 3.6. Hydrogen bond interactions in the crystal structure of $2\{\Lambda\text{-}lel_3\text{-}[Co(en)_3]^{3+}\}$ $3(terephthalate)^{2-}\cdot 10H_2O$ viewed from a C_2 axis. Only one trication is shown. Hydrogen atoms of H_2O are not shown.

The crystal structure and hydrogen bonding interactions of the decahydrated bis(cobalt) tris(terephthalate) salt, $2\{\Lambda\text{-}lel_3\text{-}[Co(en)_3]^{3+}\}$ $3(terephthalate)^{2-}\cdot 10H_2O$, are shown in Figure 3.6.[68] The terephthalate dianion is a *para*-disubstituted benzene featuring two carboxylate groups. Each Werner trication forms hydrogen bonds with

three terephthalate dianions and two H_2O molecules. The terephthalate carboxylate groups achieve triple hydrogen bonding at the two C_3 faces and double hydrogen bonding at one C_2 face.

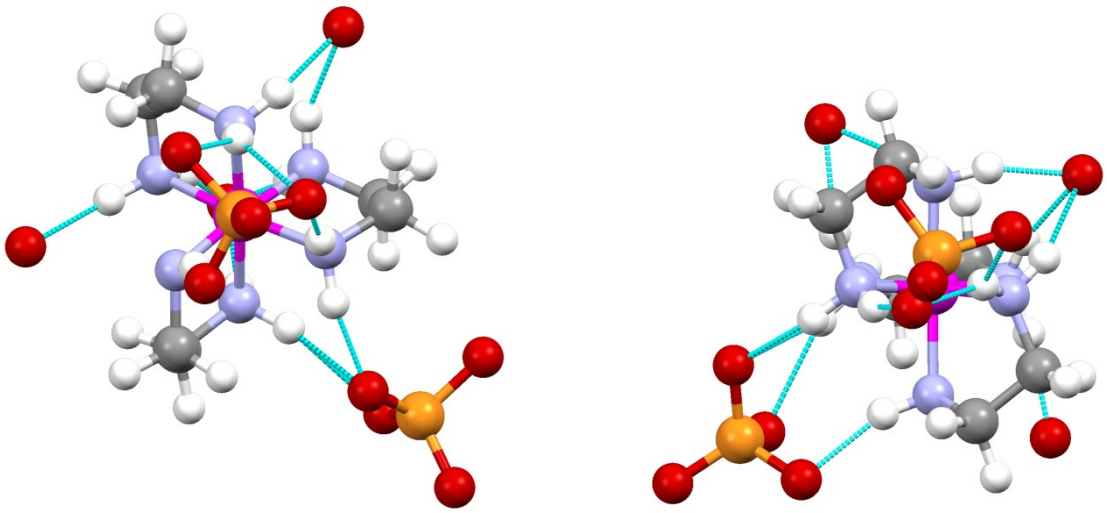

$2\{lel_3\text{-}[Co(en)_3]^{3+}\}\ 3HPO_4^{2-}\cdot 9H_2O$		
H-bond acceptor (X)	Type of H-Bond	Total number of similar interactions
HPO_4^{2-}	$[C_3,C_3,C_3][3]$	1
HPO_4^{2-}	$[C_2,C_2][2]$	1
H_2O	$[C_3,C_3,C_3][1]$	1
H_2O	$[C_2,C_2][1]$	2

Figure 3.7. Hydrogen bonding interactions in the crystal structure of racemic $2\{lel_3\text{-}[Co(en)_3]^{3+}\}$ $3HPO_4^{2-}\cdot 10H_2O$ viewed from a C_3 axis (left) and a C_2 axis (right). Only the Λ enantiomer is shown. Hydrogen atoms of H_2O and HPO_4^{2-} are not shown.

The structure of the decahydrated bis(cobalt) tris(hydrogen phosphate) salt, $2\{lel_3\text{-}[Co(en)_3]^{3+}\}\ 3HPO_4^{2-}\cdot 10H_2O$, which is derived from a racemic crystal, is shown in Figure 3.7.[69] Only those associated with the Λ enantiomer are given here. All twelve N-H units are engaged in hydrogen bonding. One HPO_4^{2-} dianion is positioned over the C_3 face. Three oxygen atoms are simultaneously engaged by the three C_3 N-H units. The position of the HPO_4^{2-} dianion is rotated counter-clockwise with respect to the orientation of the C_3 N-H units. A different HPO_4^{2-} dianion binds at a C_2 face where both C_2 N-H units engage two oxygen atoms. All other hydrogen bonding sites are occupied by H_2O molecules.

The hydrogen bonding interactions of the thiocyanate salt, $lel_3\text{-}[Co(en)_3]^{3+}\ 3NCS^-$, which is derived from a racemic crystal, are shown in Figure 3.8.[70] Only those associated with the Δ enantiomer are given here. All twelve N-H units are engaged in hydrogen bonding to NCS^- anions. Although the crystals were grown from an aqueous solution, there were no H_2O molecules in the crystal lattice. Several kinds of hydrogen bonding interactions are seen with the NCS^- anion. At one C_3 face, a single NCS^- anion is engaged by three C_3 N-H units at the nitrogen atom. On the opposite C_3 face, all three C_3 N-H units engage three different NCS^- anions at the sulfur atoms. Two of the C_2 faces feature double hydrogen bonding at the nitrogen atom of the NCS^- anion, while the third C_2 face displays a double hydrogen bond at a sulfur atom.

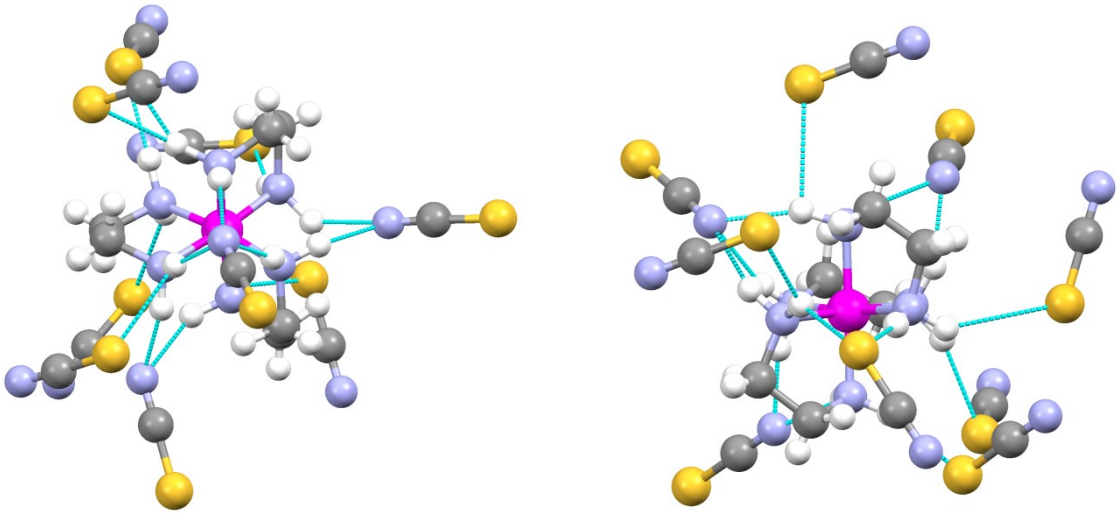

lel$_3$-[Co(en)$_3$]$^{3+}$ 3NCS$^-$		
H-bond acceptor (X)	Type of H-Bond	Total number of similar interactions
NCS$^-$	[C$_3$,C$_3$,C$_3$][1N]	1
NCS$^-$	[C$_3$][1S]	4
NCS$^-$	[C$_2$,C$_2$][1N]	2
NCS$^-$	[C$_2$,C$_2$][1S]	1
NCS$^-$	[C$_2$][1S]	1

Figure 3.8. Hydrogen bonding interactions in the crystal structure of racemic *lel*$_3$-[Co(en)$_3$]$^{3+}$ 3NCS$^-$ viewed from a C$_3$ axis (left) and a C$_2$ axis (right). Only the Δ enantiomer is shown.

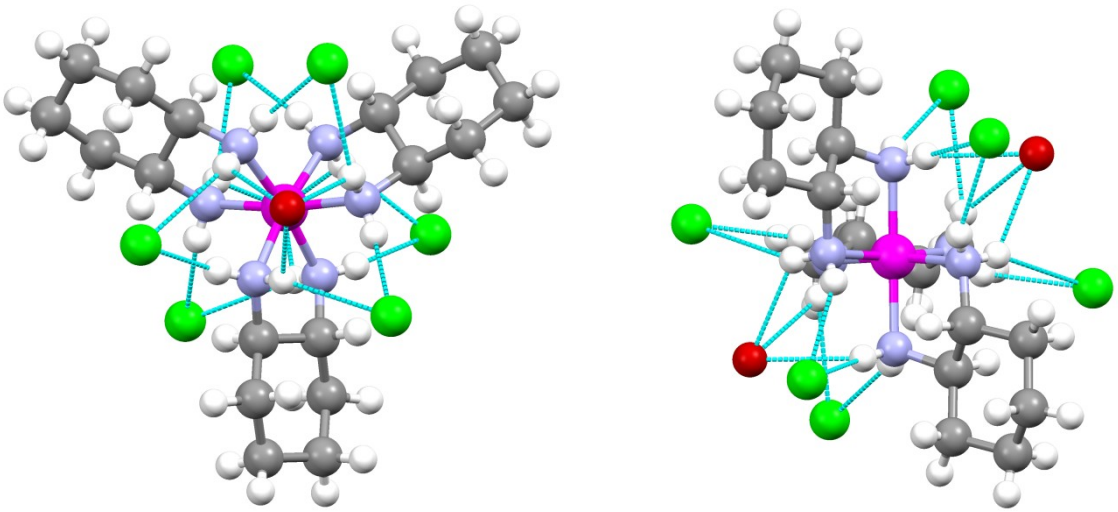

Λ-*ob*$_3$-[Co((*R*,*R*)-chxn)$_3$]$^{3+}$ 3Cl$^-$·5H$_2$O		
H-bond acceptor (X)	Type of H-Bond	Total number of similar interactions
Cl$^-$	[C$_2$,C$_3$][1]	6
H$_2$O	[C$_3$,C$_3$,C$_3$][1]	2

Figure 3.9. Hydrogen bonding interactions in the crystal structure of Λ-*ob*$_3$-[Co((*R*,*R*)-chxn)$_3$]$^{3+}$ 3Cl$^-$ ·5H$_2$O viewed from a C$_3$ axis (left) and a C$_2$ axis (right). The hydrogen atoms of H$_2$O are not shown.

The hydrogen bonding interactions of the pentahydrated trichloride salt, Λ-*ob*$_3$-[Co((*R*,*R*)-chxn)$_3$]$^{3+}$ 3Cl$^-$·5H$_2$O, are shown in Figure 3.9.[59] The diamine chelates are arranged in the *ob*$_3$ conformation, which intrinsically makes the trication a poorer hydrogen bond donor (Section 3.2). Each Werner trication forms hydrogen bonds with a total of six Cl$^-$ anions and two H$_2$O molecules. Each Cl$^-$ anion forms a double hydrogen bond between a C$_3$ N-H unit and a C$_2$ N-H unit of different diamine ligands. Both H$_2$O molecules are held by a triple hydrogen bond at the C$_3$ faces. This hydrogen bonding arrangement is notably different from that observed in the crystal structure of Λ-*lel*$_3$-

$[Co(en)_3]^{3+}$ $3Cl^{-}\cdot H_2O$ (Figure 3.3), in which the Cl^{-} anions were engaged in double hydrogen bonding with only C_3 N-H units or only C_2 N-H units.

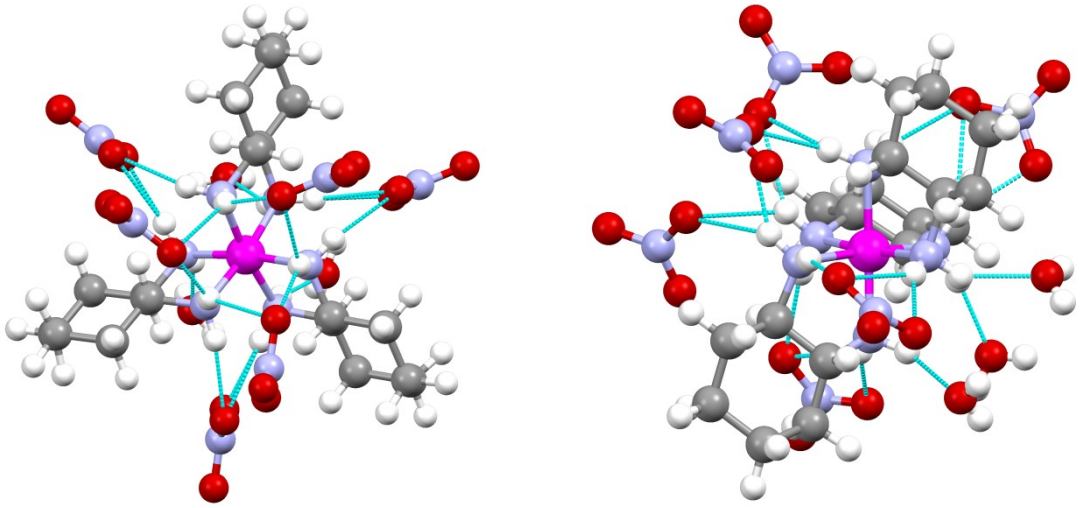

Λ-*lel*$_3$-$[Co((R,R)\text{-chxn})_3]^{3+}$ $3NO_3^{-}\cdot 3H_2O$		
H-bond acceptor (X)	Type of H-Bond	Total number of similar interactions
NO_3^{-}	$[C_3,C_3][1]$	3
NO_3^{-}	$[C_2^2,C_2][2]$	3
H_2O	$[C_3][1]$	3

Figure 3.10. Hydrogen bonding interactions in the crystal structure of Δ-*lel*$_3$-$[Co((R,R)\text{-chxn})_3]^{3+}$ $3NO_3^{-}\cdot 3H_2O$ viewed from the C_3 axis (left) and orthogonal to the C_3 axis (right).

The hydrogen bonding interactions of the trihydrated nitrate salt, Δ-*lel*$_3$-$[Co((R,R)\text{-chxn})_3]^{3+}$ $3NO_3^{-}\cdot 3H_2O$, are displayed in Figure 3.10.[58] Each Werner trication donates hydrogen bonds directly to six NO_3^{-} anions and three H_2O molecules. Three NO_3^{-} anions are simultaneously engaged at one C_3 face where a single oxygen

atom of each anion is shared by two C_3 N-H units. Each C_2 face also forms a dual hydrogen bond with a NO_3^- anion at two different oxygen atoms. At the opposite C_3 face, each N-H unit forms a hydrogen bond with a separate H_2O molecule.

3.3.3 Werner complexes with chiral anions

For many decades after Werner's original resolution, fractional crystallization of diastereomeric salts with chiral anions was the only method to separate the enantiomers of $[Co(1,2\text{-diamine})_3]^{3+}$ trications. In 1970, Yoshikawa and Yamasaki reported the complete resolution of Λ and Δ-$[Co(en)_3]^{3+}$ trications by cation exchange chromatography on a SP-Sephadex resin with aqueous Na_2((*R*,*R*)-tartrate) as the eluent.[71] In solution, the Λ enantiomer has a higher association constant with the (*R*,*R*)-tartrate dianion and is thus eluted more rapidly from the cation exchange column. The enantiomeric trications Δ-*lel*$_3$-$[Co((R,R)\text{-chxn})_3]^{3+}$ and Λ-*lel*$_3$-$[Co((S,S)\text{-chxn})_3]^{3+}$ were similarly resolved and were more efficiently discriminated with the (*R*,*R*)-tartrate dianion than the corresponding $[Co(en)_3]^{3+}$ enantiomers.[72]

Crystal structures of the mixed (*R*,*R*)-tartrate/chloride salts of Λ-*lel*$_3$-$[Co((S,S)\text{-chxn})_3]^{3+}$, the enantiomer Δ-*lel*$_3$-$[Co((R,R)\text{-chxn})_3]^{3+}$, and the diastereomer Λ-*ob*$_3$-$[Co((R,R)\text{-chxn})_3]^{3+}$ were analyzed by Miyoshi.[63,72] The association between the chiral dianion and the chiral trications are shown in Figure 3.11. Remarkably, the binding motifs are very similar for each ion pair. In each case, the (*R*,*R*)-tartrate dianion is positioned nicely across the triangular C_3 face of the cobalt trication. The C_3 N-H units form hydrogen bonds with the oxygen of one carboxylate group and both alcohol oxygen atoms. A distal carboxylate group does not form hydrogen bonds with the cobalt trication. Although the same three oxygen atoms of the (*R*,*R*)-tartrate dianion are

engaged in each case, the precise arrangements between hydrogen bond donors and acceptors are unique for each ion pairing.

The association with the (*R*,*R*)-tartrate dianion is estimated to be stronger with the Λ-*lel*$_3$-[Co((*S*,*S*)-chxn)$_3$]$^{3+}$ trication than the Δ-*lel*$_3$-[Co((*R*,*R*)-chxn)$_3$]$^{3+}$ trication.[72] In the latter, the distal carboxylate group of the (*R*,*R*)-tartrate dianion must twist into an unnatural conformation to avoid steric repulsions with the cyclohexane ring of the trication. The diastereomer Λ-*ob*$_3$-[Co((*R*,*R*)-chxn)$_3$]$^{3+}$ is estimated to have the weakest association with the (*R*,*R*)-tartrate dianion, because, as analyzed in Section 3.2, the hydrogen bonds of *ob*$_3$ trications are generally more bent and inevitably weaker.[72]

3.4 Conclusion

In summary, Werner complexes are capable of forming diverse hydrogen bonding interactions with a wide variety of counteranions and solvent molecules. These have for the first time been systematized. Perhaps the most interesting feature is the ability to form double and triple hydrogen bonding networks with Lewis basic functional groups. Both C_2 and C_3 N-H units appear equally capable of participating in hydrogen bonding. Enantiopure counteranions display different hydrogen bonding interactions with different stereoisomers of chiral Werner trications.

In consideration of their innate hydrogen bonding and chiral discrimination capabilities, Werner complexes were perceived as potential hydrogen bond mediating catalysts for enantioselective organic transformations. This theme is developed in the following chapter.

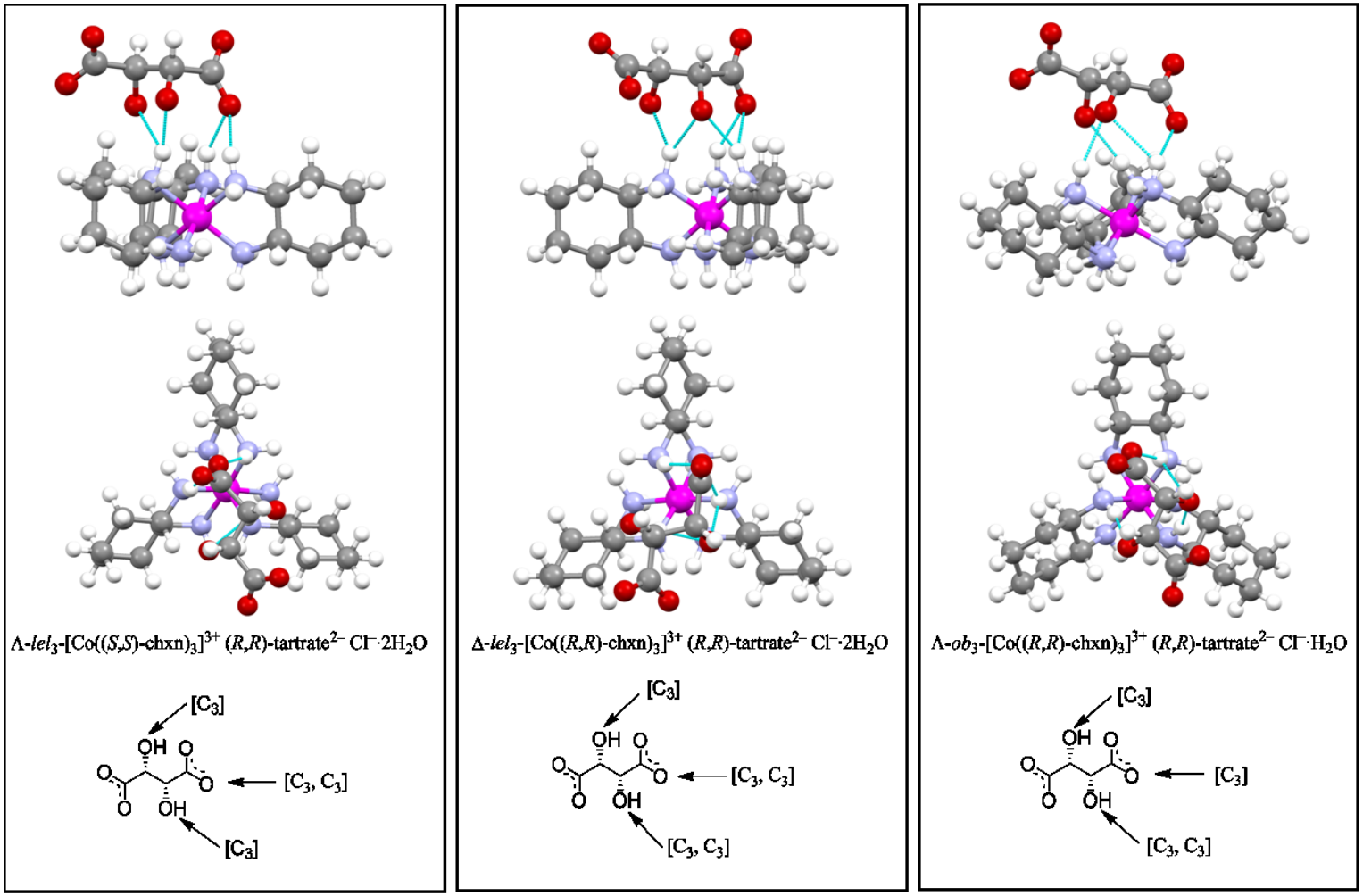

Figure 3.11. Hydrogen bonding interactions in the crystal structures of the mixed (*R*,*R*)-tartrate/chloride salt of $[Co(trans\text{-chxn})_3]^{3+}$ trications viewed orthogonal to the C_3 axis (top row) and from the C_3 axis (middle row). Chloride anions, water, and the alcohol hydrogen atoms are removed for clarity.

CHAPTER IV

WERNER COMPLEXES IN HYDROGEN BOND MEDIATED CATALYSIS

4.1 Introduction

4.1.1 An overlooked chiral hydrogen bond donor for asymmetric catalysis

Werner complexes of the type $[Co(en)_3]^{3+}$ $3X^-$, and related substituted species, possess a wealth of stereochemical possibilities. They are also extremely inexpensive and simple to prepare. In fact, the synthesis and resolution of the enantiomers of $[Co(en)_3]^{3+}$ $3Cl^-$ is a common experiment in undergraduate laboratory courses.[73] However, despite being inexpensive and readily available in enantiopure form, there have been no applications of Werner complexes in asymmetric organic synthesis. Two main reasons have impeded development. First, almost all transition metal containing catalysts involve direct activation of the substrate by the metal. Trications of the type $[Co(1,2\text{-diamine})_3]^{3+}$ are coordinatively saturated and kinetically non-labile (Section 2.2.1), rendering direct metal-substrate activation impossible. Thus, the outstanding structural integrity that has established Werner complexes as focal points of analytical study has rendered them ineffectual in traditional catalysis. Secondly, the solubility of Werner complexes has historically been limited to water. Although many organic reactions can be performed in water, it is not universally applicable for organic synthesis.

Given the recent success of small organic molecules in asymmetric hydrogen bond mediated catalysis (Chapter 1) and the innate ability for Werner complexes to form hydrogen bonds (Chapter 3), Werner-type complexes were envisioned as a new type of

chiral catalyst. The abundant N-H units would activate organic substrates *via* hydrogen bonding while the central cobalt metal serves only as a chiral, structural motif. In this mode, the previously undesired high barrier to ligand dissociation becomes an advantage, since the hydrogen bond donors would be positioned in a relatively fixed, chiral environment.

4.1.1.1 The first generation Werner complex catalyst

The $[Co(en)_3]^{3+}$ trication is typically paired with small, polar anions such as $Cl^–$, $I^–$, and $NO_3^–$ and these ionic compounds are only soluble in H_2O. Although organic synthesis can be performed in water, it was believed that hydrogen bond mediated catalysis would be most successful in aprotic solvents that are not themselves hydrogen bond donors. Previously, Wang and Kutal demonstrated that the solubility of the racemic $[Co(en)_3]^{3+}$ $3BPh_4^–$ salt, which contained lipophilic anions, could be extended to the polar organic solvent acetone.[74] Later work in the Gladysz group revealed that the incorporation of the increasingly lipophilic tetrakis[3,5-bis(trifluoromethyl)phenyl]borate ($BAr_f^–$) anion further extended the solubility of the $[Co(en)_3]^{3+}$ trication into CH_2Cl_2.[75] In the preparation of this salt, which is depicted in Scheme 4.1, a bright orange, aqueous solution of enantiopure Δ-$[Co(en)_3]^{3+}$ $3I^–·H_2O$ (Δ-$\mathbf{1}^{3+}$ $3I^–$)[76] is stirred over a nearly colorless solution of Na^+ $BAr_f^–$ in CH_2Cl_2. Within ten minutes, the orange color was transferred to the lower organic phase, and Δ-$[Co(en)_3]^{3+}$ $3BAr_f^–·14H_2O$ (Δ-$\mathbf{1}^{3+}$ $3BAr_f^–$) was isolated after removal of the aqueous layer and evaporation of the organic solvent at standard temperature and pressure. Attempts to reduce the water content by drying over chemical desiccants or under oil pump vacuum at 50 °C resulted in various levels of decomposition. The apparent importance of a

second coordination sphere of water molecules provides evidence that intermolecular hydrogen bonding interactions help to stabilize Werner complexes.

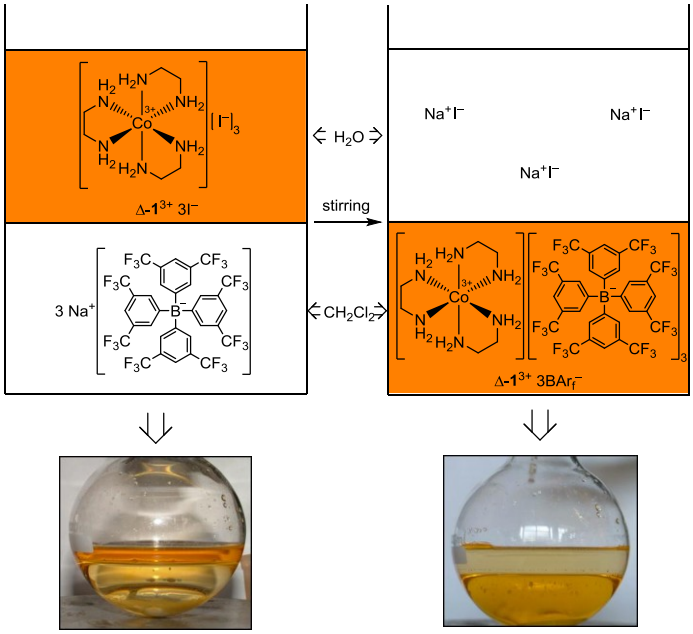

Scheme 4.1. Anion exchange between Δ-$\mathbf{1}^{3+}$ $3I^-$ and Na^+ BAr_f^-

This biphasic anion exchange method proved to be generally applicable for $[Co(1,2\text{-diamine})_3]^{3+}$ trications as the CH_2Cl_2-soluble complexes $[Co(\textit{trans}\text{-chxn})_3]^{3+}$ $3BAr_f^-\cdot 9H_2O$ and $[Co((R,R)\text{-chxn})_3]^{3+}$ $3BAr_f^-\cdot 10H_2O$ were similarly prepared.[75] More recently, incorporation of a highly fluorous version of the BAr_f^- anion has extended the solubility of the $[Co(en)_3]^{3+}$ trication to highly non-polar fluorous solvents.[77]

The enantiopure Δ-$\mathbf{1}^{3+}$ $3BAr_f^-$ complex was applied as a catalyst for a number of organic transformations. The highest enantioselectivity was achieved in the catalytic Michael addition of dimethyl malonate to 2-cyclopenten-1-one (Scheme 4.2).[75] Without a catalyst, there is no measureable product conversion in up to 24 hours at room temperature. In the presence of 9 mol% Δ-$\mathbf{1}^{3+}$ $3BAr_f^-$ and a stoichiometric amount of

Et_3N as base, the product was achieved in 78% yield and 33% ee. Though the reaction was clearly accelerated in the presence of the Werner catalyst, the enantioselectivity was modest at best.

Other reactions gave similar rate accelerations, yet low enantioselectivities and are described in the discussion section of this chapter.

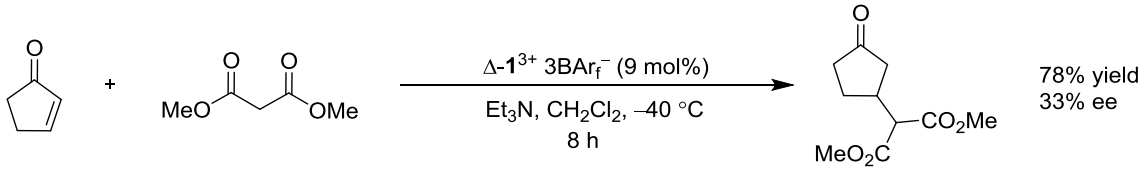

Scheme 4.2. Reaction screening with first generation Werner catalyst.

Although this first generation Werner catalyst showed promise in terms of the ability to accelerate reactions, the resulting enantioselectivities were far from competitive as compared with the best known chiral hydrogen bond mediating catalysts. The Gladysz group has pursued two main strategies to improve the enantioselectivities of Werner-type catalysts. The first involves increasing the steric parameters of the $[Co(en)_3]^{3+}$ core and is the subject of this chapter. The second focuses on the development of bifunctional Werner complexes with pendant Lewis basic ligands and is discussed elsewhere.[78]

4.1.2 Sterically enhanced Werner catalysts

The source of chirality in the Δ-**1**$^{3+}$ 3BAr_f^- catalyst is the central metal atom, which may be too distant from the newly formed product stereocenter to influence the stereochemical outcome of the catalyzed reaction. The small ethylenediamine ligands do

little to extend the chiral information established by the metal configuration into the reaction space. It was conceived that by replacing the compact ethylenediamine ligands with more extended diphenyl ethylenediamine (dpen) ligands, the chiral influence of the metal configuration would encompass a larger radial environment. In addition, the carbon stereocenters of the *trans*-dpen ligands could amplify the metal-centered chirality and thereby enhance the stereoselectivity of the catalyst.

The four possible isomers of Werner complexes with enantiopure *trans*-dpen ligands and their stereochemical relationships are shown in Figure 4.1. The overall stereochemistries of the complexes are established by the combination of the metal configuration and the chirality of the chelating *trans*-dpen ligands. Two isomers that possess opposite metal configurations but contain ligands of the same chiral orientation are diastereomers. Similarly, two isomers that possess the same metal configuration but contain ligands of opposite chiral orientation are diastereomers. Two isomers are enantiomers if both the metal configuration and ligand chirality are opposite in orientation. The stereochemical details of the four isomers, with an emphasis on the diamine chelate conformations, were also discussed in Section 2.4.3.

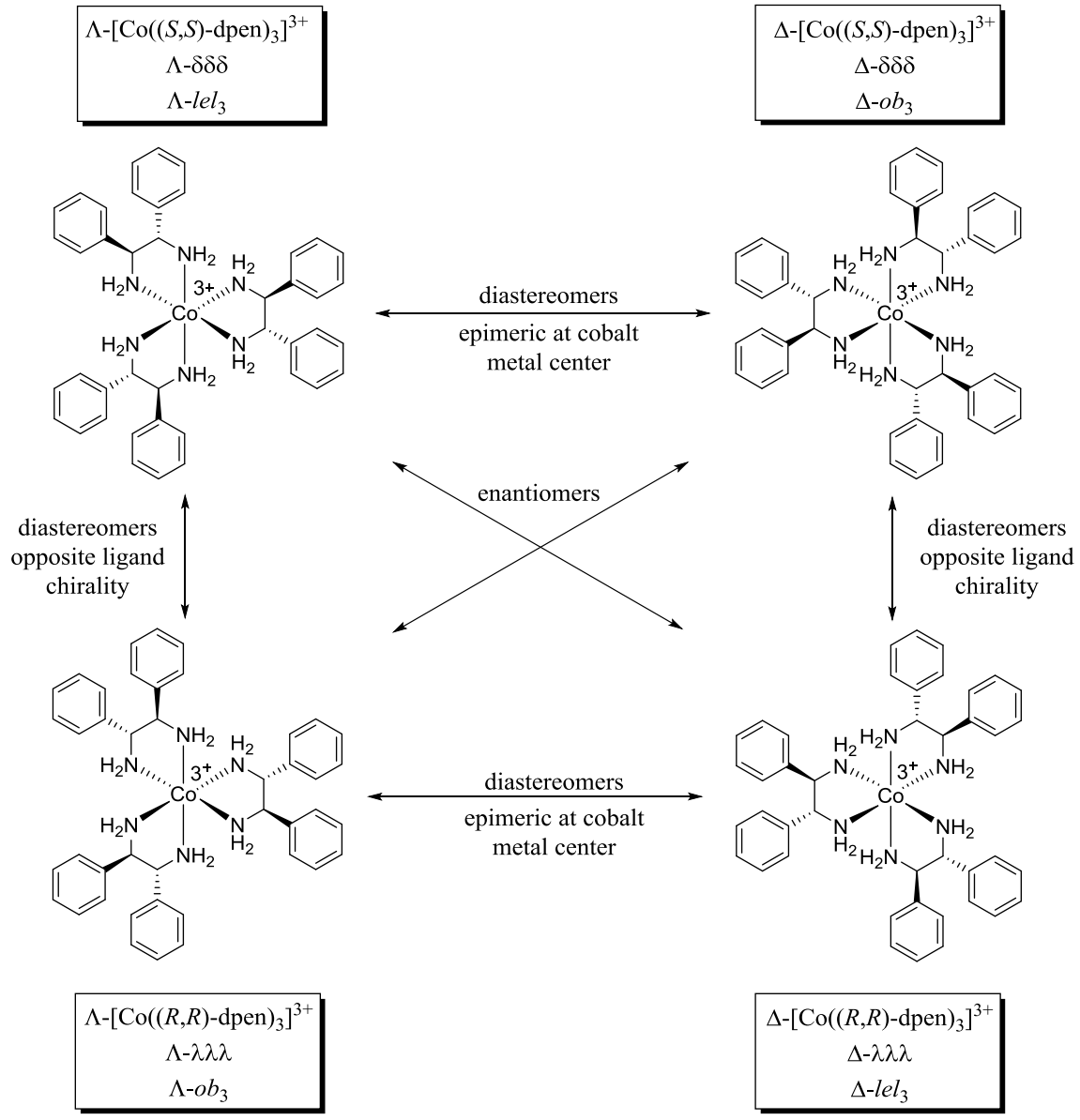

Figure 4.1. The four isomers of $[Co(\textit{trans}\text{-dpen})_3]^{3+}$ trications.

4.1.2.1 Previously reported synthesis of Co(III) complexes with dpen ligands

There are only a small number of reports concerning $[Co(dpen)_3]^{3+}$ trications. Much of the early work in preparing Co(III) metal complexes with dpen ligands was

aimed at determining the absolute configurations of the (+) and (–)-enantiomers of the chiral diamine. By comparing the optical rotary dispersion (ORD) and circular dichroism (CD) spectra of metal complexes with (–)-dpen against complexes containing chiral diamine ligands of known configuration, the absolute configuration of (–)-dpen could be deduced. The rationale is that similarly constructed ligands of the same configuration, when formed into related metal complexes, should generate CD/ORD traces of the same sign.[79] In actuality, the handful of publications in this area give conflicting conclusions about the absolute stereochemistry of the dpen ligands and metal configuration of $[Co(\textit{trans}\text{-dpen})_3]^{3+}$ trications. A brief history of the synthesis and stereochemical assignments of $[Co(\textit{trans}\text{-dpen})_3]^{3+}$ trications is outlined in Table 4.1. Because the metal configuration (Λ vs. Δ) and the ligand chirality ((*R*,*R*) vs. (*S*,*S*)) were initially unknown, the complexes are described here only by their experimentally observed optical rotations.

Table 4.1. Chronology of the stereochemical assignments of (–)-dpen ((*S*,*S*) vs. (*R*,*R*)) and (+)-$[Co\{(–)\text{-dpen}\}_3]^{3+}$ trications (Λ vs. Δ). Shading is for currently accepted stereochemistry.

	stereochemical assignment		
	(–)-dpen	(+)-$[Co\{(–)\text{-dpen}\}_3]^{3+}$	method
Gillard, 1965	(*S*,*S*)-dpen	not assigned	ORD
Mason, 1971	(*R*,*R*)-dpen	Λ-$[Co((R,R)\text{-dpen})_3]^{3+}$	CD
Bosnich, 1972	(*R*,*R*)-dpen	Λ-$[Co((R,R)\text{-dpen})_3]^{3+}$	CD
Mason, 1977	(*S*,*S*)-dpen	Λ-$[Co((S,S)\text{-dpen})_3]^{3+}$	X-ray

Lifschiltz[80] and Gillard[81] first prepared (+)-$[Co((–)\text{-dpen})_3]^{3+}$ $3Cl^–$ by combining the cobalt (II) precursor $CoCl_2$ and (–)-dpen in ethanol with concomitant air

oxidation to form the Co(III) salt. The ORD spectrum of the product gave a positive Cotton effect at 520 nm. Gillard made no attempt to predict whether the (+)-isomer possessed the Λ or Δ metal configuration, but it was assumed that the more stable isomer was obtained exclusively. Gillard concluded that the (–)-dpen ligand possessed the (*S*,*S*) configuration because the ORD curves of (+)-$[Co((–)\text{-dpen})_3]^{3+}$ $3Cl^–$ and (–)-$[Co(R\text{-}(+)\text{-pn})_3]^{3+}$ $3Cl^–$ (*R*-(+)-pn = *R*-propylenediamine) were opposite in sign and therefore possessed ligands of opposite chirality.

Bosnich was the first to characterize both configurational diastereomers of the $[Co((–)\text{-dpen})_3]^{3+}$ trications, which were isolated as the $ClO_4^–$ salts.[52a] The CD spectra of the two complexes were opposite in sign and the isomers were labeled (+)-$[Co((–)\text{-dpen})_3]^{3+}$ $3ClO_4^–$ and (–)-$[Co((–)\text{-dpen})_3]^{3+}$ $3ClO_4^–$. The synthesis route applied by Bosnich is shown in Scheme 4.3. Three equivalents of (–)-dpen were combined with the Co(II) salt $Co(OAc)_2{\cdot}4H_2O$ in methanol while ambient air oxidizes the metal to Co(III). The reaction mixture was acidified with HCl, and a crude mixture of $[Co((–)\text{-dpen})_3]^{3+}$ $3Cl^–$ salts was obtained. Washing the mixture with H_2O and hot acetone left "nearly pure" (+)-$[Co((–)\text{-dpen})_3]^{3+}$ $3Cl^–$, which was further purified by recrystallization from methanol after conversion to the $ClO_4^–$ salt. By this method, the complex was isolated as the pure hydrate, (+)-$[Co((–)\text{-dpen})_3]^{3+}$ $3ClO_4^–{\cdot}4H_2O$, in 18% overall yield. The original water and acetone washings were treated with Na^+ $ClO_4^–$, and pure (–)-$[Co((–)\text{-dpen})_3]^{3+}$ $3ClO_4^–$ was isolated in 10% overall yield after multiple recrystallizations. The authors then claim that workup of the combined reaction filtrates with excess Na^+ $ClO_4^–$ produced an additional 17% of (+)-$[Co((–)\text{-dpen})_3]^{3+}$ $3ClO_4^–{\cdot}4H_2O$ in 96% purity. Thus, in this preparation, the (+)-isomer was formed in significantly higher proportions than the (–)-isomer. The predominant (+)-isomer corresponds with the isomer obtained in the synthesis with $CoCl_2$, which Gillard assumed to be the sole, preferred isomer.

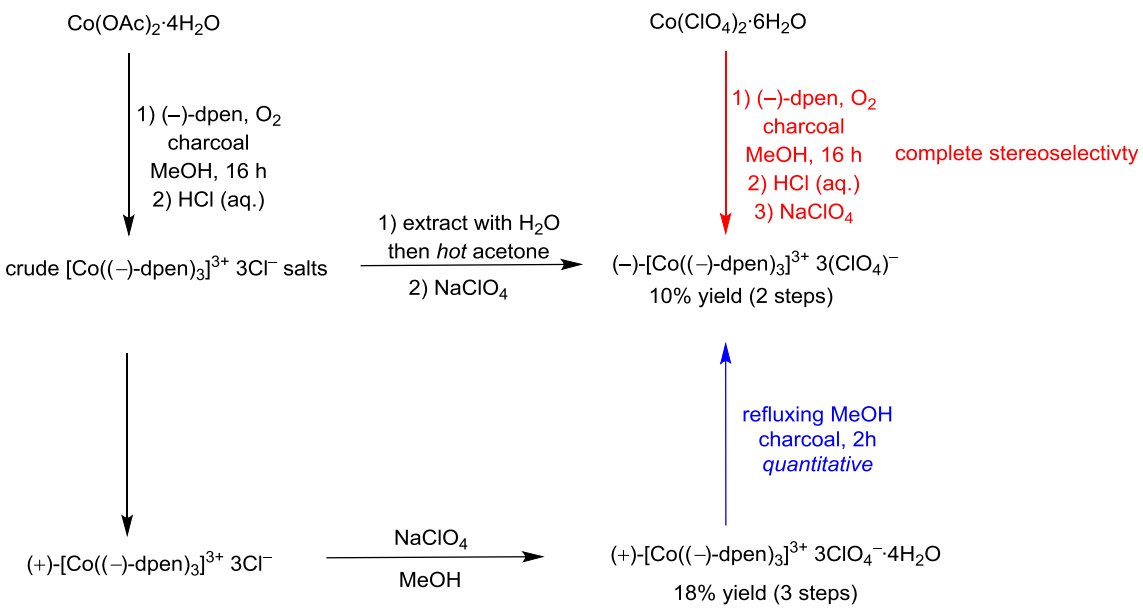

Scheme 4.3. The Bosnich synthesis of (+) and (–)-$[Co((–)\text{-dpen})_3]^{3+}$ $3ClO_4^-$.

It was previously shown that optically active $[Co(en)_3]^{3+}$ trications undergo racemization when heated in the presence of charcoal.[45,51] In equilibrium studies, it was discovered that (+)-$[Co((–)\text{-dpen})_3]^{3+}$ $3ClO_4^-$ completely isomerized to (–)-$[Co((–)\text{-dpen})_3]^{3+}$ $3ClO_4^-$ when boiled in methanol in the presence of activated charcoal (Scheme 4.3, highlighted in blue). However, when (–)-$[Co((–)\text{-dpen})_3]^{3+}$ $3ClO_4^-$ was treated under the same conditions, no detectable amount of the (+)-isomer had developed. This demonstrated that, although (+)-$[Co((–)\text{-dpen})_3]^{3+}$ $3ClO_4^-$ is isolated in greater amounts, (–)-$[Co((–)\text{-dpen})_3]^{3+}$ $3ClO_4^-$ is the thermodynamically more stable

isomer. This is opposite to the conclusion reached by Gillard. Bosnich also reported that when $Co(ClO_4)_2{\cdot}6H_2O$ was used to synthesize trication $[Co((–)\text{-dpen})_3]^{3+}$, (–)-$[Co((–)\text{-dpen})_3]^{3+}$ $3ClO_4^-$ was isolated as the sole product (Scheme 4.3, highlighted in red). However, no yield was reported.

Because the CD spectra of (–)-$[Co((–)\text{-dpen})_3]^{3+}$ $3ClO_4^-$ had the same sign as that of Δ-$[Co(en)_3]^{3+}$ $3Cl^-$, which by that time had known metal configuration,[82] Bosnich assigned the (–)-complex to the Δ-configuration. Thus, Δ-(–)-$[Co((–)\text{-dpen})_3]^{3+}$ $3ClO_4^-$ is thermodynamically more stable than Λ-(+)-$[Co((–)\text{-dpen})_3]^{3+}$ $3ClO_4^-$. It was previously reported that both $[Co(en)_3]^{3+}$ and $[Co(\textit{trans}\text{-chxn})_3]^{3+}$ trications in the $\textit{lel}_3$ conformation were more stable than the corresponding trications in the $\textit{ob}_3$ conformation.[46,51] Citing these examples, Bosnich claimed that the (–)-dpen ligands of the more stable Δ complex should also adopt the $\textit{lel}_3$ conformation. As was seen in Figure 2.11, the chelates of a $[Co(\textit{trans}\text{-dpen})_3]^{3+}$ trication with the Δ-$\textit{lel}_3$ configuration must adopt the λ conformation, which is only favored for (*R*,*R*)-dpen. This again conflicts with the earlier report by Gillard, who had determined the configuration of (–)-dpen to be (*S*,*S*).

Mason had just previously come to the same conclusion as Bosnich by independently analyzing the CD spectra of the cations (–)-$[Co((–)\text{-dpen})_3]^{3+}$, (+)-$[Co((–)\text{-dpen})_3]^{3+}$, and *trans*-$[Co((–)\text{-dpen})_2Cl_2]^+$,[83] but soon challenged his own claims when the sign of the simpler CD spectrum of $[Zn((–)\text{-dpen})_2]^{2+}$ was more consistent with an (*S*,*S*) ligand.[84]

Finally, the issue was put to rest when Mason determined the crystal structure and absolute configuration of (+)-$[Co((–)\text{-dpen})_3]^{3+}$ $3NO_3^-{\cdot}H_2O$.[85] The crystal structure is displayed in Figure 4.2. The structure revealed that the (+)-isomer of the complex possesses the Λ configuration around the metal center. Each ligand is oriented in the *lel*

conformation and each chelate adopts the δ conformation. The absolute configuration of the (–)-dpen ligand was determined to be (*S*,*S*).

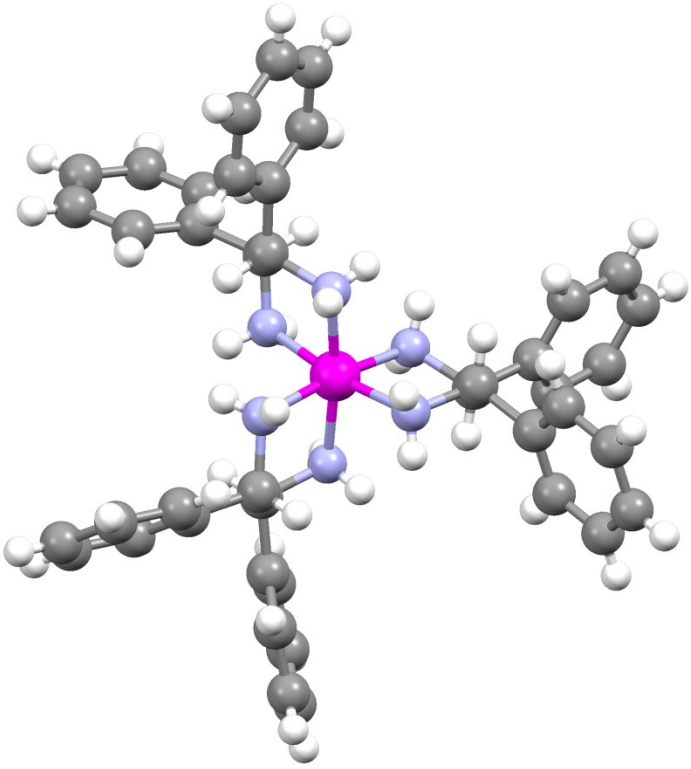

Figure 4.2. The crystal structure of Λ-(+)-$[Co((S,S)\text{-dpen})_3]^{3+}$ $3NO_3^-{\cdot}H_2O$. The anions and solvent are removed for clarity.

Therefore, Bosnich was ultimately correct in predicting that the thermodynamically preferred isomer, (–)-$[Co((-)\text{-dpen})_3]^{3+}$ $3ClO_4^-$ existed in the Δ configuration and that (+)-$[Co((-)\text{-dpen})_3]^{3+}$ $3ClO_4^-$ possessed the Λ configuration, but incorrectly assigned the absolute configuration of (–)-dpen. The error came in assuming that the lel_3 isomer was the most stable conformation for the Δ-$[Co(dpen)_3]^{3+}$ trication. Although this appears to be true for $[Co(en)_3]^{3+}$ and $[Co(trans\text{-chxn})_3]^{3+}$ trications, $[Co(trans\text{-dpen})_3]^{3+}$ trications appear to favor the ob_3 conformations.

A key feature in the synthesis of $[Co(\textit{trans}\text{-dpen})_3]^{3+}$ trications is that the configuration of the metal center is largely influenced by the anions of the starting Co(II) salt. For instance, the synthesis beginning with $CoCl_2$ or $Co(OAc_2)_2$ gave mainly the isomer Λ-(+)-$[Co((–)\text{-dpen})_3]^{3+}$. Under identical conditions, the synthesis beginning with $Co(ClO_4)_2$ led exclusively to the isomer Δ-(–)-$[Co((–)\text{-dpen})_3]^{3+}$.

Fujita was later able to prepare $[Co(\textit{meso}\text{-dpen})_3]^{3+}$ $3Cl^{-}\cdot 6H_2O$, but made no attempt to determine the metal configuration.[52c] Although stable in the solid state, the complex readily decomposed in solution.

4.2 Catalyst synthesis

4.2.1 Synthesis of cobalt complexes with (S,S)-dpen ligands

The Bosnich preparation of $[Co((S,S)\text{-dpen})_3]^{3+}$ $3X^{-}$ salts (Section 4.1.2.1) was slightly modified for the present work as shown in Scheme 4.4. A solution of $Co(OAc)_2\cdot 4H_2O$ and 3.3 equivalents of (*S*,*S*)-dpen ((*S*,*S*)-**2**) in MeOH was stirred at room temperature overnight in the presence of charcoal. Air was continuously circulated through the reaction mixture. The O_2 present in the ambient air was sufficient to oxidize the metal from Co(II) to Co(III) in the presence of the diamine ligands. After 16 hours, the charcoal was removed by filtration and HCl was added. The strong acid presumably neutralized the liberated AcO^{-} anion and exchanges with the anionic oxygen species that is formed during the oxidation event. This left Cl^{-} as the greatly dominant counteranion to the newly formed cobalt complex and workup gave crude $[Co((S,S)\text{-dpen})_3]^{3+}$ $3Cl^{-}$.

The ^{1}H and $^{13}C\{^{1}H\}$ NMR spectra of the crude material revealed a dominant set of signals that presumably represent Λ-$[Co((S,S)\text{-dpen})_3]^{3+}$ $3Cl^{-}$ (Λ-(*S*,*S*)-$\mathbf{3}^{3+}$ $3Cl^{-}$).

Other minor peaks were also observed. In accordance with the Bosnich synthesis, the crude material could be washed with hot acetone to afford essentially pure Λ-(*S*,*S*)-**3**$^{3+}$ 3Cl^{-}. This step was performed only once in a batch preparation, and the nearly pure Λ-(*S*,*S*)-**3**$^{3+}$ 3Cl^{-} was used to develop a crystal structure (Section 4.2.3.1, below) and for NMR experiments (Section 4.2.4.1, below). However, a significant amount of Λ-(*S*,*S*)-**3**$^{3+}$ 3Cl^{-} was also lost in the washing. Therefore, it was decided to bypass this step in favor of a higher yielding purification method that is described below.

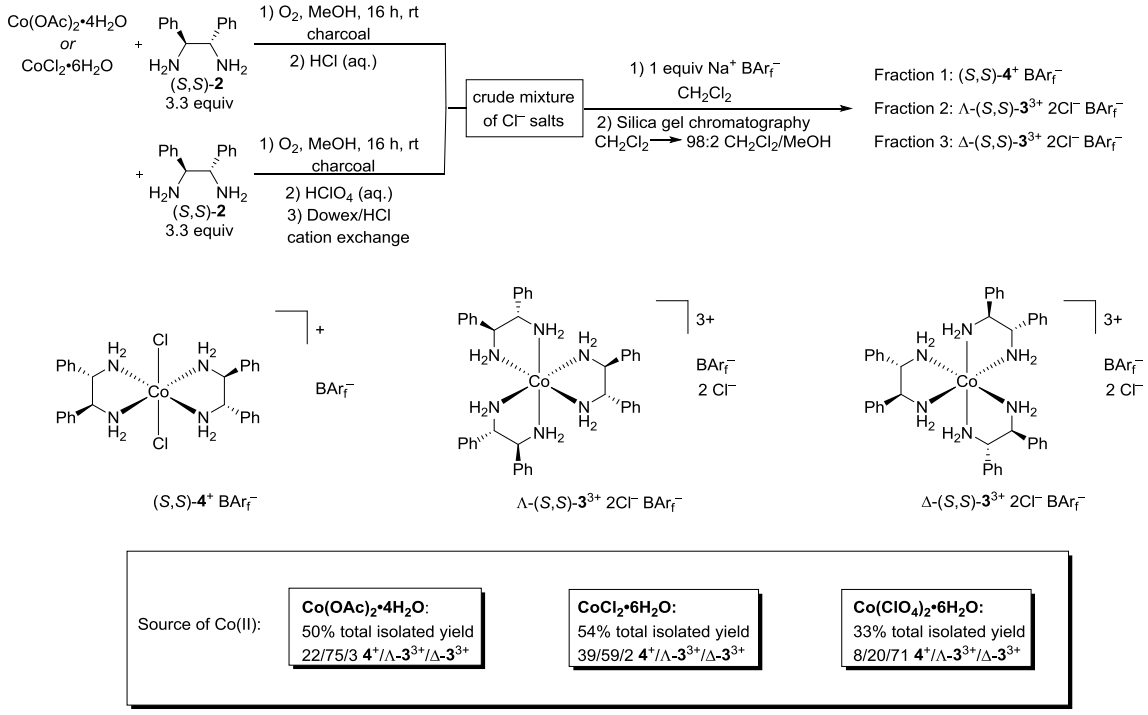

Scheme 4.4. The synthesis of Co(III) complexes containing (*S*,*S*)-dpen ligands.

The [Co((*S*,*S*)-dpen)$_3$]$^{3+}$ 3Cl^{-} salts are soluble in polar organic solvents such as MeOH and DMSO, but insoluble in less polar organic solvents such as CH_2Cl_2. Incorporation of the lipophilic BAr_f^- anion would likely render the complex soluble in

less polar solvents. However, unlike most Werner complexes, the $[Co((S,S)\text{-dpen})_3]^{3+}$ $3Cl^-$ salts are also insoluble in H_2O. Therefore, the biphasic anion metathesis previously employed with Δ-$\mathbf{1}^{3+}$ $3I^-$ (Scheme 4.1) was altered.

In this case, crude Λ-(*S*,*S*)-$\mathbf{3}^{3+}$ $3Cl^-$ was suspended directly in CH_2Cl_2 without an additional aqueous phase. In the first, unoptimized iterations of this anion exchange, three equivalents of Na^+ BAr_f^- were dissolved in the CH_2Cl_2. After sonicating the suspension for a few seconds, the solids dissolved and the colorless CH_2Cl_2 took on a bright orange color. The NaCl that resulted from the anion exchange precipitated and was removed by filtration. Surprisingly, the newly formed CH_2Cl_2-soluble cobalt complexes could be chromatographed on a silica gel column. With CH_2Cl_2 as the mobile phase, a bright green band separated from the absorbed orange band and was eluted from the column. The isolated green solid was *trans*-$[Co((S,S)\text{-dpen})_2Cl_2]^+$ BAr_f^- ((*S*,*S*)-$\mathbf{4}^+$ BAr_f^-). Although the *trans* monocation is not mentioned in the Bosnich preparation, *trans*-$[Co((S,S)\text{-dpen})_2Cl_2]^+$ $Cl^-\cdot H_2O$ was previously synthesized by a similar procedure that used only 2 equivalents of (*S*,*S*)-**2** and was isolated as bright green crystals.[86] The ^1H NMR spectrum of (*S*,*S*)-$\mathbf{4}^+$ BAr_f^- unambiguously showed a 1:2 BAr_f^-/(*S*,*S*)-**2** ligand ratio.

The major orange band was eluted from the silica gel column by introducing 1-2% MeOH to the CH_2Cl_2 eluent. Careful fractionation of the orange band separated the major, fast moving Λ-diastereomer from a minor amount of the slower moving Δ-diastereomer. The stereochemical assignments were determined from the crystal structures of the corresponding trichloride salts and are discussed in Section 4.2.3.

It was anticipated that the major product would be defined by the formula Λ-$[Co((S,S)\text{-dpen})_3]^{3+}$ $3BAr_f^-$ with a 3:1 BAr_f^-/[Co] ratio. However, integration of the ^1H NMR spectrum revealed an unambiguous 1:1 BAr_f^-/[Co] ratio. The elemental analysis

(C, H, N, Cl) also confirmed the presence of two Cl^- anions. From this it was concluded that only one Cl^- anion had been exchanged with BAr_f^- in the anion metathesis. Furthermore, it was clear that only one BAr_f^- anion was required to render the Λ-$[Co((S,S)\text{-dpen})_3]^{3+}$ trication soluble in CH_2Cl_2. Therefore, the anion exchange procedure was optimized to include only one equivalent of Na^+ BAr_f^-. The results of the anion exchange and silica gel chromatography were the same as the original procedure and resulted in three isolated products in overall yields for (S,S)-**4**$^+$ BAr_f^- (11%), Λ-(*S*,*S*)-**3**$^{3+}$ $2Cl^-$ BAr_f^- (37%), and Δ-(*S*,*S*)-**3**$^{3+}$ $2Cl^-$ BAr_f^- (1%).

Because only one of three Cl^- anions is exchanged with BAr_f^- in this procedure, the major product is isolated with a mixed set of anions. The 2:1 Cl^-/BAr_f^- anion ratio was reproduced in several batch syntheses. According to the elemental analysis, the compound is also isolated with two coordinated water molecules, despite being dried under oil pump vacuum at room temperature overnight. A water peak was also detected in the ^1H NMR spectrum. More aggressive drying procedures were not pursued as these had previously led to decomposition in the case of Δ-**1**$^{3+}$ $3BAr_f^-$. Therefore, the formula of the isolated complex is best represented as the dihydrate Λ-(*S*,*S*)-**3**$^{3+}$ $2Cl^-$ BAr_f^- $\cdot 2H_2O$.[76]

The same synthetic procedure was repeated, except that $CoCl_2\cdot 6H_2O$ was utilized as the starting Co(II) source rather than $Co(OAc)_2\cdot 4H_2O$. In this case, the three Co(III) products (*S*,*S*)-**4**$^+$ BAr_f^-, Λ-(*S*,*S*)-**3**$^{3+}$ $2Cl^-$ BAr_f^-, and Δ-(*S*,*S*)-**3**$^{3+}$ $2Cl^-$ BAr_f^- were isolated after column chromatography in overall yields of 21%, 32%, and 1%, respectively.

In both procedures, the isolated, tris-chelating $[Co((S,S)\text{-dpen})_3]^{3+}$ $2Cl^-$ BAr_f^- complexes were found to primarily exist in the Λ configuration with the Δ-diastereomer being isolated in very small amounts. According to the Bosnich preparation, however,

the Δ-diastereomer of $[Co((S,S)\text{-dpen})_3]^{3+}$ $3ClO_4^-$ was exclusively isolated when $Co(ClO_4)_2 \cdot 6H_2O$ was utilized as the source of Co(II). Therefore, the synthesis was performed beginning with $Co(ClO_4)_2 \cdot 6H_2O$, as shown in Scheme 4.4. After stirring over charcoal overnight with air oxidation, the reaction mixture was quenched with aqueous $HClO_4$ rather than aqueous HCl. The $^{13}C\{^1H\}$ NMR spectrum of the isolated salt Δ-(*S*,*S*)-**3**$^{3+}$ $3ClO_4^-$ reveals only a single isomer (Figure 4.12b).

Before conducting the BAr_f^- anion exchange with the Δ diastereomer, the Δ-(*S*,*S*)-**3**$^{3+}$ $3ClO_4^-$ complex was first converted to the trichloride salt on a Dowex cation exchange resin. First, the perchlorate salt was adsorbed on the Dowex resin, which was washed with H_2O/MeOH to remove the anion ClO_4^-. The cobalt complex was converted to the trichloride salt and released from the ion exchange resin with 4.0 M aqueous HCl in H_2O/MeOH. Removal of the solvent and excess HCl required heating at 60 °C under reduced pressure. Although Δ-(*S*,*S*)-**3**$^{3+}$ $3ClO_4^-$ is introduced to the cation exchange resin as a single isomer, the $^{13}C\{^1H\}$ NMR spectrum of the resulting Δ-(*S*,*S*)-**3**$^{3+}$ $3Cl^-$ reveals minor impurities of Λ-(*S*,*S*)-**3**$^{3+}$ $3Cl^-$ and (S,S)-**4**$^+$ Cl^-. It is likely that some degree of Cl^- substitution and complex isomerization occured during the evaporation of the solvent at elevated temperatures in the presence of the 4.0 M HCl.

The crude mixture of Cl^- salts was suspended in CH_2Cl_2 and one equivalent of Na^+ BAr_f^- was added. After sonicating the suspension for a few seconds, the solids dissolved and the CH_2Cl_2 took on a bright orange color. After removing the precipitated NaCl by filtration, the material was chromatographed on a silica gel column. A minor green band consisting of (S,S)-**4**$^+$ BAr_f^- (3%) eluted with CH_2Cl_2. Increasing the polarity of the mobile phase to 98:2 v/v CH_2Cl_2/MeOH eluted the major, orange band. Careful fractionation of the orange band separated the minor diastereomer Λ-(*S*,*S*)-**3**$^{3+}$ $2Cl^-$ BAr_f^- (7%) from the major diastereomer Δ-(*S*,*S*)-**3**$^{3+}$ $2Cl^-$ BAr_f^- (24%). In this

procedure, the Δ-diastereomer was isolated as the major product. The elemental analysis of the major product was consistent with one coordinated water molecule and the complex is best represented as the monohydrate Δ-(*S*,*S*)-**3**$^{3+}$ 2Cl^{-} BAr$_f^{-}$·H$_2$O.

In summary, the diastereoselectivity in the syntheses of Λ and Δ-[Co((*S*,*S*)-dpen)$_3$]$^{3+}$ trications is strongly influenced by the nature of the starting Co(II) salt. A synthesis that begins with a Co(II) salt containing AcO^{-} or Cl^{-} counterions leads predominately to the Λ-diastereomer of the tris-chelating complex. Also, higher amounts of the bis-chelating (S,S)-**4**$^{+}$ BAr$_f^{-}$ complex are isolated in these procedures. The same synthetic procedure, when applied to a Co(II) salt containing ClO$_4^{-}$ counteranions, ultimately leads to the dominant Δ-diastereomer of the tris-chelating complex. Although the salts of the cations *trans*-[Co((*S*,*S*)-dpen)$_2$Cl$_2$]$^{+}$ and Λ-[Co((*S*,*S*)-dpen)$_3$]$^{3+}$ were also isolated as minor byproducts, these were likely formed during the reaction workup rather than the complex synthesis.

Furthermore, the newly formed BAr$_f^{-}$ containing cobalt salts are chromatographable on silica gel with a mildly polar eluent and are independently isolated in separate fractions. This eliminates the need for repeated fractional crystallization to obtain isomerically pure material.

4.2.2 Synthesis of cobalt complexes with (R,R)-dpen ligands

The syntheses of [Co((*R*,*R*)-dpen)$_3$]$^{3+}$ 3X^{-} complexes were performed by direct analogy to the (*S*,*S*)-dpen series. In this case, the synthetic steps that had led to Λ-(*S*,*S*)-**3**$^{3+}$ 2Cl^{-} BAr$_f^{-}$ gave the opposite enantiomer, Δ-(*R*,*R*)-**3**$^{3+}$ 2Cl^{-} BAr$_f^{-}$. Likewise, the synthetic procedures that had resulted in Δ-(*S*,*S*)-**3**$^{3+}$ 2Cl^{-} BAr$_f^{-}$ gave the opposite enantiomer, Λ-(*R*,*R*)-**3**$^{3+}$ 2Cl^{-} BAr$_f^{-}$. These complexes are also isolated with a small

amount of H_2O, which is assayed by elemental analysis and ^1H NMR spectroscopy. Elemental analysis of Δ-(*S*,*S*)-**3**$^{3+}$ 2Cl$^-$ BAr$_f^-$ revealed that the complex is isolated with one coordinated water molecule so that it is best represented as the monohydrate Δ-(*R*,*R*)-**3**$^{3+}$ 2Cl$^-$ BAr$_f^-$·H_2O. Notably, this represents one fewer water molecule than was isolated with the corresponding enantiomer. However, the amount of coordinated water molecules in a particular batch is dependent on many uncontrollable factors such as atmospheric humidity and temperature. This small deviation from uniformity is of no significant consequence. For instance, one molecule of water represents only approximately 1% of the total molecular weight of the cobalt complex. At 10 mol% catalyst loading, this is only a 0.1 mol% discrepancy. In a similar manner, the elemental analysis of Λ-(*R*,*R*)-**3**$^{3+}$ 2Cl$^-$ BAr$_f^-$ revealed no coordinated water, which is one fewer than the corresponding enantiomer.

4.2.3 Crystal structures

4.2.3.1 The crystal structure of Λ-[Co((S,S)-dpen)$_3$]$^{3+}$ 3Cl$^-$·2H$_2$O·2MeOH

Orange rod-type crystals of Λ-[Co((*S*,*S*)-dpen)$_3$]$^{3+}$ 3Cl$^-$ were collected and X-ray data were obtained and refined as described in Section 4.7.1.1. The crystal structure is depicted in Figure 4.3. Besides the complex, there are two H_2O and two MeOH molecules in the asymmetric unit. The absolute stereochemistry was unambiguously determined (absolute structure parameter = 0.000(12); Table 4.20). The configuration of the metal center is Λ. Each (*S*,*S*)-dpen ligand adopts the δ chelate geometry resulting in the *lel*$_3$ conformation. Key geometrical parameters are summarized in Table 4.2.

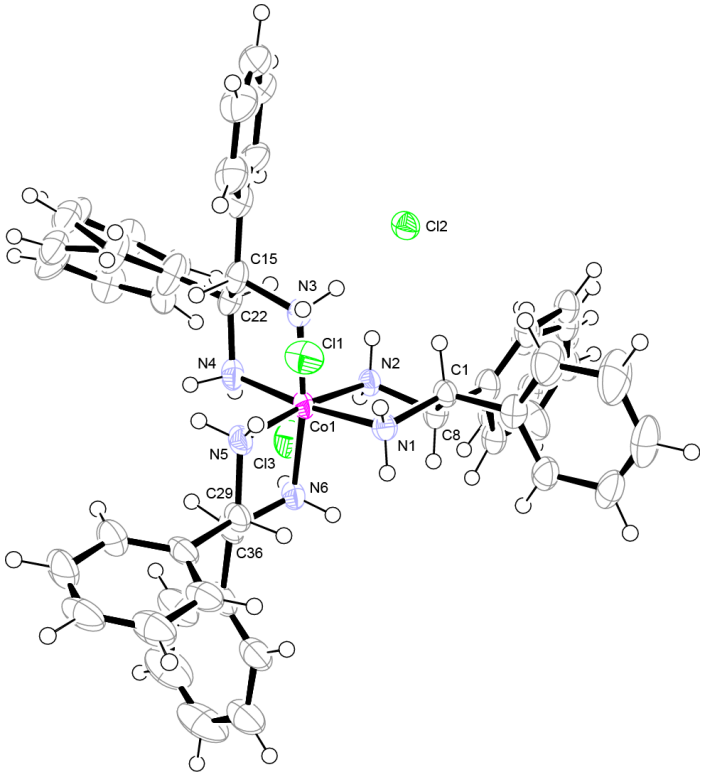

Figure 4.3. Crystal structure of Λ-[Co((*S*,*S*)-dpen)$_3$]$^{3+}$ 3Cl$^-$·2H$_2$O·2MeOH.[87] The solvent molecules do not directly hydrogen bond to the cobalt complex and are removed for clarity.

Table 4.2. Key distances [Å] and angles [°] in Λ-$[Co((S,S)\text{-dpen})_3]^{3+}$ $3Cl^-$ $\cdot 2H_2O \cdot 2MeOH$[a]

bond lengths		distances N···Cl		bond angles		torsion angles	
Co1-N1	1.910(2)	C_3		N3-Co1-N6	172.7(1)	N1-C1-C8-N2	59.4
Co1-N2	1.975(3)	N1···Cl1	3.194	N1-Co1-N4	172.7(1)	N3-C15-C22-N4	59.4
Co1-N3	1.985(2)	N3···Cl1	3.428	N2-Co1-N5	171.9(1)	N5-C29-C36-N6	52.6
Co1-N4	1.963(2)	N5···Cl1	3.269	N3-Co1-N1	90.9(1)	**Average:**	**57.1(3.9)**
Co1-N5	1.963(3)	N2···Cl3	3.259	N3-Co1-N2	96.3(1)	torsion angles H-N···N-H	
Co1-N6	1.949(3)	N4···Cl3	3.198	N3-Co1-N4	84.4(1)	C_3	
N1-C1	1.492(4)	N6···Cl3	3.195	N3-Co1-N5	90.5(1)	H–N1···N3–H	–6.8
N2-C8	1.511(4)	**Average:**	**3.257(.090)**	N6-Co1-N1	94.7(1)	H–N3···N5–H	–4.7
N3-C15	1.509(3)	C_2		N6-Co1-N2	89.0(1)	H–N5···N1–H	–7.4
N4-C22	1.502(4)	N5···Cl2	3.231	N6-Co1-N4	90.5(1)	H–N2···N4–H	–19.1
N5-C29	1.498(4)	N4···Cl2	3.266	N6-Co1-N5	84.6(1)	H–N4···N6–H	2.7
N6-C36	1.506(4)	**Average:**	**3.249(.025)**	N1-Co1-N2	84.3(1)	H–N6···N2–H	4.9
N-H···H-N distances		distances NH···Cl		N2-Co1-N4	90.7(1)	**Average:**[b]	**7.6(5.9)**
C_3		C_3		N4-Co1-N5	94.3(1)	C_2	
N1H···HN3	2.418	N1H···Cl1	2.313	N5-Co1-N1	91.3(1)	H–N1···N6–H	–24.9
N3H···HN5	2.428	N3H···Cl1	2.606	angles N-H···Cl^-		H–N3···N2–H	–35.2
N5H···HN1	2.453	N5H···Cl1	2.436	C_3		H–N5···N4–H	–28.7
N2H···HN4	2.393	N2H···Cl3	2.379	N1–H···Cl1	165.5	**Average:**[b]	**29.6(5.2)**
N4H···HN6	2.571	N4H···Cl3	2.376	N3–H···Cl1	152.4		
N6H···HN2	2.159	N6H···Cl3	2.364	N5–H···Cl1	154.0		
Average:	**2.404(.135)**	**Average:**	**2.412(.103)**	N2–H···Cl3	165.8		
C_2		C_2		N4–H···Cl3	152.2		
N1H···HN6	2.334	N5H···Cl2	2.386	N6–H···Cl3	153.6		
N3H···HN2	2.248	N4H···Cl2	2.387	**Average:**	**157.3(6.5)**		
N5H···HN4	2.187	**Average:**	**2.387(.001)**	C_2			
Average:	**2.256(.074)**			N5–H···Cl2	156.3		
				N4–H···Cl2	165.5		
				Average:	**160.9(6.5)**		

[a]The values in the bold parentheses represent the standard deviations of the average values. [b]The average of the absolute values. Positive torsion angles derive from a clockwise arrangement of measured bonds. Negative torsion angles derive from a counterclockwise arrangement of measured bonds.

The Co-N bond distances and N-Co-N bond angles show small deviations from ideal octahedronal geometries, but were similar to the related complex Λ-$[Co(en)_3]^{3+}$ $3Cl^-\cdot H_2O$.[53] The average N-C-C-N torsion angle (57.1°) of the diamine chelates approaches a near ideal gauche conformation of 60°. The N-H units can be divided into two classes (C_3 and C_2, Section 3.2) based upon the idealized D_3 symmetry of the trication. The average distance between C_2 N-H units (2.25 Å) is slightly less than that for the C_3 N-H units (2.40 Å). The average H-N···N-H torsion angle between adjacent C_3 N-H units (7.6°) is quite close to 0°, indicating that the N-H bonds on the C_3 face are roughly parallel to each other. Notably, one torsion angle (H-N_2···N_4-H, –19.1°) lies well outside of the range of the other C_3 N-H units. It is possible that this perturbation occurs to alleviate H···H repulsion between the closely oriented C_3 N-H units. The average C_2 H-N···N-H torsion angle (29.6°) is considerably more skewed than those of the C_3 axis.

A summary of all hydrogen bonding interactions between the complex and the Cl^- counteranions and solvent molecules is given in Figure 4.4. Both C_3 faces form triple hydrogen bonds with Cl^- counteranions. The third Cl^- counteranion forms a double hydrogen bond at the C_2 face. The Cl^- anions at the C_2 face form hydrogen bonding bridges between neighboring complexes that results in a continuous $\{[Co]\cdots Cl^-\cdots\}_n$ chain connected at C_2 faces. The third and final C_2 face, which is not incorporated in the $\{[Co]\cdots Cl^-\cdots\}_n$ chain, is occupied by a double hydrogen bond to H_2O and a single hydrogen bond to a MeOH. The average N-H···Cl^- bond angles (157-161°, Table 4.2) are somewhat less than the ideal, linear hydrogen bond angle of 180°.

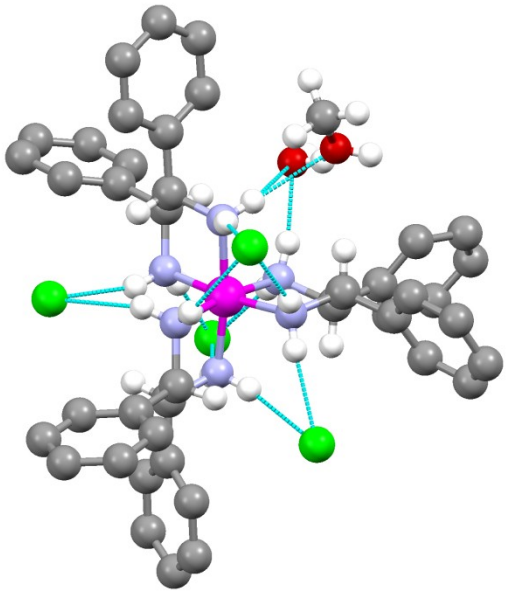

Λ-[Co((*S*,*S*)-dpen)$_3$]$^{3+}$ 3Cl$^-$·2H$_2$O·2MeOH		
H-bond acceptor (X)	Type of H-bond	Total number of similar interactions
Cl$^-$	[C$_3$,C$_3$,C$_3$][1]	2
Cl$^-$	[C$_2$,C$_2$][1]	2
H$_2$O	[C$_2$,C$_2$][1]	1
MeOH	[C$_2$][1]	1

Figure 4.4. All hydrogen bonding interactions in the crystal structure of Λ-[Co((*S*,*S*)-dpen)$_3$]$^{3+}$ 3Cl$^-$ ·2H$_2$O·2MeOH, classified per section 3.3.1. The hydrogen atoms of the phenyl rings are removed for clarity.

In accordance with the chirality of cobalt complex, the $\{[Co]\cdots Cl^{-}\cdots\}_n$ chain adopts a chiral, left-handed helical arrangement, as seen in Figure 4.5a. Interestingly, the H_2O and MeOH solvent molecules form a hydrogen bonding chain that adopts a complimentary left-handed helical arrangement. The $H_2O\cdots$MeOH helix fits inside the groove of the $\{[Co]\cdots Cl^{-}\cdots\}_n$ helix. The solvent helix is anchored to the complex helix by MeOH$\cdots Cl^{-}$ hydrogen bonds and the previously mentioned solvent interactions with the C_2 N–H units (Figure 4.4).

Space filling models that focus on the C_3 and C_2 axes of the complex are provided in Figure 4.5b-d. At the C_3 face, one Cl^{-} anion fits nicely across all three N-H units. Removing this Cl^{-} anion reveals a well-defined hydrogen bonding pocket that is surrounded by three bulky phenyl groups. At the C_2 face, one Cl^{-} anion also fits symmetrically across the two N-H units. Removing this Cl^{-} anion reveals a different hydrogen bonding pocket that is sandwiched between two approximately parallel, offset phenyl groups.

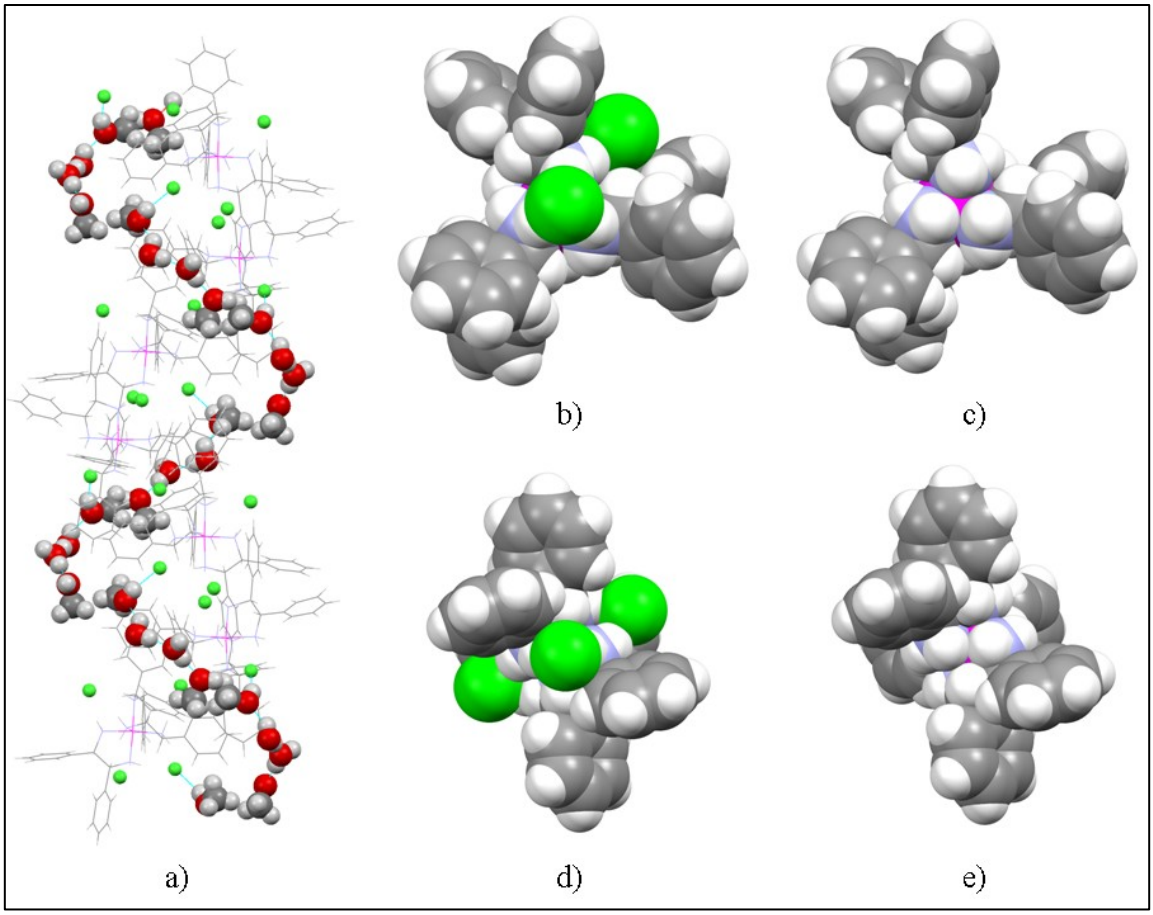

Figure 4.5. Multiple views of Λ-[Co((*S*,*S*)-dpen)$_3$]$^{3+}$ 3Cl$^-$·2H$_2$O·2MeOH including a) two unit cells viewed along the c axis; b) space filling models viewed along the C$_3$ axis with Cl$^-$ anions and c) without Cl$^-$ anions; d) space filling models viewed along the C$_2$ axis with Cl$^-$ anions and e) without Cl$^-$ anions.

4.2.3.2 The crystal structure of Δ-*[Co((R,R)-dpen)$_3$]$^{3+}$ 3Cl$^-$·H$_2$O·3MeOH*

Orange rod-type crystals of Δ-[Co((*R*,*R*)-dpen)$_3$]$^{3+}$ 3Cl$^-$ were collected and X-ray data were obtained and refined as described in Section 4.7.1.2. This complex is the opposite enantiomer of Λ-(*S*,*S*)-**3**$^{3+}$ 3Cl$^-$, the structure of which was detailed in the previous section. The crystal structure is shown in Figure 4.6. Because of different

crystallization conditions, a different solvate was obtained compared with the enantiomeric Λ-(*S*,*S*)-**3**$^{3+}$ 3Cl^{-}. Specifically, there was one H_2O and three MeOH molecules within the asymmetric unit. The absolute configuration was unambiguously determined (absolute structure parameter = 0.012(4); Table 4.21). The configuration of the metal center is Δ. Each (*R*,*R*)-dpen ligands adopts the λ chelate geometry resulting in the *lel*$_3$ conformation. Key geometrical parameters are summarized in Table 4.3.

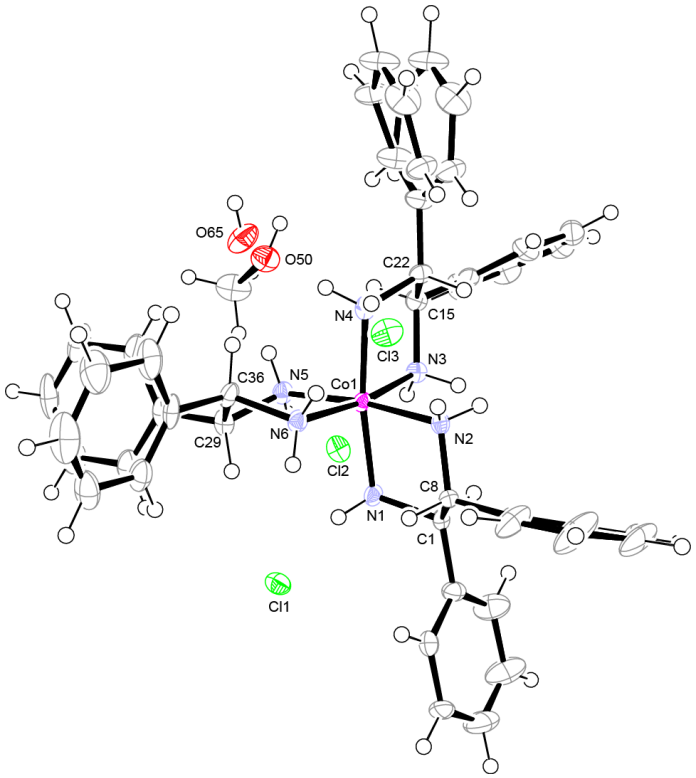

Figure 4.6. Crystal structure of Δ-[Co((*R*,*R*)-dpen)$_3$]$^{3+}$ 3Cl^{-}·H_2O·3MeOH. Solvent molecules that do not directly hydrogen bond to the cobalt complex are removed for clarity.

Table 4.3. Key distances [Å] and angles [°] in Δ-$[Co((R,R)\text{-dpen})_3]^{3+}$ $3Cl^-$ $\cdot H_2O \cdot 3MeOH$[a]

bond lengths		distances N···X		bond angles		torsion angles	
Co1-N1	1.970(3)	C_3		N3-Co1-N6	171.7(1)	N1-C1-C8-N2	–59.0
Co1-N2	1.989(3)	N1···Cl2	3.220	N1-Co1-N4	172.7(1)	N3-C15-C22-N4	–59.4
Co1-N3	1.967(3)	N3···Cl2	3.265	N2-Co1-N5	171.6(1)	N5-C29-C36-N6	–52.8
Co1-N4	1.957(3)	N5···Cl2	3.208	N3-Co1-N1	90.8(1)	**Average:**	**–57.1(3.7)**
Co1-N5	1.989(3)	N2···Cl3	3.445	N3-Co1-N2	96.7(1)	torsion angles H-N···N-H	
Co1-N6	1.962(3)	N4···Cl3	3.194	N3-Co1-N4	84.5(1)	C_3	
N1-C1	1.504(5)	N6···Cl3	3.279	N3-Co1-N5	89.6(1)	H–N1···N3–H	19.4
N2-C8	1.504(5)	**Average:**	**3.269(.093)**	N6-Co1-N1	94.4(1)	H–N3···N5–H	1.5
N3-C15	1.511(5)	C_2		N6-Co1-N2	90.4(1)	H–N5···N1–H	0.6
N4-C22	1.506(5)	N2···Cl1	3.327	N6-Co1-N4	91.0(1)	H–N2···N4–H	8.6
N5-C29	1.483(5)	N3···Cl1	3.202	N6-Co1-N5	83.8(1)	H–N4···N6–H	–0.9
N6-C36	1.484(5)	**Average:**	**3.265(.088)**	N1-Co1-N2	83.9(1)	H–N6···N2–H	0.0
N-H···H-N distances		N4···O50	3.254	N2-Co1-N4	91.1(1)	**Average:**[b]	**5.2(7.7)**
C_3		N4···O65	3.387	N4-Co1-N5	94.9(1)	C_2	
N1H···HN3	2.383	N5···O50	2.872	N5-Co1-N1	90.6(1)	H–N1···N6–H	29.5
N3H···HN5	2.163	distances NH···X		angles N-H···X		H–N3···N2–H	33.2
N5H···HN1	2.469	C_3		C_3		H–N5···N4–H	26.1
N2H···HN4	2.493	N1H···Cl2	2.398	N1–H···Cl2	151.9	**Average:**	**29.6(3.5)**
N4H···HN6	2.539	N3H···Cl2	2.379	N3–H···Cl2	168.2		
N6H···HN2	2.380	N5H···Cl2	2.324	N5–H···Cl2	161.2		
Average:	**2.405(.134)**	N2H···Cl3	2.634	N2–H···Cl3	150.5		
C_2		N4H···Cl3	2.346	N4–H···Cl3	156.9		
N1H···HN6	2.340	N6H···Cl3	2.437	N6–H···Cl3	155.7		
N3H···HN2	2.456	**Average:**	**2.420(.112)**	**Average:**	**157.4(6.5)**		
N5H···HN4	2.407	C_2		C_2			
Average:	**2.401(.058)**	N5H···Cl1	2.498	N2–H···Cl1	153.2		
		N4H···Cl1	3.356	N3–H···Cl1	156.6		
		Average:	**2.927(.607)**	**Average:**	**154.9(2.4)**		
		N4H···O50	2.410	N4H···O50	156.3		
		N4H···O65	2.708	N4H···O65	133.1		
		N5H···O50	1.957	N5H···O50	173.5		

[a]The values in the bold parentheses represent the standard deviations of the average values. [b]The average of the absolute values. Positive torsion angles derive from a clockwise arrangement of measured bonds. Negative torsion angles derive from a counterclockwise arrangement of measured bonds.

The molecular geometry of Δ-(*R*,*R*)-**3**$^{3+}$ 3Cl^{-} is very similar to that of the enantiomeric structure Λ-(*S*,*S*)-**3**$^{3+}$ 3Cl^{-} (Table 4.2). In terms of geometrical parameters, one difference is the inversion of the sign of the N-C-C-N torsion angles of the chelating diamines. The switch from positive to negative values coincides with the change from δ to λ chelate geometry. This is because, as was seen in Figure 2.11, an (*S*,*S*)-dpen ligand with the δ chelate conformation exhibits a clockwise arrangement with respect to the C-N bonds, while an (*R*,*R*)-dpen ligand with the λ chelate comformation adopts a counterclockwise arrangement. Interestingly, one value for the C_3 N-H dihedral angles (H–N1···N3–H, 19.4°) is a clear outlier compared to the other values. A similar perturbation was observed in Table 4.2.

A summary of all hydrogen bonding interactions between the complex and the Cl^{-} counteranions and solvent molecules is given in Figure 4.7. Despite the different solvation in the asymmetric unit, the total hydrogen bonding interactions are identical to those of the enantiomeric Λ-(*S*,*S*)-**3**$^{3+}$ 3Cl^{-} complex (Figure 4.4).

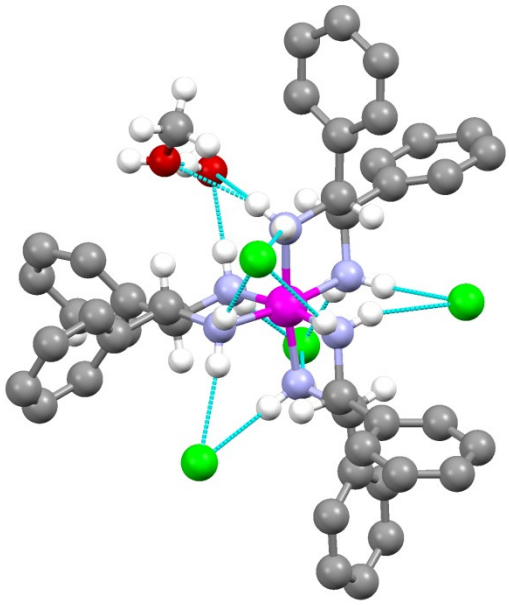

Δ-[Co((*R*,*R*)-dpen)$_3$]$^{3+}$ 3Cl$^-$·H$_2$O·3MeOH		
H-bond acceptor (X)	Type of H-bond	Total number of similar interactions
Cl$^-$	[C$_3$,C$_3$,C$_3$][1]	2
Cl$^-$	[C$_2$,C$_2$][1]	2
H$_2$O	[C$_2$,C$_2$][1]	1
MeOH	[C$_2$][1]	1

Figure 4.7. All hydrogen bonding interactions in the crystal structure of Δ-[Co((*R*,*R*)-dpen)$_3$]$^{3+}$ 3Cl$^-$ ·H$_2$O·3MeOH, classified per section 3.3.1. The hydrogen atoms of the phenyl rings are removed for clarity.

Once again, the Cl$^-$ anions that occupy the C$_2$ faces form hydrogen bonding bridges between complexes that results in a continuous {[Co]···Cl$^-$···}$_n$ chain, as shown in Figure 4.8a. In this case, the chain conforms to a right-handed helix. The solvent molecules also form hydrogen bonds among themselves, but in this structure they do not

form the well-organized complementary helix that was observed in Figure 4.5a. Also shown in Figures 4.8b-d are space filling models of the Δ-(*R*,*R*)-**3**$^{3+}$ 3Cl^{-} complex, which are the mirror-image complement to the space filling models shown in Figure 4.5b-d.

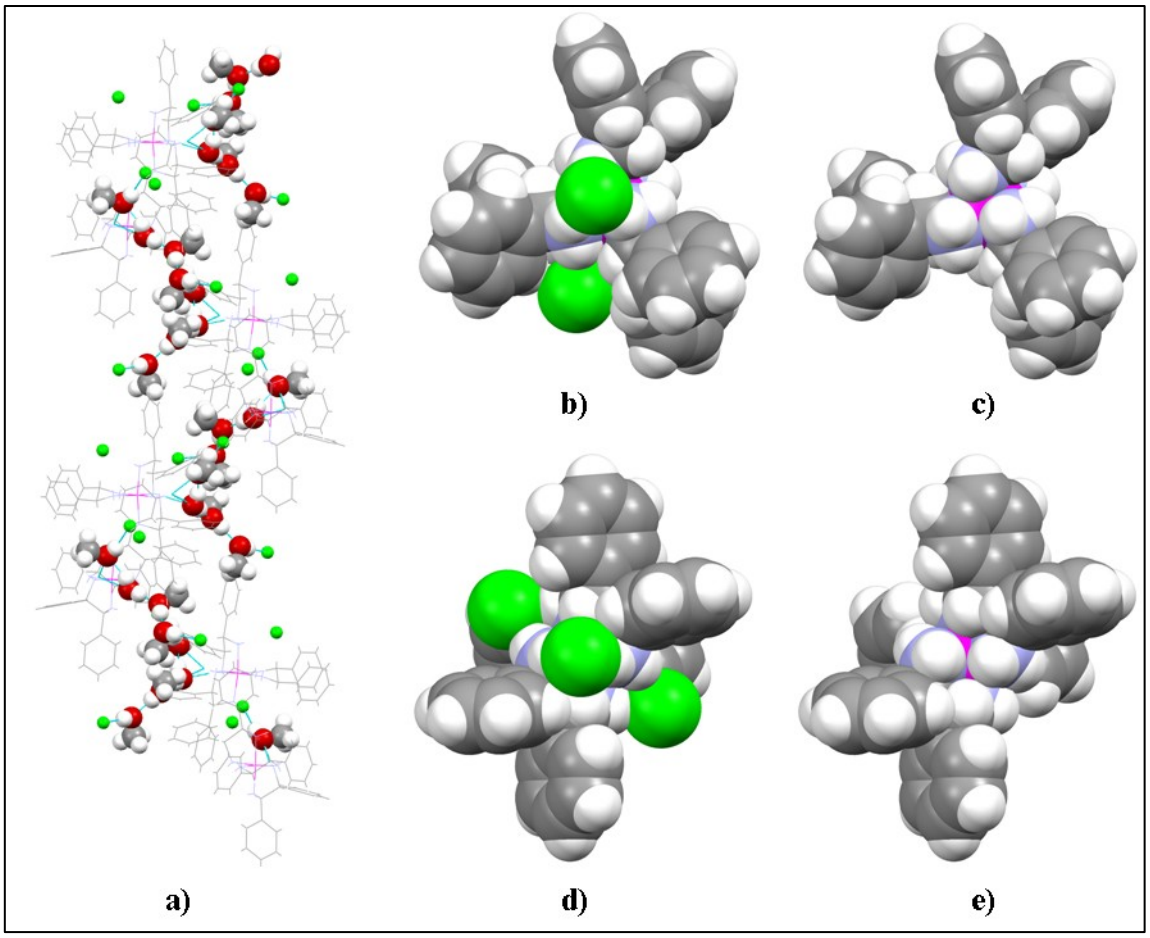

Figure 4.8. Multiple views of Δ-[Co((*R*,*R*)-dpen)$_3$]$^{3+}$ 3Cl^{-}·H$_2$O·3MeOH including a) two unit cells viewed along the c axis; b) space filling models viewed along the C$_3$ axis with Cl^{-} anions and c) without Cl^{-} anions; d) space filling models viewed along the C$_2$ axis with Cl^{-} anions and e) without Cl^{-} anions.

4.2.3.3 The crystal structure of Δ-*[Co((S,S)-dpen)$_3$]$^{3+}$ 3Cl$^-$·12.5H$_2$O*

A portion of Δ-(*S*,*S*)-**3**$^{3+}$ 3Cl$^-$, obtained after the Dowex cation exchange procedure (Scheme 4.4), was redissolved in hot H_2O. Orange blocks of Δ-[Co((*S*,*S*)-dpen)$_3$]$^{3+}$ 3Cl$^-$ were collected and X-ray data were obtained and refined as described in Section 4.7.1.3. The crystal structure is shown in Figure 4.9. The crystal structure included two cobalt molecules along with 25 water molecules in the asymmetric unit. The absolute stereochemistry was unambiguously determined (absolute structure parameter = 0.069(5); Table 4.22). The configuration of the metal center is Δ. Each (*S*,*S*)-dpen ligands adopts the δ chelate geometry resulting in the *ob*$_3$ conformation. Key geometrical parameters are summarized in Table 4.4.

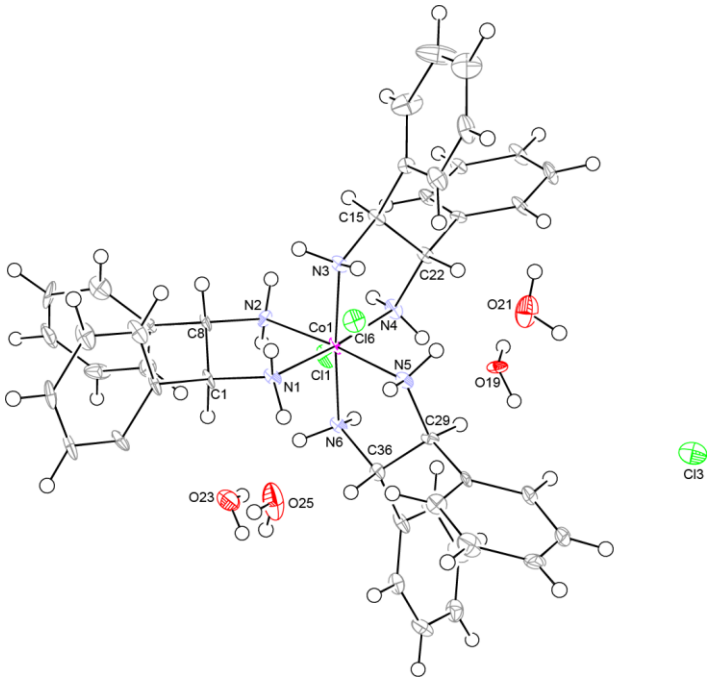

Figure 4.9. The crystal structure of one cobalt complex in the asymmetric unit of Δ-[Co((*S*,*S*)-dpen)$_3$]$^{3+}$ 3Cl$^-$·12.5H$_2$O. Molecules that are not directly hydrogen bonded to the cobalt complex are removed for clarity.

Table 4.4. Key distances [Å] and angles [°] in Δ-$[Co((S,S)\text{-dpen})_3]^{3+}$ $3Cl^{-}\cdot 12.5H_2O$[a]

bond lengths		distances N···X		bond angles		torsion angles	
Co1-N1	1.949(5)	C_3		N3-Co1-N6	175.5(2)	N1-C1-C8-N2	46.0
Co1-N2	1.963(6)	N1···Cl6	3.328	N1-Co1-N4	175.2(2)	N3-C15-C22-N4	44.9
Co1-N3	1.958(6)	N3···Cl6	3.237	N2-Co1-N5	175.3(2)	N5-C29-C36-N6	40.7
Co1-N4	1.954(5)	N5···Cl6	3.241	N3-Co1-N1	91.3(2)	**Average:**	**43.9(2.8)**
Co1-N5	1.961(6)	N2···Cl1	3.276	N3-Co1-N2	90.5(2)	torsion angles H-N···N-H	
Co1-N6	1.967(6)	N4···Cl1	3.235	N3-Co1-N4	84.4(2)	C_3	
N1-C1	1.508(9)	N6···Cl1	3.362	N3-Co1-N5	92.3(2)	H–N1···N3–H	45.0
N2-C8	1.494(9)	**Average:**	**3.280(.054)**	N6-Co1-N1	92.1(2)	H–N3···N5–H	41.8
N3-C15	1.502(9)	C_2		N6-Co1-N2	92.7(2)	H–N5···N1–H	49.8
N4-C22	1.475(9)	N1···O25	2.873	N6-Co1-N4	92.3(2)	H–N2···N4–H	55.0
N5-C29	1.489(9)	N4···O21	2.848	N6-Co1-N5	84.7(2)	H–N4···N6–H	51.8
N6-C36	1.488(9)	N5···O19	2.974	N1-Co1-N2	85.1(2)	H–N6···N2–H	47.8
N-H···H-N distances		N6···O23	3.001	N2-Co1-N4	92.7(2)	**Average:**	**48.5(4.7)**
C_3		distances NH···X		N4-Co1-N5	91.4(2)	C_2	
N1H···HN3	2.502	C_3		N5-Co1-N1	91.0(2)	H–N1···N6–H	82.7
N3H···HN5	2.624	N1H···Cl6	2.616	angles N-H···X		H–N3···N2–H	75.1
N5H···HN1	2.610	N3H···Cl6	2.421	C_3		H–N5···N4–H	86.4
N2H···HN4	2.660	N5H···Cl6	2.525	N1–H···Cl6	134.6	**Average:**	**81.4(5.8)**
N4H···HN6	2.725	N2H···Cl1	2.569	N3–H···Cl6	147.7		
N6H···HN2	2.645	N4H···Cl1	2.545	N5–H···Cl6	134.8		
Average:	**2.628(.073)**	N6H···Cl1	2.625	N2–H···Cl1	134.1		
C_2		**Average:**	**2.550(.074)**	N4–H···Cl1	132.0		
N1H···HN6	2.647	C_2		N6–H···Cl1	137.5		
N3H···HN2	2.499	N1H···O25	2.004	**Average:**	**136.8(5.6)**		
N5H···HN4	2.677	N4H···O21	1.982	C_2			
Average:	**2.608(.095)**	N5H···O19	2.100	N1H···O25	156.5		
		N6H···O23	2.120	N4H···O21	156.0		
				N5H···O19	158.2		
				N6H···O23	159.9		

[a]The values in the bold parentheses represent the standard deviations of the average values.

The Co-N bond lengths and N-Co-N bond angles reveal that the complex deviates slightly from the ideal octahedronal geometry. The positive values for the N-C-C-N torsion angles have the same sign as those found in Table 4.2, but are opposite to the values found in Table 4.3. This is consistent for a (*S*,*S*)-dpen chelate in the δ conformation. However, the average torsion angle of 44° is considerably less than the idealized gauche conformation of 60°. Also, the angles and positions of the hydrogen bond donating N-H units are significantly different than those in crystalline Λ-(*S*,*S*)-**3**$^{3+}$ 3Cl$^-$ and Δ-(*R*,*R*)-**3**$^{3+}$ 3Cl$^-$ (Table 4.2, 4.3), which are here collectively referred to as the *lel*$_3$ complexes. The average distance between adjacent N-H hydrogens atoms on the C_3 axis (2.63 Å) is approximately 0.22 Å greater than those of the *lel*$_3$ complexes and the average C_3 H-N···N-H torsion angle (48.5°) is considerably more skewed away from a parallel orientation. The C_3 N···Cl$^-$ and NH···Cl$^-$ bond distances are similar to those of the *lel*$_3$ complexes. However, the more bent C_3 N–H···Cl$^-$ bond angles (136.8°) indicate that this hydrogen bond is less direct, and likely weaker, than those observed with the *lel*$_3$ complexes.

All of the hydrogen bonding contacts between the cobalt complex and the corresponding anions or solvent molecules are shown in Figure 4.10. There are technically no C_2 NH···Cl$^-$ hydrogen bonds within the asymmetric unit. However, one such hydrogen bond is found spanning across two asymmetric units. Five H_2O molecules also form single hydrogen bonds at the C_2 faces. Both C_3 faces are fully occupied by triple hydrogen bonding with Cl$^-$ anions.

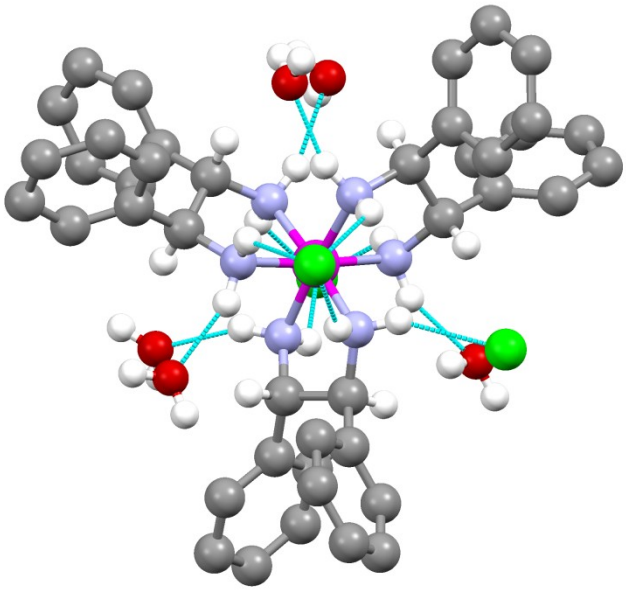

Δ-[Co((*R*,*R*)-dpen)$_3$]$^{3+}$ 3Cl$^-$·12.5H$_2$O		
H-bond acceptor (X)	Type of H-bond	Total number of similar interactions
Cl$^-$	[C$_3$, C$_3$, C$_3$][1]	2
Cl$^-$	[C$_2$][1]	1
H$_2$O	[C$_2$][1]	5

Figure 4.10. All hydrogen bonding interactions in the crystal structure of Δ-[Co((*S*,*S*)-dpen)$_3$]$^{3+}$ 3Cl$^-$ ·12.5H$_2$O, classified per section 3.3.1. The hydrogen atoms of the phenyl rings are removed for clarity.

The full asymmetric unit of the crystal structure is shown in Figure 4.11a with added emphasis on the H$_2$O molecules. There is no clear organization of the H$_2$O network around the cobalt complexes. Space-filling models of Δ-(*S*,*S*)-**3**$^{3+}$ 3Cl$^-$ that focus on the C$_3$ and C$_2$ faces are shown in Figure 4.11b-d. At the C$_3$ face, one Cl$^-$ fits symmetrically across all three N-H units. Removing the Cl$^-$ anion reveals a hydrogen bonding pocket that is surrounded by three phenyl rings. In a visible comparison to the

space-filling model in Figure 4.5c, the C_3 N-H units appear more spaced apart and more greatly skewed away from the C_3 axis. Interestingly, the C_2 N-H units are also more prominently visible when looking down the C_3 axis. In Figure 4.11d. a Cl^- anion is positioned asymmetrically across the C_2 face. The C_2 N-H hydrogen bonding pocket is bifurcated by the bulky phenyl rings, which prevents the formation of a double hydrogen bond to the Cl^- anion.

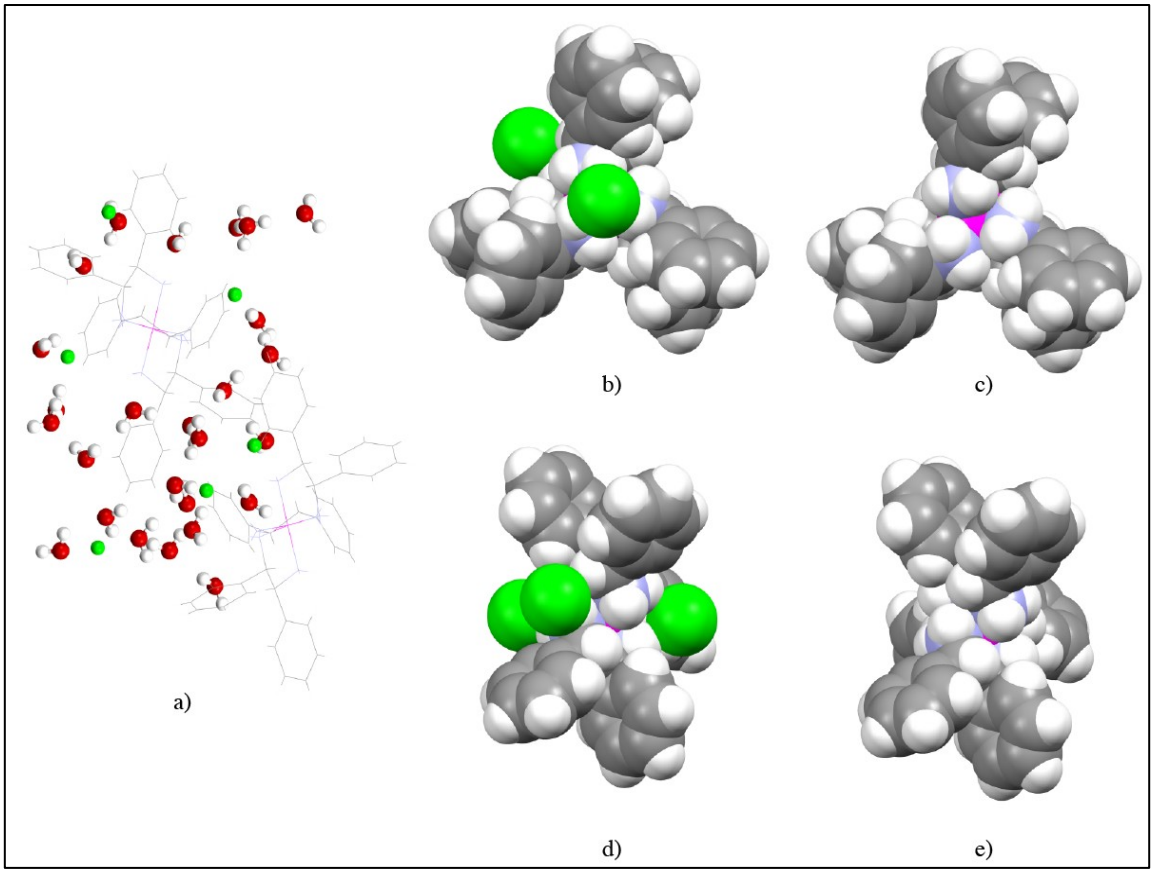

Figure 4.11. Multiple views of Δ-$[Co((S,S)\text{-dpen})_3]^{3+}$ $3Cl^-\cdot 12.5H_2O$ including a) the asymmetric unit viewed along the b axis; b) space-filling models viewed along the C_3 axis with Cl^- anions and c) without Cl^- anions; d) space-filling models viewed along the C_2 axis with Cl^- anions and e) without Cl^- anions.

4.2.4 NMR spectral features of [Co((S,S)-dpen)$_3$]$^{3+}$ 3X$^-$ complexes

The low-spin, [Co(1,2-diamine)$_3$]$^{3+}$ trications are diamagnetic and can be characterized by NMR spectroscopy. A ^{13}C NMR spectrum has been reported for [Co((*R*,*S*)-dpen)$_3$]$^{3+}$ 3Cl$^-$, which consists of *meso* dpen ligands, and in principle is capable of forming many isomers (Figure 2.14).[52c] However, there are no previously reported NMR data for [Co(*trans*-dpen)$_3$]$^{3+}$ trications.

4.2.4.1 Determination of diastereomeric purity by ^{13}C{^{1}H} NMR.

Bosnich assayed the diastereomeric purity of isolated [Co((*S*,*S*)-dpen)$_3$]$^{3+}$ trications by analysis of their CD spectra. However, ^{13}C{^{1}H} NMR is a more precise and convenient method by which to distinguish the diastereomers of the cobalt complexes. The diastereomerically related Λ-(*S*,*S*)-**3**$^{3+}$ and Δ-(*S*,*S*)-**3**$^{3+}$ trications should have similar, yet distinguishable NMR features.

Towards this end, the diastereomerically pure salts of Λ-(*S*,*S*)-**3**$^{3+}$ 3ClO$_4^-$ and Δ-(*S*,*S*)-**3**$^{3+}$ 3ClO$_4^-$ were prepared according the original Bosnich procedure (Scheme 4.3). The ^{13}C{^{1}H} NMR spectra are compared in Figure 4.12. There are only slight differences between the aromatic carbon signals (127-137 ppm). In contrast, the chemical shift of the aliphatic carbon atoms of the dpen ligands (C̲HNH$_2$) is more informative. Due to the idealized D_3 symmetry of the trication, all six aliphatic carbon atoms are equivalent, and appear as a single peak. For Λ-(*S*,*S*)-**3**$^{3+}$ 3ClO$_4^-$, this peak appears as a singlet at 61.4 ppm while the analogous peak for Δ-(*S*,*S*)-**3**$^{3+}$ 3ClO$_4^-$ is shifted slightly downfield to 63.2 ppm. Thus, each diastereomer gives a unique and clearly distinguishable peak in the range of 60-65 ppm. Because both complexes only

show one peak in this range, they are considered to exist as single configurational diastereomers.

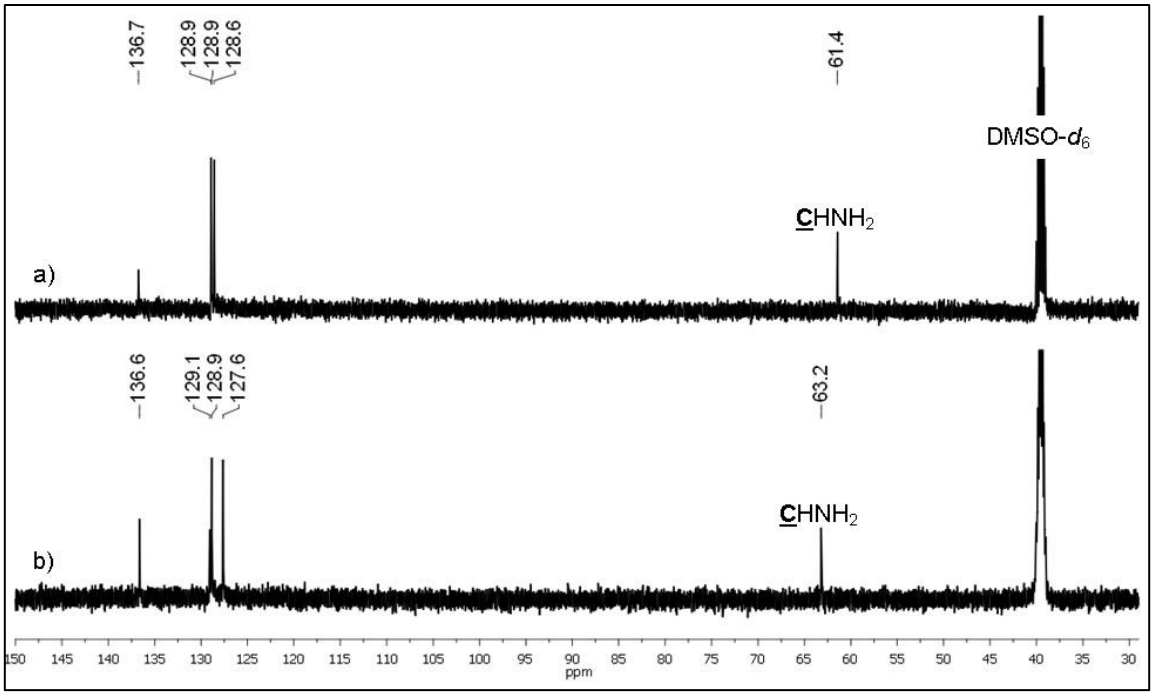

Figure 4.12. The $^{13}C\{^1H\}$ NMR spectra (DMSO-d_6) of a) Λ-(*S*,*S*)-**3**$^{3+}$ 3ClO_4^- and b) Δ-(*S*,*S*)-**3**$^{3+}$ 3ClO_4^-.

A similar relationship is observed in the $^{13}C\{^1H\}$ NMR spectra of the isolated Λ-(*S*,*S*)-**3**$^{3+}$ 2Cl^- BAr_f^- and Δ-(*S*,*S*)-**3**$^{3+}$ 2Cl^- BAr_f^- diastereomers, as shown in Figure 4.13. Once again, the aliphatic carbons of the dpen ligands of the two diastereomers are easily distinguishable. This peak is shifted downfield by more than 3 ppm for the Δ-diastereomer compared to the Λ-diastereomer. It must also be noted that, although Λ-(*S*,*S*)-**3**$^{3+}$ 2Cl^- BAr_f^- is readily soluble in CD_2Cl_2, Δ-(*S*,*S*)-**3**$^{3+}$ 2Cl^- BAr_f^- is very poorly soluble. The presence of a small amount of a polar additive such as MeOH is required to dissolve the complex.

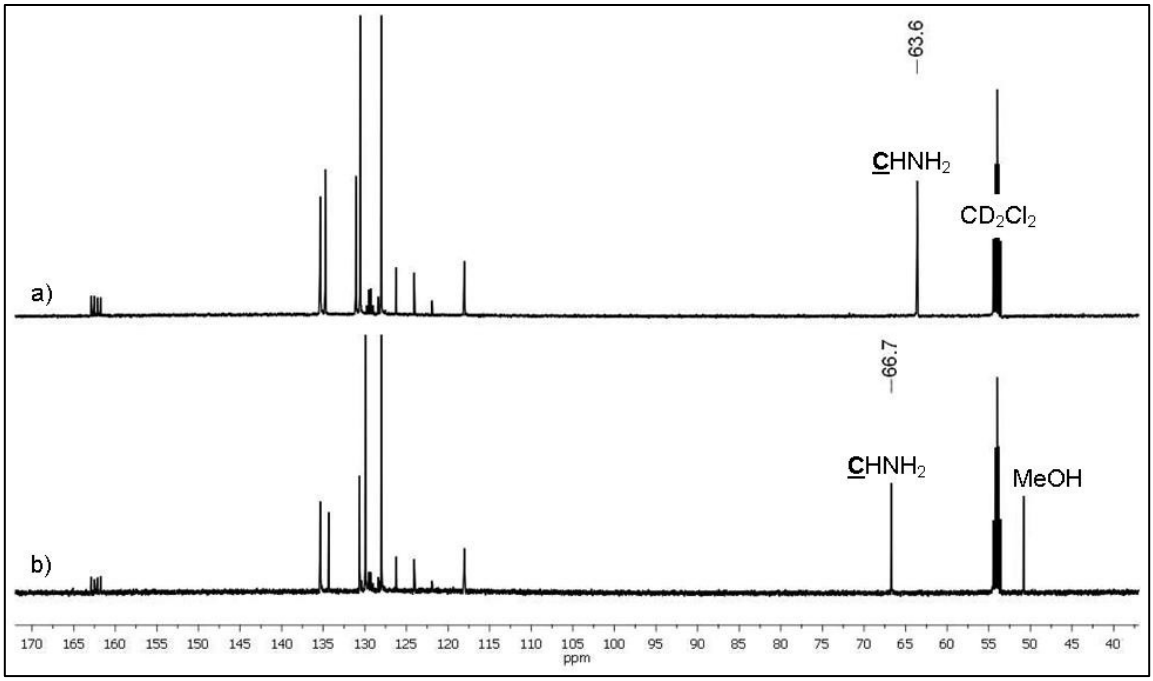

Figure 4.13. The $^{13}C\{^{1}H\}$ NMR spectra of Λ-(*S*,*S*)-**3**$^{3+}$ 2Cl^{-} BAr_f^{-} in CD_2Cl_2 and b) Δ-(*S*,*S*)-**3**$^{3+}$ 2Cl^{-} BAr_f^{-} in CD_2Cl_2/MeOH 0.40:0.0010 mL.

4.2.4.2 ^{1}H NMR evidence for hydrogen bonding

Many hydrogen bonding features of $[Co(S,S\text{-dpen})_3]^{3+}$ trications can be examined by ^{1}H NMR spectroscopy. As a general rule, a peak of the type X-*H* (X = O, N) is shifted downfield when engaged in a hydrogen bond compared to a non-hydrogen bonded analog.[88]

The ^{1}H NMR spectra of the diastereomers Λ-(*S*,*S*)-**3**$^{3+}$ 2Cl$^-$ BAr$_f^-$ and Δ-(*S*,*S*)-**3**$^{3+}$ 2Cl$^-$ BAr$_f^-$ are compared in Figure 4.14. The diastereotopic C_3 and C_2 N-H groups are expected to give slightly different chemical shifts. However, the chemical shift difference of 4.31 ppm between the C_3 and C_2 N-H units of Λ-(*S*,*S*)-**3**$^{3+}$ 2Cl$^-$ BAr$_f^-$ was much larger than initially expected. This is considered to arise from more than just shielding differences associated with geometry. It seemed more likely that one class of N-H units was engaged in strong hydrogen bonding with the two Cl$^-$ counteranions. Due to the apparent preference for the Cl$^-$ anions to form triple hydrogen bonds to the C_3 N-H units (Figure 4.4), the downfield shifted peak at 8.17 ppm was assigned to the two sets of C_3 N-H units. In contrast, the three sets of C_2 N-H units, with no coordinated Cl$^-$ anions, are assigned to the signals at 3.86 ppm.

A significant, yet smaller, chemical shift difference also occurs between the C_3 and C_2 N-H units of the diastereomer Δ-(*S*,*S*)-**3**$^{3+}$ 2Cl$^-$ BAr$_f^-$. Notably, the C_3 N-H units appear at only 6.58 ppm, which is considerably less downfield as compared to those of the Λ-diastereomer. This is likely due to weaker C_3 N-H···Cl$^-$ hydrogen bonding interactions, which is consistent with the bent N-H···Cl$^-$ bond angles in the crystal structure of Δ-$[Co(S,S\text{-dpen})_3]^{3+}$ 3Cl$^-$ (Table 4.4).

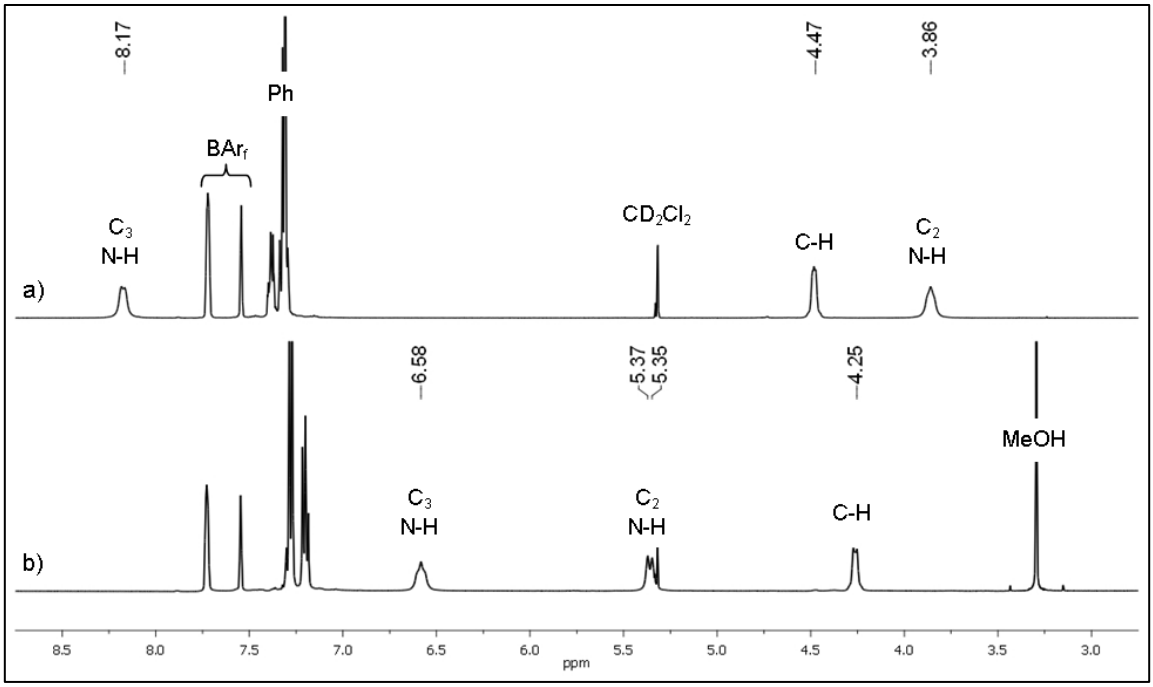

Figure 4.14. The ^{1}H NMR spectra of a) Λ-(*S*,*S*)-**3**$^{3+}$ 2Cl$^-$ BAr$_f^-$ in CD_2Cl_2 and b) Δ-(*S*,*S*)-**3**$^{3+}$ 2Cl$^-$ BAr$_f^-$ in CD_2Cl_2/MeOH 0.40:0.0010 mL.

Because Δ-(*S*,*S*)-**3**$^{3+}$ 2Cl$^-$ BAr$_f^-$ requires a small amount of MeOH to dissolve in CD_2Cl_2, it could be argued that Figure 4.14 represents an unfair comparison of the hydrogen bonding characteristics of the two diastereomers. For this reason, the ^{1}H NMR spectra were also recorded in acetone-d_6, in which both complexes are highly soluble. The comparative analysis, depicted in Figure 4.15, shows the same general hydrogen bonding characteristics for the two diastereomers as was seen in Figure 4.14. For the Λ-diastereomer, the downfield shifted peak at 8.28 ppm indicates that the strong C_3 N-H···Cl$^-$ is not disrupted by the hydrogen bond accepting acetone. However, the C_2 N-H units (5.21 ppm) are shifted downfield compared to those depicted in Figure 4.14a, possibly due to hydrogen bonding interactions with acetone. For the Δ-diastereomer

(Figure 4.15b), the difference in chemical shift between the C_3 and C_2 N-H peaks is again smaller with the C_3 N-H unit appearing at only 7.12 ppm.

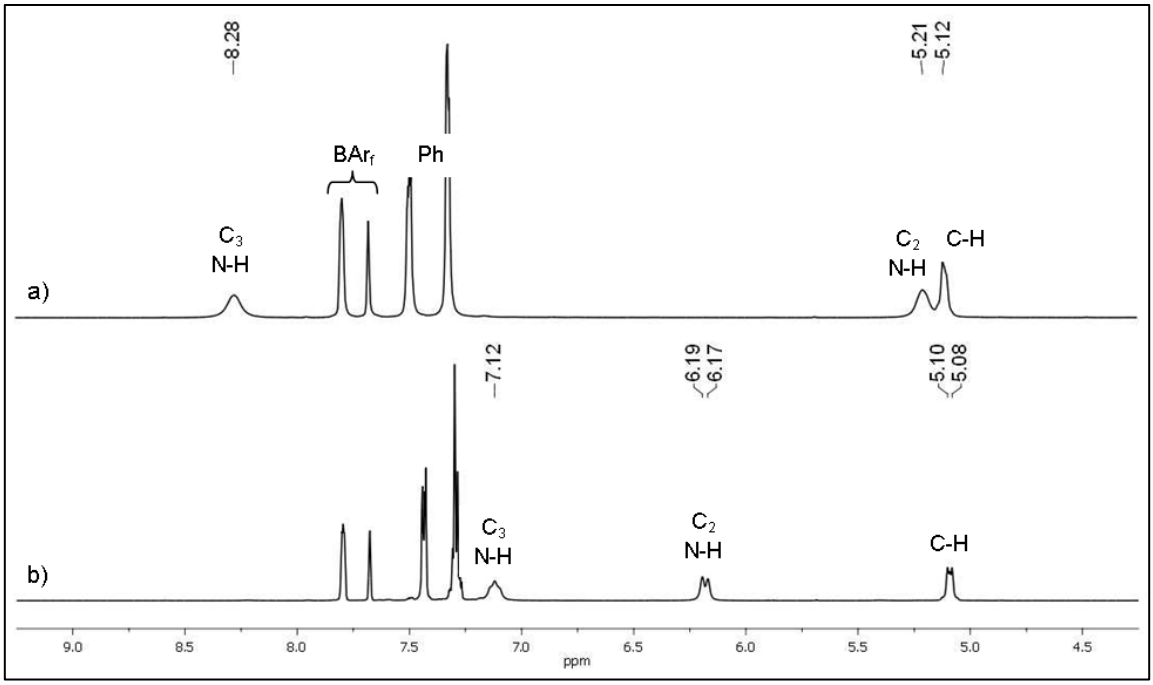

Figure 4.15. The ^{1}H NMR spectra (acetone-d_6) of a) Λ-(*S*,*S*)-**3**$^{3+}$ 2Cl$^-$ BAr$_f^-$ and b) Δ-(*S*,*S*)-**3**$^{3+}$ 2Cl$^-$ BAr$_f^-$.

4.2.5 The introduction of additional non-coordinating counteranions

The two Cl$^-$ counteranions of Λ-(*S*,*S*)-**3**$^{3+}$ 2Cl$^-$ BAr$_f^-$ could be replaced with weakly coordinating and hydrogen bonding counteranions by metathesis with silver salts. The salt Λ-(*S*,*S*)-**3**$^{3+}$ 2BF$_4^-$ BAr$_f^-$ was prepared by adding Ag$^+$ BF$_4^-$ to a solution of Λ-(*S*,*S*)-**3**$^{3+}$ 2Cl$^-$ BAr$_f^-$ in CH_2Cl_2. In this case, Ag$^+$ BF$_4^-$ has no appreciable solubility in CH_2Cl_2 and no reaction takes place when it is initially added. However, after sonicating the heterogeneous mixture for ten minutes, the colorless crystalline Ag$^+$

BF_4^- is replaced by a new powdery white precipitate of Ag^+ Cl^-. After filtration and solvent removal, the product is obtained as an orange-yellow crystalline solid in 96% yield.

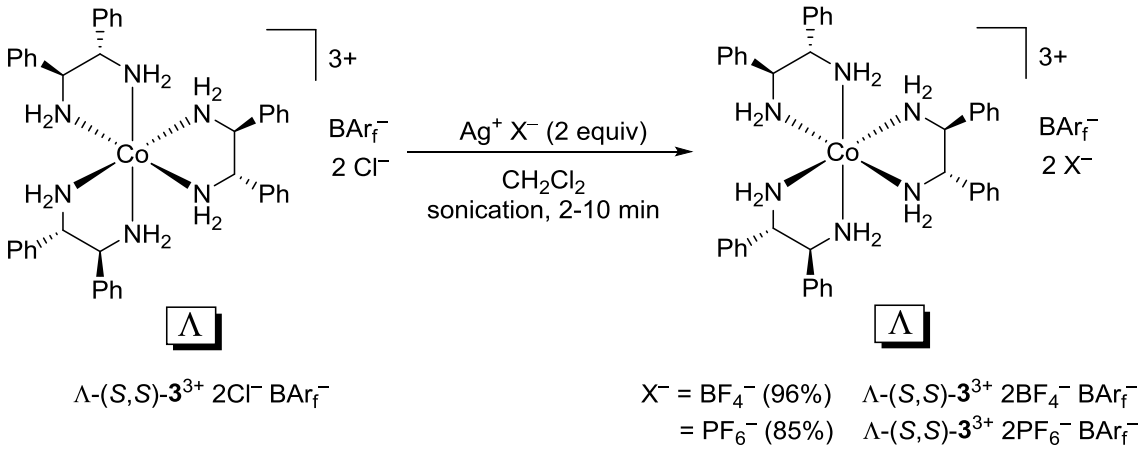

Scheme 4.5. The exchange of Cl^- with additional non-coordinating anions.

The $^{13}C\{^1H\}$ NMR spectrum reveals, among other signals, a single $\underline{C}HNH_2$ peak at 64.5 ppm, which strongly suggests that the new salt is still a single diastereomer. The ^{19}F NMR spectrum demonstrates the expected 3:1 integration for the BAr_f^-/BF_4^- fluorine atoms, indicating a 1:2 ratio of BAr_f^-/BF_4^- counteranions. The elemental analysis data are consistent for both the dihydrate Λ-(*S*,*S*)-**3**$^{3+}$ $2BF_4^-$ $BAr_f^-\cdot 2H_2O$ and the trihydrate Λ-(*S*,*S*)-**3**$^{3+}$ $2BF_4^-$ $BAr_f^-\cdot 3H_2O$.

The analogous Λ-(*S*,*S*)-**3**$^{3+}$ $2PF_6^-$ BAr_f^- salt is prepared by combining CH_2Cl_2 solutions of Λ-(*S*,*S*)-**3**$^{3+}$ $2Cl^-$ BAr_f^- and Ag^+ PF_6^-. The resulting Ag^+ Cl^- precipitate is removed by filtration and the cobalt complex is isolated after solvent removal as a crystalline yellow solid in 85% yield. The $^{13}C\{^1H\}$ NMR spectrum reveals, among other signals, a single $\underline{C}HNH_2$ peak at 64.0 ppm, which strongly suggests that the new salt still

exists as a single diasteromer. The ^{19}F NMR demonstrates a 2:1 integration of BAr_f^- /PF_6^- fluorine atoms, indicating a 1:2 ratio of BAr_f^-/PF_6^- counteranions. The elemental analysis data are consistent for both anhydrous Λ-(*S*,*S*)-**3**$^{3+}$ 2PF_6^- BAr_f^- and the monohydrate Λ-(*S*,*S*)-**3**$^{3+}$ 2PF_6^- BAr_f^-·H_2O.

4.2.5.1 The effect of the counteranion on hydrogen bonding

The ^1H NMR spectra of Λ-(*S*,*S*)-**3**$^{3+}$ 2Cl^- BAr_f^-, Λ-(*S*,*S*)-**3**$^{3+}$ 2BF_4^- BAr_f^-, and Λ-(*S*,*S*)-**3**$^{3+}$ 2PF_6^- BAr_f^- are compared in Figure 4.16. Replacing the two strong hydrogen bond accepting Cl^- anions with two poorly coordinating anions creates a significant upfield shift in the C_3 N-H peaks. In the absence of the N-H···Cl^- interaction, the C_3 N-H chemical shift relaxes into a more normal position. Notably, the C_3 N-H chemical shift of Λ-(*S*,*S*)-**3**$^{3+}$ 2BF_4^- BAr_f^- (6.04 ppm) appears slightly more downfield than the corresponding peak of Λ-(*S*,*S*)-**3**$^{3+}$ 2PF_6^- BAr_f^- (5.77 ppm), indicating that the BF_4^- anion still engages in weak hydrogen bonding. As a consequence of the diminished hydrogen bonding interactions at the C_3 face, the C_2 N-H peaks experience a downfield shift in the ^1H NMR spectra.

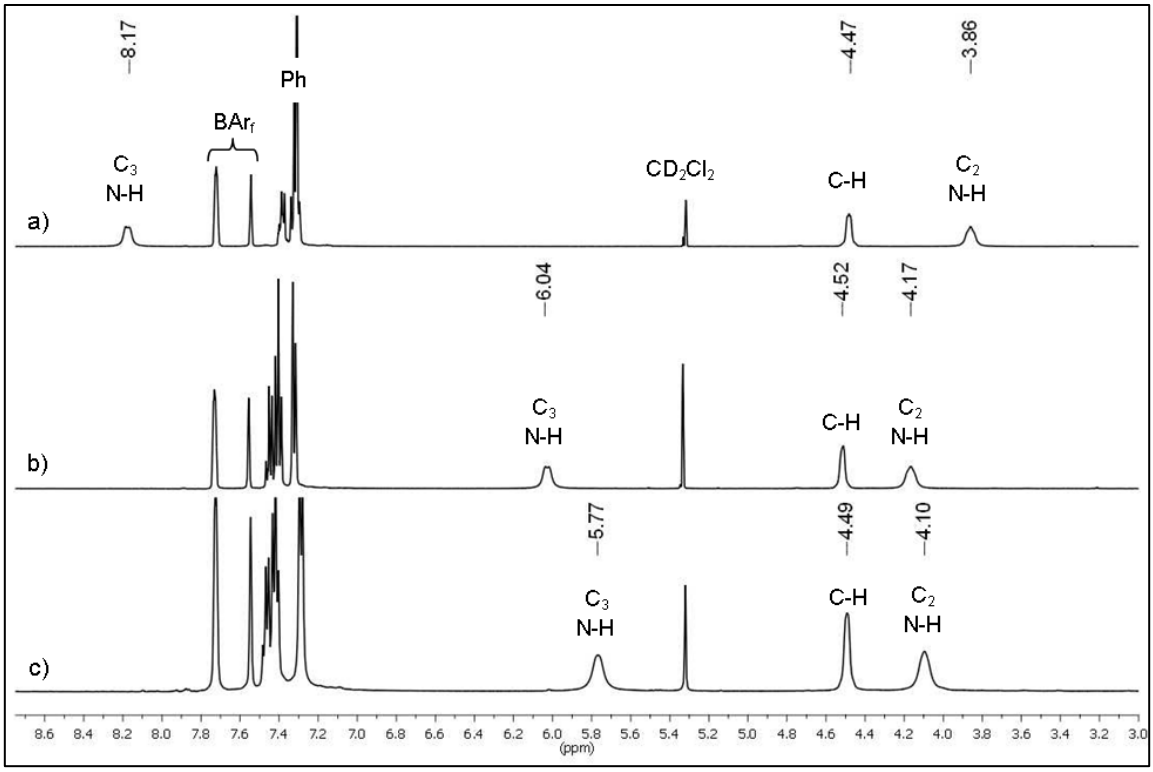

Figure 4.16. The ^{1}H NMR spectra (CD_2Cl_2) of a) Λ-(*S*,*S*)-**3**$^{3+}$ 2Cl$^-$ BAr$_f^-$, b) Λ-(*S*,*S*)-**3**$^{3+}$ 2BF$_4^-$ BAr$_f^-$, and c) Λ-(*S*,*S*)-**3**$^{3+}$ 2PF$_6^-$ BAr$_f^-$.

4.2.6 The introduction of a chiral counteranion

The ammonium salt of (+)-3-bromocamphor-8-sulfonic acid (**5**; camphSO$_3^+$ NH$_4^-$) was used to replace the Cl$^-$ anions of Λ-(*S*,*S*)-**3**$^{3+}$ 2Cl$^-$ BAr$_f^-$, as shown in Scheme 4.6. A biphasic anion exchange method was employed in which a solution of **5** in H_2O was vigorously stirred over a solution of Λ-(*S*,*S*)-**3**$^{3+}$ 2Cl$^-$ BAr$_f^-$ in CH_2Cl_2. The newly formed NH$_4^+$ Cl$^-$ was removed with the aqueous phase and Λ-[Co((*S*,*S*)-dpen)$_3$]$^{3+}$ 2camphSO$_3^-$ BAr$_f^-$ (Λ-(*S*,*S*)-**3**$^{3+}$ 2camphSO$_3^-$ BAr$_f^-$) was isolated from the CH_2Cl_2 phase and chromatographed on silica gel. Although an excess of four equivalents of **5** were used, only the two Cl$^-$ anions were exchanged under these

conditions. Considering the high yield of the BAr_f^- containing salt, there was not a significant anion exchange between **5** and BAr_f^-.

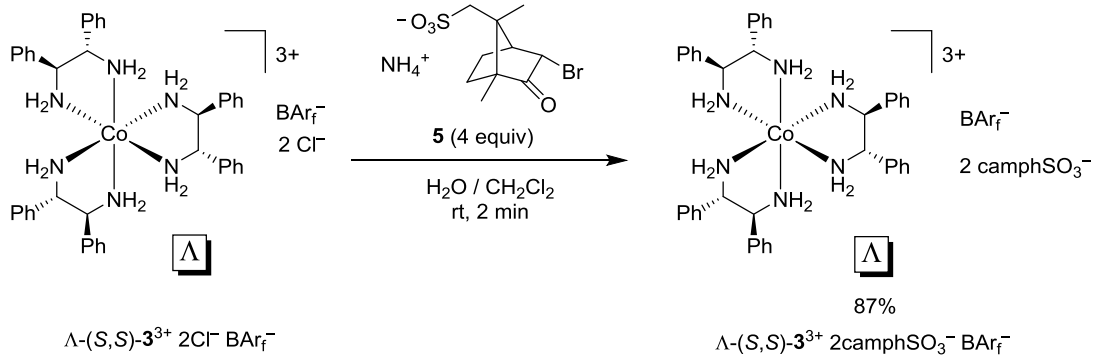

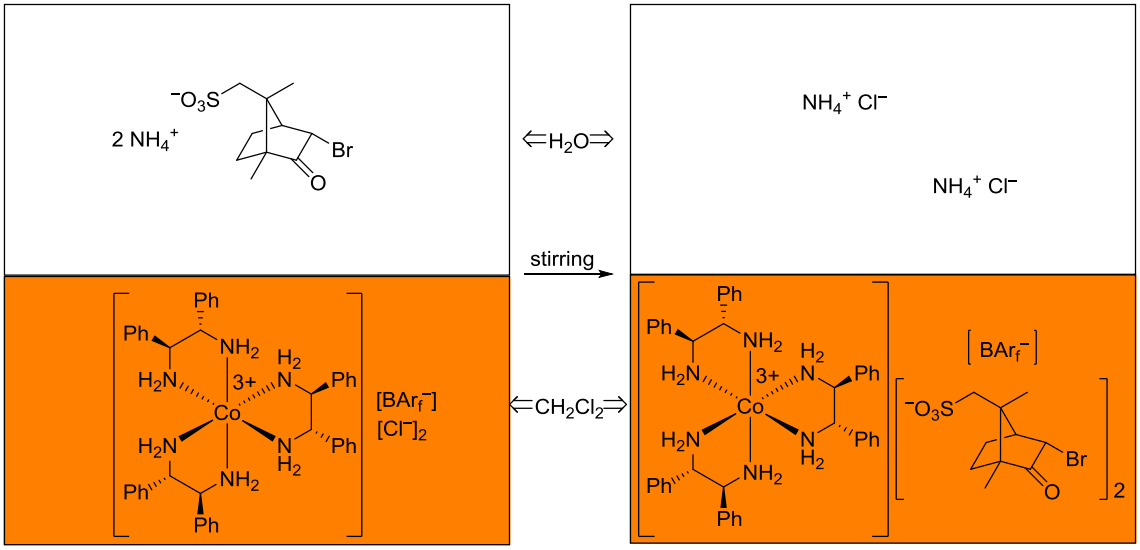

Scheme 4.6. The biphasic exchange of the chloride ions of Λ-(*S*,*S*)-**3**$^{3+}$ 2Cl$^-$ BAr_f^- with a chiral anion.

In the ^{1}H NMR spectrum of the product, which is shown in Figure 4.17, the C_3 N-H peak appears at 7.89 ppm, indicating a strong hydrogen bonding interaction with the alkyl sulfonate groups of the counteranion. The $^{13}C\{^1H\}$ NMR spectrum reveals, among other signals, a single $\underline{C}HNH_2$ peak at 63.2 ppm, which strongly suggests that the complex exists as a single diastereomer. The elemental analysis fits within the

acceptable range for both anhydrous Λ-(*S*,*S*)-**3**$^{3+}$ 2camphSO$_3^-$ BAr$_f^-$ and the monohydrate Λ-(*S*,*S*)-**3**$^{3+}$ 2camphSO$_3^-$ BAr$_f^-$·H$_2$O.

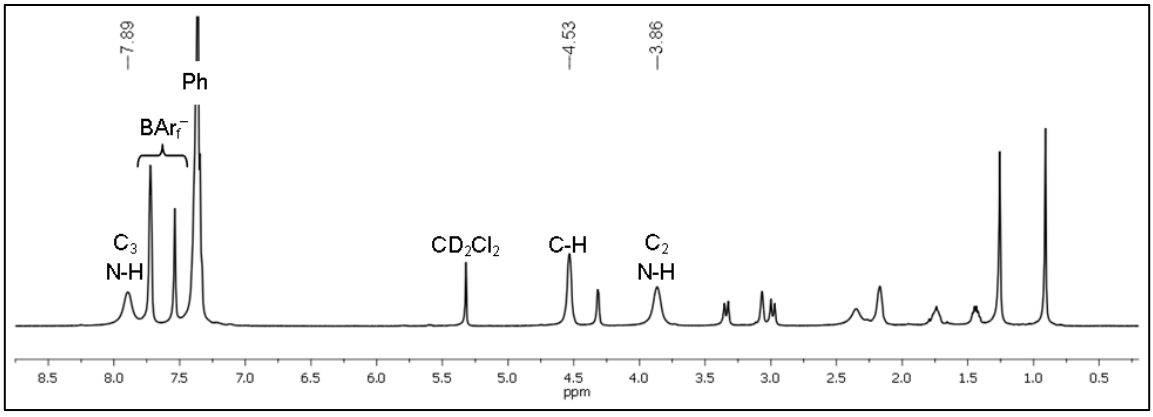

Figure 4.17. The ^{1}H NMR spectrum (CD$_2$Cl$_2$) of Λ-(*S*,*S*)-**3**$^{3+}$ 2camphSO$_3^-$ BAr$_f^-$.

4.2.7 The synthesis of Co(III) complexes with functionalized dpen ligands

The synthesis of Co(III) complexes with (*S*,*S*)-dpen ligands that contain extra functionalities would result in a broad family of related complexes with tunable electronic and steric features. For instance, a dpen ligand with electron withdrawing groups would have more acidic NH$_2$ groups and likely form stronger hydrogen bonds, while a dpen ligand with electron donating groups is expected to form weaker hydrogen bonds. Also, a bulky dpen ligand could provide controlled steric crowding around the hydrogen bonding sites.

A very clever route to substituted (*S*,*S*)-dpen ligands was previously reported and is depicted in Scheme 4.7.[89] The synthesis involves initial formation of a diimine with commercially available (*R*,*R*)-1,2-bis-(2-hydroxyphenyl)-1,2-diaminoethane ((*R*,*R*)-**6**) and a corresponding aldehyde. A spontaneous stereospecific aza-Cope rearrangement of

the diimine, followed by hydrolysis, results in a new disubstituted diamine in the (*S*,*S*) configuration. Therefore, from a single "mother diamine", a series of enantiopure "daughter diamines" can be prepared by introducing different aldehydes, abundant numbers of which are commercially available. In this way, four functionalized (*S*,*S*)-dpen ligands were prepared, including an electron rich ((*S*,*S*)-**7**), a strongly electron withdrawing ((*S*,*S*)-**8**), a weakly electron withdrawing ((*S*,*S*)-**9**), and a bulky diamine ligand ((*S*,*S*)-**10**).

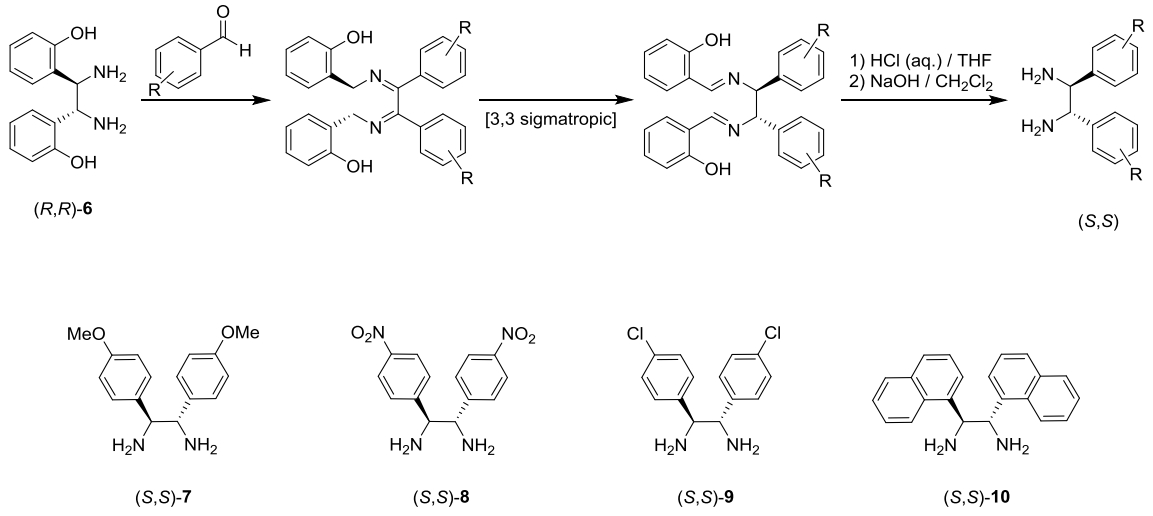

Scheme 4.7. The modular synthesis of functionalized (*S*,*S*)-dpen ligands.

4.2.7.1 The synthesis of cobalt complexes with (S,S)-p-OMe-dpen ((S,S)-7) ligands

The *para*-methoxy substituted ligand (*S*,*S*)-**7** represents a moderately electron rich derivative of the dpen ligands. The Hammett constant for a methoxy group in the *para* position is –0.12 (σ_p).[90] The synthesis of diastereomeric Co(III) complexes with (*S*,*S*)-**7** ligands is depicted in Scheme 4.8. The synthesis beginning with $Co(OAc)_2 \cdot 4H_2O$

ultimately led to Λ-[Co((*S*,*S*)-*p*-OMe-dpen)$_3$]$^{3+}$ 2Cl$^-$ BAr$_f^-$ (Λ-(*S*,*S*)-**11**$^{3+}$ 2Cl$^-$ BAr$_f^-$) after anion metathesis and column chromatography. According to the elemental analysis, the compound is also isolated with three coordinated water molecules so that the complex is best represented as the trihydrate Λ-(*S*,*S*)-**11**$^{3+}$ 2Cl$^-$ BAr$_f^-$·3H$_2$O.

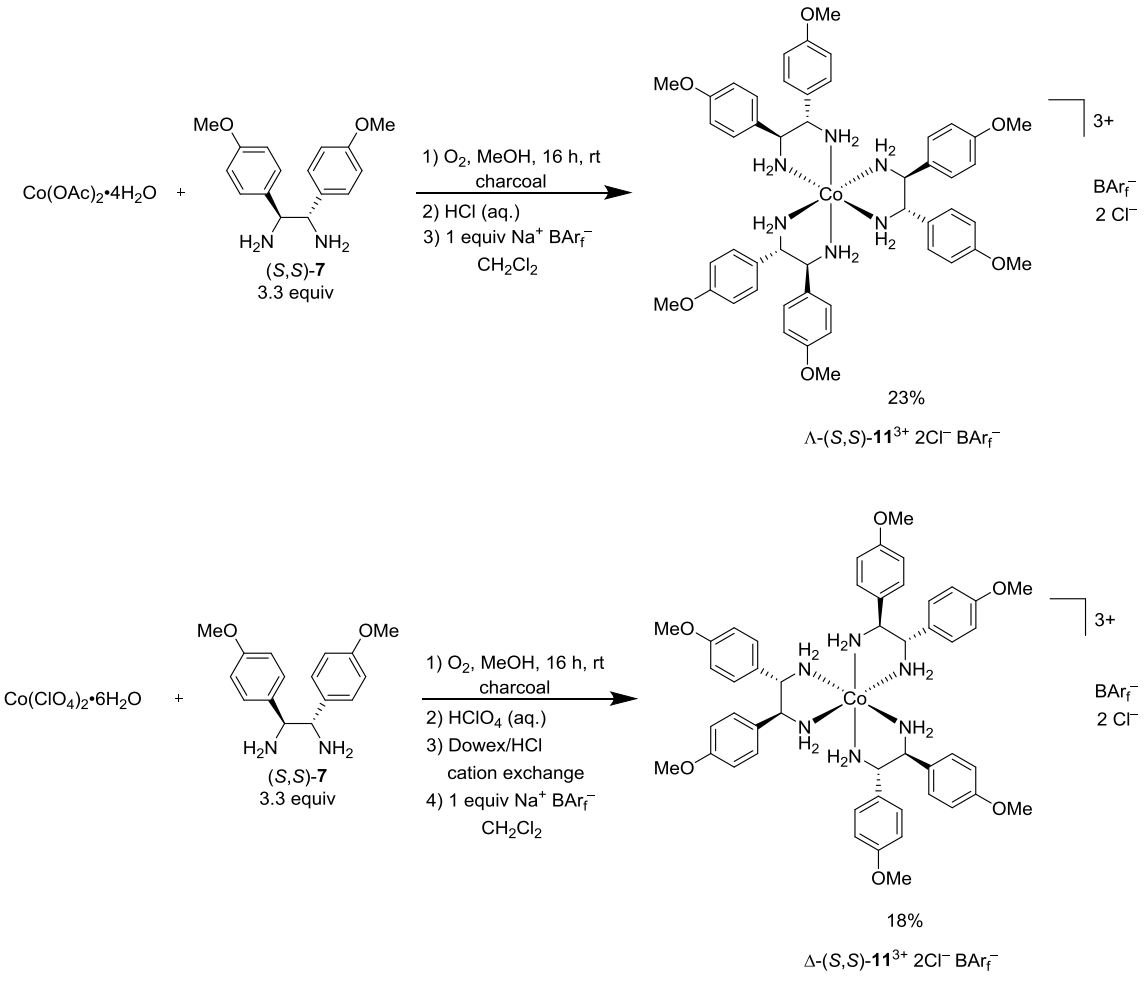

Scheme 4.8. The synthesis of Λ and Δ-(*S*,*S*)-**11**$^{3+}$ 2Cl$^-$ BAr$_f^-$.

The ^{1}H NMR spectrum of Λ-(*S*,*S*)-**11**$^{3+}$ 2Cl$^-$ BAr$_f^-$, depicted in Figure 4.18, shows two separate peaks for the two sets of diastereotopic N-H units. Notably, the more

downfield peak, which results from the strong C_3 N-H···Cl^- hydrogen bonding interaction, appears at 7.67 ppm. Compared to the analogous C_3 N-H peak of Λ-(*S*,*S*)-**3**$^{3+}$ 2Cl^- BAr_f^- (8.17 ppm, Figure 4.15), this indicates a somewhat weaker, but still substantial, cation-anion hydrogen bonding interaction. This is likely due to the electron rich character of the (*S*,*S*)-**7** ligands, which could make Λ-(*S*,*S*)-**11**$^{3+}$ 2Cl^- BAr_f^- a poorer hydrogen bond donor. The $^{13}C\{^1H\}$ NMR spectrum reveals, among other signals, a single $\underline{C}HNH_2$ peak at 62.9 ppm, which strongly suggests that the isolated complex exists as a single diastereomer.

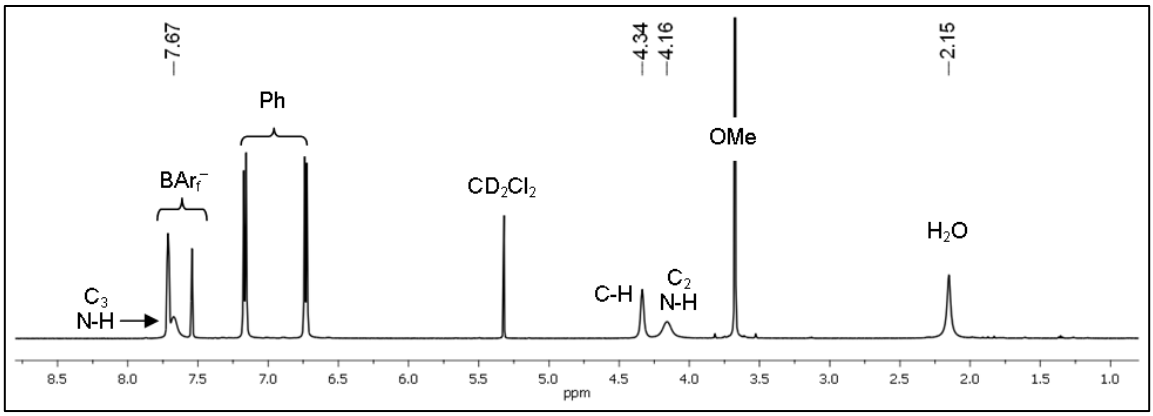

Figure 4.18. The ^1H NMR spectrum of Λ-(*S*,*S*)-**11**$^{3+}$ 2Cl^- BAr_f^- in CD_2Cl_2.

The other diastereomer, Δ-(*S*,*S*)-**11**$^{3+}$ 2Cl^- BAr_f^-, was also prepared according to Scheme 4.8, beginning from $Co(ClO_4)_2 \cdot 6H_2O$ in an overall 18% yield. Like Δ-(*S*,*S*)-**3**$^{3+}$ 2Cl^- BAr_f^-, Δ-(*S*,*S*)-**11**$^{3+}$ 2Cl^- BAr_f^- is mostly insoluble in CD_2Cl_2. A small amount of CD_3OD was added to make a homogeneous solution for NMR analysis. The ^1H NMR spectrum shows peaks for the two diastereotopic N-H moieties at 5.82 and 5.67 ppm. The ^{13}C NMR spectrum reveals, among other signals, a single $\underline{C}HNH_2$ peak at 64.9 ppm, which strongly suggests that the complex is isolated as a single diasteromer that is

unique from Λ-(*S*,*S*)-**11**$^{3+}$ 2Cl$^-$ BAr$_f^-$. The elemental analysis data are consistent with two molecules of coordinated water so that the complex is best represented as the dihydrate Δ-(*S*,*S*)-**11**$^{3+}$ 2Cl$^-$ BAr$_f^-$·2H$_2$O.

It should be noted here that there is no absolute structural proof for the stereochemical assignments for the complexes isolated in Scheme 4.8. However, Λ and Δ-(*S*,*S*)-**11**$^{3+}$ 2Cl$^-$ BAr$_f^-$ each possess unique properties that were also observed to be differentiating features for the diastereomers of Λ and Δ-(*S*,*S*)-**3**$^{3+}$ 2Cl$^-$ BAr$_f^-$. These include the above mentioned NMR characteristics (chemical shift trends, $\underline{C}$HNH$_2$ ^{13}C{^{1}H} signals) as well as the observation that both complexes with the Δ configuration are poorly soluble in CH$_2$Cl$_2$. Also, the similarity between measured optical rotations ([α]$_{18}^{546}$ = 23.1°/25.0° Λ-(*S*,*S*)-**3**$^{3+}$ 2Cl$^-$ BAr$_f^-$/Λ-(*S*,*S*)-**11**$^{3+}$ 2Cl$^-$ BAr$_f^-$) and ([α]$_{18}^{546}$ = –419.0°/–516.4° Δ-(*S*,*S*)-**3**$^{3+}$ 2Cl$^-$ BAr$_f^-$/Δ-(*S*,*S*)-**11**$^{3+}$ 2Cl$^-$ BAr$_f^-$) provides additional support for the stereochemical assignment.

*4.2.7.2 The synthesis of cobalt complexes with (S,S)-p-NO$_2$-dpen ((S,S)-**8**) ligands*

A synthesis was attempted with the strongly electron withdrawing, *para*-nitro substituted ligand, (*S*,*S*)-**8**. The Hammett constant for a nitro group in the para position is 0.81 (σ_p).[90] The procedure in Scheme 4.9 beginning with Co(OAc)$_2$·4H$_2$O was investigated. However, after acidifying with HCl, the crude product was isolated as a bright green solid rather than the customary orange solid. The colors of cobalt complexes are very sensitive to the oxidation state of the metal and the arrangement and type of coordinated ligands. There is an extensive literature of monocations of the type *trans*-[Co(1,2-diamine)$_2$Cl$_2$]$^+$ X$^-$, with diamines ranging from ethylenediamine[91] to dpen.[53] In all cases, these are isolated as bright green solids, consistent with (*S*,*S*)-**4**$^+$

BAr_f^- in Scheme 4.4, which was isolated as a minor product. Hence, the product in Scheme 4.9 is provisionally assigned the structure *trans*-$[Co((S,S)\text{-}p\text{-}NO_2\text{-dpen})_2Cl_2]^+$ Cl^-. This is consistent with the reduced Lewis basicity of (*S*,*S*)-**8**, which makes it a poorer ligand for Co(III) complexes, allowing appropriate counteranions to compete for binding to the metal. Under the conditions studied, only two (*S*,*S*)-**8** ligands are able to coordinate to the metal at one time.

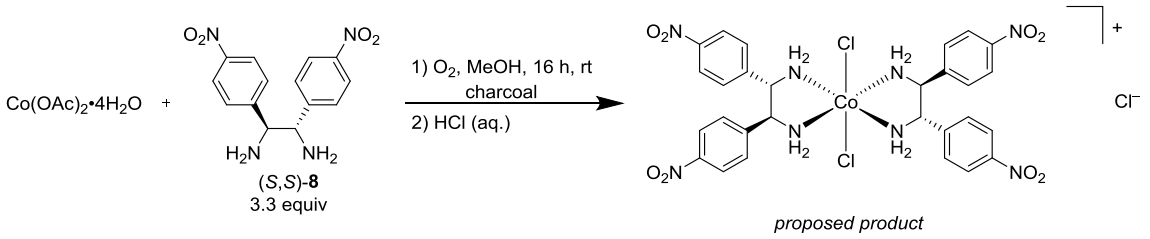

Scheme 4.9. The attempted synthesis of Λ-$[Co((S,S)\text{-}p\text{-}NO_2\text{-dpen})_3]^{3+}$ $2Cl^-$ BAr_f^-

*4.2.7.3 The synthesis of cobalt complexes with (S,S)-p-Cl-dpen ((S,S)-**9**) ligands*

The *para*-chloro substituted (*S*,*S*)-dpen ligand, (*S*,*S*)-**9**, represents a less electron withdrawing alternative to (*S*,*S*)-**8**. The Hammett constant of a chloro group in the *para* position is 0.24 (σ_p).[90] The synthesis from $Co(OAc)_2{\cdot}4H_2O$ successfully yielded Λ-$[Co((S,S)\text{-}p\text{-Cl-dpen})_3]^{3+}$ $2Cl^-$ BAr_f^- (Λ-(*S*,*S*)-$\mathbf{12}^{3+}$ $2Cl^-$ BAr_f^-), which was isolated as an orange solid in 34% yield. The stereochemical assignment is made by analogy to Λ-(*S*,*S*)-$\mathbf{3}^{3+}$ $2Cl^-$ BAr_f^-, based on similarities in the ^1H and $^{13}C\{^1H\}$ NMR spectra.

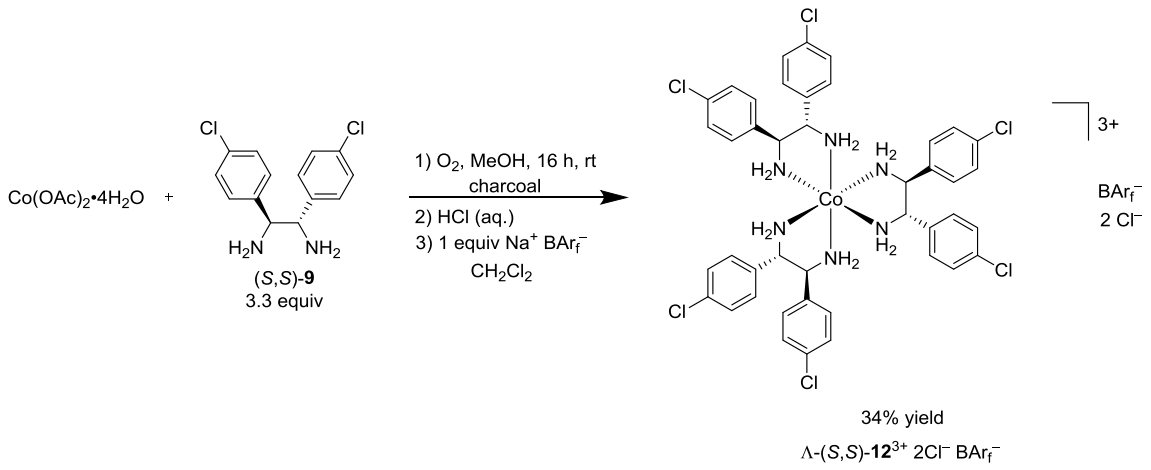

Scheme 4.10. The synthesis of Λ-(*S*,*S*)-**12**$^{3+}$ 2Cl^{-} BAr$_f^{-}$.

The complex formed a homogeneous CD_2Cl_2 solution and the ^{1}H NMR spectrum revealed the diagnostic downfield shifted N-H peak that is expected for the Λ diastereomer at 7.98 ppm. An overnight $^{13}C\{^1H\}$ NMR spectrum was recorded. After the first hour, the preliminary scans suggested that there was only one $\underline{C}HNH_2$ peak at 62.4 ppm, as seen in Figure 4.19 (bottom). However, the final spectrum after 12 hours revealed that a second peak at 65.6 ppm of greater intensity had developed. Meanwhile, a significant amount of solid had precipitated in the NMR tube. In all previous cases, the Δ-diastereomer is less soluble in CD_2Cl_2 than the corresponding Λ-diastereomer and requires a polar additive to form a homogeneous solution. From this, and the gradual development of a second signal in the $^{13}C\{^1H\}$ NMR spectrum that is shifted approximately 3 ppm downfield, it seemed most likely that the isolated Λ complex had epimerized to the Δ complex during the course of the data acquisition. Although the tris-chelated complex Λ-(*S*,*S*)-**12**$^{3+}$ 2Cl^{-} BAr$_f^{-}$ is initially isolated, its ready isomerization in a non-coordinating solvent at room temperature compromised its efficacy as an enantioselective catalyst and it was not studied further.

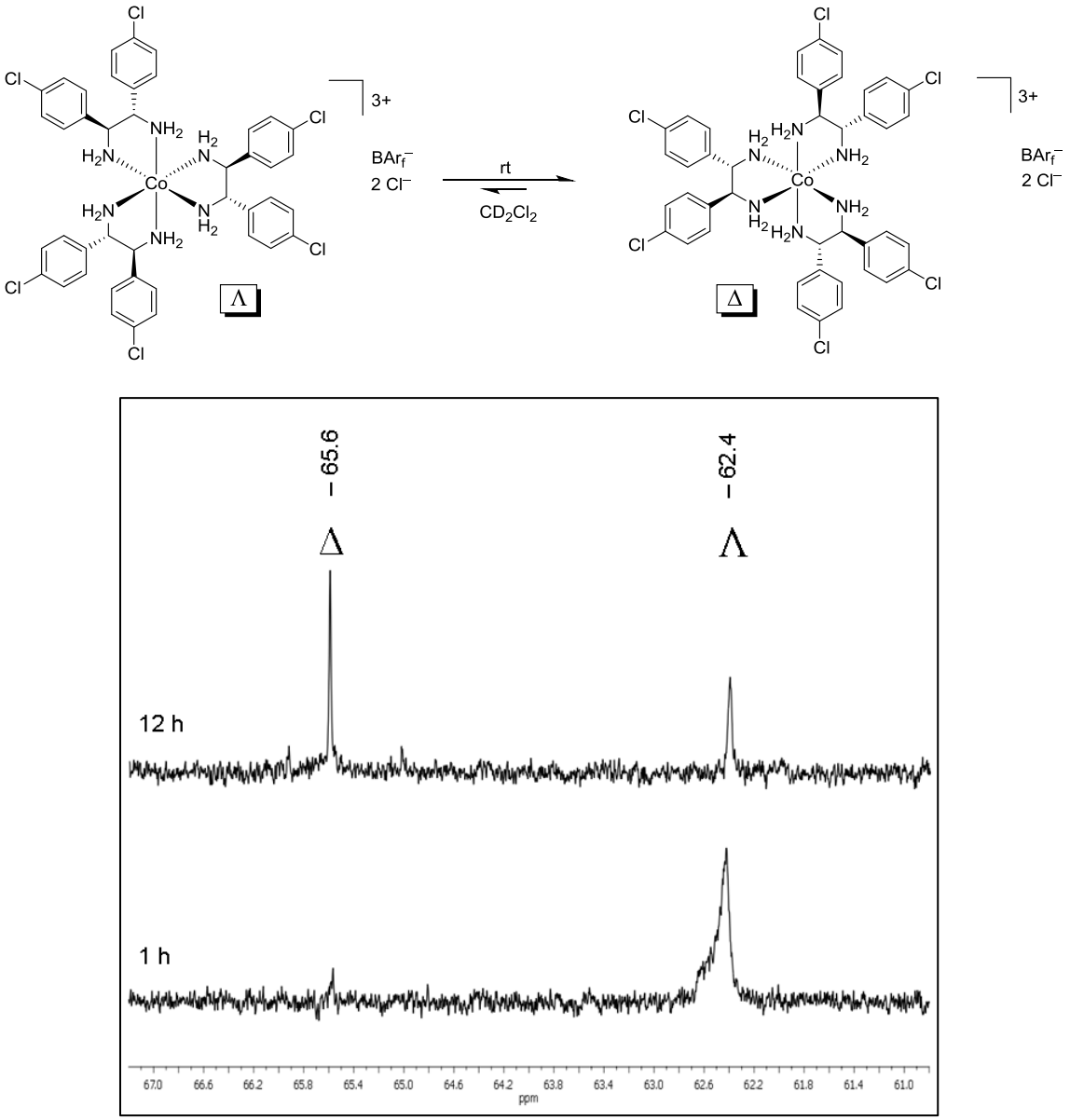

Figure 4.19. The isomerization of Λ-(*S*,*S*)-**12**$^{3+}$ 2Cl^{-} BAr$_f^{-}$ in CD_2Cl_2 at room temperature during a single overnight $^{13}C\{^1H\}$ experiment.

*4.2.7.4 The synthesis of a cobalt complex with (S,S)-1-dnen ((S,S)-**10**, dnen = 1,2-di(1-naphthyl)ethylenediamine) ligands*

The synthesis of a tris-chelating Co(III) complex with the bulky diamine ligand, (*S*,*S*)-**10**, was also achieved as seen in Scheme 4.11. Some particular details distinguish this synthesis from those of other Λ-[Co((*S*,*S*)-dpen)$_3$]$^{3+}$ 3X$^-$ type complexes. Notably, the addition of aqueous HCl immediately precipitated a bright yellow solid, presumably consisting primarily of Λ-[Co((*S*,*S*)-1-dnen)$_3$]$^{3+}$ 3Cl$^-$ (Λ-(*S*,*S*)-**13**$^{3+}$ 3Cl$^-$), suggesting that this trichloride salt is uniquely insoluble in MeOH. The subsequent anion metathesis with Na$^+$ BAr$_f^-$ proceeded as expected and the mixture was chromatographed on silica gel. A bright green band was eluted with CH_2Cl_2 to give *trans*-[Co((*S*,*S*)-1-dnen)$_2$Cl$_2$]$^+$ BAr$_f^-$ (12%). A dark orange band was then eluted with 98:2 v/v CH_2Cl_2/MeOH to give Λ-[Co((*S*,*S*)-1-dnen)$_3$]$^{3+}$ 2Cl$^-$ BAr$_f^-$ (Λ-(*S*,*S*)-**13**$^{3+}$ 2Cl$^-$ BAr$_f^-$, 45%) The stereochemical assignment of Λ-(*S*,*S*)-**13**$^{3+}$ 2Cl$^-$ BAr$_f^-$ was made by analogy to Λ-(*S*,*S*)-**3**$^{3+}$ 2Cl$^-$ BAr$_f^-$ based on similarities in the ^{1}H and ^{13}C{^{1}H} NMR spectra. There was no evidence of the formation or isolation of the Δ-diastereomer in this procedure.

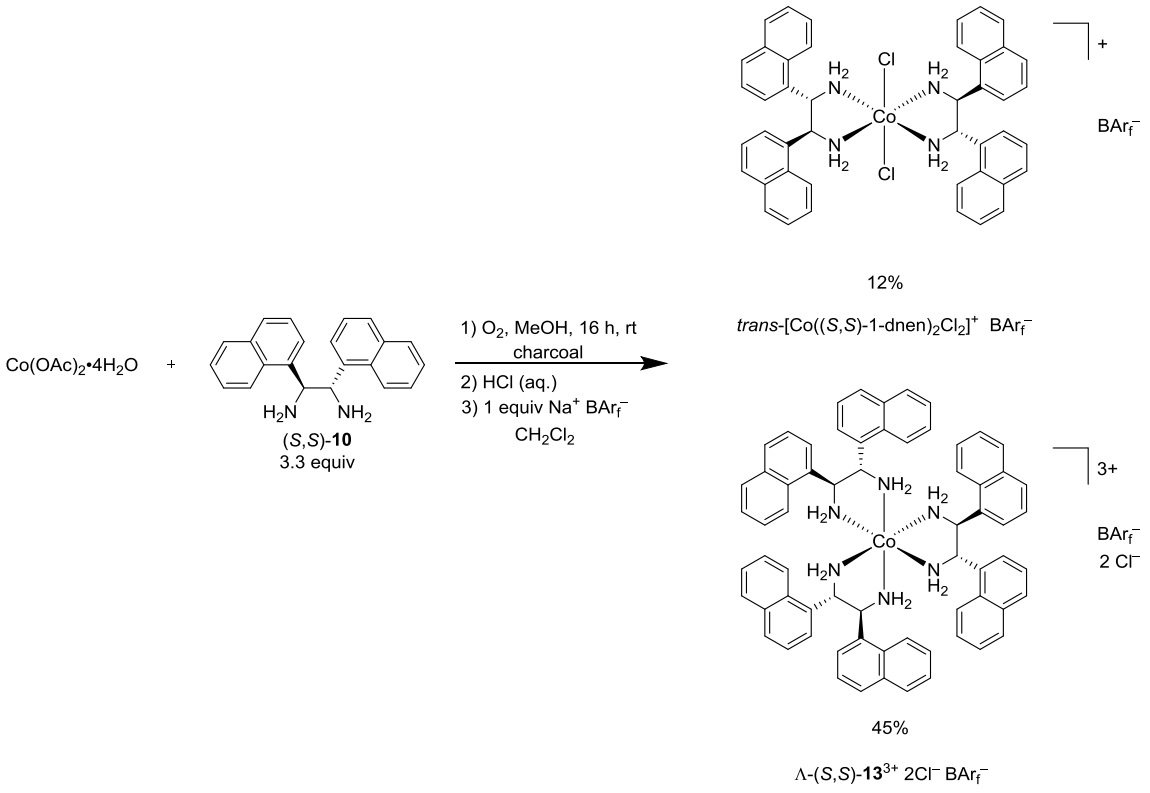

Scheme 4.11. The synthesis of Λ-(*S*,*S*)-**13**$^{3+}$ 2Cl^{-} BAr$_f^{-}$.

The ^{1}H NMR spectrum of Λ-(*S*,*S*)-**13**$^{3+}$ 2Cl^{-} BAr$_f^{-}$ is shown in Figure 4.20a. The C_3 N-H peak (9.73 ppm) appears significantly more downfield than the corresponding peak of Λ-(*S*,*S*)-**3**$^{3+}$ 2Cl^{-} BAr$_f^{-}$ (Figure 4.14a). This indicates a stronger hydrogen bonding interaction at the C_3 face, and/or a deshielding effect of the more spatially extended naphthyl system. The ^{13}C{^{1}H} spectrum, among other peaks, reveals only a single C$\underline{\text{H}}$NH$_2$ peak at 59.7 ppm, which strongly suggests that the complex exists as a single isomer. The elemental analysis and the integration of the H_2O peak in the ^{1}H NMR spectrum of the isolated material are consistent for the dihydrate Λ-(*S*,*S*)-**13**$^{3+}$ 2Cl^{-} BAr$_f^{-}$·2H_2O.

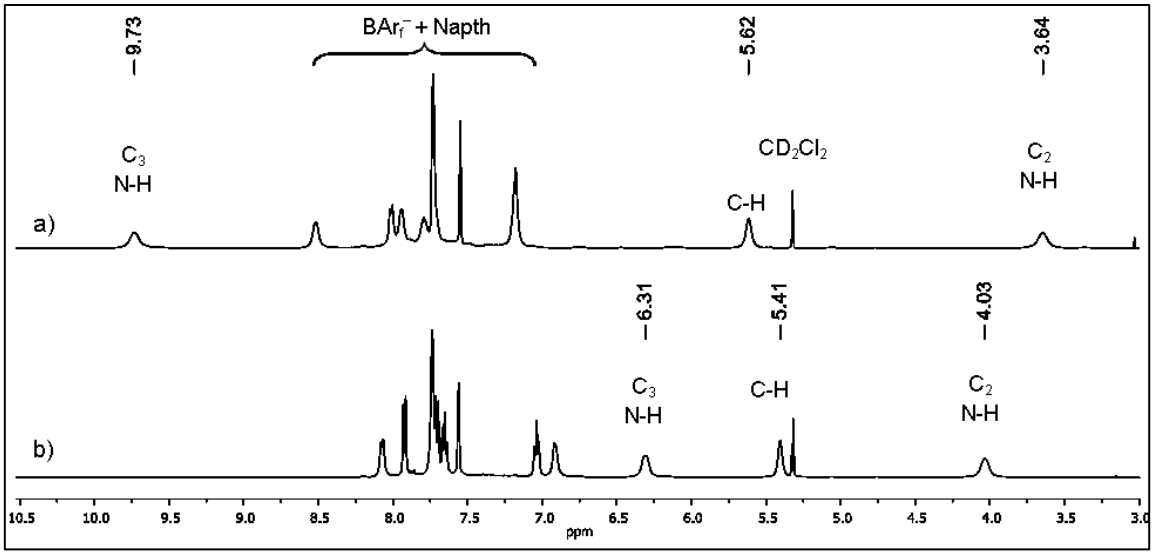

Figure 4.20. The ^{1}H NMR spectra (CD_2Cl_2) of a) Λ-(*S*,*S*)-**13**$^{3+}$ 2Cl$^-$ BAr$_f^-$ and b) Λ-(*S*,*S*)-**13** $^{3+}$ 2BF$_4^-$ BAr$_f^-$.

The two Cl$^-$ counteranions of Λ-(*S*,*S*)-**13**$^{3+}$ 2Cl$^-$ BAr$_f^-$ were replaced with the poor hydrogen bond accepting BF$_4^-$ anions, as depicted in Scheme 4.12. The ^{1}H NMR spectrum of Λ-(*S*,*S*)-**13**$^{3+}$ 2BF$_4^-$ BAr$_f^-$ is illustrated in Figure 4.20b. The C_3 N-H peak shifts to a more natural position of 6.31 ppm. This indicates that the strong C_3 N-H···Cl$^-$ hydrogen bond has been replaced by a weaker anion interaction. The corresponding signal in Λ-(*S*,*S*)-**3**$^{3+}$ 2BF$_4^-$ BAr$_f^-$ is 6.04 ppm, suggesting that any naphthyl deshielding effect is modest (ca. 0.27 ppm). The isomer purity is maintained, as the ^{13}C{^{1}H} NMR spectrum reveals only one single $\underline{C}HNH_2$ peak at 59.4 ppm. The elemental analysis and the integration of the H_2O peak in the ^{1}H NMR spectrum are best fit by the trihydrate Λ-(*S*,*S*)-**13**$^{3+}$ 2BF$_4^-$ BAr$_f^-$·3H_2O.

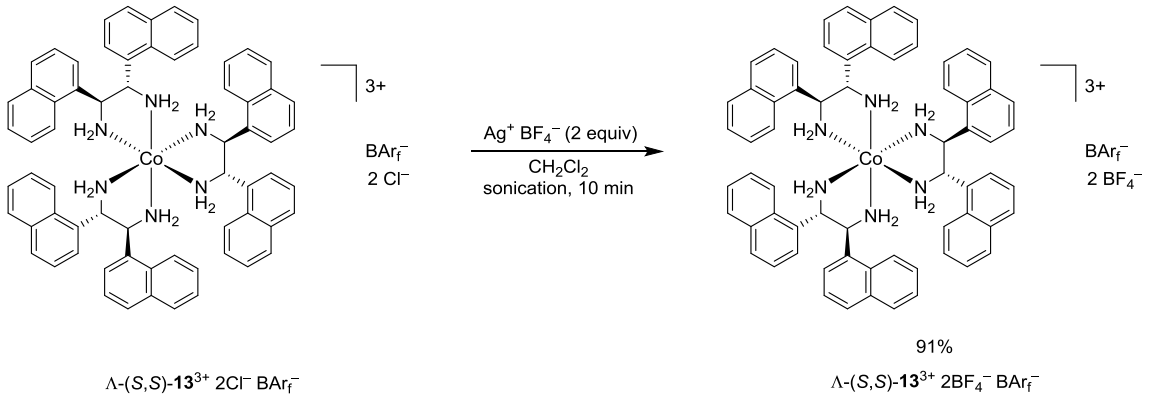

Scheme 4.12. The synthesis of Λ-(*S*,*S*)-**13**$^{3+}$ 2BF_4^- BAr_f^-.

4.2.8 Thermal isomerization studies of [Co(S,S)-dpen)$_3$]$^{3+}$ trications

In the syntheses of the [Co((*S*,*S*)-dpen)$_3$]$^{3+}$ trications, the preference for a particular metal configuration is strongly dependent on the complex counteranion. When Cl^- or AcO^- is the counteranion, the Λ-diastereomer is formed almost exclusively. However, Bosnich reported that Λ-(*S*,*S*)-**3**$^{3+}$ 3ClO_4^- completely isomerized to Δ-(*S*,*S*)-**3**$^{3+}$ 3ClO_4^- when refluxed in MeOH over charcoal for 3 hours (Scheme 4.3).[52a] Although Bosnich does not make this connection, it was conceived here that the preference for a particular metal configuration is influenced by hydrogen bonding interactions between the cobalt complex and the counteranion. Perhaps for a compact, strong hydrogen bond accepting anion such as Cl^-, the Λ-diastereomer is favored. In the presence of a relatively poor hydrogen bond accepting anion such as ClO_4^-, the Δ-diastereomer then appears to be favored.

The complex Λ-(*S*,*S*)-**3**$^{3+}$ 2BF_4^- BAr_f^-, which contains only poor hydrogen bond acceptors, was heated in DMSO-d_6 at 80 °C in the absence of charcoal. The progress of the isomerization is shown in Figure 4.21. The degree of isomerization is measured by

tracking the decrease of the Λ-diastereomer $^{13}C\{^1H\}$ peak at 61.4 ppm ($\underline{C}HNH_2$) and the increase of the corresponding Δ-diastereomer peak at 63.2 ppm. After one day at 80 °C, approximately 20% of the complex had isomerized to the Δ-diastereomer. The reaction continued at this temperature for several days and the relative amount of the Δ-diastereomer continued to increase. After 30 days, the isomerization had proceeded almost completely to Δ-(*S*,*S*)-**3**$^{3+}$ $2BF_4^-$ BAr_f^-. During this time, no additional peaks were observed in the $^{13}C\{^1H\}$ NMR spectrum, indicating a clean isomerization.

In a related experiment, the complex Δ-(*S*,*S*)-**3**$^{3+}$ $2Cl^-$ BAr_f^-, which contains two strong hydrogen bond accepting anions, was heated in DMSO-d_6 to 80 °C for 24 hours, as shown in Figure 4.22. During this time, no isomerization to the Λ-diastereomer was detected. Upon increasing the temperature to 110 °C, several additional peaks appeared in the region between 60-65 ppm. The color of the solution also changed from bright orange to green, which strongly indicates the formation of some (*S*,*S*)-**4**$^+$ BAr_f^- (Scheme 4.4). At this temperature, dpen substitution by Cl^- apparently competes with complex isomerization. The other peaks likely represent a mixture of *cis*-$[Co((S,S)\text{-dpen})_2Cl_2]^+$ BAr_f^-, Λ-(*S*,*S*)-**3**$^{3+}$ $2Cl^-$ BAr_f^-, and the free ligand (*S*,*S*)-**2**.

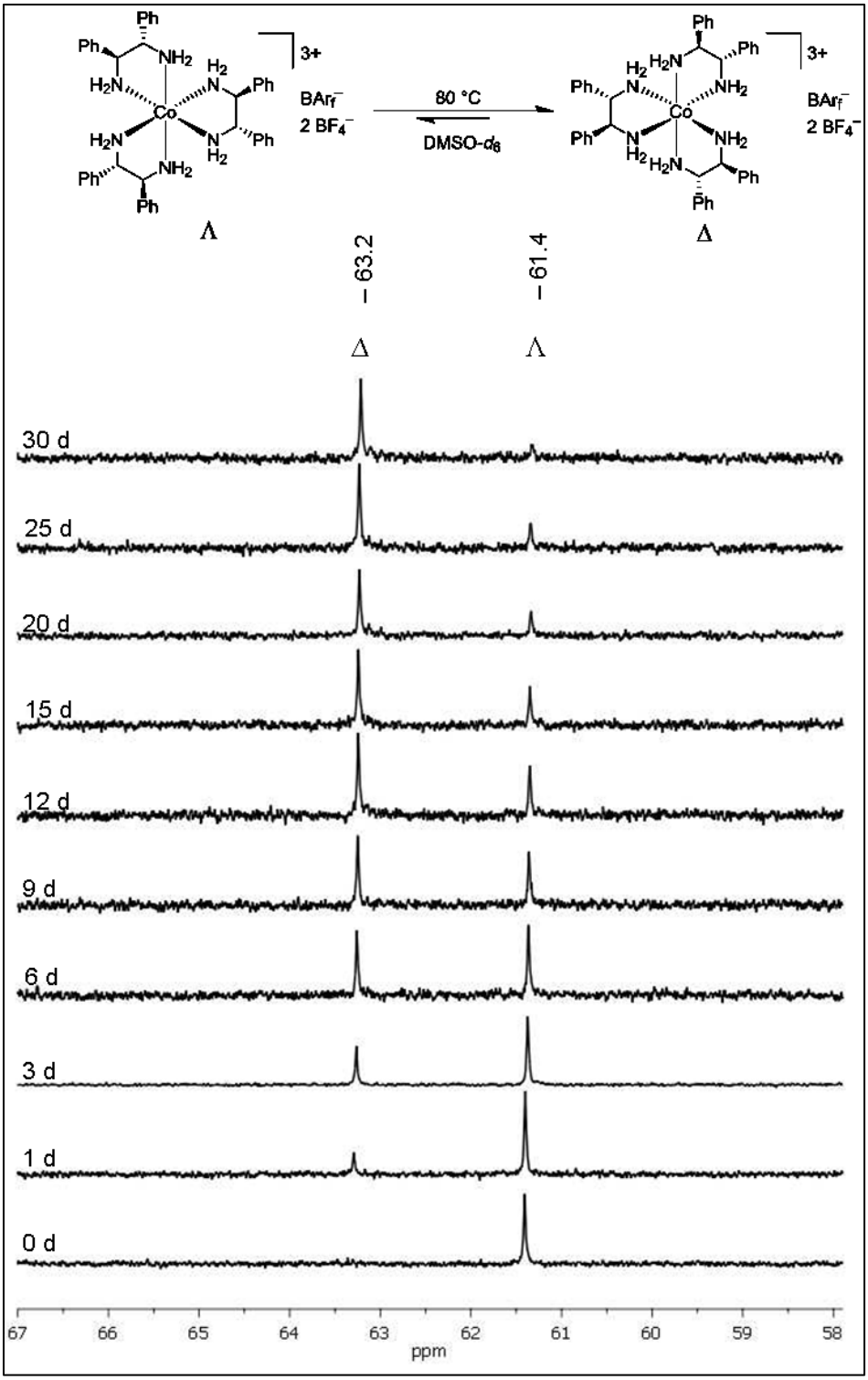

Figure 4.21. The thermal isomerization of Λ-(*S*,*S*)-**3**$^{3+}$ 2BF$_4^-$ BAr$_f^-$ in DMSO-d_6 at 80 °C monitored by $^{13}C\{^1H\}$ NMR.

The thermal isomerizations of the trichloride salts Λ-(*S*,*S*)-**3**$^{3+}$ 3Cl^{-} and Δ-(*S*,*S*)-**3**$^{3+}$ 3Cl^{-} were also attempted. Orange solutions of each complex in CD_3OD were heated in an NMR tube at 60 °C for 15 hours (b.p. CD_3OD = 65 °C). No changes in the $^{13}C\{^1H\}$ spectra were observed. Then a small amount of charcoal was added to each NMR tube and the temperature increased to 67 °C to afford a gentle reflux, as per the Bosnich conditions in the isomerization of Λ-(*S*,*S*)-**3**$^{3+}$ 3ClO_4^-.[52a] However, within 5 minutes of boiling, both solutions change from bright orange to bright green, which strongly suggests that a substitution reaction with the Cl^{-} counteranion to form the bis-chelating complex (*S*,*S*)-**4**$^{+}$ Cl^{-} had occurred.

Although Λ-(*S*,*S*)-**3**$^{3+}$ 3Cl^{-} is readily soluble in DMSO-d_6, Δ-(*S*,*S*)-**3**$^{3+}$ 3Cl^{-} is poorly soluble and a sufficient $^{13}C\{^1H\}$ signal of the latter could not be achieved during an overnight acquisition. Therefore, the isomerization was not attempted in this solvent.

The complex Λ-(*S*,*S*)-**3**$^{3+}$ 2BF_4^- BAr_f^- readily isomerized to Δ-(*S*,*S*)-**3**$^{3+}$ 2BF_4^- BAr_f^- at 80 °C, but Δ-(*S*,*S*)-**3**$^{3+}$ 2Cl^{-} BAr_f^- did not undergo isomerization under identical conditions and attempts to force an isomerization at higher temperatures led to competing reactions. Therefore, the Δ-diastereomer of the $[Co(S,S\text{-dpen})_3]^{3+}$ trication is thermally more stable in the presence of three non-coordination counteranions, but the thermally preferred isomer of the trication with two or three Cl^{-} counteranions could not be accurately determined.

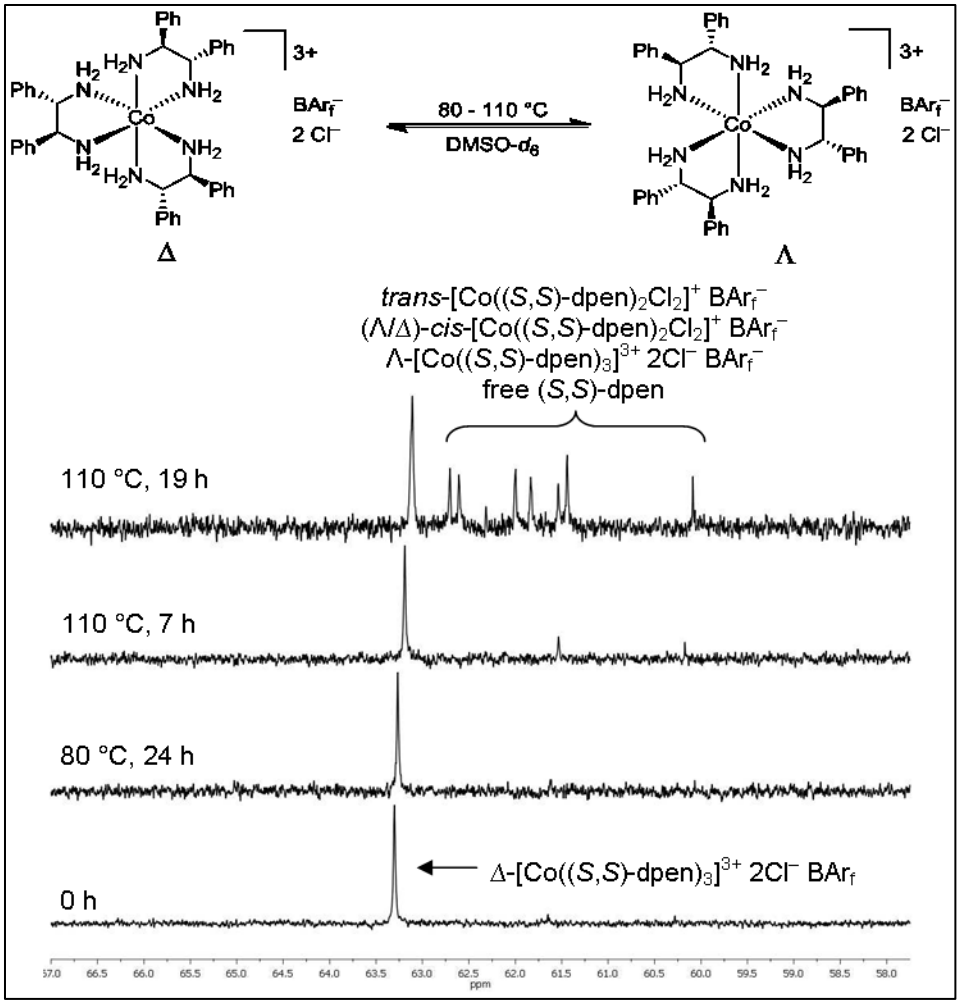

Figure 4.22. The attempted thermal isomerization of Δ-(*S*,*S*)-**3**$^{3+}$ 2Cl$^-$ BAr$_f^-$ in DMSO-d_6 at 80 °C and 110 °C monitored by ^{13}C{^{1}H} NMR.

4.2.9 Additional hydrogen bonding interactions of Werner complexes probed by ^{1}H NMR spectroscopy

The effects of the stereochemistry and counteranion of [Co(*S*,*S*)-dpen)$_3$]$^{3+}$ trications have already been examined (Sections 4.2.4.2 and 4.2.5.1). This section

describes the hydrogen bonding interactions between these trications and external hydrogen bond accepting and donating molecules.

The ^{1}H NMR spectra of Λ-(*S*,*S*)-**3**$^{3+}$ 2Cl$^-$ BAr$_f^-$ in CD_2Cl_2 and in the presence of various Brønsted acids are shown in Figure 4.23. In the presence of acetic acid or an organic phosphoric acid, the C_3 N-H peak is shifted significantly upfield to 6.79 and 4.86 ppm (Figure 4.23a,b), respectively, compared to the corresponding peak in Figure 4.14a (8.17 ppm). In the case of Figure 4.23c, a homogeneous solution containing two equivalents of Et_3NH^+ BF_4^- in CD_2Cl_2 is added to a solution of Λ-(*S*,*S*)-**3**$^{3+}$ 2Cl$^-$ BAr$_f^-$ in CD_2Cl_2. A heavy white precipitate, presumably Et_3NH^+ Cl$^-$, immediately crashed out. The ^{1}H NMR spectrum revealed a significant upfield shift of the C_3 N-H unit that is remarkably similar to that observed for Λ-(*S*,*S*)-**3**$^{3+}$ 2BF_4^- BAr$_f^-$ in Figure 4.16b (6.04 ppm).

It is likely that the strong C_3 N-H···Cl$^-$ hydrogen bonding interactions in Λ-(*S*,*S*)-**3**$^{3+}$ 2Cl$^-$ BAr$_f^-$ are disrupted in the presence of competing hydrogen bond donors. In the above cases, the newly introduced protic hydrogen atoms can also bind with the Cl$^-$ anion and partially displace it from the C_3 N-H binding site of the Werner complex. This would result in the observed upfield chemical shift of the C_3 N-H units.

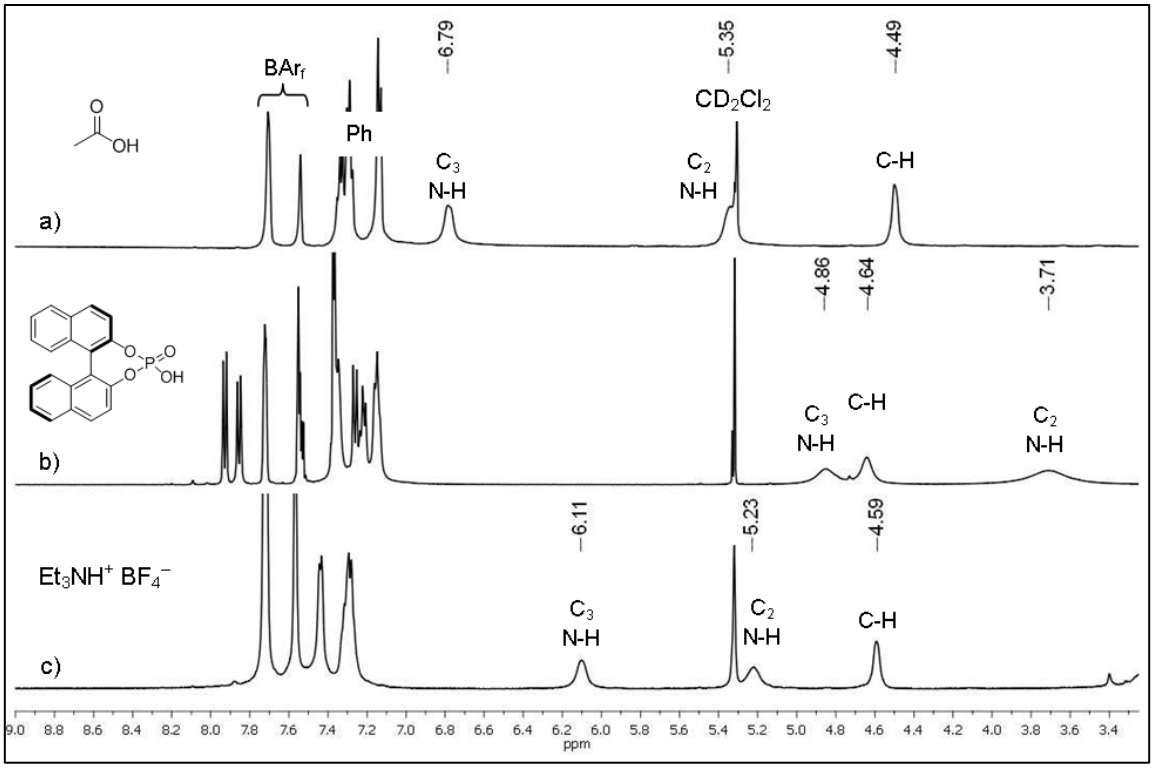

Figure 4.23. The ^{1}H NMR spectra (CD_2Cl_2) of Λ-(*S*,*S*)-**3**$^{3+}$ 2Cl$^-$ BAr$_f^-$ in the presence of one equivalent of the protic additives a) acetic acid, b) (*R*)-1,1′-binapthyl-2,2′-diyl hydrogenphosphate, and c) Et_3NH^+ BF_4^-.

4.2.9.1 ^{1}H NMR titrations of Λ-[Co(S,S)-dpen)$_3$]$^{3+}$ 3X$^-$ complexes with hydrogen bond acceptors

The hydrogen bonding characteristics of [Co(*S*,*S*)-dpen)$_3$]$^{3+}$ trications with neutral, organic molecules were also examined. The complexes Λ-(*S*,*S*)-**3**$^{3+}$ 2Cl$^-$ BAr$_f^-$ and Λ-(*S*,*S*)-**3**$^{3+}$ 2BF$_4^-$ BAr$_f^-$ were independently titrated in CD_2Cl_2 with gradually increasing concentrations of *trans*-β-nitrostyrene (**14**) and dimethyl malonate (**15a**) (Figure 4.24), resulting in gradual peak shifts in the ^{1}H NMR spectra.

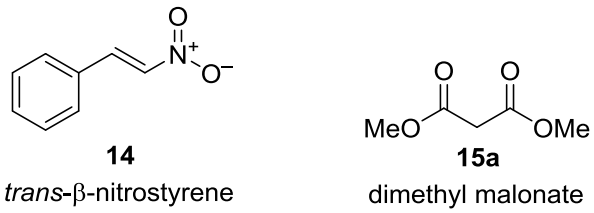

14 *trans*-β-nitrostyrene

15a dimethyl malonate

Figure 4.24. The hydrogen bond donors used in the ^{1}H NMR titrations.

The titration of Λ-(*S*,*S*)-**3**$^{3+}$ 2Cl$^-$ BAr$_f^-$ with **15a** is depicted in Figure 4.25. An initial ^{1}H NMR spectrum of the cobalt complex in the absence of **15a** is recorded. Incremental amounts of **15a** are introduced and a spectrum recorded after each addition. The C_2 N-H peaks experience a significant downfield shift from 3.95 to 4.77 ppm upon the addition of **15a**, indicating the presence of a hydrogen bonding interaction. As a consequence, the adjacent aliphatic C-H peak also shifts slightly downfield. Surprisingly, the chemical shift of the C_3 N-H peak is virtually unchanged even in the presence of 10 equivalents of **15a**, indicating that the organic substrate does not disrupt the strong C_3 N-H···Cl$^-$ hydrogen bond. Another interesting point concerns the shift of the H_2O peak. In commercial CD_2Cl_2, the H_2O impurity appears at 1.56 ppm. The peak of the H_2O that is isolated with Λ-(*S*,*S*)-**3**$^{3+}$ 2Cl$^-$ BAr$_f^-$ is initially shifted to 2.06 ppm due to hydrogen bonding. Upon the addition of increasing amounts of **15a**, the H_2O peak gradually shifts upfield to 1.72 ppm. Figure 4.26 gives a quantitative representation of the C_3 N-H, C_2 N-H, C-H, and H_2O peak shifts with respect to the added equivalents of **15a**. The C_2 N-H peak experiences the greatest shift of approximately 0.8 ppm.

The titration of Λ-(*S*,*S*)-**3**$^{3+}$ 2Cl$^-$ BAr$_f^-$ with **14**, depicted in Figure 4.27, yielded a similar, albeit less pronounced effect on the chemical shifts. The C_3 N-H peak remains virtually unchanged even in the presence of 12 equivalents of **14**. The C_2 N-H peak

again experiences the largest shift, but in this case it only shifts approximately 0.5 ppm downfield (Figure 4.28).

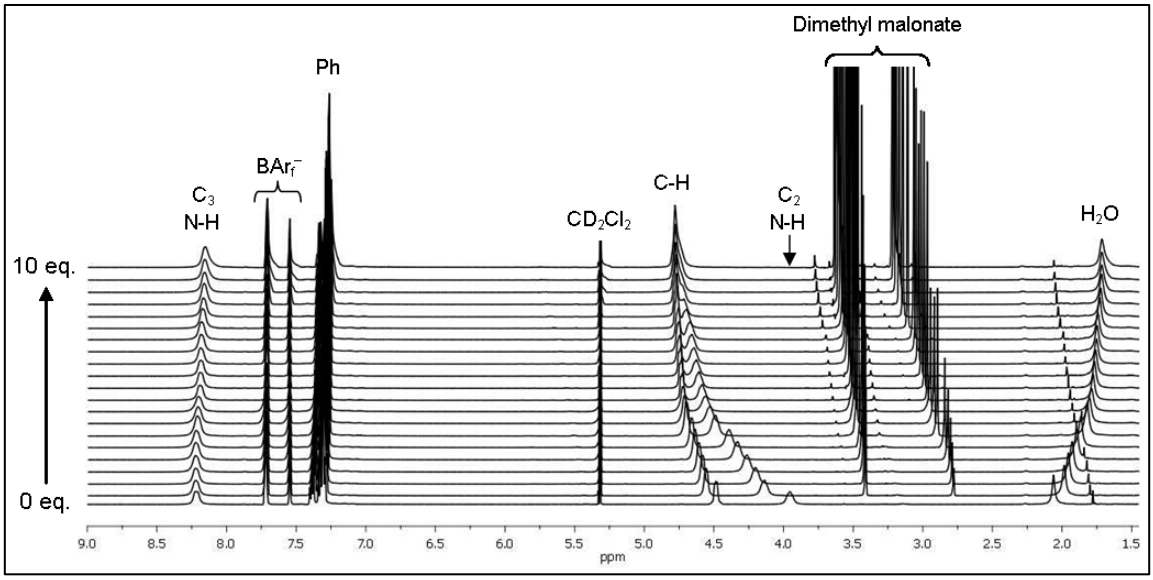

Figure 4.25. The ^{1}H NMR titration (CD_2Cl_2) of Λ-(*S*,*S*)-**3**$^{3+}$ 2Cl$^-$ BAr$_f^-$ with **15a**.

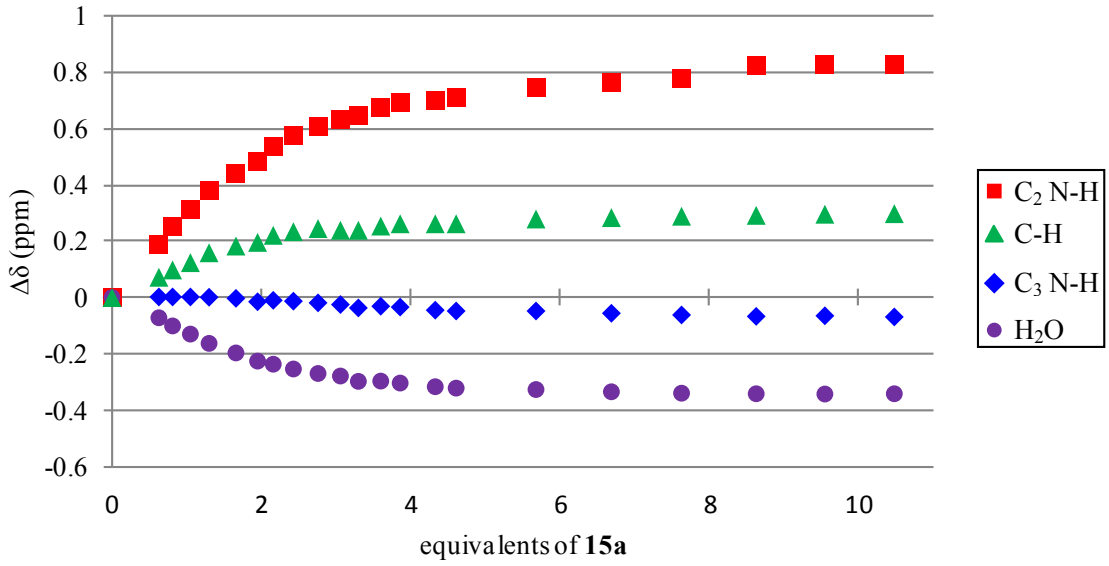

Figure 4.26. The change in chemical shift (Δδ) of various signals for the titration examined in Figure 4.25.

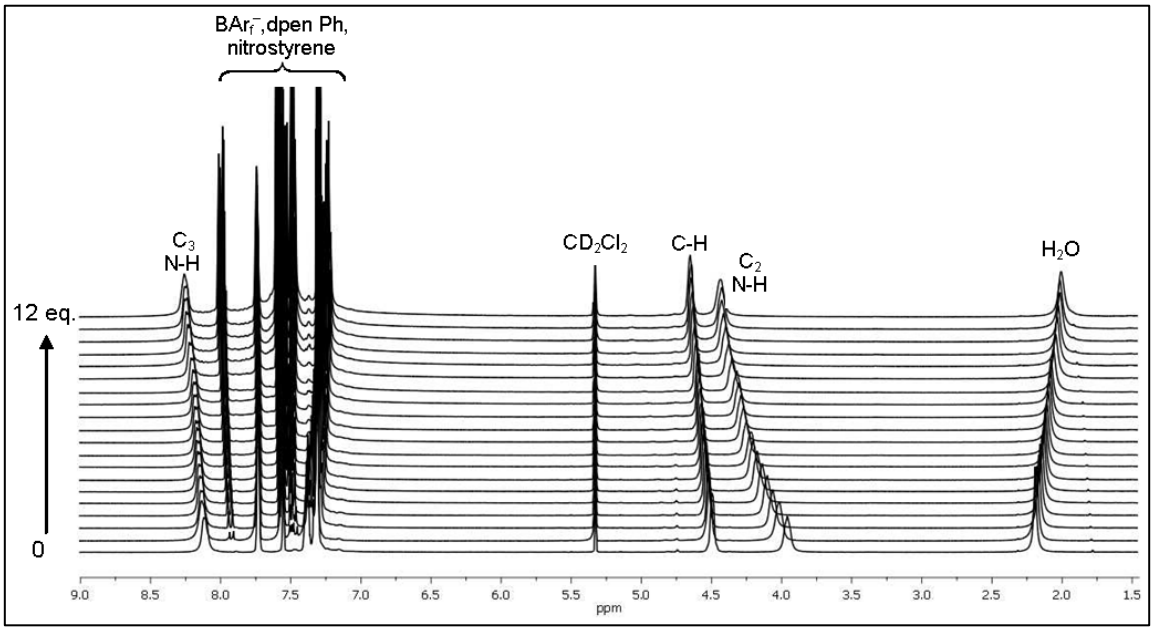

Figure 4.27. The ^{1}H NMR titration (CD_2Cl_2) of Λ-(*S*,*S*)-**3**$^{3+}$ 2Cl$^-$ BAr$_f^-$ with **14**.

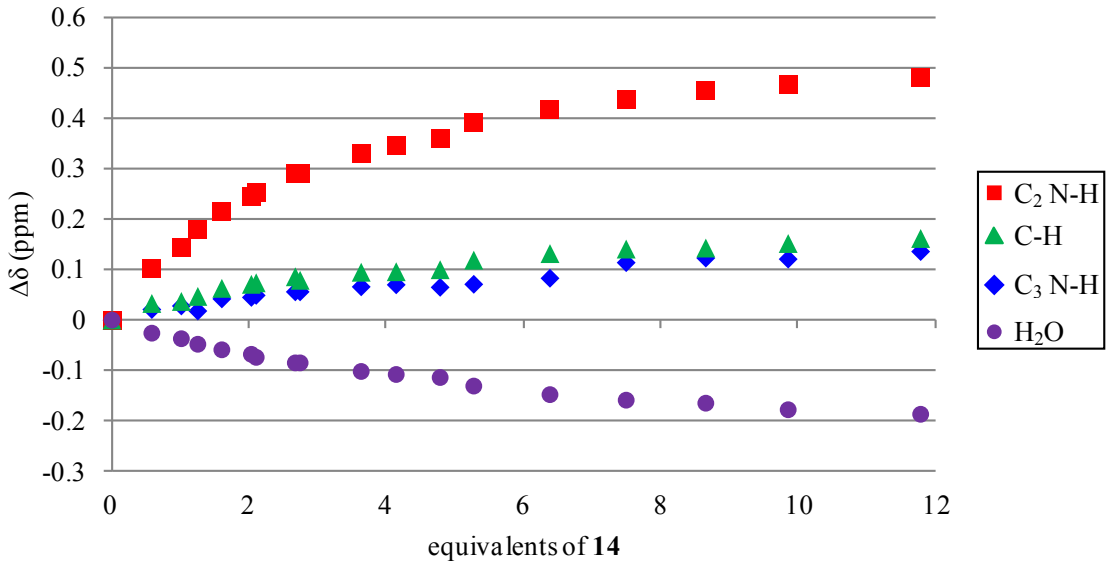

Figure 4.28. The change in chemical shift (Δδ) of various signals for the titration examined in Figure 4.27.

The titration of the mixed BF_4^-/BAr_f^- salt Λ-(*S*,*S*)-**3**$^{3+}$ 2BF_4^- BAr_f^- with **15a** in CD_2Cl_2 is depicted in Figure 4.29. In the absence of **15a** the C_3 N-H peak appears at 6.52 ppm. It was thought that the weaker hydrogen bonding involving the C_3 N-H hydrogen atoms (section 4.2.5.1) could lead – in contrast to the situations in Figures 4.25-4.28 – to downfield shifts upon addition of increasing quantities of **15a**. Instead, the peak gradually shifts upfield and simultaneously broadens to the point that it is nearly indistinguishable from the baseline. The C_2 N-H peak experiences a drastic downfield shift from 3.98 to 5.20 ppm while the H_2O peak again shifts upfield. As seen in Figure 4.30, the C_2 N-H peak shifts by a total of 1.22 ppm after the addition of 10 equivalents of **15a**, which is a noticeably greater shift than was observed in Figure 4.25. This indicates that **15a** binds to the C_2 site of Λ-(*S*,*S*)-**3**$^{3+}$ 2BF_4^- BAr_f^- more strongly than the C_2 site of Λ-(*S*,*S*)-**3**$^{3+}$ 2Cl^- BAr_f^-. Interestingly, the change in chemical shift for all hydrogens changes linearly until 3 equivalents of **15a** have been added. Then the change in chemical shift abruptly levels off. This demonstrates a clear 3:1 binding stoichiometry[92] between **15a** and Λ-(*S*,*S*)-**3**$^{3+}$ 2BF_4^- BAr_f^-, which nicely corresponds with the 3 C_2 N-H binding sites.

Lastly, the analogous titration of Λ-(*S*,*S*)-**3**$^{3+}$ 2BF_4^- BAr_f^- with the nitroolefin **14** in CD_2Cl_2 is depicted in Figure 4.31. The C_3 N-H peak experiences virtually no change in chemical shift and only marginal peak broadening. According to Figure 4.32, the C_2 N-H peaks shift by nearly 0.77 ppm from 3.93 to 4.70 ppm. This is a more significant change than was observed in the same titration with Λ-(*S*,*S*)-**3**$^{3+}$ 2Cl^- BAr_f^- (Figure 4.28). This indicates that **14** binds to the C_2 site of Λ-(*S*,*S*)-**3**$^{3+}$ 2BF_4^- BAr_f^- more strongly than the C_2 site of Λ-(*S*,*S*)-**3**$^{3+}$ 2Cl^- BAr_f^-.

From this evidence, it is understood that **15a** forms stronger hydrogen bonds with both complexes than **14**. Furthermore, Λ-(*S*,*S*)-**3**$^{3+}$ 2BF_4^- BAr_f^- binds both organic

substrates more strongly than Λ-(*S*,*S*)-**3**$^{3+}$ 2Cl$^-$ BAr$_f^-$. In each titration, the C_2 N-H peak shifts downfield with increasing concentrations of organic substrate, clearly indicating hydrogen bonding interactions at this site. The C_3 N-H units of Λ-(*S*,*S*)-**3**$^{3+}$ 2Cl$^-$ BAr$_f^-$ have a greater hydrogen bonding affinity for the Cl$^-$ counteranions than for the organic substrates. Given the absence of a downfield shift in the C_3 N-H peak of Λ-(*S*,*S*)-**3**$^{3+}$ 2BF$_4^-$ BAr$_f^-$ with increasing amounts of **15a** or **14** (Figure 4.29-4.32), there is apparently a greater bonding affinity for BF$_4^-$ than for the organic substrates. However, none of these experiments exclude the possibility of small equilibrium concentrations of organic substrate binding to the C_3 N-H site, as long as these interactions are rapidly reversible on the NMR time scale.

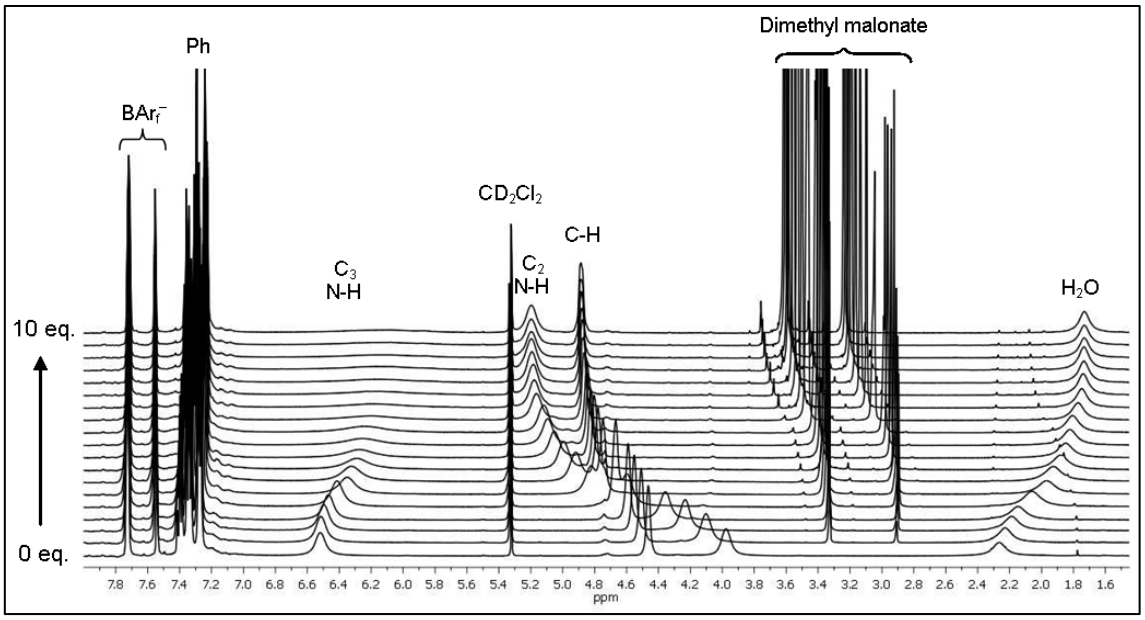

Figure 4.29. The ^{1}H NMR titration (CD$_2$Cl$_2$) of Λ-(*S*,*S*)-**3**$^{3+}$ 2BF$_4^-$ BAr$_f^-$ with **15a**.

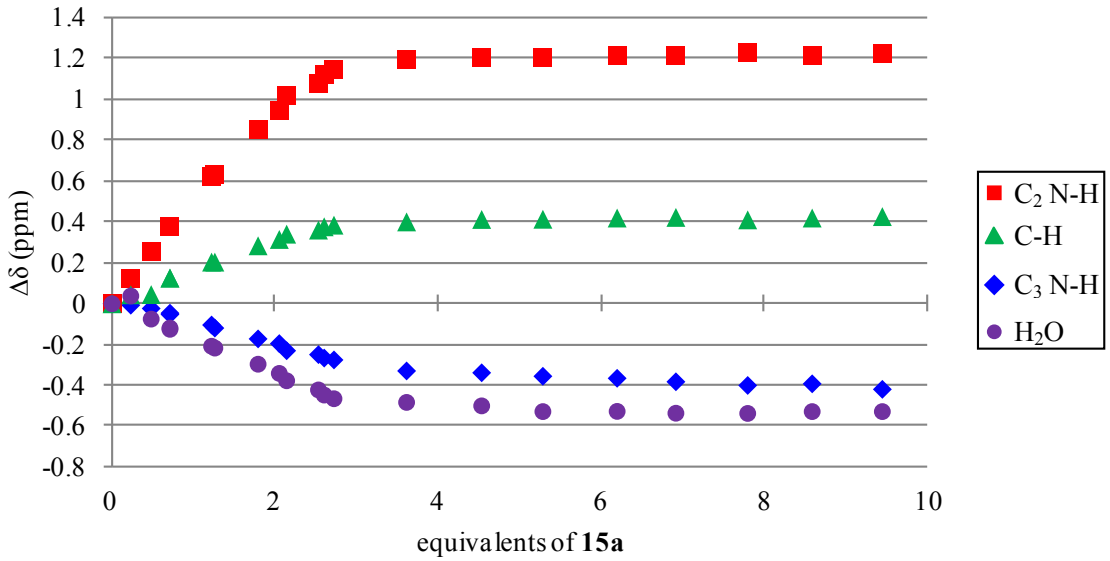

Figure 4.30. The change in chemical shift (Δδ) of various signals for the titration examined in Figure 4.29.

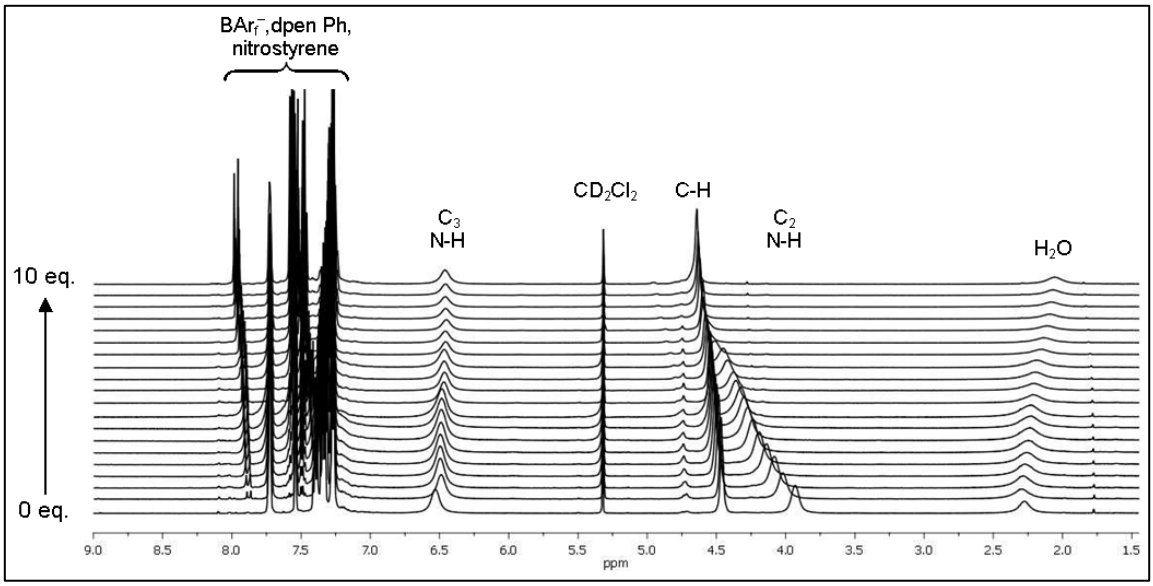

Figure 4.31. The ^{1}H NMR titration (CD_2Cl_2) of Λ-(*S*,*S*)-**3**$^{3+}$ 2BF_4^- BAr_f^- with **14**.

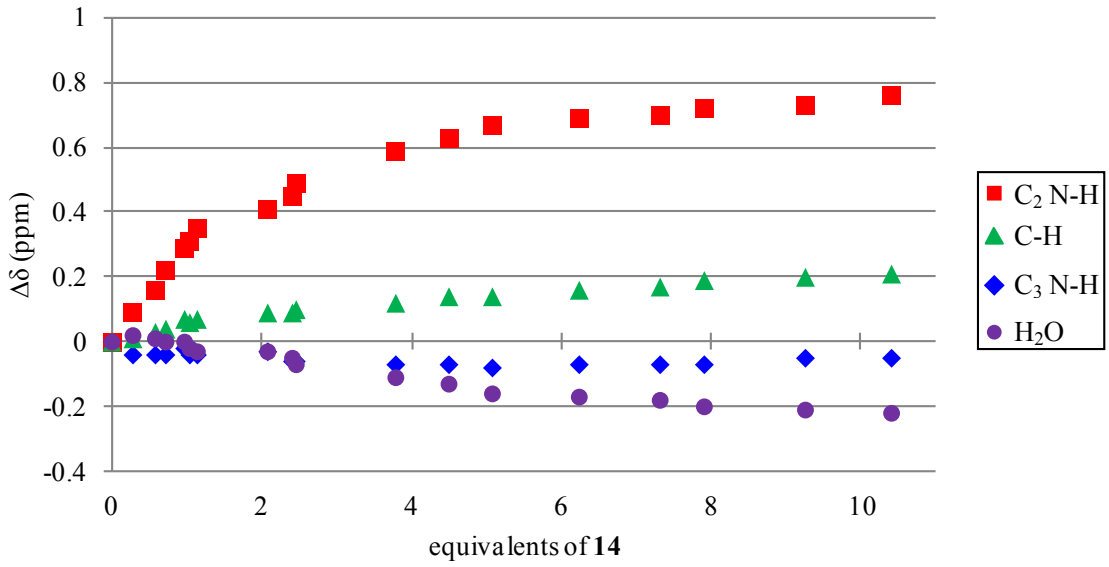

Figure 4.32. The change in chemical shift (Δδ) of various signals for the titration examined in Figure 4.31.

4.2.9.2 Interactions of small prochiral and chiral organic molecules with Λ-[Co(S,S)-dpen)$_3$]$^{3+}$ trications

The enantiotopic protons of an achiral organic molecule are symmetry equivalent and therefore give rise to a single ^{1}H NMR signal. The two methylene protons of ethyl acetate (EtOAc) give a simple quartet signal as shown in Figure 4.33a. However, in the presence of approximately one equivalent of the chiral Werner complex Λ-(*S*,*S*)-**3**$^{3+}$ 2Cl$^-$ BAr$_f^-$ or Λ-(*S*,*S*)-**3**$^{3+}$ 2BF$_4^-$ BAr$_f^-$, these methylene protons become inequivalent, which results in two distinct doublet of quartet signals (Figure 4.33b,c).

Similar effects were observed with achiral organic molecules containing different kinds of hydrogen bond accepting functional groups. Figure 4.34 shows that the enantiotopic methylene protons of 1-methyl-2-oxindole are separated into two distinct doublet signals. Likewise, the enantiotopic protons of cyclohexene oxide become nonequivalent when hydrogen bonded to Λ-[Co(*S*,*S*)-dpen)$_3$]$^{3+}$ cations, as shown in Figure 4.35.

These Werner-type complexes were also effective as chiral shift reagents with racemic mixtures of D,L-lactide, as shown in Figure 4.36. The racemic lactide gives a single quartet peak for the protons on the carbon atom α to the carbonyl group. In the presence of Λ-(*S*,*S*)-**3**$^{3+}$ 2Cl$^-$ BAr$_f^-$ or Λ-(*S*,*S*)-**3**$^{3+}$ 2BF$_4^-$ BAr$_f^-$, this peak is resolved into two separate quartet signals. The assignment of the resolved lactide enantiomers, shown in Figure 4.37, was achieved by spiking the solution with a small portion of enantiopure L-lactide.

The desymmetrization of enantiotopic protons and the chiral resolution of racemic substrates by ^{1}H NMR spectroscopy require an intimate hydrogen bonding contact between the organic substrate and the Werner complex. Furthermore, the Werner

complex must have sufficient chiral influence over the hydrogen bonded organic group so as to position each enantiotopic proton in a unique geometric environment. Lastly, the reversibility of the hydrogen bonding interaction must be relatively slow to be observed on the NMR time scale.

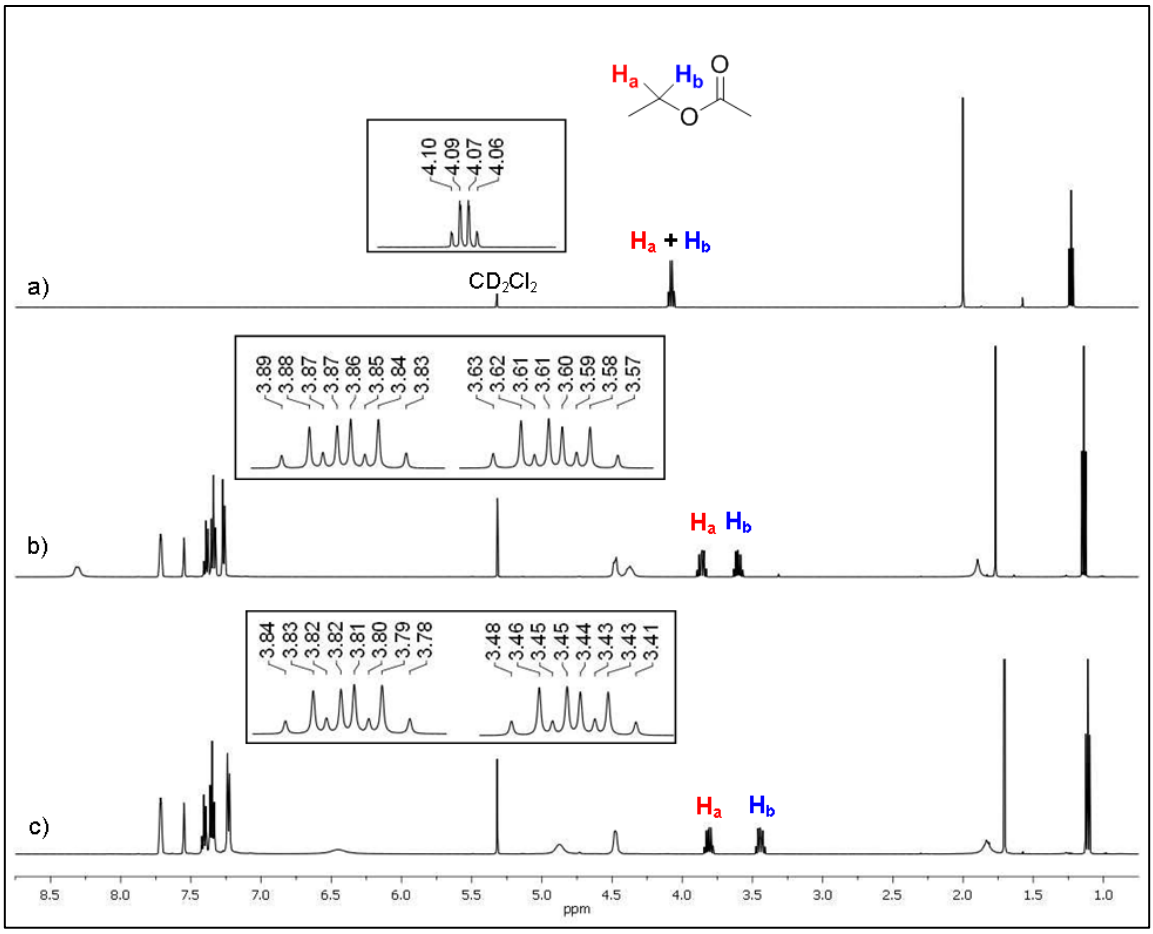

Figure 4.33. The ^{1}H NMR spectra (CD_2Cl_2) of a) EtOAc, b) Λ-(*S*,*S*)-**3**$^{3+}$ 2Cl^{-} BAr_f^{-} with one equivalent of EtOAc, and c) Λ-(*S*,*S*)-**3**$^{3+}$ 2BF_4^{-} BAr_f^{-} with one equivalent of EtOAc.

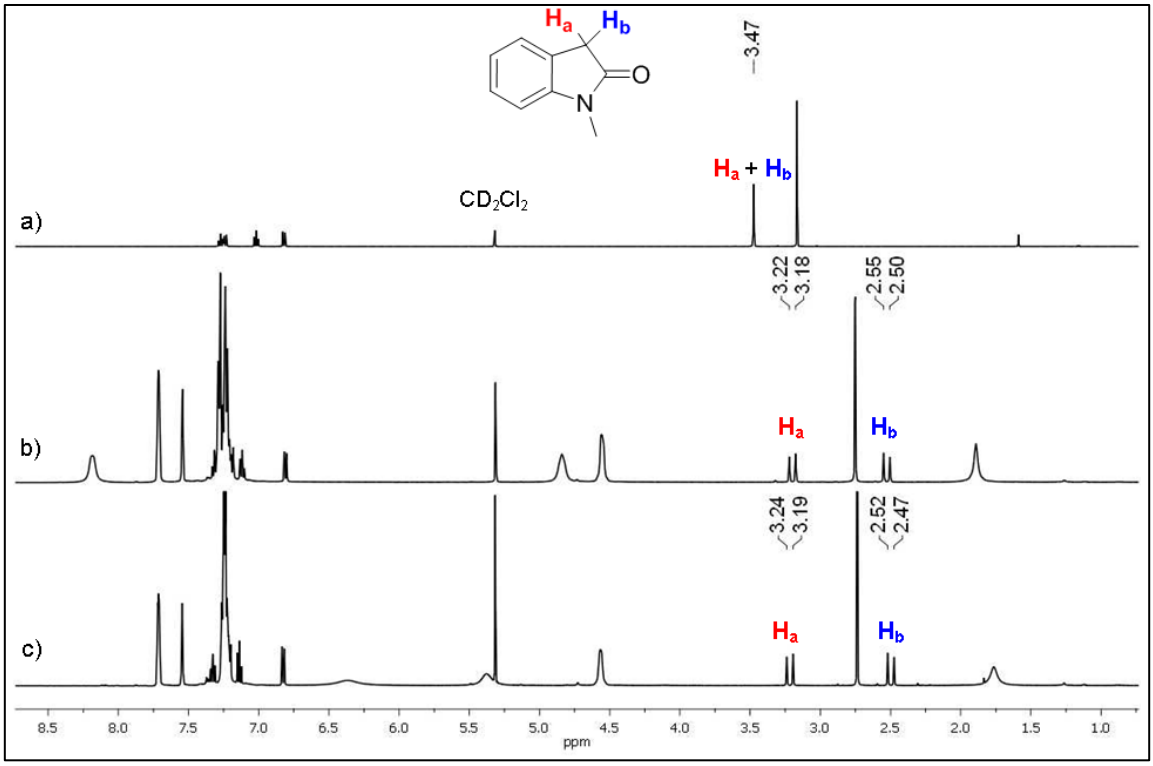

Figure 4.34. The ^{1}H NMR spectra (CD_2Cl_2) of a) 1-methyl-2-oxindole, b) Λ-(*S*,*S*)-**3**$^{3+}$ 2Cl^- BAr_f^- with one equivalent of 1-methyl-2-oxindole, and c) Λ-(*S*,*S*)-**3**$^{3+}$ 2BF_4^- BAr_f^- with one equivalent of 1-methyl-2-oxindole.

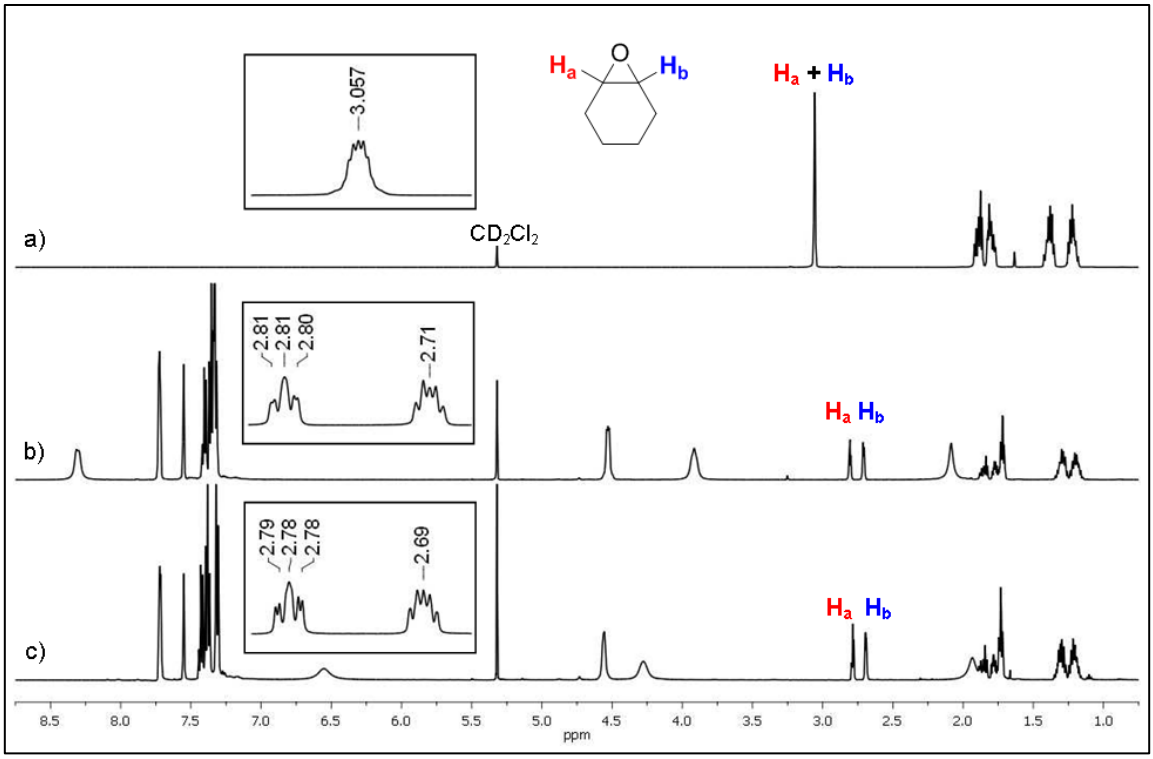

Figure 4.35. The ^{1}H NMR spectra (CD_2Cl_2) of a) cyclohexene oxide, b) Λ-(*S*,*S*)-**3**$^{3+}$ 2Cl^{-} BAr_f^{-} with one equivalent of cyclohexene oxide, and c) Λ-(*S*,*S*)-**3**$^{3+}$ 2BF_4^{-} BAr_f^{-} with one equivalent of cyclohexene oxide.

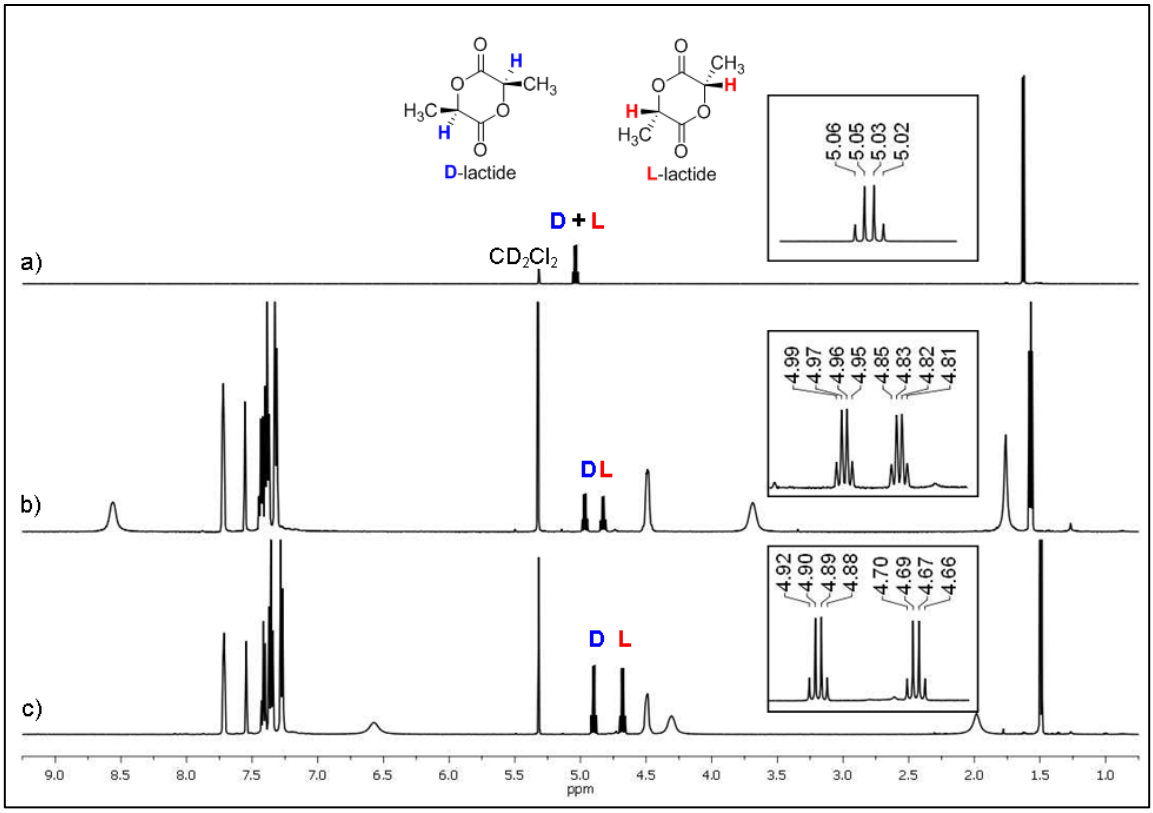

Figure 4.36. The ^{1}H NMR spectra (CD_2Cl_2) of a) racemic D,L-lactide, b) Λ-(*S*,*S*)-**3**$^{3+}$ 2Cl^{-} BAr_f^{-} with one equivalent of racemic D,L-lactide, and c) Λ-(*S*,*S*)-**3**$^{3+}$ 2BF_4^{-} BAr_f^{-} with one equivalent of racemic D,L-lactide.

4.3 Enantioselective catalysis

4.3.1 The enantioselective Michael addition of dialkyl malonates to nitroolefins

The title reaction of this section has been successfully developed for a number of chiral, hydrogen bond mediating catalysts as well as chiral, organometallic catalysts.[93,94] It was chosen here as a "benchmark" reaction to compare Werner-type complexes to the best known catalysts. The proposed mechanism is shown in Scheme

4.13. A base, in this case Et_3N, must first deprotonate the dialkyl malonate. The electron deficient nitroolefin is expected to engage in hydrogen bonding with the catalyst, thus rendering it more electrophilic. After the addition of the malonate to the nitroolefin, the Et_3NH^+ will transfer a proton to the anionic organic intermediate to form the Michael addition adduct and regenerate the base.

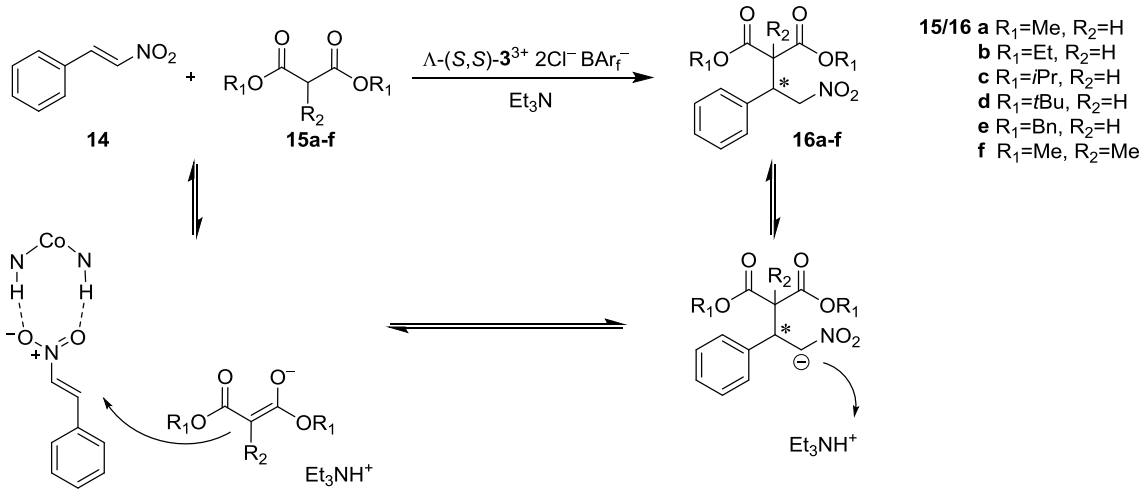

Scheme 4.13. The proposed mechanism for the catalyzed Michael addition.

In the initial reaction screenings and optimizations, catalysis was performed and analyzed on an NMR scale. In a typical experiment, **14** (1.0 equiv), dialkyl malonate (1.2 equiv), Λ-(*S*,*S*)-**3**$^{3+}$ 2Cl$^-$ BAr$_f^-$ (10 mol%), diphenyldimethylsilane (internal standard), and CD_2Cl_2 were combined in an NMR tube. Because no reaction occurs before the addition of base, a ^{1}H NMR spectrum was recorded at this point to measure the initial relative ratio of the starting material to the internal standard. Then Et_3N (1.0 equiv) was added and the conversion of **14** was periodically measured by ^{1}H NMR. In all cases, the catalysis gave a clean conversion to the desired Michael addition adduct with no detectable byproducts. Thus, the product conversion measured by ^{1}H NMR can be

assumed to be equivalent to the yield of the desired product. The reaction mixture is then passed through silica gel with 1:1 hexanes/EtOAc to remove the catalyst. The enantiomeric ratio of the organic products was measured by chiral HPLC. The enantioselectivities are reported in terms of both %ee and er.[95] The stereochemical assignment of the product enantiomers was made by comparisons of products **16a-c** with previously reported chiral HPLC data.[96]

4.3.1.1 The effect of metal and ligand chirality in catalysis

The Michael addition of diisopropyl malonate (**15c**) to *trans*-β-nitrostyrene (**14**) was catalyzed by Λ-(*S*,*S*)-**3**$^{3+}$ 2Cl$^-$ BAr$_f^-$ and three related stereoisomers in the presence of one equivalent of Et_3N in CD_2Cl_2. The results are summarized in Table 4.5. After 2 hours, the reaction catalyzed by Λ-(*S*,*S*)-**3**$^{3+}$ 2Cl$^-$ BAr$_f^-$ had reached 88% conversion and the product was achieved in 80% ee with the *R* enantiomer predominating (Entry 1). The catalyst Δ-(*S*,*S*)-**3**$^{3+}$ 2Cl$^-$ BAr$_f^-$, which bears the same ligand chirality but the opposite sense of chirality at the metal center, catalyzes the same reaction with a faster rate of conversion, reaching full conversion within 2 hours (Entry 2). The product is achieved in 76% ee, but, remarkably, the *S* enantiomer predominates. Both diastereomers of the catalyst are nearly equally enantioselective in this Michael addition, yet each gives the opposite product enantiomer.

Table 4.5. Data for the catalyzed Michael addition of **15c** to **14**.

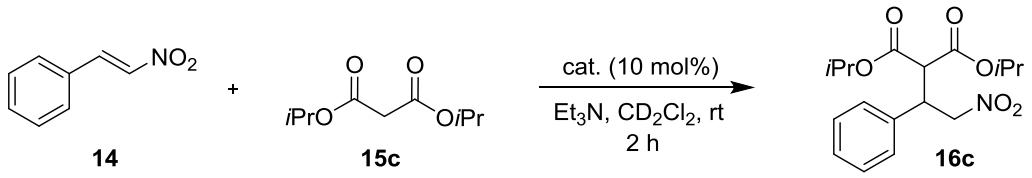

entry	catalyst	conversion (%)[a]	er (R:S)[b]	ee (%)[b]
1	Λ-(*S*,*S*)-**3**$^{3+}$ 2Cl$^-$ BAr$_f^-$	88	**90**:10	80 *R*
2	Δ-(*S*,*S*)-**3**$^{3+}$ 2Cl$^-$ BAr$_f^-$	>99	12:**88**	76 *S*
3	Λ-(*R*,*R*)-**3**$^{3+}$ 2Cl$^-$ BAr$_f^-$	>99	**87**:13	74 *R*
4	Δ-(*R*,*R*)-**3**$^{3+}$ 2Cl$^-$ BAr$_f^-$	89	10:**90**	80 *S*

[a]The conversion was determined by ^{1}H NMR integration of **14** versus an internal standard. [b]Enantioselectivities were determined by chiral HPLC analyses.

This catalyst system contains chiral elements in both the metal configuration and the stereochemistry of the ligands. Although both elements are expected to have influence over the stereoselectivity of the reaction, the metal chirality is the overwhelmingly dominant factor in governing the absolute configuration of the product. The chiral ligands have less influence and serve only to slightly reinforce or detract from the chiral arrangement set by the metal center.

To further emphasize this point, the catalysis was performed with the (*R*,*R*)-dpen catalyst series. It was found that Λ-(*R*,*R*)-**3**$^{3+}$ 2Cl$^-$ BAr$_f^-$ gave the *R* product in 74% ee (Entry 3), which is very similar to the result obtained with Λ-(*S*,*S*)-**3**$^{3+}$ 2Cl$^-$ BAr$_f^-$ even though the chirality of the ligands have been reversed. Likewise, Δ-(*R*,*R*)-**3**$^{3+}$ 2Cl$^-$ BAr$_f^-$ gives the *S* product in 80% ee (Entry 4), which is the same product enantiomer obtained with Δ-(*S*,*S*)-**3**$^{3+}$ 2Cl$^-$ BAr$_f^-$. In this representative Michael addition, catalysts with the

same metal configuration give the same enantiomer of the product with virtually identical enantioselectivity regardless of the chirality of the ligand.

4.3.1.2 The influence of the dialkyl malonate

The catalyst screening was extended to include other dialkyl malonates that range in steric parameters. The screening of dialkyl malonates was performed with both Λ-(*S*,*S*)-**3**$^{3+}$ 2Cl^{-} BAr$_f^{-}$ and Δ-(*S*,*S*)-**3**$^{3+}$ 2Cl^{-} BAr$_f^{-}$ in CD_2Cl_2 in the presence of one equivalent of Et_3N at room temperature. The results are summarized in Table 4.6.

In all cases, the Λ-(*S*,*S*)-**3**$^{3+}$ 2Cl^{-} BAr$_f^{-}$ catalyst gives the *R* product as the predominant enantiomer while Δ-(*S*,*S*)-**3**$^{3+}$ 2Cl^{-} BAr$_f^{-}$ provides the opposite *S* product. With Λ-(*S*,*S*)-**3**$^{3+}$ 2Cl^{-} BAr$_f^{-}$ as catalyst, the highest level of enantioselectivity is achieved with dimethyl malonate as the nucleophile. A slight decrease in selectivity as well as reaction rate is observed when the somewhat bulkier diethyl and diisopropyl malonates are employed. The enantioselectivities drastically drop off as the steric bulk further increases with dibenzyl malonate and again to a greater extent with di-*t*-butyl malonate.

Table 4.6. Data for the catalyzed Michael addition of various dialkyl malonates to **14**.

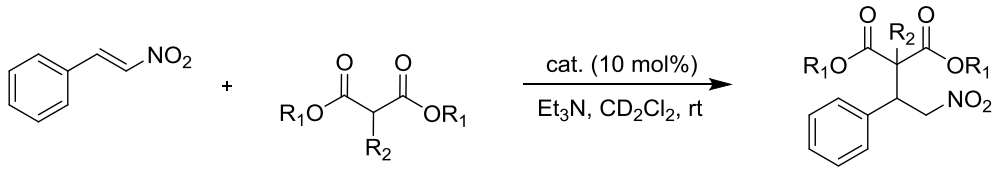

14 **15a-f** **16a-f**

				Λ-(*S*,*S*)-**3**$^{3+}$ 2Cl$^-$ BAr$_f^-$		Δ-(*S*,*S*)-**3**$^{3+}$ 2Cl$^-$ BAr$_f^-$	
entry	R_1	R_2	**15/16**	conversion (%)[a]	er (R:S)[b] ee (%)	conversion (%)[a]	er (R:S)[b] ee (%)
1	Me	H	**a**	>99 (2 h)	**91**:9 82 *R*	>99 (1 h)	30:**70** 40 *S*
2	Et	H	**b**	94 (3 h)	**90**:10 79 *R*	99 (1 h)	24:**76** 51 *S*
3[c]	*i*Pr	H	**c**	88 (2 h)	**90**:10 80 *R*	>99 (2 h)	12:**88** 76 *S*
4	Bn	H	**d**	>99 (2 h)	**84**:16 67 *R*	>99 (2 h)	17:**83** 67 *S*
5	*t*Bu	H	**e**	43 (6 h)	**72**:28 44 *R*	44 (6 h)	36:**64** 28 *S*
6	Me	Me	**f**	94 (10 h)	**86**:14 71 *R*	97 (5 h)	36:**64** 28 *S*

[a]The conversion was determined by ^{1}H NMR integration of **14** versus an internal standard. [b]Enantioselectivities were determined by chiral HPLC analyses. [c]The data are reproduced from Table 4.5, Entries 1 and 2.

With Δ-(*S*,*S*)-**3**$^{3+}$ 2Cl^{-} BAr$_f^{-}$ as catalyst, the Michael addition with diisopropyl malonate is achieved with the highest enantioselectivity. The enantioselectivity diminishes as the steric bulk either decreases or increases in comparison to diisopropyl malonate. While the trend for Λ-(*S*,*S*)-**3**$^{3+}$ 2Cl^{-} BAr$_f^{-}$ follows "smaller is better", the Δ-(*S*,*S*)-**3**$^{3+}$ 2Cl^{-} BAr$_f^{-}$ catalyst has a "sweet spot" in which a dialkyl malonate of intermediate size gives the highest enantioselectivity.

Both catalysts gave poorer enantioselectivities and slower reaction rates with dimethyl methylmalonate (Entry 6) compared to the unsubstituted dimethyl malonate (Entry 1).

In general, Δ-(*S*,*S*)-**3**$^{3+}$ 2Cl^{-} BAr$_f^{-}$ catalyzes the Michael addition reactions with higher conversion rates than Λ-(*S*,*S*)-**3**$^{3+}$ 2Cl^{-} BAr$_f^{-}$, but with lower enantioselectivities.

The Michael addition of **15a** to **14** was catalyzed by both Λ-(*S*,*S*)-**3**$^{3+}$ 2Cl^{-} BAr$_f^{-}$ and Δ-(*S*,*S*)-**3**$^{3+}$ 2Cl^{-} BAr$_f^{-}$ at 2 mol% loading, as seen in Figure 4.37. The Δ-diastereomer affords a faster rate than the Λ-diastereomer. According to Table 4.7, both catalysts afford the Michael addition product with the opposite enantiomer predominating, but the Λ-diasteromer is more enantioselective.

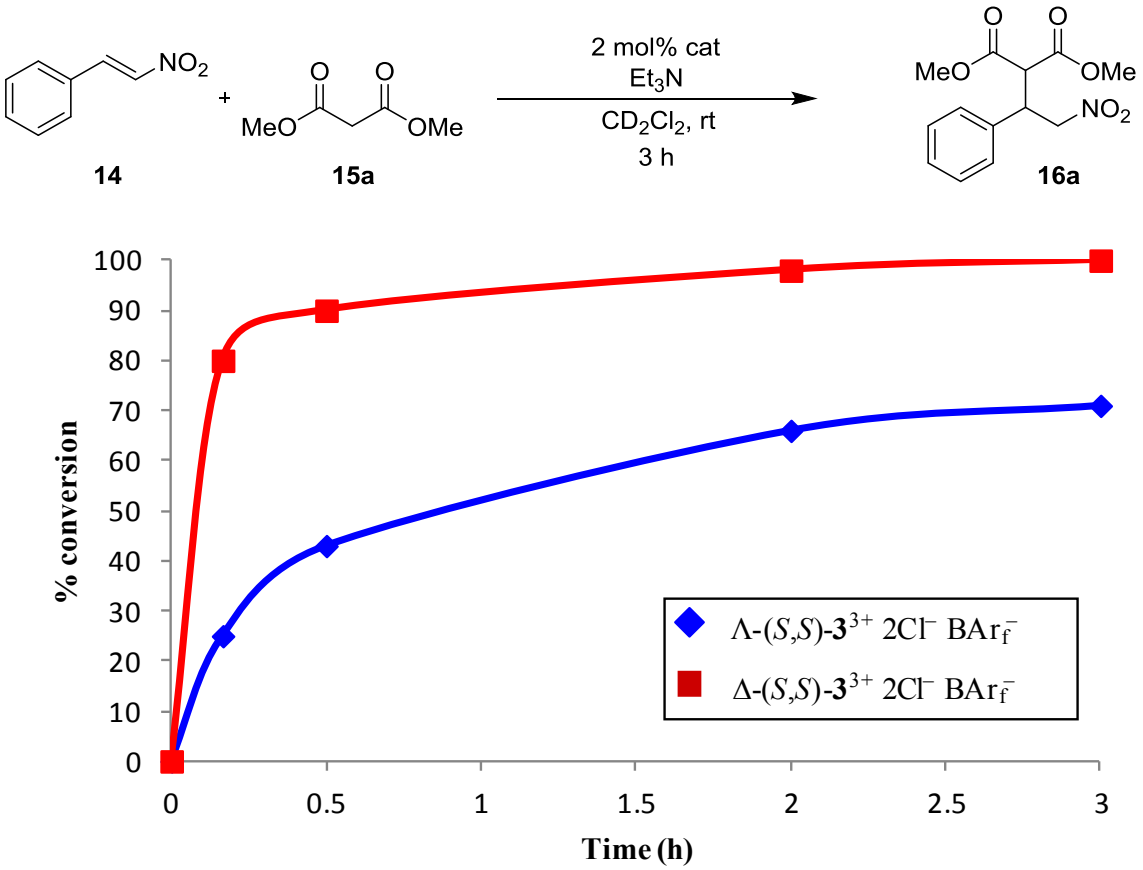

Figure 4.37: Reaction rate profiles for the Michael addition of **15a** to **14** at 2 mol% catalyst loading.

Table 4.7. Data for the catalyzed Michael addition of **15a** to **14** with various catalysts at 2 mol%.

entry	catalyst	conversion (%)[a]	er (R:S) ee (%)[b]
1	Λ-(*S*,*S*)-**3**$^{3+}$ 2Cl^{-} BAr$_f^{-}$	88	**85**:15 70 *R*
2	Δ-(*S*,*S*)-**3**$^{3+}$ 2Cl^{-} BAr$_f^{-}$	>99	23:**77** 53 *S*

[a]The conversion was determined by ^{1}H NMR integration of **14** versus an internal standard. [b]Enantio-selectivities were determined by chiral HPLC analyses.

4.3.1.3 The influence of the base

The catalyst screening was extended to include a range of nitrogen containing organic bases of various strengths. The data are summarized along with $pK_a(BH^+)$ values in H_2O (and DMSO where known)[97] of the protonated nitrogen bases in Table 4.8. Activation of the dialkyl malonate by deprotonation (pK_a = 13.0, 15.9; H_2O, DMSO)[98] is required since no conversion is observed in up to 24 hours in the presence of catalyst without base (Entry 1). It is also conceivable that the base could deprotonate an amino group of the catalyst dpen ligand. However, the pK_a (H_2O) of the related Werner trication, $[Co(en)_3]^{3+}$, could only be estimated as >14.[99] At best, a base such as Et_3N (pK_a = 10.8, 9.0; H_2O, DMSO) could only deprotonate Λ-(*S*,*S*)-**3**$^{3+}$ 2Cl^- BAr_f^- in very small equilibrium proportions.

Although the accepted mechanism of the Michael addition allows for the use of a catalytic amount of base, a stoichiometric amount of base is utilized in most cases herein. The exception is Entry 3 in which only 0.1 equivalents of Et_3N is used.

The enantioselectivities of the catalyzed Michael addition were fairly constant with nitrogen bases with $pK_a(BH^+)$ values within the 5-11 range. However, despite performing the reaction at –78 °C, catalysis in the presence of the strong base diazabicycloundecene (DBU) gave the product in only 15% ee (Entry 8).

To compliment Table 4.8, the conversions for entries 2,3-7 were periodically monitored by ^1H NMR for the first 7 hours and are shown in Figure 4.38. The rate of reaction is directly related to the strength of the base. With 1 equivalent of Et_3N, complete conversion is achieved within 2 hours. Surprisingly, reducing the base loading to 0.1 equivalents had little measureable effect on the rate, since 89% conversion was achieved in 30 minutes (not shown) and 97% conversion was achieved within 2 hours

(Table 4.8, Entry 3). With the weaker bases 4-dimethylamino pyridine (DMAP) and 1,4-diazabicyclo[2.2.2]octane (DABCO), the rate of catalysis was somewhat slower, but high levels of product conversion (>90%) were still achieved within 7 hours. With the even weaker bases N-methylmorpholine (NMM) and pyridine, a drastic rate reduction is observed and the reaction remains incomplete even after 24 hours.

Table 4.8. Data for the catalyzed Michael addition of **15a** to **14** in the presence of various bases.

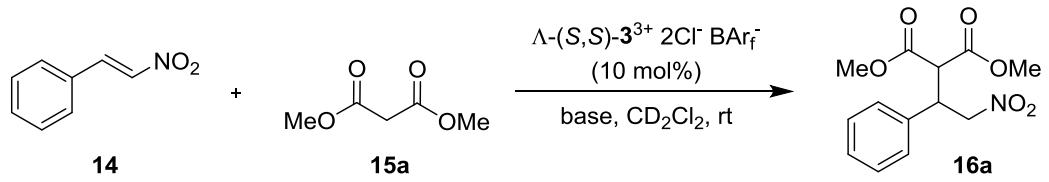

entry	base	$pK_a(BH)^+$ H_2O (DMSO)	conversion (%)[a]	er (R:S)[b]	ee (%)[b]
1	none	---	<1	---	---
2[c]	Et_3N	10.8 (9.0)	>99 (2 h)	**91**:9	82 *R*
3	Et_3N[d]	10.8 (9.0)	97 (2 h)	**90**:10	80 *R*
4	DMAP	9.2	>99 (7 h)	**91**:9	82 *R*
5	DABCO	8.8 (9.1)	92 (7 h)	**90**:10	80 *R*
6	NMM	7.4	70 (24 h)	**89**:11	79 *R*
7	pyridine	5.2 (3.4)	24 (24 h)	**92**:8	84 *R*
8[e]	DBU	(12)	>99 (15 h)	**58**:42	15 *R*

[a]The conversion was determined by ^{1}H NMR integration of **14** versus an internal standard. [b]Enantioselectivities were determined by chiral HPLC analyses. [c]Data are reproduced from Table 4.6, Entry 1. [d]Reaction performed with 10 mol% base. [e]Reaction performed at –78 °C.

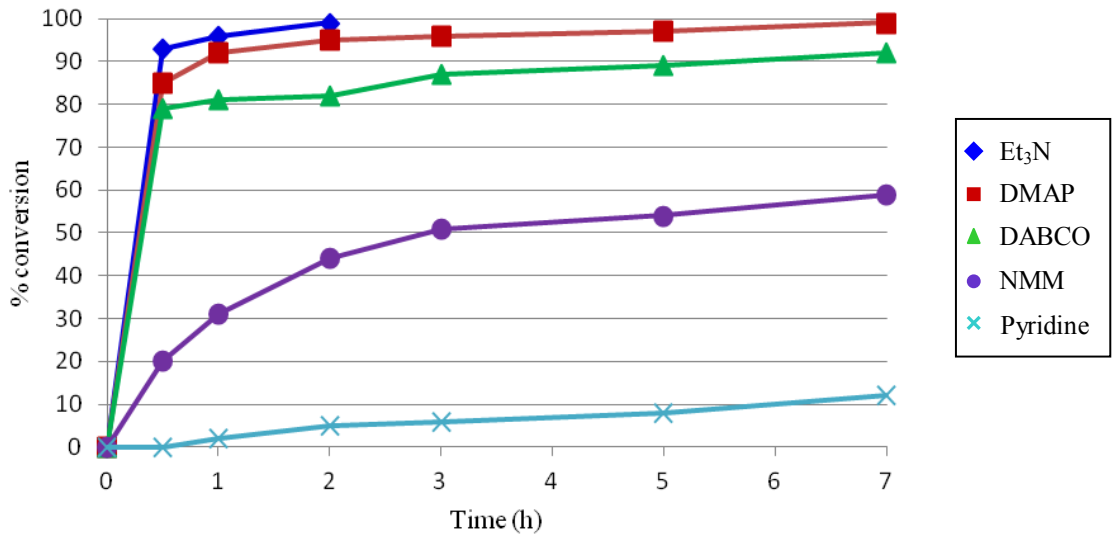

Figure 4.38. The effect of base on the rate of the catalyzed Michael addition.

4.3.1.4 The influence of the solvent and temperature

The reaction screening was performed in different solvents and at various temperatures. The data are summarized in Table 4.9. The Michael addition was catalyzed by Λ-(*S*,*S*)-**3**$^{3+}$ 2Cl^{-} BAr$_f^{-}$ in CD_2Cl_2 at 4 different temperatures (Entries 1-4). As expected, reactions conducted at lower temperatures resulted in slower conversions. Surprisingly, the selectivity of the catalysis is diminished at temperatures lower than room temperature. Heating the reaction to 35 °C did not erode the selectivity of the catalyst and complete conversion was reached within 1 hour.

The catalysis was performed in acetone-d_6 at room temperature (Entry 5). A slight increase in enantioselectivity was achieved at the cost of decreased reaction rate. Decreasing the temperature to 0 °C in acetone-d_6 led to a modest increase in enantioselectivity (Entry 6), yet the reaction requires 24 hours to reach 93% conversion.

The complex Δ-(*S*,*S*)-**3**$^{3+}$ 2Cl$^-$ BAr$_f^-$ catalyzes the Michael addition in acetone-d_6 at 0 °C with a significantly faster rate than Λ-(*S*,*S*)-**3**$^{3+}$ 2Cl$^-$ BAr$_f^-$. Once again, the opposite *S* product isomer is the major enantiomer, yet it is only achieved in 73% ee (Entry 7).

Catalysis with Λ-(*S*,*S*)-**3**$^{3+}$ 2Cl$^-$ BAr$_f^-$ in CD_3CN at 0 °C also showed a decrease in reaction rate as compared to catalysis in CD_2Cl_2, achieving 98% conversion after 7 hours (Entry 8). However, a slightly higher level of enantioselectivity of 83% ee was realized. Under the same conditions, Δ-(*S*,*S*)-**3**$^{3+}$ 2Cl$^-$ BAr$_f^-$ achieves complete conversion within 45 minutes and gives the product in 80% ee as the opposite *S* enantiomer (Entry 9).

Catalysis with Λ-(*S*,*S*)-**3**$^{3+}$ 2Cl$^-$ BAr$_f^-$ in the polar, protic solvent CD_3OD led to a significant decrease in enantioselectivity (Entry 10), consistent with the presence of the competing hydrogen bond donors.

The catalysts have very poor solubility in less polar solvents such as chloroform, hexane, and toluene. Therefore, these obvious solvents were not screened.

Table 4.9. Data for the catalyzed Michael addition of **15a** to **14** in various solvents.

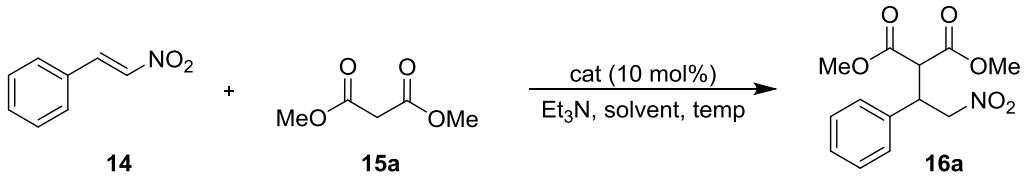

14 **15a** **16a**

entry	catalyst	solvent	temp (°C)	conv (%)[a]	er (R:S) ee (%)[b]
1	Λ-(*S*,*S*)-**3**$^{3+}$ 2Cl$^-$ BAr$_f^-$	CD_2Cl_2	–78	61 (48 h)	**85**:15 70 *R*
2	Λ-(*S*,*S*)-**3**$^{3+}$ 2Cl$^-$ BAr$_f^-$	CD_2Cl_2	0	91 (3 h)	**89**:11 78 *R*
3[c]	Λ-(*S*,*S*)-**3**$^{3+}$ 2Cl$^-$ BAr$_f^-$	CD_2Cl_2	rt	>99 (2 h)	**91**:9 82 *R*
4	Λ-(*S*,*S*)-**3**$^{3+}$ 2Cl$^-$ BAr$_f^-$	CD_2Cl_2	35	>99 (1 h)	**91**:9 82 *R*
5	Λ-(*S*,*S*)-**3**$^{3+}$ 2Cl$^-$ BAr$_f^-$	acetone-d_6	rt	>99 (24 h)	**92**:8 83 *R*
6	Λ-(*S*,*S*)-**3**$^{3+}$ 2Cl$^-$ BAr$_f^-$	acetone-d_6	0	93 (24 h)	**93**:7 87 *R*
7	Δ-(*S*,*S*)-**3**$^{3+}$ 2Cl$^-$ BAr$_f^-$	acetone-d_6	0	98 (12 h)	12:**88** 76 *S*
8	Λ-(*S*,*S*)-**3**$^{3+}$ 2Cl$^-$ BAr$_f^-$	CD_3CN	0	98 (7 h)	**91**:9 83 *R*
9	Δ-(*S*,*S*)-**3**$^{3+}$ 2Cl$^-$ BAr$_f^-$	CD_3CN	0	>99 (1 h)	10:**90** 80 *S*
10	Λ-(*S*,*S*)-**3**$^{3+}$ 2Cl$^-$ BAr$_f^-$	CD_3OD	0	>99 (14 h)	**81**:19 62 *R*

[a]The conversion was determined by ^{1}H NMR integration of **14** versus an internal standard. [b]Enantioselectivities were determined by chiral HPLC analyses. [c]Data are reproduced from Table 4.6, Entry 1.

4.3.1.5 The influence of substituents on the nitroolefin

Thus far, extensive catalyst screening has revealed that Λ-(*S*,*S*)-**3**$^{3+}$ 2Cl$^-$ BAr$_f^-$ gives higher enantioselectivities than Δ-(*S*,*S*)-**3**$^{3+}$ 2Cl$^-$ BAr$_f^-$ across all reaction conditions. Dimethyl malonate and Et_3N comprise the combination of nucleophile and base required to achieve the best catalyst rate and selectivity. Catalysis in CD_2Cl_2 at room temperature leads to very fast reaction rates and good enantioselectivities. Catalysis in acetone-d_6 at 0°C gives better enantioselectivities at the cost of significantly longer reaction times. Since catalysis in each solvent has its own advantages, both solvents were employed in the screening of a large range of substituted aromatic nitroolefins. The results are summarized in Table 4.10.

In every case, the conversion of each Michael acceptor proceeds at a significantly faster rate in CD_2Cl_2 (room temperature) compared to acetone-d_6 (0 °C). In CD_2Cl_2, conversion of at least 90% is generally achieved within 3 hours. In acetone-d_6, conversion of at least 90% generally requires 20 to 24 hours. Nitroolefin substrates that are electron rich (Entries 3 and 4) are intrinsically less reactive and are converted at slower rates. The nitroolefin **26** contains a bulkier group at the *ortho* position, which may explain the need for extended reaction times during catalysis in both solvents.

In general, catalysis in acetone-d_6 gives a significant boost in the enantioselectivity compared to the same reaction in CD_2Cl_2.

Nitroolefins with bulkier substituents in the *ortho* position were converted to Michael addition products with especially high enantioselectivities in acetone-d_6 (≥90% ee, Entries 1, 8-11). The best enantioselectivity is achieved with nitroolefin **27** (Entry 11, 94% ee), which contains an O-benzyl group at the *ortho* position.

Table 4.10. Data for the catalyzed Michael addition of **15a** to various nitroolefins.

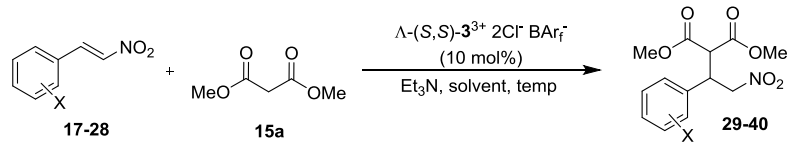

			CD_2Cl_2, rt		acetone-d_6, 0 °C					CD_2Cl_2, rt		acetone-d_6, 0 °C	
entry	Ar	react/prod	conv (%)[a]	er (R:S) ee (%)[b]	conv (%)[a]	er (R:S) ee (%)[b]	entry	Ar	react/prod	conv (%)[a]	er (R:S) ee (%)[b]	conv (%)[a]	er (R:S) ee (%)[b]
1		**17**/**29**	98 (3 h)	**83**:17 66 *R*	>99 (20 h)	**96**:4 92 *R*	7		**23**/**35**	97 (2 h)	**92**:8 85 *R*	96 (20 h)	**92**:8 85 *R*
2		**18**/**30**	95 (2 h)	**89**:11 77 *R*	95 (20 h)	**94**:6 88 *R*	8		**24**/**36**	93 (3 h)	**90**:10 81 *R*	>99 (20 h)	**95**:5 90 *R*
3	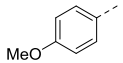	**19**/**31**	94 (6 h)	**86**:14 73 *R*	95 (20 h)	**91**:9 82 *R*	9		**25**/**37**	>99 (2 h)	**92**:8 84 *R*	98 (21 h)	**95**:5 91 *R*
4	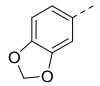	**20**/**32**	95 (2 h)	**92**:8 84 *R*	54 (20 h)	**87**:13 74 *R*	10		**26**/**38**	92 (20 h)	**87**:13 74 *R*	94 (48 h)	**95**:5 92 *R*
5	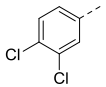	**21**/**33**	>99 (2 h)	**87**:13 74 *R*	>99 (20 h)	**90**:10 80 *R*	11		**27**/**39**	98 (2 h)	**95**:5 89 *R*	98 (22 h)	**97**:3 94 *R*
6		**22**/**34**	>99 (1 h)	**85**:15 70 *R*	98 (24 h)	**90**:10 81 *R*	12		**28**/**40**	>99 (1 h)	**90**:10 80 *R*	94 (21 h)	**92**:8 85 *R*

[a]The conversion was determined by ^{1}H NMR integration of the nitroolefin signal versus an internal standard. [b]Enantioselectivities were determined by chiral HPLC analyses.

*4.3.1.6 Semi-preparative scale catalysis with Λ-(S,S)-**3**$^{3+}$ 2Cl$^-$ BAr$_f^-$*

The preceding catalyst screenings with Λ-(*S*,*S*)-**3**$^{3+}$ 2Cl$^-$ BAr$_f^-$ were performed on NMR scales. Some of these experiments were subsequently performed on larger, semi-preparative scales that are more useful for synthetic chemists. The reactions were performed on a 0.33 mmol scale for the nitroolefins, which yields approximately 100 mg of enantioenriched product upon full conversion. The results of the larger scale catalysis are summarized in Table 4.11. In all cases, the products are isolated in good yields after column chromatography. The enantioselectivities are nearly identical to those obtained on NMR scales (Table 4.10).

Table 4.11. Catalysis with Λ-(*S*,*S*)-**3**$^{3+}$ 2Cl$^-$ BAr$_f^-$ on a semi-preparative scale.

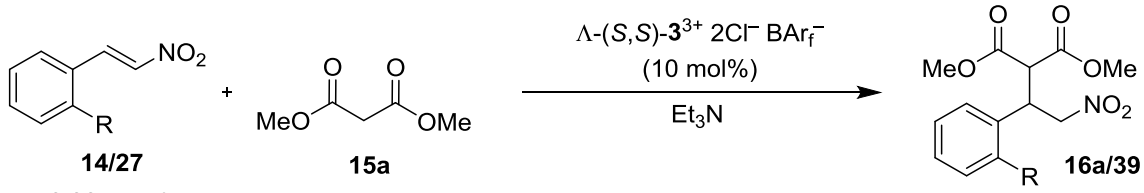

entry	reactant	react/prod	solvent/temp	time (h)	yield (%)[a]	er (R:S) ee (%)[b]
1	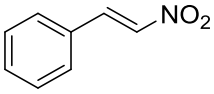	**14**/**16a**	CH_2Cl_2, rt	2	95	**91**:9 81 *R*
2	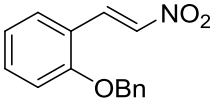	**27**/**39**	CH_2Cl_2, rt	2	96	**95**:5 91 *R*
3	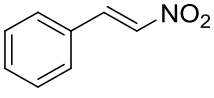	**14**/**16a**	acetone, 0 °C	15	94	**94**:6 87 *R*
4	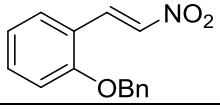	**27**/**39**	acetone, 0 °C	15	90	**97**:3 94 *R*

[a]Isolated yields after column chromatography. [b]The enantioselectivities were determined by chiral HPLC.

4.3.1.7 Catalyst recovery

The catalyst Λ-(*S*,*S*)-**3**$^{3+}$ 2Cl$^-$ BAr$_f^-$ can be recovered in high yields upon completion of the reactions. In a typical workup, the acetone is removed and the reaction mixture dissolved in CH_2Cl_2. Extraction with aqueous 1 M HCl removes the Et_3N. Despite the presence of a nearly 100-fold excess of aqueous HCl, the BAr$_f^-$ anion does not undergo metathesis with a Cl$^-$ anion. Furthermore, there is no visible color leaching from the organic phase to the aqueous phase, demonstrating that the cobalt complex remains completely soluble in CH_2Cl_2. The separated organic phase is loaded directly onto a silica gel column. The organic products are eluted with 9:1 v/v hexanes/EtOAc. Under these conditions, the orange band consisting of the catalyst does not move from the top of the column. The column is purged with CH_2Cl_2 and then Λ-(*S*,*S*)-**3**$^{3+}$ 2Cl$^-$ BAr$_f^-$ is eluted with 95:5 v/v CH_2Cl_2/MeOH. The catalyst, after drying overnight at room temperature under oil pump vacuum, is recovered in up to 97% yield. The ^{1}H NMR spectrum (Figure 4.39) of the recovered catalyst was similar to that of the fresh catalyst, albeit with some minor impurities in the alkane region between 1 and 2 ppm. However, these are negligible as the elemental analysis is consistent for the monohydrate Λ-[Co(*S*,*S*-dpen)$_3$]$^{3+}$ 2Cl$^-$ BAr$_f^-$·H_2O. The ^{1}H NMR integration also allows for 1-2 molecules of H_2O. The ^{13}C{^{1}H} NMR spectrum gives only a single CNH_2 peak at 63.6 ppm, proving that the catalyst is recovered as the pure Λ-diastereomer.

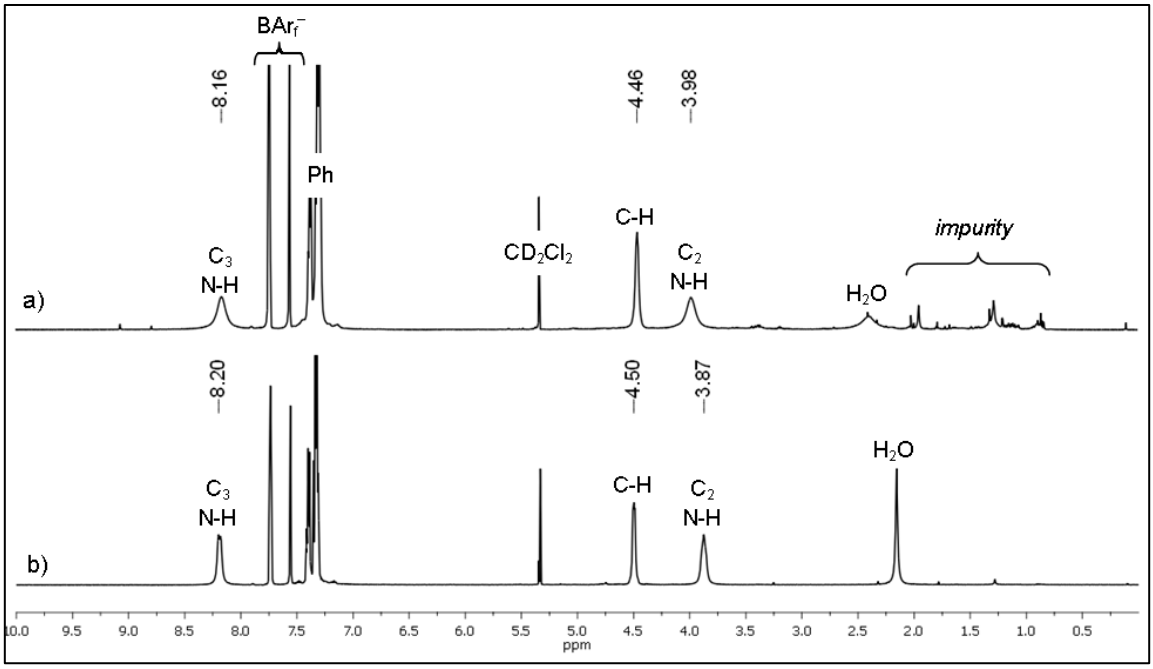

Figure 4.39. Comparison of the ^{1}H NMR spectra (CD_2Cl_2) of a) recovered and b) newly prepared Λ-(*S*,*S*)-**3**$^{3+}$ 2Cl$^-$ BAr$_f^-$.

4.3.1.8 The influence of the catalyst counteranions

Both the crystal structure of Λ-(*S*,*S*)-**3**$^{3+}$ 3Cl$^-$ (Figure 4.4) and the ^{1}H NMR spectrum of Λ-(*S*,*S*)-**3**$^{3+}$ 2Cl$^-$ BAr$_f^-$ (Figure 4.14a) reveal strong hydrogen bonding interactions between the N-H groups of the (*S*,*S*)-**2** ligands and the Cl$^-$ counteranions. These interactions could have a negative effect on the rate of catalysis because the Cl$^-$ counteranion would compete with the nitroolefin for hydrogen bonding sites on the catalyst. Faster reaction rates may be achieved by replacing the two Cl$^-$ counteranions with two less-coordinating counteranions that are poorer hydrogen bond acceptors. To this end, Λ-(*S*,*S*)-**3**$^{3+}$ 2BF$_4^-$ BAr$_f^-$ and Λ-(*S*,*S*)-**3**$^{3+}$ 2PF$_6^-$ BAr$_f^-$ were introduced as catalysts for the Michael addition of dialkyl malonates to nitroolefins.

Reaction conditions that promoted particularly slow rates of conversion were required to accurately compare the catalysts. The Michael addition was performed with **15a** and the electron rich nitroolefin **19**. The catalysts Λ-(*S*,*S*)-$\mathbf{3}^{3+}$ $2Cl^-$ BAr_f^-, Δ-(*S*,*S*)-$\mathbf{3}^{3+}$ $2Cl^-$ BAr_f^-, Λ-(*S*,*S*)-$\mathbf{3}^{3+}$ $2BF_4^-$ BAr_f^-, and Λ-(*S*,*S*)-$\mathbf{3}^{3+}$ $2PF_6^-$ BAr_f^- were employed at 2 mol% loadings in the presence of only 35 mol% of Et_3N. The conversions for the first 3 hours of reaction were measured by ^1H NMR and are shown in Figure 4.40.

The catalyst that gave the slowest rate of conversion was Λ-(*S*,*S*)-$\mathbf{3}^{3+}$ $2Cl^-$ BAr_f^-. For the Λ-diastereomer series, faster rates were achieved when the chloride counteranions were replaced with less coordinating anions. An increase in catalysis rate was achieved with Λ-(*S*,*S*)-$\mathbf{3}^{3+}$ $2BF_4^-$ BAr_f^- and then, to an even greater extent, with Λ-(*S*,*S*)-$\mathbf{3}^{3+}$ $2PF_6^-$ BAr_f^-. Surprisingly, the fastest reaction rate was found with the diastereomeric Δ-(*S*,*S*)-$\mathbf{3}^{3+}$ $2Cl^-$ BAr_f^-. This catalyst achieved nearly complete conversion within 3 hours, despite the presence of the two hydrogen bonding Cl^- counteranions.

The enantioselectivities, as well as the overall reaction conversions after 24 hours, are summarized in Table 4.12. Notably, the reaction catalyzed by Λ-(*S*,*S*)-$\mathbf{3}^{3+}$ $2Cl^-$ BAr_f^- only reached 88% conversion after one full day while the other three catalysts each achieved >95% conversion. However, at only 2 mol% loading, each catalyst appears to level off before reaching quantitative conversion.

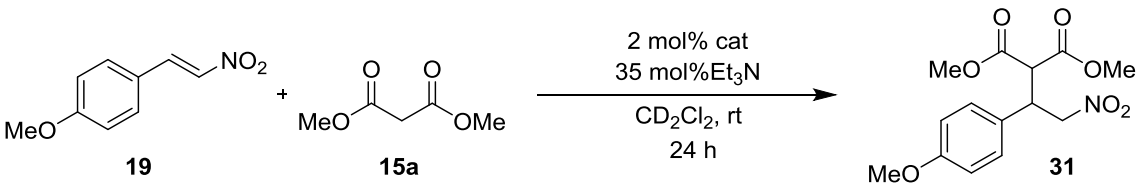

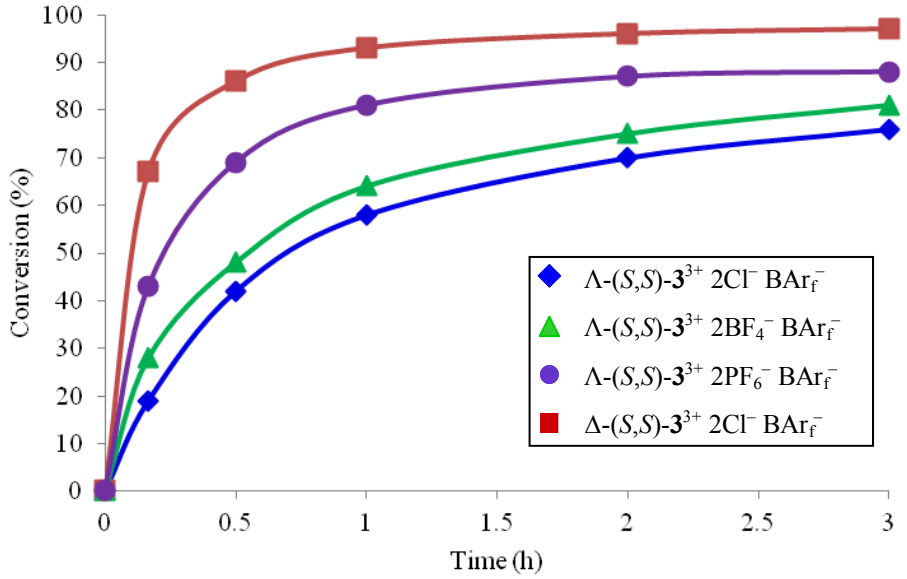

Figure 4.40. Reaction rate profiles for the Michael addition of **15a** to **19** at 2 mol% catalyst loading.

Table 4.12. Data for the catalyzed Michael addition of **15a** to **19** with various catalysts at 2 mol%.

entry	catalyst	conversion (%)[a]	er (R:S) ee (%)[b]
1	Λ-(*S*,*S*)-**3**$^{3+}$ 2Cl^{-} BAr$_f^{-}$	88	**81**:19 63 *R*
2	Λ-(*S*,*S*)-**3**$^{3+}$ 2BF$_4^{-}$ BAr$_f^{-}$	96	**83**:17 66 *R*
3	Λ-(*S*,*S*)-**3**$^{3+}$ 2PF$_6^{-}$ BAr$_f^{-}$	96	**85**:15 69 *R*
4	Δ-(*S*,*S*)-**3**$^{3+}$ 2Cl^{-} BAr$_f^{-}$	98	27:**73** 47 *R*

[a]The conversion was determined by ^{1}H NMR integration of **19** versus an internal standard. [b]Enantio-selectivities were determined by chiral HPLC analyses.

For the catalysts with the Λ configurations, the stepwise increase in rate is matched by a gradual increase in enantioselectivity. Thus, Λ-(*S*,*S*)-**3**$^{3+}$ 2BF_4^- BAr_f^- catalyzed the Michael addition in slightly higher selectivity (66% ee) than Λ-(*S*,*S*)-**3**$^{3+}$ 2Cl^- BAr_f^- (63% ee). The even faster catalyst Λ-(*S*,*S*)-**3**$^{3+}$ 2PF_6^- BAr_f^- gives still better enantioselectivity (69% ee). The opposite diastereomer, Δ-(*S*,*S*)-**3**$^{3+}$ 2Cl^- BAr_f^-, gives the opposite product enantiomer, but with lower absolute enantioselectivity (47%) than the catalysts with the Λ configuration.

The enantioselectivity decreased when the catalyst loading of Λ-(*S*,*S*)-**3**$^{3+}$ 2Cl^- BAr_f^- decreased from 10 mol% (73% ee, Table 4.10, Entry 3) to 2 mol% (63% ee, Table 4.12, Entry 1). It was hoped that the modest improvement in enantioselectivities afforded by Λ-(*S*,*S*)-**3**$^{3+}$ 2BF_4^- BAr_f^- and Λ-(*S*,*S*)-**3**$^{3+}$ 2PF_6^- BAr_f^- in Table 4.12 could be further amplified when applied at higher catalyst loadings.

Accordingly, the Michael addition of **15a** to nitroolefins was catalyzed by Λ-(*S*,*S*)-**3**$^{3+}$ 2BF_4^- BAr_f^- and Λ-(*S*,*S*)-**3**$^{3+}$ 2PF_6^- BAr_f^- at 10 mol% loading in various solvents. The data are summarized in Table 4.13. With **14** as the electrophile, catalysis with Λ-(*S*,*S*)-**3**$^{3+}$ 2BF_4^- BAr_f^- was performed in three polar organic solvents (Entries 1-3). The data follows the same trends that were established with Λ-(*S*,*S*)-**3**$^{3+}$ 2Cl^- BAr_f^- (Table 4.9). Higher enantioselectivities are achieved in CD_3CN (88% ee) and acetone-d_6 (90% ee) as compared to CD_2Cl_2 (84% ee).

The catalyst Λ-(*S*,*S*)-**3**$^{3+}$ 2Cl^- BAr_f^- had previously achieved the highest enantioselectivity with **27** as the Michael acceptor in acetone-d_6 at 0 °C (94% ee, Table 4.10, Entry 11). These optimized conditions were applied to the catalyst Λ-(*S*,*S*)-**3**$^{3+}$ 2BF_4^- BAr_f^-, and also afforded the Michael addition product in excellent enantioselectivity (97% ee, Entry 4). In every case, the enantioselectivity achieved with Λ-(*S*,*S*)-**3**$^{3+}$ 2BF_4^- BAr_f^- is higher than that achieved with Λ-(*S*,*S*)-**3**$^{3+}$ 2Cl^- BAr_f^- under

otherwise identical conditions. Likewise, the reaction rate with Λ-(*S*,*S*)-**3**$^{3+}$ 2BF_4^- BAr_f^- is universally higher than that of reactions catalyzed by Λ-(*S*,*S*)-**3**$^{3+}$ 2Cl^- BAr_f^-.

Catalysis with Λ-(*S*,*S*)-**3**$^{3+}$ 2PF_6^- BAr_f^- in acetone-d_6 at 0 °C results in even faster rates and complete conversions are achieved within 4 hours (Table 4.13, Entries 5 and 6). Although Λ-(*S*,*S*)-**3**$^{3+}$ 2PF_6^- BAr_f^- afforded the highest enantioselectivities under the conditions outlined in Figure 4.40, this catalyst gave slightly lower enantioselectivities than Λ-(*S*,*S*)-**3**$^{3+}$ 2BF_4^- BAr_f^- in acetone-d_6.

Table 4.13. Data for the optimized Michael addition of **15a** to nitroolefins with various catalysts.

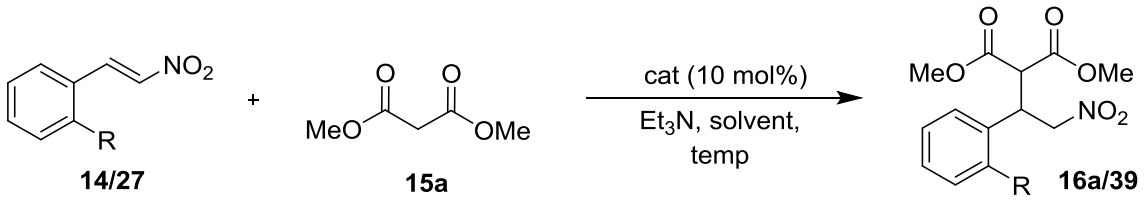

entry	catalyst	react/ prod	R	solvent	temp (°C)	conv (%)[a]	er (R:S) ee (%)[b]
1	Λ-(*S*,*S*)-**3**$^{3+}$ 2BF_4^- BAr_f^-	**14**/**16a**	H	CD_2Cl_2	rt	>99 (1 h)	**92**:8 84 *R*
2	Λ-(*S*,*S*)-**3**$^{3+}$ 2BF_4^- BAr_f^-	**14**/**16a**	H	CD_3CN	0	99 (3 h)	**94**:6 88 *R*
3	Λ-(*S*,*S*)-**3**$^{3+}$ 2BF_4^- BAr_f^-	**14**/**16a**	H	acetone-d_6	0	94 (10 h)	**95**:5 90 *R*
4	Λ-(*S*,*S*)-**3**$^{3+}$ 2BF_4^- BAr_f^-	**27**/**39**	OBn	acetone-d_6	0	99 (7 h)	**98**:2 97 *R*
5	Λ-(*S*,*S*)-**3**$^{3+}$ 2PF_6^- BAr_f^-	**14**/**16a**	H	acetone-d_6	0	>99 (4 h)	**92**:8 85 *R*
6	Λ-(*S*,*S*)-**3**$^{3+}$ 2PF_6^- BAr_f^-	**27**/**39**	OBn	acetone-d_6	0	>99 (4 h)	**97**:3 94 *R*[c]

[a]The conversion was determined by ^{1}H NMR integration of the nitroolefin versus an internal standard. [b]Enantioselectivities were determined by chiral HPLC analyses. [c]Average of two experiments.

*4.3.1.9 Semi-preparative scale catalysis with Λ-(S,S)-**3**$^{3+}$ 2BF_4^- BAr_f^-*

The optimized reaction conditions for the enantioselective Michael addition of **15a** to nitroolefins employed Λ-(*S*,*S*)-**3**$^{3+}$ 2BF_4^- BAr_f^- as the catalyst in acetone at 0 °C. Therefore, this catalyst was applied towards larger scale reactions across a full range of nitroolefin substrates. Similar to Section 4.3.1.6, catalysis on this scale was designed to isolate approximately 100 mg of enantioenriched product. In a typical experiment, a nitroolefin (0.330 mmol) was combined with **15a** and Λ-(*S*,*S*)-3^{3+} 2BF_4^- BAr_f^- in acetone (3.33 mL). The reaction was conducted at 0 °C with one equivalent of Et_3N. The enantioenriched Michael addition products were isolated after column chromatography. The results of the semi-preparative scale catalysis with Λ-(*S*,*S*)-**3**$^{3+}$ 2BF_4^- BAr_f^- are summarized in Table 4.14.

Nearly all reactions exhibit complete conversion of the nitroolefin after 12 hours by TLC. The exceptions (Entries 1 and 9) still show some starting material even after extending the reaction to 18 hours. Despite the perceived quantitative conversion of the nitroolefins to Michael addition products, some product is inevitably lost during the purification procedure. However, the isolated yields are still quite high and in most cases exceed 90%.

The lowest enantioselectivity is achieved from the electron-rich nitroolefin (**19**, 78% ee, Entry 1). However, a wide range of nitroolefins (Entries 4-11) is converted to the Michael addition product in excellent enantioselectivity (>90% ee). This includes an unfunctionalized aromatic nitroolefin (**14**, Entry 4), a nitroolefin containing an electron withdrawing group (**21**, Entry 5), a heterocyclic aromatic nitroolefin (**41**, Entry 6), and a bulky aromatic nitroolefin (**17**, Entry 7). Once again, aromatic nitroolefins with substituents in the *ortho* position are obtained with the highest enantioselectivity (Entries

8-11, 93-96% ee). An aliphatic nitroolefin (**42**) was also isolated in good yield and 80% ee.

Table 4.14. Catalysis with Λ-(*S*,*S*)-**3**$^{3+}$ 2BF_4^- BAr_f^- on a semi-preparative scale.

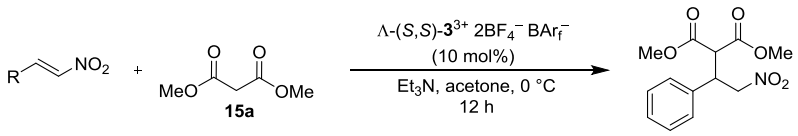

entry	nitroolefin	react/ prod	yield (%)[a]	er (R:S) ee (%)[b]	entry	nitroolefin	react/ prod	yield (%)[a]	er (R:S) ee (%)[b]
1	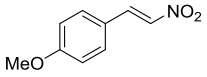	**19/31**	87[c]	**89**:11 78 *R*	7	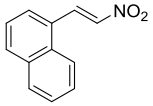	**17/29**	98	**96**:4 93 *R*
2	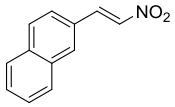	**18/30**	92	**92**:8 83 *R*	8	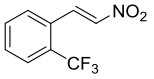	**24/36**	98	**97**:3 93 *R*
3	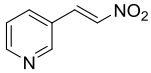	**22/34**	90	**93**:7 86 *R*	9	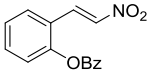	**26/38**	86[c]	**96**:4 93 *R*
4	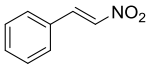	**14/16a**	97	**95**:5 90 *R*	10	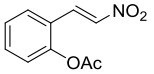	**25/37**	96	**97**:3 94 *R*
5	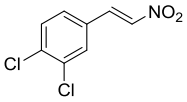	**21/33**	94	**95**:5 90 *R*	11	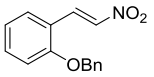	**27/39**	95	**98**:2 96 *R*
6	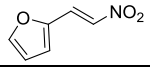	**41/43**	91	5:**95** 91 *S*[100]	12	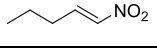	**42/44**	83	**10**:90 80 *S*[100]

[a]Isolated yield after column chromatography. [b]Enantioselectivities were determined by chiral HPLC analyses. [c]reaction time increased to 18 h.

Recovery of the Λ-(*S*,*S*)-**3**$^{3+}$ 2BF_4^- BAr_f^- catalyst proved to be more complicated. The removal of base by acid extraction with aqueous HCl generated Λ-(*S*,*S*)-**3**$^{3+}$ 2Cl^- BAr_f^-, which was recovered in up to 74% yield. Performing the extraction with the weaker acid, acetic acid (AcOH), resulted in a high catalyst recovery of 99% after column chromatography. However, the ^{1}H NMR spectrum of the isolated

catalyst was consistent for a Λ-[Co((*S*,*S*)-dpen)$_3$]$^{3+}$ 2AcO$^-$ BAr$_f^-$ salt. Extracting the reaction with aqueous HBF$_4$·OEt$_2$ allowed for the successful recovery of Λ-(*S*,*S*)-**3**$^{3+}$ 2BF$_4^-$ BAr$_f^-$. Unfortunately, Et$_3$NH$^+$ BF$_4^-$ coelutes from the silica gel column with the catalyst and the isolated material is approximately a 1:9 [Co]/Et$_3$NH$^+$ BF$_4^-$ mixture. The recovery of Λ-[Co((*S*,*S*)-dpen)$_3$]$^{3+}$ 2BF$_4^-$ BAr$_f^-$ was also attempted without an acid extraction workup. In this case the reaction mixture was loaded directly onto a silica gel column. The recovered catalyst material was approximately a 1.0:0.7 [Co]/Et$_3$N mixture. The base could not be removed even after drying the material under oil pump vacuum for 24 hours at 50 °C. Furthermore, the ^{1}H NMR integrations of the BAr$_f^-$ peaks were double that of the expected value, indicating that further anion reorganization had occurred. However, the ^{13}C{^{1}H} NMR spectrum revealed only a single peak at 63.8 ppm, which is consistent with the Λ-diastereomer.

For future applications of the catalyst Λ-(*S*,*S*)-**3**$^{3+}$ 2BF$_4^-$ BAr$_f^-$, it is recommended that the catalyst be recovered as Λ-(*S*,*S*)-**3**$^{3+}$ 2Cl$^-$ BAr$_f^-$ and regenerated with the addition of Ag$^+$ BF$_4^-$ as described in Scheme 4.5.

4.3.1.10 The influence of water and biphasic reaction conditions

Nearly all of the catalysts are isolated with a small amount of coordinated H$_2$O. Because of this, no attempt was made to rigorously dry the solvents or glassware and reactions were conducted under ambient atmosphere. In theory, H$_2$O could occupy substrate binding sites of the catalyst, diminishing rates, or serve as an alternative hydrogen bond donor, diminishing enantioselectivities. Several experiments were conducted to test the effect of this adventitious H$_2$O on the catalyzed Michael addition reaction. The results are summarized in Table 4.15.

Table 4.15. The effect of H_2O on the catalyzed Michael addition of dimethyl malonate to nitroolefins.

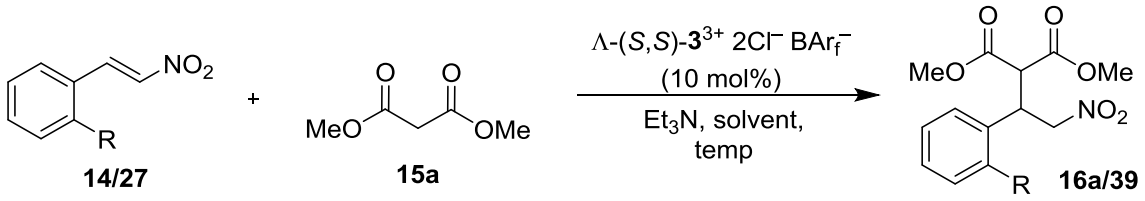

entry	react/prod	R	solvent	temp (°C)	conv (%)[a]	er (R:S) ee (%)[b]
1	**14**/**16a**	H	acetone-d_6 (dry)[c]	0	96 (24 h)	**93**:7 86 *R*
2	**27**/**39**	OBn	acetone-d_6 (dry)[c]	0	71 (22 h) 93 (63 h)	**97**:3 94 *R*
3	**14**/**16a**	H	9:1 acetone-d_6/ D_2O	0	>99 (15 h)	**78**:22 56 *R*
4	**27**/**39**	OBn	7:1 CH_2Cl_2/H_2O	rt	96 (1 h)[d]	**88**:12 75 *R*

[a]The conversion was determined by ^{1}H NMR integration of the nitroolefin versus an internal standard. [b]Enantioselectivities were determined by chiral HPLC analyses. [c]The solvent is freshly distilled and the catalysis performed over activated 3Å sieves. [d]Isolated yield after column chromatography.

An "anhydrous" Michael addition of **15a** to nitroolefin **14** was catalyzed by Λ-(*S*,*S*)-**3**$^{3+}$ 2Cl$^–$ BAr$_f^–$ in distilled acetone-d_6 (Table 4.15, Entry 1). Before the Et_3N base was added, the catalyst reaction mixture was dried over activated molecular sieves for 3 hours during which time the H_2O ^{1}H NMR peak disappeared. The enantioselectivity of the "anhydrous" catalyzed reaction was virtually the same as that in the presence of adventitious water (Table 4.9, Entry 6). Similarly, the "anhydrous" Michael addition to nitroolefin **27** (Entry 2) was achieved with the same selectivity as the analogous "wet" reaction (Table 4.10, Entry 11), but in this particular case a drastic decrease in reaction rate was observed. Whereas in the presence of a small amount of water, the reaction

reached 98% conversion after 22 hours, the anhydrous reaction only achieves 71% conversion in the same time. Even after 63 hours, the conversion had only reached 93%.

A similar reaction was carried out in the presence of an artificially high concentration of H_2O (Table 4.15, Entry 3). Catalysis in a homogeneous solution of 9/1 v/v acetone-d_6:D_2O resulted in quantitative conversion of nitroolefin **14** within 15 hours but severely diminished the enantioselectivity to 56% ee. Overall, the presence of an adventitious amount of H_2O in acetone increases the reaction rate without sacrificing selectivity, but catalysis with artificially "wet" acetone erodes the selectivity.

Surprisingly, catalysis with artificially "wet" CH_2Cl_2 only slightly decreased the enantioselectivity (Table 4.15, Entry 4). In this case, the 7/1 v/v CH_2Cl_2:H_2O solvent mixture results in an organic/aqueous bilayer. Despite the excess H_2O, the product is isolated in high yields after only one hour and the selectivity (75% ee) is comparable to that of analogous catalysis in the absence of H_2O (82% ee, Table 4.6, Entry 1).

Since relatively good enantioselectivity was achieved even in the presence of an aqueous bilayer, it was conceived that this catalyst system could support phase-transfer catalysis. In this case, the catalyst and organic substrates are dissolved in CH_2Cl_2 while the inorganic base Na_2CO_3 is dissolved in H_2O, as depicted in Scheme 4.14. During the course of the reaction, an anion exchange equilibrium could be established in which the carbonate anion (CO_3^{2-}) transfers to the organic phase and becomes ion paired with the Werner complex. The now CH_2Cl_2 soluble CO_3^{2-} dianion can serve as a base to deprotonate the dimethyl malonate and initiate the catalytic reaction.

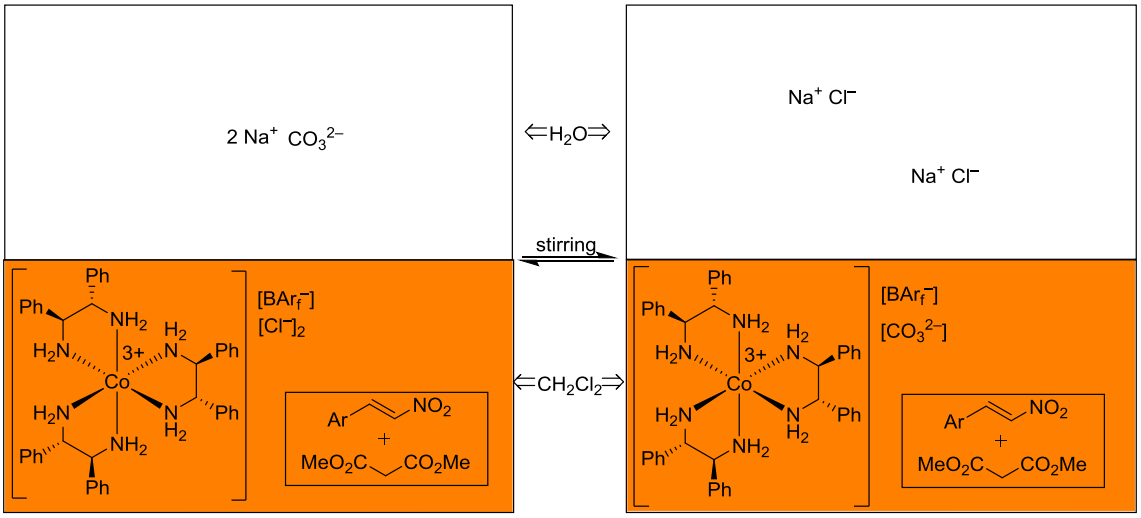

Scheme 4.14. Proposed phase transfer when $2Na^+ CO_3^{2-}$ is employed as a base in the Michael addition catalyzed by Λ-(*S*,*S*)-$\mathbf{3}^{3+}$ $2Cl^-$ BAr_f^- (Table 4.16).

The biphasic conditions were applied to the Michael addition of **15a** to various nitroolefins as seen in Table 4.16. Catalysis was performed with one equivalent of Na_2CO_3 with respect to the nitroolefin, meaning a 10-fold excess of the CO_3^{2-} dianion compared to the catalyst. In each case, the products were isolated in good yields after 15 hours. All enantioselectivities were higher under these biphasic conditions than in CH_2Cl_2 alone (Table 4.10). During the course of the reaction, the lower CH_2Cl_2 phase remained bright orange and there was no visible leaching of color to the upper aqueous phase. Attempts were made to recover the catalyst directly from the reaction mixture as the carbonate salt, Λ-[Co((*S*,*S*)-dpen)$_3$]$^{3+}$ CO_2^{2-} BAr_f^-, but the complex rapidly decomposed after the removal of the aqueous layer and evaporation of the CH_2Cl_2. However, the catalyst could be recovered as Λ-(*S*,*S*)-$\mathbf{3}^{3+}$ $2Cl^-$ BAr_f^- in 91% yield after an aqueous quench with HCl and column chromatography.

Table 4.16. Data for the biphasic catalyzed Michael addition of **15a** to nitroolefins.

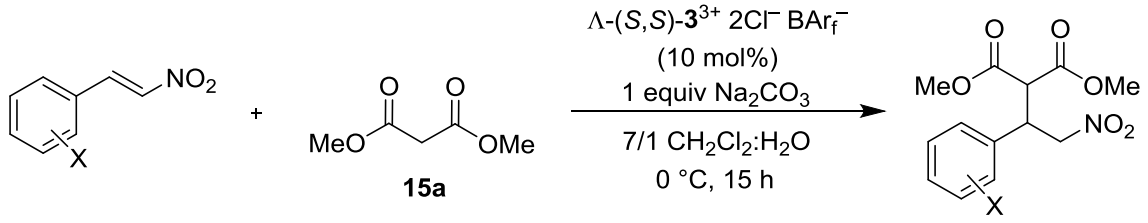

entry	nitroolefin	react/prod	yield (%)[a]	er (R:S) ee (%)[b]
1	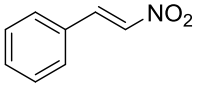	**14**/**16a**	88	**92**:8 84 *R*
2	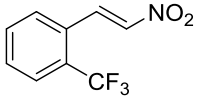	**24**/**36**	84	**93**:7 87 *R*
3	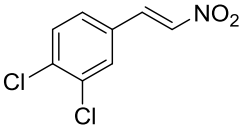	**21**/**33**	85	**94**:6 88 *R*
4	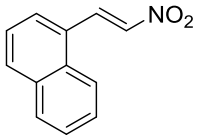	**17**/**29**	85	**94**:6 89 *R*
5	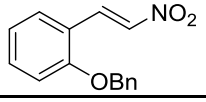	**27**/**39**	84	**95**:5 90 *R*

[a]Isolated yield after column chromatography. [b]Enantioselectivities were determined by chiral HPLC analyses.

4.3.1.11 Screening of miscellaneous catalysts

Various other catalysts were screened for the Michael addition of **15a** to **14** and the results are summarized in Table 4.17. The conditions applied were identical to those of the previously optimized conditions for Λ-(*S*,*S*)-**3**$^{3+}$ 2Cl^{-} BAr$_f^{-}$ (Table 4.9, Entry 6). The catalyst with a chiral counteranion, Λ-(*S*,*S*)-**3**$^{3+}$ 2camphSO$_3^{-}$ BAr$_f^{-}$, achieves the

product in 72% ee. It is not known whether this decrease in enantioselectivity is a result of a mismatched chiral arrangement between the anion and Werner complex or due to some other unfavorable interaction with the new anion. Catalysis with both Λ- and Δ-(*S*,*S*)-**11**$^{3+}$ 2Cl^{-} BAr$_f^{-}$, which possess electron donating *p*-methoxyphenyl groups, gave lower enantioselectivities than the corresponding catalysts with unfunctionalized dpen ligands (Entries 2 and 3).

Catalysis with the bulky, α-naphthyl substituted Λ-(*S*,*S*)-**13**$^{3+}$ 2Cl^{-} BAr$_f^{-}$ resulted in a remarkably low rate of conversion and poor enantioselectivity. Even after 48 hours, the reaction had only reached 60% conversion. The reaction rate was significantly improved with the mixed BF$_4^{-}$/BAr$_f^{-}$ salt Λ-(*S*,*S*)-**13**$^{3+}$ 2BF$_4^{-}$ BAr$_f^{-}$. The enantioselectivity was also significantly improved, but under these conditions the best enantioselectivities that had previously been achieved with Λ-(*S*,*S*)-**3**$^{3+}$ 2BF$_4^{-}$ BAr$_f^{-}$ (Table 4.13, Entry 3) were not be matched.

For each of the catalysts screened in Table 4.17, those that contained the Λ metal configuration afforded the *R* product enantiomer while the catalyst containing the Δ metal configuration afforded the *S* product enantiomer. This is consistent with the observed stereoselectivities achieved with the unfunctionalized Λ-(*S*,*S*)-**3**$^{3+}$ 2Cl^{-} BAr$_f^{-}$ and Δ-(*S*,*S*)-**3**$^{3+}$ 2Cl^{-} BAr$_f^{-}$ catalysts.

Table 4.17. Data for the screening of miscellaneous catalysts in the Michael addition of **15a** to **14**.

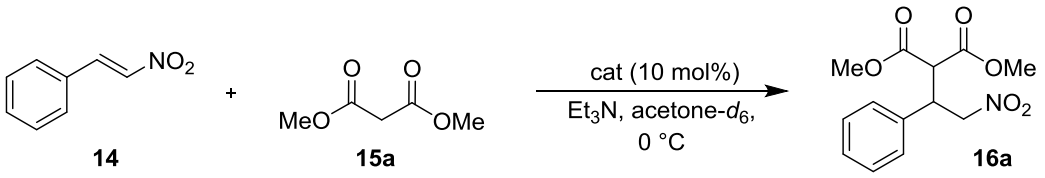

entry	catalyst	diamine aryl group	conversion (%)[a]	er (R:S) ee (%)[b]
1	Λ-(*S*,*S*)-**3**$^{3+}$ 2camphSO$_3^-$ BAr$_f^-$	Ph	>99 (24 h)	**86**:14 72 *R*
2	Λ-(*S*,*S*)-**11**$^{3+}$ 2Cl$^-$ BAr$_f^-$	*p*-OMe-C$_6$H$_4$	>99 (24 h)	**87**:13 74 *R*
3	Δ-(*S*,*S*)-**11**$^{3+}$ 2Cl$^-$ BAr$_f^-$	*p*-OMe-C$_6$H$_4$	>99 (24 h)	16:**84** 69 *S*
4	Λ-(*S*,*S*)-**13**$^{3+}$ 2Cl$^-$ BAr$_f^-$	α-naphthyl	25 (5 h) 60 (48 h)	**64**:36 28 *R*
5	Λ-(*S*,*S*)-**13**$^{3+}$ 2BF$_4^-$ BAr$_f^-$	α-naphthyl	58 (5 h) 90 (48 h)	**86**:14 71 *R*

[a]The conversion was determined by ^{1}H NMR integration of **14** versus an internal standard. [b]Enantioselectivities were determined by chiral HPLC analyses.

4.3.2 The enantioselective Michael addition of diphenyl phosphite to nitroolefins

Besides dialkyl malonates, other nucleophiles can be added to **14**. The Michael addition of diphenyl phosphite (**45**) to nitroolefins has been catalyzed with high enantioselectivities by chiral, bifunctional organocatalysts.[101] This Michael addition was also catalyzed by the Werner catalysts and the data are summarized in Table 4.18. Both of the diastereomeric catalysts Λ- and Δ-(*S*,*S*)-**3**$^{3+}$ 2Cl$^-$ BAr$_f^-$ afforded complete conversion within 2 hours. Once again, the two catalysts yielded products with opposite configurations. Surprisingly, the catalyst with the Δ configuration, which was less

enantioselective in all previously described reactions, achieved far better selectivity in the addition of **45**.

Table 4.18. Data for the catalyzed Michael addition of diphenyl phosphite to **14.**

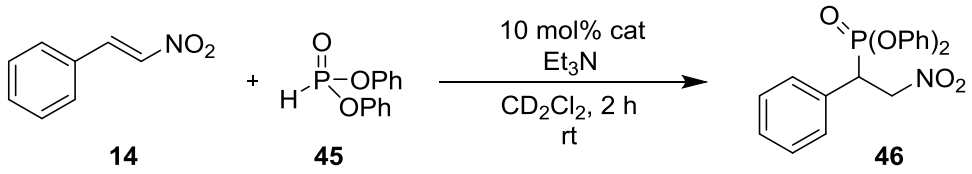

14 **45** **46**

entry	catalyst	conversion (%)[a]	er (R:S) ee (%)[b]
1	Λ-(*S*,*S*)-**3**$^{3+}$ 2Cl$^-$ BAr$_f^-$	>99	**68**:32 35 *R*
2	Δ-(*S*,*S*)-**3**$^{3+}$ 2Cl$^-$ BAr$_f^-$	>99	7:**93** 85 *S*

[a]The conversion was determined by ^{1}H NMR integration of **14** versus an internal standard. [b]Enantioselectivities were determined by chiral HPLC analyses. The assignments of the enantiomers (*R*/*S*) were made by comparisons of the elution orders with those under previously reported HPLC conditions.[99a]

4.3.3 The Michael addition of nitroethane to nitroolefins

The Werner complexes were also screened as catalysts for the Michael addition of nitroethane (**47**) to **14**, which has previously been catalyzed with high enantioselectivity by a chiral Lewis acid.[102] The results are summarized in Table 4.19. In this case, the yield of the expected Michael adduct was always lower than the conversion of **14**, indicating the formation of side-products. Because two new stereocenters are generated in the reaction, up to four *syn*/*anti* diastereomers of the product are possible. For each reaction, four previously characterized stereoisomers[102] were obtained, as assayed by ^{1}H NMR and HPLC. In all cases, the diastereoselectivity

(*syn* vs. *anti*) was poor. Overall, the enantioselectivity achieved for each diastereomer was low, reaching a maximum of 30% ee (Entries 3 and 4). As usual, the Λ and Δ-(*S*,*S*)-**3**$^{3+}$ 2Cl$^-$ BAr$_f^-$ diastereomers gave products of opposite absolute configurations (Table 4.19, Entries 1 and 4).

Table 4.19. Data for the Michael addition of nitroethane to **14.**

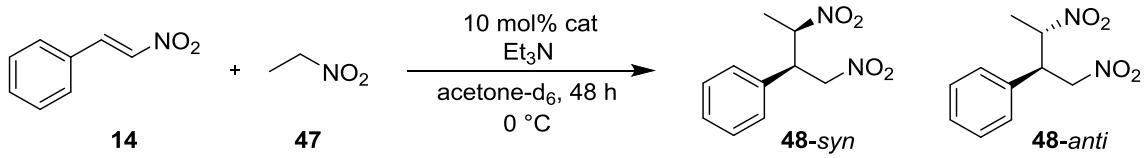

14 **47** **48-*syn*** **48-*anti***

entry	catalyst	conv (%)[a]	yield (%)[a]	dr[b] (*syn*:*anti*)	ee (%)[c] (*syn*)	ee (%)[c] (*anti*)
1	Λ-(*S*,*S*)-**3**$^{3+}$ 2Cl$^-$ BAr$_f^-$	74	43	55:45	28	20
2	Λ-(*S*,*S*)-**3**$^{3+}$ 2BF$_4^-$ BAr$_f^-$	87	50	52:48	30	25
3	Λ-(*S*,*S*)-**3**$^{3+}$ 2PF$_6^-$ BAr$_f^-$	93	60	54:46	29	30
4	Δ-(*S*,*S*)-**3**$^{3+}$ 2Cl$^-$ BAr$_f^-$	95	55	54:46	–13	–6

[a]The conversion/yield was determined by ^{1}H NMR integration of **14**/**48** versus an internal standard. [b]Diastereoselectivities were determined by *in situ* ^{1}H NMR integration of the *syn*/*anti* products. [c]Enantioselectivities were determined by chiral HPLC analyses. [d]The stereochemistries of the products (*R*/*S*) were not determined.

4.3.4 The Friedel-Crafts addition of 1-methylindole to nitroolefins

The Werner complexes were also screened as catalysts for the Friedel-Crafts addition of 1-methylindole (**49**) to **14**, which has previously been catalyzed with modest enantioselectivity by a chiral organocatalyst.[103] The results are summarized in Table

4.20. The reaction is similar to the Michael additions previously examined in that the nucleophile adds to the β position of the nitroolefin. A significant difference, however, is that this reaction does not require a base to activate the nucleophile.

When the Friedel-Crafts addition is catalyzed by Λ-(*S*,*S*)-**3**$^{3+}$ 2Cl^{-} BAr$_f^{-}$, the reaction requires 9 hours to reach 90% conversion. Similarly, the reaction catalyzed by the diastereomer Δ-(*S*,*S*)-**3**$^{3+}$ 2BF$_4^{-}$ BAr$_f^{-}$ requires 6 hours to reach 96% conversion. However, under identical conditions, the mixed BF$_4^{-}$/BAr$_f^{-}$ salt Λ-(*S*,*S*)-**3**$^{3+}$ 2BF$_4^{-}$ BAr$_f^{-}$ achieves complete conversion within 30 minutes. It is clear from this result that the two Cl^{-} counteranions of Λ and Δ-(*S*,*S*)-**3**$^{3+}$ 2Cl^{-} BAr$_f^{-}$ strongly inhibit the activation of the nitroolefin by the N-H units of the trication.

Table 4.20. Data for the catalyzed Friedel-Crafts addition of 1-methylindole to **14**.

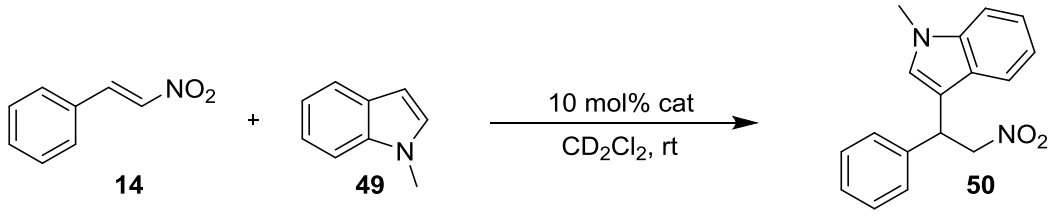

14 **49** **50**

entry	catalyst	conversion (%)[a]	ee (%)[b,c]
1	Λ-(*S*,*S*)-**3**$^{3+}$ 2Cl^{-} BAr$_f^{-}$	90 (9 h)	11
2	Λ-(*S*,*S*)-**3**$^{3+}$ 2BF$_4^{-}$ BAr$_f^{-}$	>99 (0.5 h)	15
3	Δ-(*S*,*S*)-**3**$^{3+}$ 2Cl^{-} BAr$_f^{-}$	96 (6 h)	4

[a]The conversion was determined by ^{1}H NMR integration of **14** versus an internal standard. [b]Enantioselectivities were determined by chiral HPLC analyses. [c]The stereochemistries of the products (*R*/*S*) were not determined.

4.3.5 Notable reactions that gave no conversion

Several Michael acceptors besides nitroolefins were also screened in catalysis with Werner-type catalysts. Unfortunately, the Michael acceptors **51**-**54** shown in Scheme 4.15 gave no conversion with **15a** and Et_3N in the presence of 10 mol% of Λ-(*S*,*S*)-$\mathbf{3}^{3+}$ 2Cl$^-$ BAr_f^-, Δ-(*S*,*S*)-$\mathbf{3}^{3+}$ 2Cl$^-$ BAr_f^-, or Λ-(*S*,*S*)-$\mathbf{3}^{3+}$ 2BF_4^- BAr_f^-. However, Michael additions to acceptors **51**-**53** were previously effected in high enantioselectivities with chiral thiourea organocatalysts.[104]

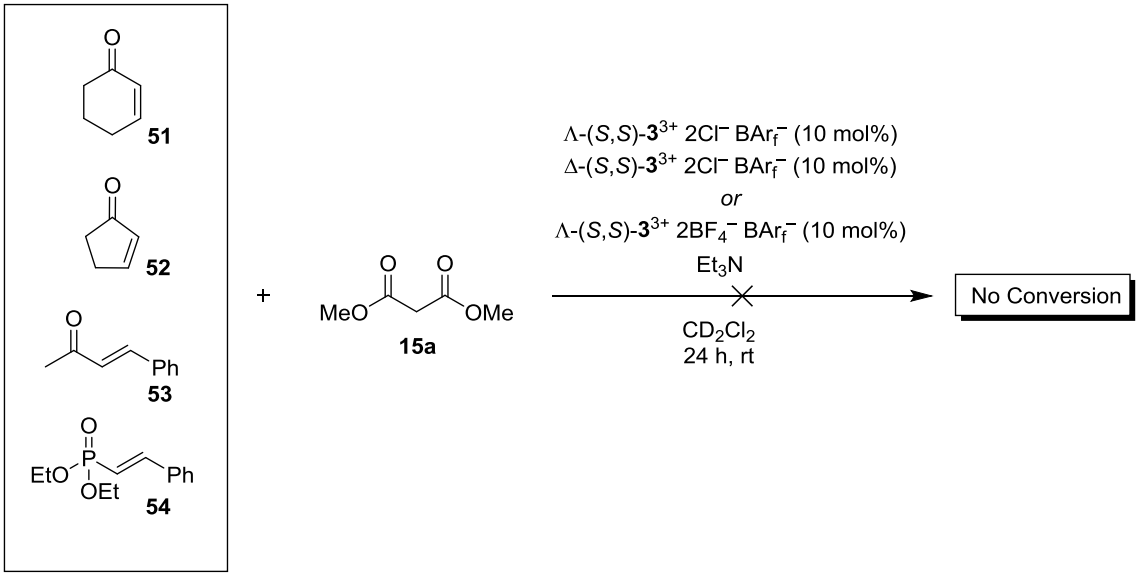

Scheme 4.15. Michael acceptors that gave no conversion in catalyst screening.

Another notable reaction that was not successfully catalyzed by Λ-(*S*,*S*)-$\mathbf{3}^{3+}$ 2Cl$^-$ BAr_f^- is the Michael addition of nitromethane (**56**) to dimethyl 2-benzylidenemalonate (**55**) as shown in Scheme 4.16. Although the expected product is identical to that of the previously studied Michael additions, here the relationship between the functional group and the nucleophile/electrophile have been reversed. Compound **56** (pK_a = 17.2,

DMSO)[105] is only approximately 20-fold less acidic than **15a** (pK_a = 15.9, DMSO),[98] so it is reasonable to assume that the nucleophile is still deprotonated by the base, albeit with a smaller equilibrium distribution. One possibility is that the lack of conversion is a result of insufficient activation of the electrophile *via* hydrogen bonding to promote the reaction.

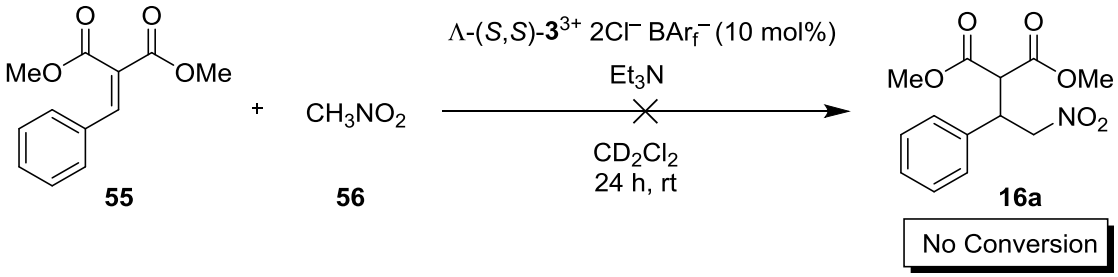

Scheme 4.16. The unsuccessful Michael addition of nitromethane to dimethyl 2-benzylidenemalonate (**55**).

4.4 Discussion

4.4.1 The stereoselective synthesis of Λ and Δ-(S,S)-3^{3+} trications

Bosnich reported that the metal configurations of isolated $[Co(S,S\text{-dpen})_3]^{3+}$ trications were strongly influenced by the starting Co(II) salt. As shown in Scheme 4.3, and summarized in Scheme 4.17, the Λ-diastereomer (lel_3 conformation) is achieved as the major product when $Co(OAc)_2{\cdot}4H_2O$ is the Co(II) source and the Δ-diastereomer (ob_3 conformation) is achieved as the major product when $Co(ClO_4)_2{\cdot}6H_2O$ is the Co(II) source, despite otherwise identical synthetic procedures. The same general trend was observed in this work during the syntheses of Λ and Δ-(*S*,*S*)-**3**$^{3+}$ 2Cl$^-$ BAr$_f^-$ (Scheme 4.4). It was also discovered here that the synthesis beginning with $CoCl_2{\cdot}6H_2O$ led

predominately to the isolation of crude Λ-(*S*,*S*)-$\mathbf{3}^{3+}$ $3Cl^-$, which after metathesis gave Λ-(*S*,*S*)-$\mathbf{3}^{3+}$ $2Cl^-$ BAr_f^- (Scheme 4.4).

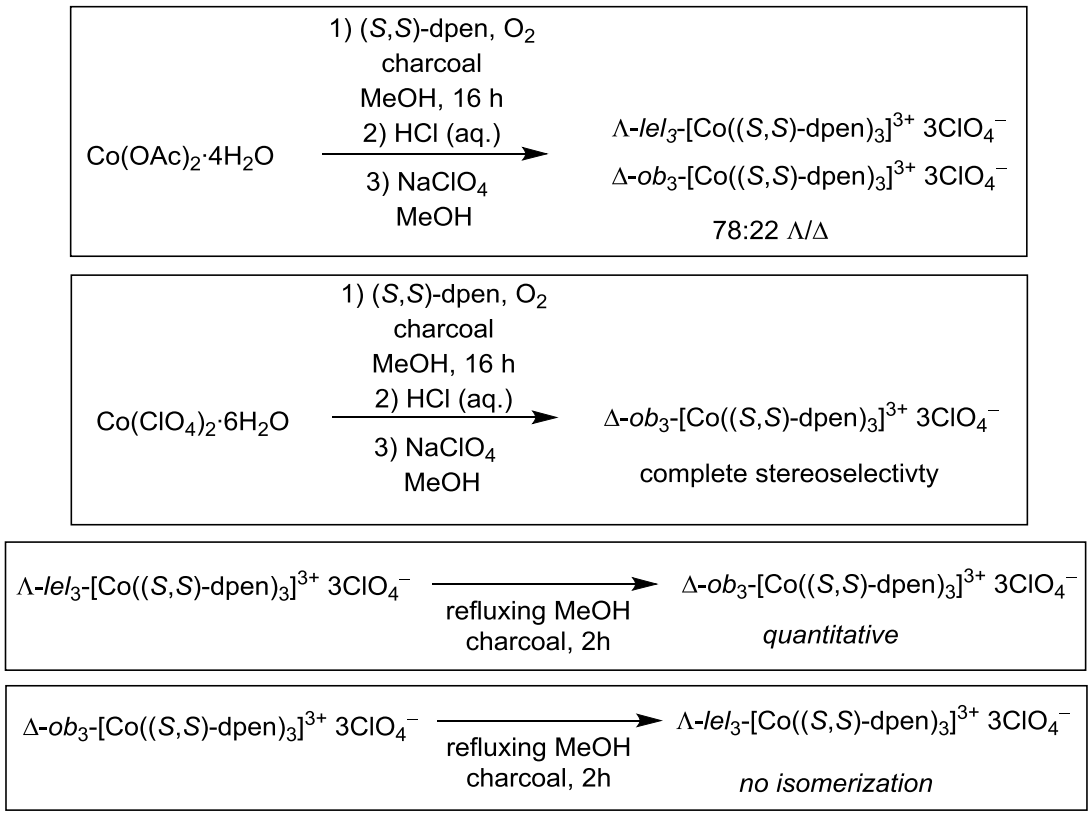

Scheme 4.17: The Bosnich synthesis revisited.

Even though Bosnich could isolate Λ-(*S*,*S*)-$\mathbf{3}^{3+}$ $3ClO_4^-$ as the major product, this is not the thermodynamically preferred diastereomer of this salt. Heating the complex in MeOH over charcoal resulted in the isomerization to the Δ-diastereomer (Scheme 4.3, highlighted in blue, and Scheme 4.17). In a similar manner, Λ-(*S*,*S*)-$\mathbf{3}^{3+}$ $2BF_4^-$ BAr_f^- isomerized nearly completely to the Δ-diastereomer when heated at 80 °C in DMSO-d_6 (Figure 4.21).

Many would assume that the Δ-diastereomer of the trichloride salt (*S*,*S*)-**3**$^{3+}$ 3Cl^{-} would also be thermodynamically more stable than the Λ-diastereomer. Bosnich then rationalized the isolation of Λ-(*S*,*S*)-**3**$^{3+}$ 3Cl^{-} based upon a lower solubility in MeOH, with the equilibrium being driven by precipitation. This explanation has two errors. First, both Λ and Δ-(*S*,*S*)-**3**$^{3+}$ 3Cl^{-} are highly soluble in MeOH. Secondly, the Co(III) salts do not readily isomerize at room temperature and therefore an equilibrium between the product diastereomers would not be established under the experimental conditions.

It is possible that both the geometry of the trication, as well as the hydrogen bonding interactions with the counteranions, play roles in determining the relative stabilities of the Λ and Δ-diastereomers of the [Co((*S*,*S*)-dpen)]$^{3+}$ trication. In all of the cases that equilibria could be established by Bosnich or in this work (Figure 4.21), the counteranions of the trication were non-coordinating and the Δ-diastereomer was always favored. Because there were only very weak interactions between the trications and the counteranions in these experiments, it seemed that the results primarily reflected the geometrical stabilities of the core Co(III) trications. The key differentiating parameters might be identified in the crystal structures of Λ-(*S*,*S*)-**3**$^{3+}$ 3Cl^{-} (Section 4.2.3.1), the enantiomer Δ-(*R*,*R*)-**3**$^{3+}$ 3Cl^{-} (Section 4.2.3.2)), and the diastereomer Δ-(*S*,*S*)-**3**$^{3+}$ 3Cl^{-} (Section 4.2.3.3). Although each of these structures were obtained as the trichloride salt, only the geometry of the core Co(III) trication is considered at first. For the sake of discussion, these features are assumed to be largely independent of the counteranion.

One can attempt to identify features that would render the Δ-diastereomer thermodynamically preferred. It has been crystallographically demonstrated that Δ-(*S*,*S*)-**3**$^{3+}$ trications adopt the *ob*$_3$ conformation (Figure 4.9). In contrast, the Λ-(*S*,*S*)-**3**$^{3+}$ trication, as well as the enantiomeric Δ-(*R*,*R*)-**3**$^{3+}$ trication, adopt the *lel*$_3$ conformation (Figure 4.3 and 4.6). There are a number of attendant structural consequences as can be

appreciated in the list of bond angles and distances for Λ-(*S*,*S*)-**3**$^{3+}$ 3Cl^{-} (Table 4.2), Δ-(*R*,*R*)-**3**$^{3+}$ 3Cl^{-} (Table 4.3), and Δ-(*S*,*S*)-**3**$^{3+}$ 3Cl^{-} (Table 4.4). Most notable are the different arrangements of the C_3 N-H units. For the *lel*$_3$ complexes, these hydrogen atoms are positioned closely together and the adjacent N-H bonds are roughly parallel. Said another way, the hydrogen atoms of the H-N···N-H torsion angle are approximately eclipsed. Interestingly, the crystal structures of both *lel*$_3$ complexes each give one C_3 H-N···N-H torsion angle of approximately ± 19°, which is significantly larger than the other torsion angles. This deviation could indicate a "pressure release" mechanism to alleviate some of the intramolecular H···H strain.

By contrast, the hydrogen atoms of the C_3 N-H units in the *ob*$_3$ structure are separated by a greater distance (2.63 Å vs. 2.40 Å). The C_3 H-N···N-H torsion angles also reveal that adjacent N-H bonds closely approach a gauche conformation (avg. 48.5°) while the analogous *lel*$_3$ N-H bonds are nearly eclipsed (avg. 7.6°). Therefore, the *ob*$_3$ isomer could be the more stable isomer due to decreased intramolecular H···H repulsions at the C_3 axis. Note that interactions between the bulky phenyl rings might also play a role here. However, there appears to be sufficient space between phenyl rings, so it is difficult to rationalize whether these interactions might favor the *lel*$_3$ or *ob*$_3$ conformation.

The *lel*$_3$ complex is the thermodynamically less preferred isomer with non-coordinating anions, but one can argue that it should form stronger hydrogen bonds than the *ob*$_3$ isomer, especially with Cl^{-} counteranions, which are good hydrogen bond acceptors. For example, one can consider the C_3 N-H···Cl^{-} angles (Tables 4.2 and 4.4). These are more nearly linear for the *lel*$_3$ complex (157°) than for the *ob*$_3$ complex (137°). Additional evidence is provided in the ^{1}H NMR spectra of Λ-(*S*,*S*)-**3**$^{3+}$ 2Cl^{-} BAr$_f^{-}$ and Δ-(*S*,*S*)-**3**$^{3+}$ 2Cl^{-} BAr$_f^{-}$ (Figure 4.14) in which the signal for the C_3 N-H of

the *lel*$_3$ complex is shifted further downfield due to a stronger hydrogen bond with the Cl^- counteranion. The C_2 N-H···Cl^- hydrogen bond is also stronger for the *lel*$_3$ complex. The crystal structure of Λ-(*S*,*S*)-**3**$^{3+}$ 3Cl^- demonstrates double hydrogen bonding between two C_2 N-H units and a Cl^- anion (Figure 4.4). However, the space-filling model of Δ-(*S*,*S*)-**3**$^{3+}$ 3Cl^- (Figure 4.11) reveals that only a single N-H···Cl^- hydrogen bond can be formed at the congested C_2 face.

It is conceived here that the formation of stronger hydrogen bonds with the counteranions would allow the *lel*$_3$ isomer to at least partially compensate for the intrinsic intramolecular H···H strain. In other words, a greater fraction of the Λ-diastereomer would be present at equilibrium in the presence of a good hydrogen bond accepting counteranion. Unfortunately, none of the experiments in this dissertation could prove that the Λ-diastereomer is thermodynamically preferred in this situation. Specifically, attempts to equilibrate samples of the trichloride salts Λ-(*S*,*S*)-**3**$^{3+}$ 3Cl^- and Δ-(*S*,*S*)-**3**$^{3+}$ 3Cl^- in CD_3OD at 67 °C in the presence of charcoal resulted in the apparent substitution of dpen ligands by the Cl^- counteranions (Section 4.2.8). However, the fact that the Λ-diastereomer of the trication is isolated in greater proportions in the presence of hydrogen bonding anions suggests the importance of this interaction.

A proposed model for this selectivity is provided in Figure 4.41. While in the Co(II) oxidation state, the metal center can adopt either the lambda or delta configuration. To our knowledge, there is no information regarding such equilibria for any 1,2-diamine. However, important considerations would include stabilizing contributions of both intramolecular sterics and hydrogen bonding to the counteranion. Extrapolating from Co(III), strong hydrogen bonding to the counteranion has an overall greater influence with the Λ-diastereomer, but intramolecular steric factors favor the Δ-diastereomer. Subsequent oxidation will greatly reduce the substitution lability of the

cobalt, and it is therefore proposed that the Co(II) equilibria dictate the diastereoselectivity in the Co(III) products. Figure 4.41a depicts this situation when Cl^- is the counteranion. In effect, the Cl^- counteranions serve as templates that help organize the diamine ligands into the Λ-configuration. When ClO_4^- is the counteranion (Figure 4.41b), the steric factors of the core Co(III) trication still favor the Δ-diastereomer. The poor hydrogen bonding interactions with the counteranion create less of a bias toward the Λ-configuration and do not overcome the steric preference. Therefore, the Δ-diastereomer is isolated after oxidation.

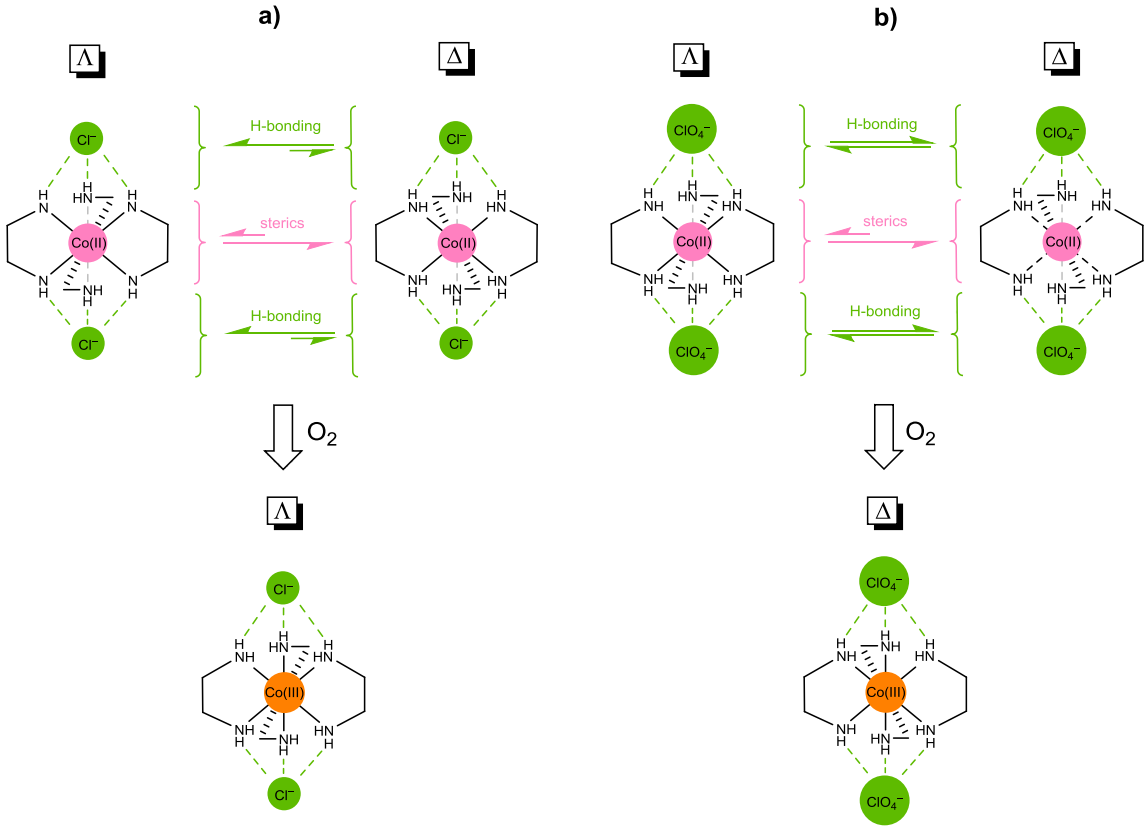

Figure 4.41. Stereoselective syntheses of $[Co((S,S)\text{-dpen})_3]^{3+}$ cations. The phenyl rings are removed for clarity.

4.4.2 The anion exchange with Na^+ BAr_f^-

When Λ-(*S*,*S*)-**3**$^{3+}$ 3Cl^- is combined with 3 equivalents of Na^+ BAr_f^- in CH_2Cl_2, the product that is isolated after column chromatography is Λ-(*S*,*S*)-**3**$^{3+}$ 2Cl^- BAr_f^-, indicating that only one of the three Cl^- anions is replaced by BAr_f^- in this anion exchange. In the crystal structure of Λ-(*S*,*S*)-**3**$^{3+}$ 3Cl^- (Figure 4.4), two Cl^- counteranions are held by triple hydrogen bonds with the C_3 N-H units. The third Cl^- anion only forms a double hydrogen bond with the C_2 N-H units. It is suggested that only the latter, weakly held Cl^- anion is exchanged in this procedure. Unexpectedly, the anion exchange reaction cannot overcome the high barrier involved in breaking the strong C_3 N-H···Cl^- triple hydrogen bond. Therefore, optimized anion exchange procedures include adding only one equivalent of Na^+ BAr_f^-. It should also be noted that the more compact $[Co(en)_3]^{3+}$ trication requires three BAr_f^- counteranions to be rendered soluble in CH_2Cl_2 due to the lack of substituents on the ethylene diamine ligand.

It is a fortuitous advantage that only one BAr_f^- anion is required to render Λ-(*S*,*S*)-**3**$^{3+}$ trications soluble in organic solvents. First, the bulky BAr_f^- anion is the most expensive part of the catalyst system and is responsible for approximately 52% of the molecular weight of Λ-(*S*,*S*)-**3**$^{3+}$ 2Cl^- BAr_f^-. The use of a total of three BAr_f^- anions would drastically increase both the cost and the molecular weight of the catalyst. Secondly, it allows for the two remaining anions to be treated as optimization variables. For instance, the two Cl^- counteranions of Λ-(*S*,*S*)-**3**$^{3+}$ 2Cl^- BAr_f^- have been exchanged for additional non-coordinating anions (BF_4^-, PF_6^-), a chiral anion ($camphSO_3^-$), and a basic anion (CO_3^{2-}, *in situ*). This provides opportunities for catalyst fine tuning and a

broader range of applications without fundamentally changing the properties of the Λ-(*S*,*S*)-**3**$^{3+}$ trication.

4.4.3 The catalytic active site

It was hoped that by combining the hydrogen bonding and catalysis data examined in this chapter that a thorough understanding of the interaction between the catalyst and the organic substrate could be achieved. The most important aspect to rationalize is whether the C_3 or C_2 face (Section 3.2) of the Λ-(*S*,*S*)-**3**$^{3+}$ trication is the primary active site in the Michael addition of dialkyl malonates to nitroolefins.

First, it is clear that the electrophilic nitroolefin must hydrogen bond with the Λ-(*S*,*S*)-**3**$^{3+}$ trication to be sufficiently "activated" for the catalytic reaction. Although the nucleophilic dialkyl malonate is also observed to form hydrogen bonds with the Λ-(*S*,*S*)-**3**$^{3+}$ trication (Figure 4.25 and 4.29), this is not necessarily relevant to the mechanism. Hydrogen bonding would actually render the dialkyl malonate *less* nucleophilic. On the other hand, hydrogen bonding to the dialkyl malonate will render it *more* acidic and therefore more readily deprotonated by the base. At this point, the least that can be said is that the nitroolefin binds to the Λ-(*S*,*S*)-**3**$^{3+}$ trication with the possibility of simultaneous hydrogen bonding of the dialkyl malonate.

The NO_3^- anion shares several structural features with the hydrogen bonding nitro group of a nitroolefin. Therefore, Mason's crystal of Λ-[Co((*S*,*S*)-dpen)$_3$]$^{3+}$ 3NO_3^- ·H_2O (Figure 4.2), is further examined in Figure 4.42 with respect to the hydrogen bonding interactions with the counteranions. The hydrogen bonding sites could represent potential catalytic binding sites.

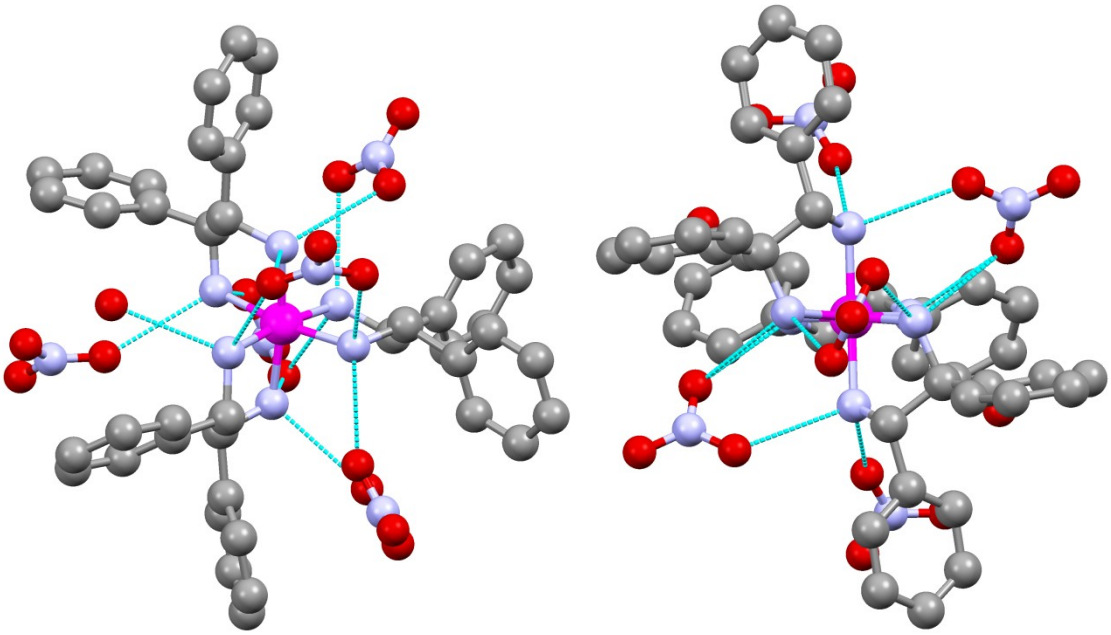

Λ-[Co((*S*,*S*)-dpen)$_3$]$^{3+}$ 3NO_3^-·H_2O		
H-bond acceptor (X)	Type of H-bond	Total number of similar interactions
NO_3^-	[C_3, C_3, C_3][2]	2
NO_3^-	[C_2, C_2][2]	1
NO_3^-	[C_2][1]	2
H_2O	[C_2][1]	2

Figure 4.42. All hydrogen bonding interactions in the crystal structure of Λ-[Co((*S*,*S*)-dpen)$_3$]$^{3+}$ 3NO_3^- ·H_2O. Hydrogen atoms are not depicted since they were not put in calculated positions by the original author.

At both C_3 faces, the trication forms triple hydrogen bonding to two oxygen atoms of the NO_3^- anion. At one C_2 face, there is a double hydrogen bond to two oxygen atoms of a NO_3^- anion. At the remaining two C_2 faces, each N-H unit simultaneously binds to a molecule of H_2O and a single oxygen atom of a NO_3^- anion.

4.4.3.1 Considering the C_2 face as the catalytic active site

From the crystal structure of Λ-$[Co((S,S)\text{-dpen})_3]^{3+}$ $3NO_3^- \cdot H_2O$ (Figure 4.42) and the hydrogen bond titration experiments (Figure 4.27 and 4.31), it is clear that a nitroolefin will form hydrogen bonds with the C_2 N-H units. However, evidence of hydrogen bonding does not necessarily prove that this is the primary site for catalysis.

Chiral catalysts with overall C_2 symmetry are ubiquitous in the chemical literature. A well-accepted four quadrant model for steric biasing in C_2 symmetric catalysts has been previously developed, and is extended here to the C_2 face of the Λ-(*S*,*S*)-$\mathbf{3}^{3+}$ trication.[106] In this case, the environment of the C_2 binding site is divided into four quadrants, as depicted in Figure 4.43. The center of the quadrant represents the position of the cobalt atom (not shown) and the horizontal line is congruent with the N-Co-N plane. The shaded regions of the quadrant represent areas that are sterically hindered by the bulky phenyl rings. The non-shaded regions represent areas that are more accessible. For reference, this diagram is best compared to the space-filling model of Λ-(*S*,*S*)-$\mathbf{3}^{3+}$ $3Cl^-$ (Figure 4.5e). The nitrostyrene can bind at the C_2 site in such a way that the pendant phenyl ring is oriented on the right-hand side (Figure 4.43, top). Consequently, this also places the β-carbon, which will be the site of the new C-C bond, on the right-hand side. Due to the location of the bulky phenyl rings, the incoming dialkyl malonate favors an approach from the top-right quadrant. This will result in the *S* product enantiomer. The nitroolefin is equally likely to bind to the C_2 site with the phenyl ring on the left-hand side (Figure 4.43, bottom). In this case, the dialkyl malonate favors an approach from the bottom-left quadrant, which again leads to the *S* product enantiomer. *However, in all cases, catalysis with the Λ-(S,S)-$\mathbf{3}^{3+}$ trication gives the R*

product of ***16a*** *as the major enantiomer.* Hence, these transitions state models can be rejected.

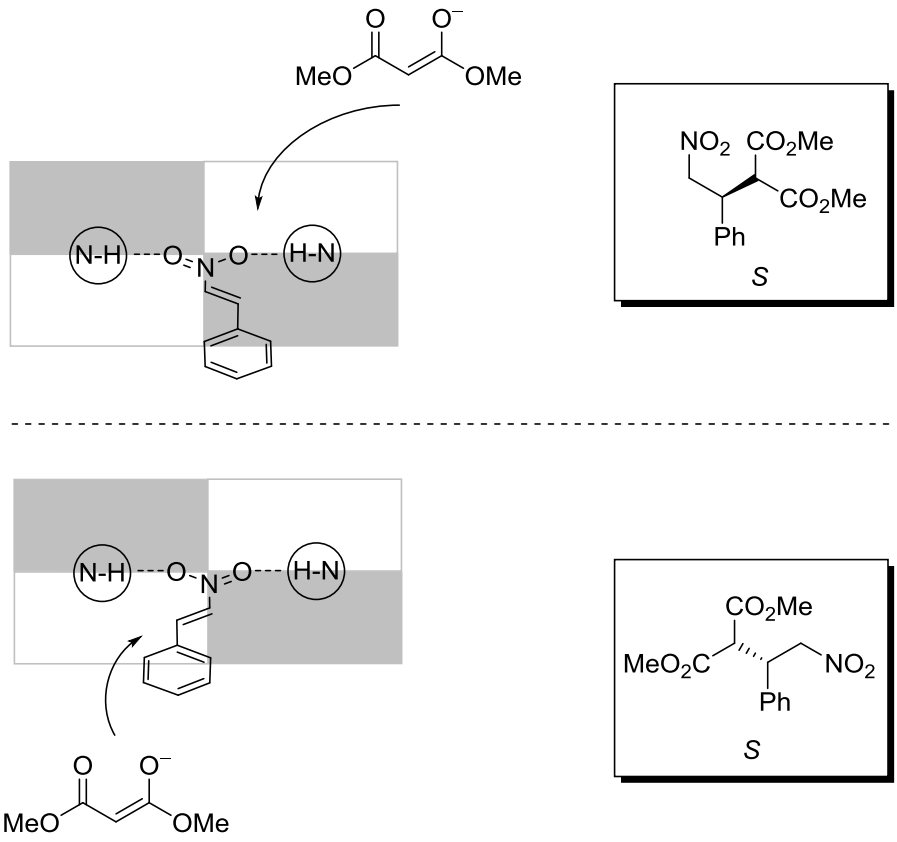

Figure 4.43. A stereochemical model for a potential C_2 catalytic active site.

4.4.3.2 Considering the C_3 face as the catalytic active site

Due to the incompatibility between the stereochemical model involving binding at the C_2 site and the actual catalyst results, the C_3 face should be given serious consideration as the catalytically active site. The Cl^- anions of Λ-(*S*,*S*)-**3**$^{3+}$ 2Cl^- BAr_f^-

were previously shown above to preferentially occupy the C_3 N-H hydrogen bonding sites (Figure 4.14a). Catalysis at this site would require the displacement of at least small equilibrium quantities of Cl^-. However, this C_3 N-H···Cl^- interaction is so strong that it is not appreciably disrupted even in the presence of 10 equivalents of either **14** or **15a** (Figures 4.27 and 4.31). At first glance, this would appear to make the C_3 face a less likely candidate to be the catalytically active site. However, it was also shown that the Cl^- counteranions could be readily displaced from the C_3 N-H binding sites in the presence of a mild acid such as Et_3NH^+ BF_4^- (Figure 4.23c) which has pK_a values of pK_a = 10.8 (H_2O) and 9.0 (DMSO). During catalysis, the Et_3N base will deprotonate **15a**, as seen in Scheme 4.18. The resulting triethylammonium cation, Et_3NH^+, can form a hydrogen bonded ion pair with Cl^- and dislodge it from the C_3 site. In fact, during catalysis with Λ-(*S*,*S*)-**3**$^{3+}$ 2Cl^- BAr_f^- in CH_2Cl_2, a faint white suspension develops immediately after the addition of Et_3N. This white turbidity likely results from the formation of the Et_3NH^+ Cl^- salt, which is poorly soluble in CH_2Cl_2. With the Cl^- anion removed from the C_3 site, the organic substrates now have access to the C_3 N-H units.

The formation of the Et_3NH^+ Cl^- ion pair must be reversible, because the proton is transferred back to the organic product to form **16a** (Scheme 4.13). Therefore, after each catalytic cycle the Cl^- counteranion could return the C_3 N-H binding site. Although access to the C_3 N-H hydrogen bonding site could be achieved after simple dissociation of the Cl^- counteranions, it is believed that the formation of the Et_3NH^+ Cl^- hydrogen bonded ion pair greatly accelerates this dissociation.

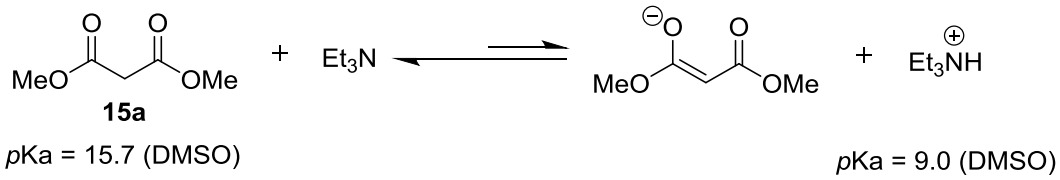

Scheme 4.18. The deprotonation of dimethyl malonate with Et_3N.

Catalysis with mixed salts with less coordinating anions, Λ-(*S*,*S*)-**3**$^{3+}$ 2BF_4^- BAr_f^- and Λ-(*S*,*S*)-**3**$^{3+}$ 2PF_6^- BAr_f^-, was also performed and directly compared to catalysis with Λ-(*S*,*S*)-**3**$^{3+}$ 2Cl^- BAr_f^- (Figure 4.40). For each catalyst, the C_2 binding site is equally exposed. If catalysis occurs through the C_2 binding site, then each catalyst should give nearly the same rate and enantioselectivity. In contrast, the C_3 sites might become available by dissociation of a small amount of Cl^- or larger equilibrium quantities of the poorer hydrogen bond accepting anions BF_4^- and PF_6^-. When the C_3 axis is less hindered by the counteranion, the reaction rate should be markedly increased and the enantioselectivities could be enhanced either by proximity effects or less competitive background catalysis. Indeed, as was seen in Figure 4.40, Table 4.12, and Table 4.13, both the reaction rate and the enantioselectivity increased when the catalyst contained only non-coordinating anions.

One particularly instructive example concerning the effect of the C_3 N-H···Cl^- hydrogen bond on catalyst rate is observed in the Friedel-Crafts addition of 1-methylindole (**49**) to **14** (Table 4.20). In this reaction, no base is required, and therefore there is no formation of the Et_3NH^+ cation. In this catalyst system, there is no mechanism by which to actively displace the Cl^- counteranions from the C_3 binding site. The C_3 N-H binding site only becomes accessible after self-dissociation of small equilibrium quantities of Cl^-. Both Λ-(*S*,*S*)-**3**$^{3+}$ 2Cl^- BAr_f^- and Λ-(*S*,*S*)-**3**$^{3+}$ 2BF_4^- BAr_f^- are explored as catalysts in this reaction. In each case, the C_2 binding sites are

equally exposed, but the C_3 site is more readily accessible with Λ-(*S*,*S*)-**3**$^{3+}$ 2BF_4^- BAr_f^-. The catalysis reaction with Λ-(*S*,*S*)-**3**$^{3+}$ 2Cl^- BAr_f^- is still incomplete after 9 hours, but that with Λ-(*S*,*S*)-**3**$^{3+}$ 2BF_4^- BAr_f^- proceeds to full conversion within 30 minutes. This provides very strong evidence that the C_3 N-H units are responsible for activating the nitroolefin. It also suggests the importance of the generation of the Et_3NH^+, or related, cation during any catalysis with Λ-(*S*,*S*)-**3**$^{3+}$ 2Cl^- BAr_f^- to accelerate the dissociation of the Cl^- anion and expose the C_3 N-H hydrogen bond donors.

4.4.3.3 Literature examples of catalysts with C_3 symmetric active site

Chiral catalysts with C_3 symmetry are less prevalent in the chemical literature than asymmetric catalysts or chiral catalysts with C_2 symmetry. However, a few examples of chiral catalysts with C_3 symmetry or C_3 symmetric ligands are known.

The C_3 symmetric phosphite **57** has been employed as a ligand in the enantioselective rhodium catalyzed hydrogenation of alkenes (Scheme 4.19).[107] The phosphite ligand adopts a helical conformation. When the axially chiral BINOL moieties are in the *S* configuration, the phosphite ligand adopts an *M* (counterclockwise) helicity, as depicted in the space-filling model in Scheme 4.19. This space filling model, which features a deep binding pocket for the rhodium atom, is strikingly similar to the space filling models of the Werner catalysts (Section 4.2.3). Alternatively, when the BINOL moieties are in the *R* configuration, the phosphite ligand adopts a *P* (clockwise) helicity. The ligands are configurationally stable, and rapid equilibration between the helical conformations does not occur.

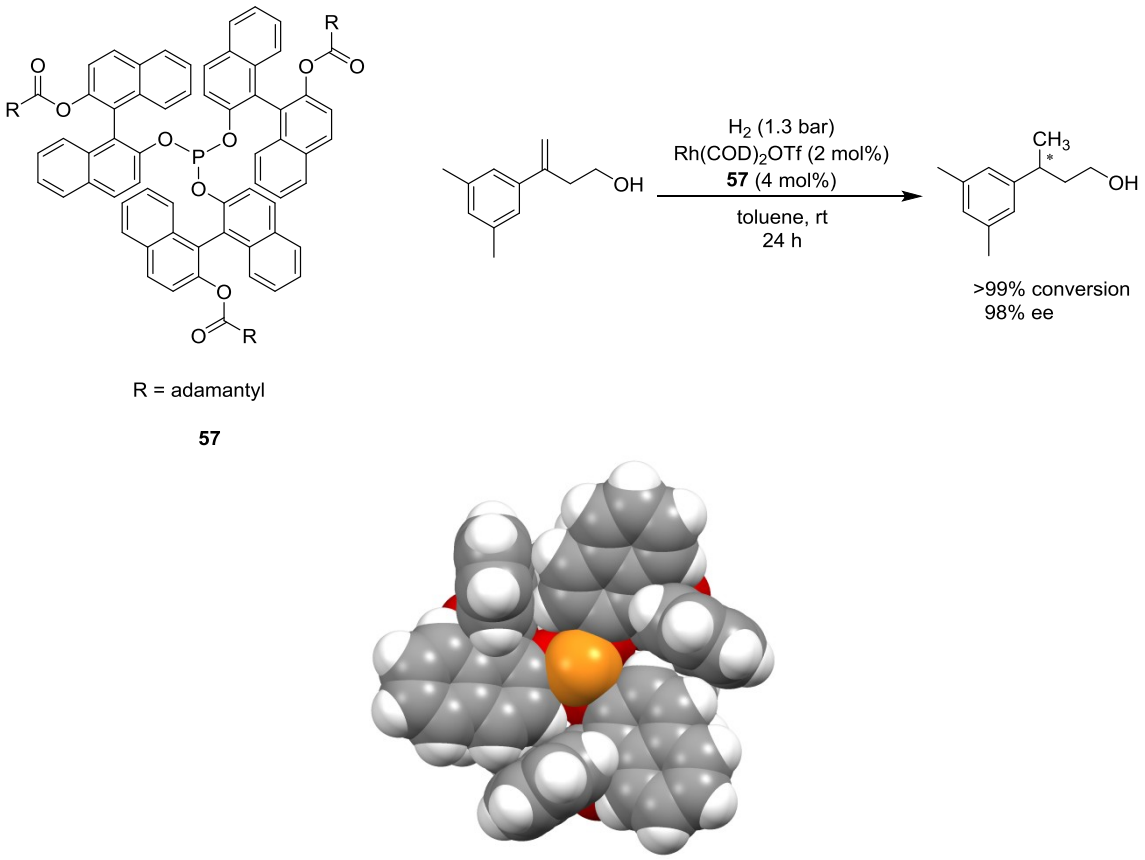

Scheme 4.19. A C_3 symmetric chiral phosphite ligand (**57**) in the rhodium catalyzed hydrogenation of alkenes (top) and a space filling model (bottom).

In another example, the C_3 symmetric chiral trisimidazoline **58** was employed as a catalyst in enantioselective bromolactonization reactions (Scheme 4.20).[108] The chirality of the catalyst is provided by three (*S*,*S*)-dpen derived imidazoline units. The authors propose a substrate binding motif in which a carboxylic acid simultaneously engages in two hydrogen bonds with two different imidazoline units.

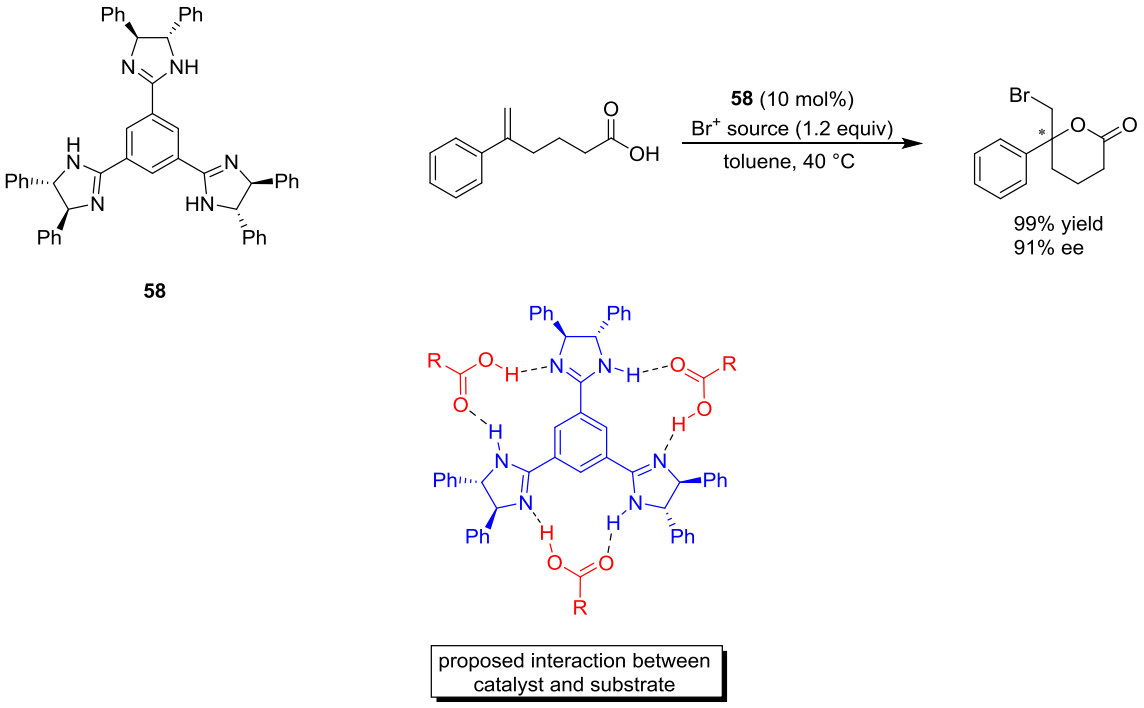

Scheme 4.20. A C_3 symmetric trisimidazoline catalyst (**58**) in an enantioselective bromolactonization reaction (top) and a proposed hydrogen bonding interaction (bottom).

4.4.4 Enantioselectivity

The Λ-(*S*,*S*)-**3**$^{3+}$ 2Cl$^-$ BAr$_f^-$ catalyst system, and related complexes, were found to give much higher enantioselectivities than the first generation Werner catalyst, Δ-**1**$^{3+}$ 3BAr$_f^-$ (Scheme 4.1). For instance, Δ-**1**$^{3+}$ 3BAr$_f^-$ catalyzed the Michael addition of diethyl malonate (**15b**) to *trans*-β-nitrostyrene (**14**) in only 33% ee as shown in Scheme 4.21.[78] Under nearly identical conditions, Λ-(*S*,*S*)-**3**$^{3+}$ 2Cl$^-$ BAr$_f^-$ catalyzed the same reaction in 79% ee (Table 4.6, Entry 2).

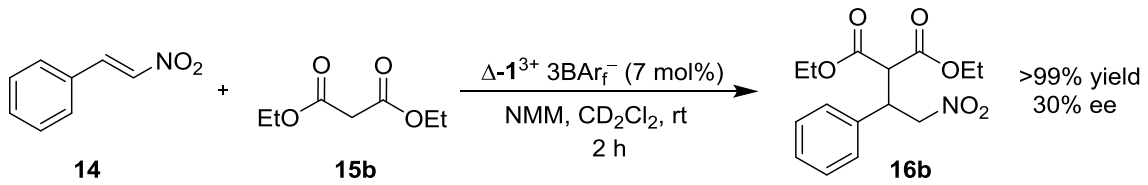

Scheme 4.21. The Michael addition of a dialkyl malonate to a nitroolefin catalyzed by Δ-$\mathbf{1}^{3+}$ $3BAr_f^-$.

The additional steric features in Λ-(*S*,*S*)-$\mathbf{3}^{3+}$ $2Cl^-$ BAr_f^-, as well as the chiral influence of the ligands, certainly play roles in increasing the selectivity of the catalyst. A more subtle point that also deserves consideration involves the geometry of the chelate conformations (Chapter 2). An unsubstituted ethylenediamine chelate may rapidly interconvert between the λ and δ conformations (Figure 2.2). The result is that the enantiopure Δ-$\mathbf{1}^{3+}$ $3BAr_f^-$ catalyst actually exists as a mixture of four rapidly interconverting isomers. In contrast, a *trans*-dpen ligand will preferentially adopt only one chelate conformation (Figure 2.10), and an enantiopure $[Co(\textit{trans}\text{-dpen})_3]^{3+}$ trication will exist predominantly in a single, structurally rigid conformation.

In all of the catalysis reactions explored in this chapter, the Λ-(*S*,*S*)-$\mathbf{3}^{3+}$ $2Cl^-$ BAr_f^- and Δ-(*S*,*S*)-$\mathbf{3}^{3+}$ $2Cl^-$ BAr_f^- catalysts give opposite enantiomers of the organic product. In many cases, especially in the Michael addition of dialkyl malonates to nitroolefins, the enantioselectivities achieved with the two diastereomeric catalysts are nearly "equal and opposite", with the Λ-diastereomer giving products of slightly better enantiopurity. The two catalysts are constructed with dpen ligands of the same chirality, but have the opposite sense of chirality at the metal center. It is clear then that the configuration of the metal center, and the implicit geometrical consequences, has the greatest influence over the stereochemical outcome of the catalyzed reaction.

It is difficult, based upon existing data, to propose a stereochemical model for a catalytic binding site containing C_3 symmetry. However, from the space-filling models of Λ-(*S*,*S*)-**3**$^{3+}$ 3Cl$^-$ and Δ-(*S*,*S*)-**3**$^{3+}$ 3Cl$^-$ (Figures 4.5c and 4.11c), it is clear that the C_3 axis of the two trications are roughly mirror-images, which explains why each diastereomer of the catalyst gives the opposite product enantiomer.

Although the catalyst Δ-(*S*,*S*)-**3**$^{3+}$ 2Cl$^-$ BAr$_f^-$ gives lower enantioselectivities, it affords faster reaction rates. A likely explanation is that the C_3 N-H site forms weaker hydrogen bonds with the Cl$^-$ anions, which are more readily exchanged for the nitroolefin substrate.

One of several possible substrate binding models is proposed in Figure 4.44. This entails the simultaneous hydrogen bonding of the nitroolefin and the deprotonated dialkyl malonate in a side by side orientation on the C_3 face. This dual activation of the electrophile and nucleophile may be one factor responsible for achieving high enantioselectivity. It was previously shown that the Λ-(*S*,*S*)-**3**$^{3+}$ 2BF$_4^-$ BAr$_f^-$ catalyzed addition of 1-methylindole (**49**), which has no hydrogen bond accepting groups, to **14** proceeded with very low enantioselectivity (15% ee, Table 4.20, Entry 2). Under identical conditions, the hydrogen bond accepting dimethyl malonate (**15a**) underwent addition to **14** in 84% ee (Table 4.13, Entry 1). The crystal structure of Λ-*lel*$_3$-[Co(en)$_3$]$^{3+}$ 3NO$_3^-$ (Figure 3.4) is a particularly informative example of a related hydrogen bonding arrangement. In this structure, two approximately parallel NO$_3^-$ anions are simultaneously hydrogen bonded at the C_3 face of the trication.

The three C_3 N-H units of the Λ-(*S*,*S*)-**3**$^{3+}$ 2Cl$^-$ BAr$_f^-$ catalyst, which adopts the *lel*$_3$ conformation, are arranged more closely together and may produce a tighter binding arrangement between the nitroolefin and the dialkyl malonate than the *ob*$_3$ catalyst Δ-(*S*,*S*)-**3**$^{3+}$ 2Cl$^-$ BAr$_f^-$. This may explain why the Λ-diastereomer gives somewhat higher

enantioselectivities. However, this model is not yet detailed enough to explain why the *R* product enantiomer is formed in greater amounts than the *S* enantiomer. This objective will require further experimentation with a broader range of substrates and catalysts.

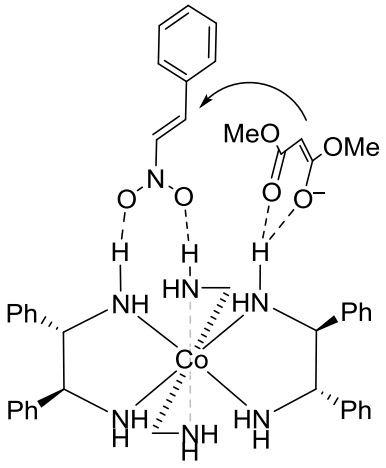

Figure 4.44. A proposed catalyst-substrate binding model.

As was seen in the Michael addition of diphenyl phosphite (**31**) to **14**, the catalyst Δ-(*S*,*S*)-$\mathbf{3}^{3+}$ $2Cl^-$ BAr_f^- was actually more selective than the diastereomer Λ-(*S*,*S*)-$\mathbf{3}^{3+}$ $2Cl^-$ BAr_f^-. Therefore, the Δ-diastereomer should not be automatically discarded as the less selective catalyst, but should always be considered when screening new reactions.

4.4.5 Water and biphasic catalysis

Schreiner previously demonstrated that 1 mol% of a thiourea catalyst (**59**) could promote increased reaction rates for a Diels-Alder reaction even with H_2O as solvent (Scheme 4.22).[109] The rationale for the increased reaction rate involved the hydrophobic aggregation of the organic substrates and thiourea catalyst in H_2O.

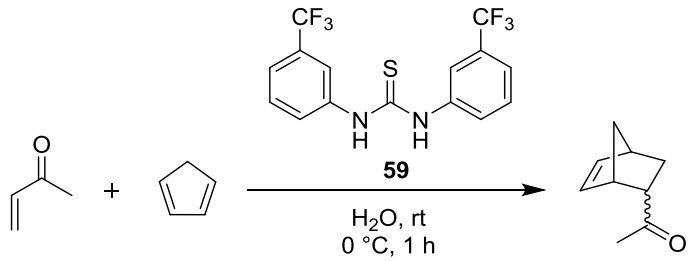

cat. loading **59** (mol%)	yield (%)
--	74
1	85

Scheme 4.22. Schreiner's hydrophobically driven Diels-Alder reaction.

Most of the Werner-type catalysts prepared are isolated with small amounts of H_2O. The difficulty in removing this residual H_2O under reduced pressure is a testament to the hydrogen bonding with the cobalt complex. Rigorous drying under forcing conditions was not pursued, as this had previously led to decomposition with Δ-**1**$^{3+}$ 3BAr_f^-.[78] Although H_2O has the potential to act as a competing hydrogen bond donor during catalysis, it is not found to have any deleterious effects here. According to the ^1H NMR titrations of Λ-(*S*,*S*)-**3**$^{3+}$ 2Cl^- BAr_f^- and Λ-(*S*,*S*)-**3**$^{3+}$ 2BF_4^- BAr_f^- (Section 4.2.9.1), both the nitroolefin and dialkyl malonate will displace coordinated H_2O from the binding site of the catalysts. In addition, the presence of an adventitious amount of H_2O is beneficial to the rate of catalysis, without sacrificing enantioselectivity (Table 4.15).

Unlike most Werner complexes, $[Co(dpen)_3]^{3+}$ trications are insoluble in H_2O, even with small, hard anions such as Cl^- and ClO_4^-. The six bulky phenyl rings render such complexes more organic in nature, although they are only soluble in very polar organic solvents such as MeOH and DMSO. Consider also the interaction between the solvent molecules and the Λ-(*S*,*S*)-**3**$^{3+}$ 3Cl^- complex in Figure 4.5a. The self hydrogen bonding H_2O-MeOH chain appears to form an encapsulating helix surrounding the core Λ-(*S*,*S*)-**3**$^{3+}$ 3Cl^- helix. The partial close up view depicted in Figure 4.45 reveals that a

large portion of the solvent chain perfectly envelops the outside edge of a phenyl ring, which is the most non-polar portion of the trication. These combined features point toward a hydrophobic effect, in which the catalyst (and potential organic substrates) will aggregate together surrounded by a cage-like assembly of H_2O. Therefore, a second coordination sphere of H_2O could help to organize the catalyst and substrates into a more beneficial arrangement, leading to enhanced selectivity.

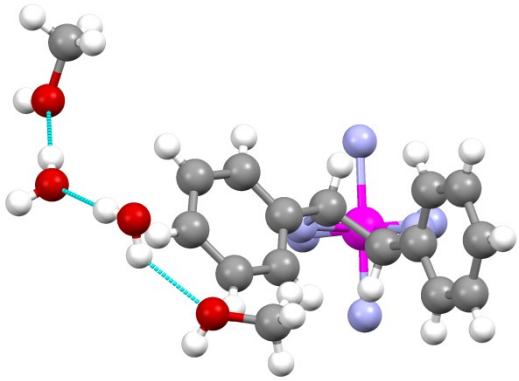

Figure 4.45. A fragment of the crystal structure of Λ-(*S*,*S*)-**3**$^{3+}$ 3Cl$^-$·2H_2O·2MeOH displaying the hydrophobic interaction between the solvent molecules and the trication.

One well-known example of a phase-transfer catalysis system was reported by Maruoka.[110] A chiral quaternary ammonium bromide salt (**60**) is employed as a phase transfer catalyst for the alkylation of a glycine ester derived imine, as depicted in Scheme 4.23. The mechanism involves a phase-transfer anion exchange to form a new ammonium hydroxide salt. The newly soluble hydroxide anion (OH^-) can deprotonate the imine. The close ion association between the chiral ammonium cation and the deprotonated imine allows the alkylation step to proceed with high enantioselectivity.

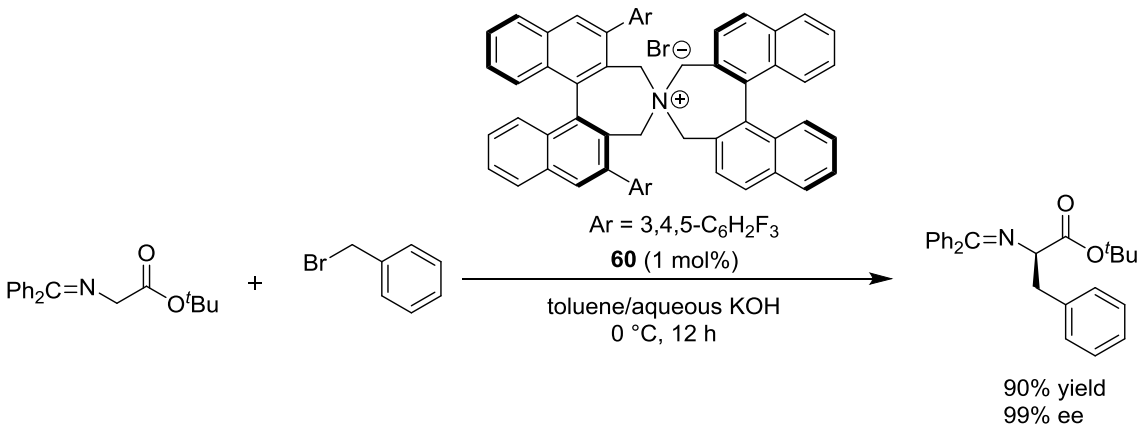

Scheme 4.23. A chiral quaternary ammonium salt for the phase-transfer alkylation of an imine.

The Λ-(*S*,*S*)-**3**$^{3+}$ 2Cl^{-} BAr$_f^{-}$ catalyst was applied under CH_2Cl_2/H_2O biphasic conditions with Na_2CO_3 as base (Figure 4.14 Table 4.16). Even though the bulk of the H_2O separates from the organic phase in the formation of a bilayer, it is safe to assume that a significant amount of H_2O is also dissolved in the CH_2Cl_2. During catalysis the CO_3^{2-} dianion must first phase-transfer to the lower organic phase (Figure 4.14) where it can deprotonate the dialkyl malonate. There should then be a close ion association between the chiral cobalt cation and the deprotonated malonate. At the same time, the nitroolefin is activated by hydrogen bonding to the chiral cobalt cation. It is possible that this double activation of the organic substrates, in addition to the previously described hydrophobic influence, gives rise to the increased enantioselectivity under biphasic conditions.

4.4.6 Miscellaneous catalysts

In order to gain some further insight into some of the issues described in this chapter, additional complexes were targeted but could not be fully characterized. As

noted in Scheme 4.11, the complex with α-substituted naphthyl groups, Λ-(*S*,*S*)-**13**$^{3+}$ 2Cl$^-$ BAr$_f^-$, was prepared. It would be of obvious interest to compare the catalytic properties of this system with an analog with β-substituted naphthyl groups ((*S*,*S*)-**61**). The synthesis of the latter was pursued as described in Scheme 4.24. The ^{1}H NMR spectrum of the isolated product after BAr$_f^-$ anion exchange and column chromatography strongly supports the formation of [Co((*S*,*S*)-**61**)$_3$] 2Cl$^-$ BAr$_f^-$. However, there were many additional signals in the ^{1}H NMR spectrum that could not be assigned. These potential impurities or byproducts could not be removed after multiple purification attempts. There were also multiple peaks in the 60-70 ppm region of the ^{13}C{^{1}H} NMR spectrum, providing evidence that multiple configurational isomers could be present.

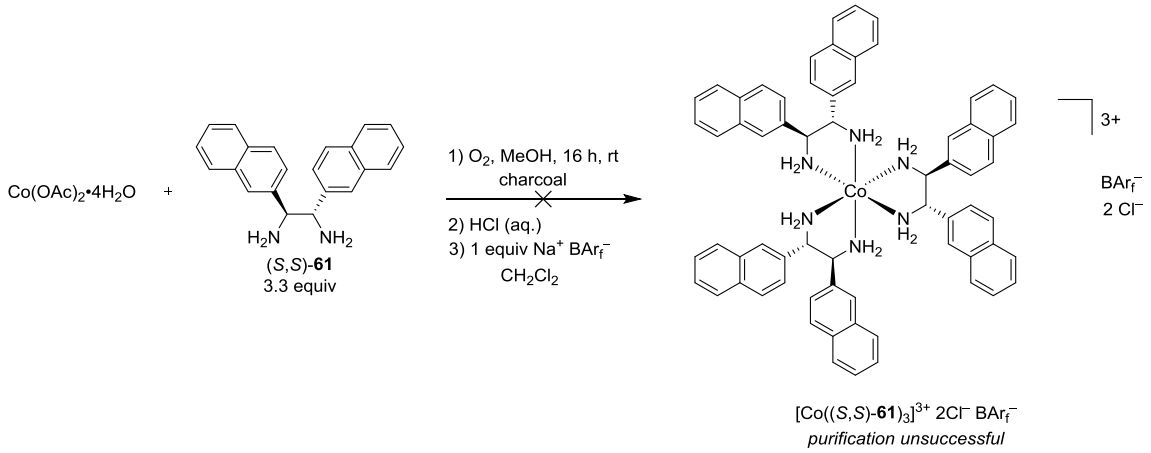

Scheme 4.24. The attempted synthesis of [Co((*S*,*S*)-**61**)$_3$]$^{3+}$ 2Cl$^-$ BAr$_f^-$.

The two Cl$^-$ anions of Λ-(*S*,*S*)-**3**$^{3+}$ 2Cl$^-$ BAr$_f^-$ were exchanged with the non-coordinating anions BF$_4^-$ and PF$_6^-$ (Scheme 4.5). The synthesis of the tris-BAr$_f^-$ complex Λ-(*S*,*S*)-**3**$^{3+}$ 3 BAr$_f^-$ from Λ-(*S*,*S*)-**3**$^{3+}$ 2Cl$^-$ BAr$_f^-$ was also pursued (Scheme

4.25). In one attempt, Λ-(*S*,*S*)-$\mathbf{3}^{3+}$ $2Cl^-$ BAr_f^- was combined with two equivalents of Ag^+ BAr_f^- in a manner analogous to Scheme 4.5. Surprisingly, no precipitate (AgCl) formed, even after sonicating the solution for 10 min. In a second attempt, a CH_2Cl_2 solution of Λ-(*S*,*S*)-$\mathbf{3}^{3+}$ $2Cl^-$ BAr_f^- and two equivalents of Na^+ BAr_f^- were stirred in the presence of an aqueous bilayer. It was thought that the H_2O might assist in the formation and removal of the NaCl ion pair. An orange solid was isolated after separation of the aqueous phase and subsequent column chromatography. The ^1H NMR spectrum exhibited many uncharacteristic signals that could not reliably be assigned to Λ-(*S*,*S*)-$\mathbf{3}^{3+}$ 3 BAr_f^-.

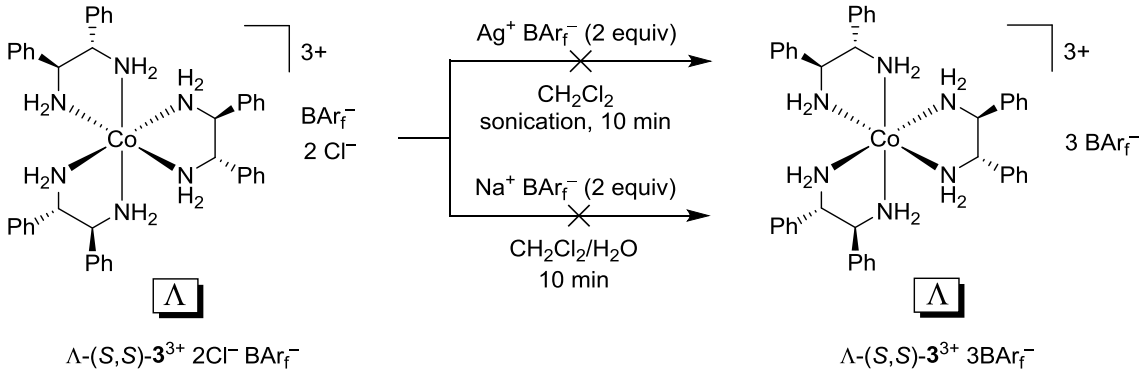

Scheme 4.25. The attempted synthesis of the tris-BAr_f^- complex Λ-(*S*,*S*)-$\mathbf{3}^{3+}$ $3BAr_f^-$.

4.4.7 Future work

The complexes and the reactions examined in this chapter should be considered only the first step towards a promising field of highly enantioselective Werner-type catalysts. The continuation of catalyst development and the application of these catalysts towards new reactions deserve attention.

The $[Co((S,S)\text{-dpen})_3]^{3+}$ trication is a highly modifiable platform for hydrogen bond mediated catalysis. Already described in this chapter is the introduction of functionalized dpen ligands and chiral anions, which will continue to be pursued. Other diversity elements that deserve attention include varying the metal center[37-41] and extensions to diamine ligands with other kinds of substituents besides aryl rings.[49-51]

The Λ-(*S*,*S*)-**3**$^{3+}$ $2Cl^-$ BAr_f^- catalyst system is well-suited for a variety of non-polar and polar solvents. Perhaps most intriguing is the ability to yield products of high enantiopurities under biphasic conditions. This opens the door for catalysis with a wide range of water soluble reagents and nucleophiles. This could include oxidizing agents such as permanganate (MnO_4^-) or peroxides (HOO^-), which would be unlikely to affect the cobalt(III), or good nucleophiles such as cyanide (CN^-) or azide (N_3^-) anions.

Hydrogen bond mediation is a very general mode of activation for organic electrophiles. In principal, enantioselective catalysis with the $[Co(dpen)_3]^{3+}$ trication should be possible with a wide range of organic functional groups including carbonyls, imines, epoxides, aziridines, etc. Many of these transformations have been catalogued with other hydrogen bond mediating catalysts and are summarized in review articles.[19] The $[Co(dpen)_3]^{3+}$ trication could be summarily applied to any of these transformations as well.

One interesting mode of catalysis that the $[Co(dpen)_3]^{3+}$ trication could be particularly suited for is the activation of cationic species by hydrogen bond assisted anion binding. Jacobsen has explored this mechanism with a chiral thiourea catalyst in nucleophilic additions to oxocarbenium ions (Scheme 4.26).[111] The thiourea forms a double hydrogen bond with the Cl^- anion, thus stabilizing the oxocarbenium ion pair. Due to the tight ion pair between the oxocarbenium cation and the Cl^- bound to the chiral thiourea, the silyl enol ether can add with high enantioselectivity. Knowing that

the Λ-(*S*,*S*)-**3**$^{3+}$ trication forms strong, triple hydrogen bonds with Cl^- anions at the C_3 face, the Werner-type catalysts could be applied to this kind of transformation in a similar way (Scheme 4.26, insert).

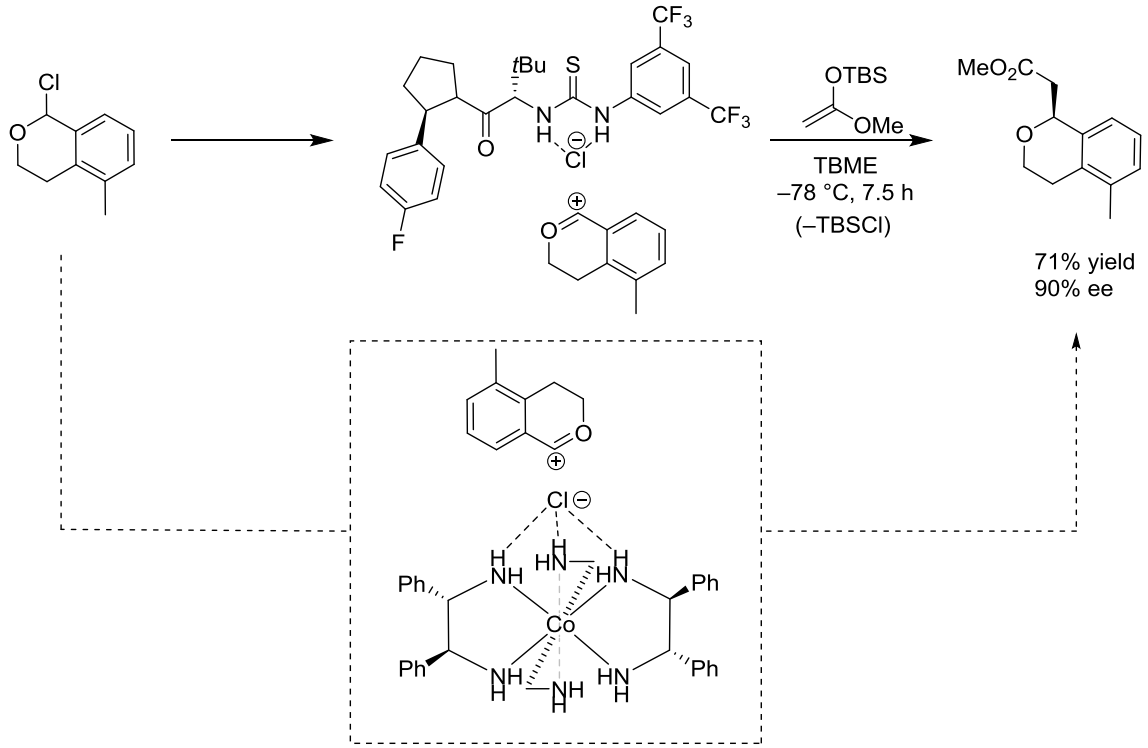

Scheme 4.26. Enantioselective addition to an oxocarbenium intermediate by hydrogen bond assisted anion binding.

4.5 Conclusion and outlook

For the first time, Werner-type complexes have been applied as highly enantioselective (>95% ee) catalysts for asymmetric organic synthesis. The catalysts Λ-(*S*,*S*)-**3**$^{3+}$ 2Cl^- BAr_f^- and Δ-(*S*,*S*)-**3**$^{3+}$ 2Cl^- BAr_f^- were prepared by a stereoselective synthesis and further purified by silica gel chromatography to efficiently afford

isomerically pure complexes. In the catalytic Michael addition of dialkyl malonates to nitroolefins, both catalysts achieved high yields and good enantioselectivities. The absolute stereochemistry of the isolated product was found to primarily depend on the chirality of the metal center. Catalysts with additional non-coordinating anions such as Λ-(*S*,*S*)-$\mathbf{3}^{3+}$ $2BF_4^-$ BAr_f^- and Λ-(*S*,*S*)-$\mathbf{3}^{3+}$ $2PF_6^-$ BAr_f^- gave increased reaction rates and improved enantioselectivities.

The hydrogen bonding features of the catalysts were thoroughly examined by crystal structures and through ^{1}H NMR titration experiments. The Λ-(*S*,*S*)-$\mathbf{3}^{3+}$ trication was also employed as a ^{1}H NMR chiral shift reagent.

A roadmap for future iterations of this catalyst system was clearly defined, including the introduction of functionalized dpen ligands and chiral anions.

The catalysts are user-friendly, easily synthesized from an inexpensive metal source, and can be stored on the bench top under ambient atmosphere for long periods of time. No special effort to rigorously dry solvents or glassware is required. The catalyst is stable under the applied reaction conditions and can be recycled in high purity and excellent yields (97%).

This catalyst system is one of the first contributions to what should be a large pool of related Werner-type catalysts. Many elements of the catalysts presented here are easily modifiable, allowing for continued fine tuning to match specific catalyst needs.

4.6 Experimental

4.6.1 General data

^{1}H, $^{13}C\{^{1}H\}$, and ^{19}F NMR spectra were recorded on a Varian NMRS 500 MHz spectrometer at ambient probe temperatures. Chemical shifts were referenced to residual solvent signals (^{1}H NMR: $CHCl_3$, 7.26 ppm; DMSO-d_5, 2.50 ppm; $CDHCl_2$, 5.32 ppm; CHD_2CN, 1.94 ppm; acetone-d_5, 2.05 ppm; $^{13}C\{^{1}H\}$ NMR: $CDCl_3$, 77.2 ppm; DMSO-d_6, 39.5 ppm; CD_2Cl_2, 54.0 ppm; CD_3CN, 118.3 ppm; acetone-d_6, 206.3 ppm; ^{19}F NMR: C_6F_6 (external standard), –164.9 ppm).

IR spectra were recorded on a Shimadzu IRAffinity-1 spectrometer with a Pike MIRacle ATR system (diamond/ZnSe crystal). Optical rotations were measured with a Rudolph Autopol II Automatic Polarimeter.

Melting point and thermal behavior were analyzed using an OptiMelt MPA 100 instrument. Microanalyses were performed by Atlantic Microlab. HPLC analyses were conducted with a Shimadzu instrument package (pump/autosampler/detector LC-20AD/SIL-20A/SPD-M20A; columns Chiralpak AD, Chiralpak AS-H, Chiralcel OD).

NMR solvents (Cambridge Isotopes) were treated as follows: DMSO-d_6 was distilled under vacuum and stored over molecular sieves; $CDCl_3$, CD_2Cl_2, acetone-d_6, CD_3CN, and CD_3OD were stored over molecular sieves. The HPLC solvents hexanes (Fischer, HPLC Grade) and isopropanol (JT Baker, HPLC Grade) were degassed before use. Other solvents were treated as follows: DMSO (Fischer, ACS grade) was distilled under vacuum and stored over molecular sieves; CH_2Cl_2 (EMD Chemicals, ACS grade), MeOH (EMD, anhydrous, 99.8%), hexanes (Macron, ACS grade), EtOAc (Macron, ACS grade), and acetone (BDH, ACS grade) were used as received.

Chemicals were treated as follows: *trans*-β-nitrostyrene (**14**, Alfa Aesar, 98%) was purified by column chromatography (9:1 v/v hexanes/EtOAc). The commercially available nitroolefins **20** (Alfa Aesar, 98%), 3,4-dichloro-β-nitrostyrene **21** (Alfa Aesar, 98%), and **29** (Alfa Aesar, 98%) were used as received. Other previously reported nitroolefins (**17-19, 22-24, 27, 28, 30**, see Tables 4.10 and 4.14) were prepared by known Henry addition procedures from the corresponding aldehydes.[112] Dimethyl malonate (**15a**, Alfa Aesar, 98%), diethyl malonate (**15b**, Alfa Aesar, 99%), diisopropyl malonate (**15c**, TCI), dibenzylmalonate (**15d**, Aldrich, 95%), di-*t*-butyl malonate (**15e**, Alfa Aesar, 98%), dimethyl methylmalonate (**15f**, Aldrich, 99%), diphenyl phosphite (**45**, Aldrich), nitroethane (**47**, Aldrich, >98%), 1-methylindole (**49**, Acros, 98%), $CoCl_2 \cdot 6H_2O$ (Alfa Aesar, 99.9%), $Co(OAc)_2 \cdot 4H_2O$ (Alfa Aesar, 98%), $Co(ClO_4)_2 \cdot 6H_2O$ (Alfa Aesar, reagent grade), (*S*,*S*)-dpen ((*S*,*S*)-**2**, dpen = 1,2-diphenylethylenediamine, Oakwood), (*R*,*R*)-dpen ((*R*,*R*)-**2**, Oakwood), charcoal (Acros, Norit SX 4), $HClO_4$ (70%, Macron, ACS grade), (*R*,*R*)-1,2-bis(2-hydroxyphenyl)ethylenediamine ((*R*,*R*)-**6**, Aldrich, 95%), Ag^+ BF_4^- (Aldrich, 98%), Ag^+ PF_6^- (Strem, 99%), (+)-3-bromocamphor-8-sulfonic acid ammonium salt (**5**, camphSO_3^- NH_4^+, Alfa Aesar, 98%), Et_3N (Alfa Aesar, 98%), DMAP (Alfa Aesar, 99%), DABCO (Alfa Aesar, 99%), *N*-methyl morpholine (NMM, Alfa Aesar, 99%), pyridine (EMD, anhydrous, 99.8%), DBU (Alfa Aesar, 99%), DOWEX 50WX2 (Aldrich), silica gel (Silicycle SiliaFlash® F60), Celite 545 (Aldrich), and Na_2SO_4 (EMD) were used as received.

Na^+ BAr_f^- was prepared according to the literature.[113] The diamines (*S*,*S*)-*p*-OMe-dpen ((*S*,*S*)-**7**), (*S*,*S*)-*p*-NO_2-dpen ((*S*,*S*)-**8**), (*S*,*S*)-*p*-Cl-dpen ((*S*,*S*)-**9**), and (*S*,*S*)-1-dnen ((*S*,*S*)-**10**, dnen = 1,2-di(1-naphthyl)ethylenediamine) were prepared according to the literature.[89]

4.6.2 Experimental procedures

4.6.2.1 Syntheses of cobalt complexes

Λ-[Co((*S*,*S*)-dpen)$_3$]$^{3+}$ 2Cl$^-$ BAr$_f^-$ (Λ-(*S*,*S*)-3^{3+} 2Cl$^-$ BAr$_f^-$). A gas circulating flask (Figure 4.46) was charged with a solution of $Co(OAc)_2{\cdot}6H_2O$ (0.8888 g, 3.57 mmol) in MeOH (50 mL). Activated charcoal (0.1 g) and (*S*,*S*)-**2** (2.5439 g, 12.0 mmol, 3.36 equiv) were added with stirring. Air was passed through the vigorously stirred suspension for 16 h. The mixture was filtered through Celite and 12.0 M aq. HCl (3.0 mL) was added. The solvent was removed by rotary evaporation to give an orange paste. Then H_2O (100 mL) was added. The suspension was filtered and the orange filter cake was washed with H_2O (100 mL). The cake was dissolved in MeOH. The solvent was removed by rotary evaporation to give an orange solid that was dried by oil pump vacuum at room temperature overnight. The crude trichloride salt (1.7506 g; see text) was suspended in CH_2Cl_2 (30 mL) and Na^+ BAr$_f^-$ (1.9656 g, 2.22 mmol) was added. The mixture was sonicated for 1 min during which time the CH_2Cl_2 became bright orange and a white precipitate (NaCl) developed. The mixture was filtered and the filtrate was loaded onto a silica gel column, giving an orange band. The column was eluted with CH_2Cl_2 and a green band consisting of *trans*-[Co((*S*,*S*)-dpen)$_2$Cl$_2$]$^+$ BAr$_f^-$ ((*S*,*S*)-**4**$^+$ BAr$_f^-$, see text) separated and was collected. The column was eluted with 98:2 v/v CH_2Cl_2/MeOH and the main orange band was collected. Careful fractionation separated the major Λ-diastereomer from the minor Δ-diastereomer. The solvent was removed from the green and two orange fractions. Each residue was dried by oil pump vacuum at room temperature overnight to give (*S*,*S*)-**4**$^+$ BAr$_f^-{\cdot}(1\pm1)H_2O$ (0.5631 g,

0.397 mmol, 11%),[114] Λ-(*S*,*S*)-**3**$^{3+}$ 2Cl$^-$ BAr_f^-·2H_2O (2.2234 g, 1.33 mmol, 37%),[114] and Δ-(*S*,*S*)-**3**$^{3+}$ 2Cl$^-$ BAr_f^- (0.0762 g, 0.046 mmol, 1.3%).[115]

Data for Λ-(*S*,*S*)-**3**$^{3+}$ 2Cl$^-$ BAr_f^-·2H_2O; mp 116-119 °C dec (open capillary). Anal. Calcd. for $C_{74}H_{60}BCl_2CoF_{24}N_6$·2$H_2O$ (1665.95): C 53.35, H 3.87, N 5.04, Cl 4.26; found C 53.50, H 3.82, N 4.84, Cl 3.94.

^{1}H NMR (500 MHz, CD_2Cl_2, δ in ppm, Figure 4.14a): BAr_f^- at 7.73 (s, 8H, *o*), 7.54 (s, 4H, *p*); (*S*,*S*)-**2** ligand at 8.17 (br s, 6H, N**H**H′), 7.40-7.37 (m, 6H, *p*), 7.34-7.30 (m, 24H, *o*, *m*), 4.48 (s, 6H, C**H**NH_2), 3.86 (br s, 6H, NH**H′**); 2.14 (br s, 7H, **H**$_2$O); ^{13}C NMR (125 MHz, CD_2Cl_2, δ in ppm, Figure 4.13a): BAr_f^- at 162.3 (q, $^1J_{BC}$ = 49.4 Hz, *i*), 135.4 (s, *o*), 129.4 (q, $^2J_{CF}$ = 31.3 Hz, *m*), 125.2 (q, $^1J_{CF}$ = 271.0 Hz, **C**F_3), 118.1 (s, *p*); (*S*,*S*)-**2** ligand at 134.8 (s, *i*), 131.1 (s, *p*), 130.6 (s, *o*), 128.0 (s, *m*), 63.6 (s, **C**HNH_2).[116]

IR (powder film, cm^{-1}): 3039 (m, ν_{NH}), 1609 (m, δ_{NH}), 1354 (s, $\nu_{Ar\text{-}CF_3}$), 1275 (vs, ν_{CF}), 1119 (vs, δ_{CCN}); UV-visible (nm, 1.66 × 10^{-3} M in CH_2Cl_2 (ε, M^{-1} cm^{-1})): 455 (157). $[\alpha]_{18}^{589}$ = 0.0° (5.18 mg mL^{-1}, CH_2Cl_2); $[\alpha]_{18}^{546}$ = 23.1° (5.18 mg mL^{-1}, CH_2Cl_2).[117]

Data for (*S*,*S*)-**4**$^+$ BAr_f^-·(1±1)H_2O; dec. pt 62-74 °C (no melting), liquefies at 87 °C (open capillary). Anal. Calcd. for $C_{60}H_{44}BCl_2CoF_{24}N_4$/$C_{60}H_{44}BCl_2CoF_{24}N_4$·$H_2O$ (1417.64/1435.66): C 50.84/50.20, H 3.13/3.23, N 3.95/3.90, Cl 5.00/4.94; found C 50.57, H 3.36, N 3.95, Cl 4.94.

^{1}H NMR (500 MHz, CD_2Cl_2, δ in ppm): BAr_f^- at 7.72 (s, 8H, *o*), 7.56 (s, 4H, *p*); (*S*,*S*)-**2** ligand at 7.38-7.34 (m, 12H), 7.29-7.26 (m, 8H), 4.73 (br s, 12H, N**H**H′, NH**H′**, and C**H**NH_2); 1.65 (s, 2H, **H**$_2$O); ^{13}C{^{1}H} NMR (125 MHz, CD_2Cl_2, δ in ppm): BAr_f^-

at 162.3 (q, $^{1}J_{BC}$ = 49.8 Hz, *i*), 135.4 (s, *o*), 129.4 (q, $^{2}J_{CF}$ = 28.6 Hz, *m*), 125.2 (q, $^{1}J_{CF}$ = 270.9 Hz, **C**F_3), 118.0 (s, *p*); (*S*,*S*)-**2** ligand at 135.4 (s, *i*), 130.8 (s, *p*), 130.4 (s, *o*), 127.6 (s, *m*), 66.2 (s, **C**HNH_2).

IR (powder film, cm^{-1}): 3335 (m, ν_{NH}), 3255 (m, ν_{NH}), 1609 (m, δ_{NH}), 1576 (m, δ_{NH}), 1354 (s, $\nu_{Ar\text{-}CF_3}$), 1275 (vs, ν_{CF}), 1118 (vs, δ_{CCN}); UV-visible (nm, 1.65 × 10^{-3} M in CH_2Cl_2 (ε, M^{-1} cm^{-1})): 597 (52), 457 (56); $[\alpha]_{18}^{589}$ = –34.3° (4.66 mg mL^{-1}, CH_2Cl_2).

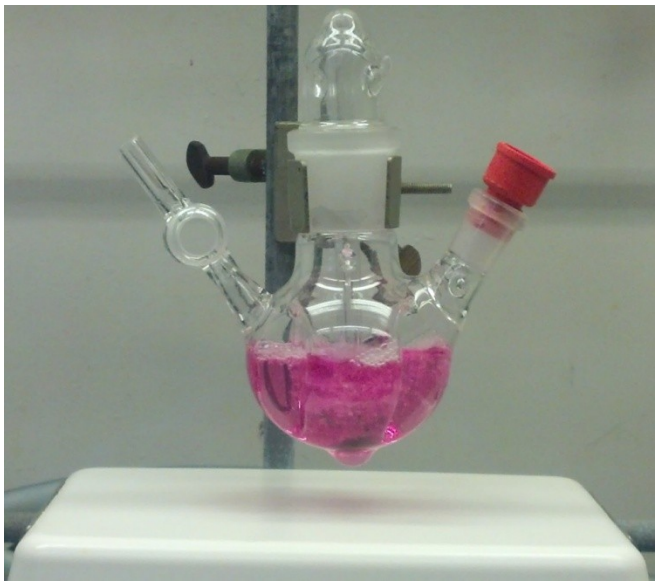

Figure 4.46. A gas circulating flask bubbles the air atmosphere through a vigorously stirred solution of $Co(OAc)_2{\cdot}4H_2O$ in MeOH.

Δ-[Co((*S*,*S*)-dpen)$_3$]$^{3+}$ 2Cl$^-$ BAr$_f^-$ (Δ-(*S*,*S*)-3^{3+} 2Cl$^-$ BAr$_f^-$). *The following synthesis involves the use and preparation of perchlorate salts that are potentially explosive.*[118] *Although no mishaps were experienced in this work, special protection should always be used when working with the perchlorate salts or $HClO_4$ solutions.* A gas circulating flask was charged with a solution of $Co(ClO_4)_2{\cdot}6H_2O$ (0.2601 g, 0.711

mmol) in MeOH (50 mL). Activated charcoal (0.1 g) and (*S*,*S*)-**2** (0.5002 g, 2.35 mmol, 3.31 equiv) were added with stirring. Air was passed through the vigorously stirred suspension at room temperature for 16 h. The mixture was filtered through Celite and $HClO_4$ (2.0 mL, 35% in H_2O) was added. The solution was loaded onto a Dowex cation exchange column, giving an orange band. The column was washed with 1:1 v/v H_2O/MeOH (100 mL) and gradient eluted with increasing concentrations of aq. 12.0 M HCl in MeOH (9:1 v/v MeOH/HCl (100 mL), 8:2 v/v MeOH/HCl (100 mL), 7:3 v/v MeOH/HCl (100 mL), 6:4 v/v MeOH/HCl (100 mL)). An orange band was collected and taken to dryness by rotary evaporation (60 °C bath; base trap to scavenge HCl). A portion of the bright orange crude trichloride salt (0.2765 g; see text) was suspended in CH_2Cl_2 (5 mL), and Na^+ BAr_f^- (0.3040 g, 0.343 mmol) and MeOH (0.05 mL) were added. The mixture was sonicated for a few seconds and the CH_2Cl_2 became bright orange as a faint white precipitate (NaCl) developed. The mixture was filtered and the orange filtrate was loaded onto a silica gel column, giving an orange band. The column was eluted with CH_2Cl_2 and a green band consisting of (*S*,*S*)-**4**$^+$ BAr_f^- was separated and collected. The column was eluted with 97:3 v/v CH_2Cl_2/MeOH and the main orange band was collected. Careful fractionation separated the major Λ-diastereomer from the minor Δ-diastereomer. The solvent was removed from the green and two orange fractions by rotary evaporation. Each residue was dried by oil pump vacuum at room temperature overnight to give (*S*,*S*)-**4**$^+$ BAr_f^- (0.0234 g, 0.0165 mmol, 2.5%, see characterization above),[115] Λ-(*S*,*S*)-**3**$^{3+}$ $2Cl^-$ BAr_f^- (0.0723 g, 0.0432 mmol, 6.6%, see characterization above),[115] and Δ-(*S*,*S*)-**3**$^{3+}$ $2Cl^-$ $BAr_f^-{\cdot}H_2O$ (0.2536 g, 0.1539 mmol, 24%).[114,119]

Data for Δ-(*S*,*S*)-**3**$^{3+}$ 2Cl$^-$ BAr$_f^-$·H$_2$O; The complex Δ-(*S*,*S*)-**3**$^{3+}$ 2Cl$^-$ BAr$_f^-$·H$_2$O continually darkens then liquefies at 110 °C. Anal. Calcd. for $C_{74}H_{60}BCl_2CoF_{24}N_6$·H$_2$O (1647.94): C 53.93, H 3.79, N 5.10, Cl 4.30; found C 53.96, H 4.02, N 4.98, Cl 4.20.

^{1}H NMR (500 MHz, CD_2Cl_2/MeOH (0.40:0.001 mL), δ in ppm, Figure 4.14b): BAr$_f^-$ at 7.73 (s, 8H, *o*), 7.55 (s, 4H, *p*); (*S*,*S*)-**2** ligand at 7.30-7.27 (m, 18H, *o*, *p*), 7.22-7.19 (t, $^3J_{HH}$ = 7.5 Hz, 12H, *m*), 6.58 (br s, 6H, N**H**H′), 5.35 (br s, 6H, NH**H′**), 4.25 (s, 6H, C**H**NH$_2$); 2.53 (br s, 14H, **H**$_2$O);[34] ^{13}C{^{1}H} NMR (125 MHz, CD_2Cl_2/MeOH (0.40:0.001 mL), δ in ppm, Figure 4.13b): BAr$_f^-$ at 162.3 (q, $^1J_{BC}$ = 49.6 Hz, *i*), 135.4 (s, *o*), 129.4 (q, $^2J_{CF}$ = 31.4 Hz, *m*), 125.2 (q, $^1J_{CF}$ = 271.0 Hz, **C**F$_3$), 118.0 (s, *p*); (*S*,*S*)-**2** ligand at 134.3 (s, *i*), 130.6 (s, *p*), 129.9 (s, *o*), 128.0 (s, *m*), 66.7 (s, **C**HNH$_2$).

IR (powder film, cm^{-1}): 3068 (m, ν_{NH}), 1608 (m, δ_{NH}), 1574 (m, δ_{NH}), 1354 (s, $\nu_{Ar\text{-}CF_3}$), 1275 (vs, ν_{CF}), 1119 (vs, δ_{CCN}); UV-visible (nm, 1.66 × 10^{-3} M in CH_2Cl_2 (ε, M^{-1} cm^{-1})): 462 (191); $[\alpha]_{18}^{546}$ = –419.0° (5.25 mg mL^{-1}, CH_2Cl_2).

Δ-[Co((*R*,*R*)-dpen)$_3$]$^{3+}$ 2Cl$^-$ BAr$_f^-$ (Λ-(*R*,*R*)-3^{3+} 2Cl$^-$ BAr$_f^-$). The complex was prepared analogously to Λ-(*S*,*S*)-**3**$^{3+}$ 2Cl$^-$ BAr$_f^-$·2H$_2$O; Anal. Calcd. for $C_{74}H_{60}BCl_2CoF_{24}N_6$·H$_2$O (1647.94): C 53.91, H 3.79, N 5.10, Cl 4.30; found C 53.86, H 3.92, N 4.92, Cl 3.90. $[\alpha]_{18}^{546}$ = –29.5° (5.42 mg mL^{-1}, CH_2Cl_2).

Λ-[Co((*R*,*R*)-dpen)$_3$]$^{3+}$ 2Cl$^-$ BAr$_f^-$ (Λ-(*R*,*R*)-3^{3+} 2Cl$^-$ BAr$_f^-$). The complex was prepared analogously to Δ-(*S*,*S*)-**3**$^{3+}$ 2Cl$^-$ BAr$_f^-$·H$_2$O; Anal. Calcd. for $C_{74}H_{60}BCl_2CoF_{24}N_6$ (1629.92): C 54.53, H 3.71, N 5.16, Cl 4.35; found C 54.44, H 4.08, N 5.15, Cl 4.2. $[\alpha]_{18}^{546}$ = 502.8° (5.33 mg mL^{-1},CH_2Cl_2).

Λ-[Co((*S*,*S*)-dpen)$_3$]$^{3+}$ 2BF$_4^-$ BAr$_f^-$ (Λ-(*S*,*S*)-3^{3+} 2BF$_4^-$ BAr$_f^-$). A round bottom flask was charged with a solution of Λ-(*S*,*S*)-**3**$^{3+}$ 2Cl$^-$ BAr$_f^-$·2H$_2$O (0.9985 g, 0.599 mmol) in CH_2Cl_2 (4 mL) and Ag^+ BF_4^- (0.2412 g, 1.24 mmol, 2.07 equiv) was added. The heterogeneous mixture was sonicated for 10 min. The mixture was filtered through Celite. The solvent was removed from the filtrate by rotary evaporation. The residue was dried by oil pump vacuum at room temperature overnight to give Λ-(*S*,*S*)-**3**$^{3+}$ 2BF$_4^-$ BAr$_f^-$·(2±1)H$_2$O as a bright orange solid (1.0191 g, 0.576 mmol, 96%);[31] mp 140-147 °C dec (open capillary). Anal. Calcd. for $C_{74}H_{60}B_3CoF_{32}N_6{\cdot}2H_2O$ /$C_{74}H_{60}B_3CoF_{32}N_6{\cdot}3H_2O$ (1768.42/1786.43): C 50.25/49.75, H 3.65/3.72, N 4.75/4.70; found C 49.94, H 3.69, N 4.52.

^{1}H NMR (500 MHz, CD_2Cl_2, δ in ppm, Figure 4.16b): BAr$_f^-$ at 7.73 (s, 8H, *o*), 7.56 (s, 4H, *p*); (*S*,*S*)-**2** ligand at 7.45 (t, $^1J_{HH}$ = 7.0 Hz, 6H, *p*), 7.40 (t, $^1J_{HH}$ = 7.0 Hz, 12H, *m*), 7.32 (d, $^1J_{HH}$ = 7.0 Hz, 12H, *o*), 6.04 (br s, 6H, N**H**H′), 4.52 (s, 6H, C**H**NH$_2$), 4.17 (br s, 6H, NH**H′**); 2.01 (s, 8H, **H**$_2$O); ^{13}C{^{1}H} NMR (125 MHz, CD_2Cl_2, δ in ppm): BAr$_f^-$ at 162.2 (q, $^1J_{BC}$ = 48.8 Hz, *i*), 135.3 (s, *o*), 129.4 (q, $^2J_{CF}$ = 27.5 Hz, *m*), 125.1 (q, $^1J_{CF}$ = 271.3 Hz, **C**F$_3$), 118.1 (s, *p*); (*S*,*S*)-**2** ligand at 133.6 (s, *p*), 131.4 (s, *i*), 130.7, (s, *o*), 127.8 (s, *m*), 64.5 (s, **C**HNH$_2$); ^{19}F NMR (470 MHz, CD_2Cl_2, δ in ppm): –62.8 (s, 24F, BAr$_f^-$), –142.9 (s, 8F, BF_4^-).

IR (powder film, cm^{-1}): 3254 (m, ν_{NH}), 1608 (m, δ_{NH}), 1354 (s, $\nu_{Ar\text{-}CF_3}$), 1277 (vs, ν_{CF}), 1121 (vs, δ_{CCN}); UV-visible (nm, 1.67 × 10^{-3} M in CH_2Cl_2 (ε, M^{-1} cm^{-1})): 451 (*sh*, 231); $[\alpha]_{18}^{546}$ = 50.6° (4.74 mg mL^{-1}, CH_2Cl_2).

Λ-[Co((*S*,*S*)-dpen)$_3$]$^{3+}$ 2PF$_6^-$ BAr$_f^-$ (Λ-(*S*,*S*)-3^{3+} 2PF$_6^-$ BAr$_f^-$). A round bottom flask was charged with a solution of Λ-(*S*,*S*)-**3**$^{3+}$ 2Cl$^-$ BAr$_f^-$·2H$_2$O (0.1200 g, 0.072 mmol) in CH_2Cl_2 (2 mL). A solution of Ag^+ PF_6^- (0.0373 g, 0.148 mmol, 2.1

equiv) in CH_2Cl_2 (2 mL) was added and a white precipitate immediately formed. The mixture was sonicated for 1 min. The mixture was filtered through Celite. The orange filtrate was washed with H_2O (2 × 1 mL) and the solvent was removed by rotary evaporation. The residue was dried by oil pump vacuum at room temperature for 5 h to give Λ-(*S*,*S*)-**3**$^{3+}$ 2PF_6^- BAr_f^-·(1±1)H_2O as a bright orange solid (0.1121 g, 0.061 mmol, 85%).[31] Compound Λ-(*S*,*S*)-**3**$^{3+}$ 2PF_6^- BAr_f^-·(1±1)H_2O continually darkens and liquefies at 160 °C. Anal. Calcd. for $C_{74}H_{60}BCoF_{36}N_6P_2$/ $C_{74}H_{60}BCoF_{36}N_6P_2$·$H_2O$ (1848.94/1866.96): C 48.07/47.61, H 3.27/3.35, N 4.55/4.50; found C 47.86, 3.49, 4.62.

^{1}H NMR (500 MHz, CD_2Cl_2, δ in ppm, Figure 4.16c): BAr_f^- at 7.71 (s, 8H, *o*), 7.55 (s, 4H, *p*); (*S*,*S*)-**2** ligand at 7.47 (t, $^3J_{HH}$ = 7.0 Hz, 6H, *p*), 7.42 (t, $^3J_{HH}$ = 7.5 Hz, 12H, *m*), 7.29 (d, $^3J_{HH}$ = 7.0 Hz, 12H, *o*), 5.66 (br s, 6H, N**H**H′), 4.49 (s, 6H, C**H**NH_2), 4.37 (br s, 6H, NH**H**′); 1.85 (br s, 18H, **H**$_2$O); ^{13}C NMR (125 MHz, CD_2Cl_2, δ in ppm): BAr_f^- at 162.2 (q, $^1J_{BC}$ = 48.8 Hz, *i*), 135.3 (s, *o*), 129.4 (q, $^2J_{CF}$ = 33.8 Hz, *m*), 125.1 (q, $^1J_{CF}$ = 271.2 Hz, **C**F_3), 118.1 (s, *p*); (*S*,*S*)-**2** ligand at 133.0 (s, *i*), 131.9 (s, *p*), 131.0 (s, *o*), 127.8 (s, *m*), 64.0 (s, **C**HNH_2); ^{19}F NMR (470 MHz, CD_2Cl_2, δ in ppm): –62.8 (s, 24F, BAr_f^-), –68.3 (d, $^1J_{PF}$ = 718.6 Hz, 12F, PF_6^-).

IR (powder film, cm^{-1}): 3287 (m, ν_{NH}), 1609 (m, δ_{NH}), 1354 (s, $\nu_{Ar\text{-}CF_3}$), 1276 (vs, ν_{CF}), 1122 (vs, δ_{CCN}); UV-visible (nm, 1.67 × 10^{-3} M in CH_2Cl_2 (ε, M^{-1} cm^{-1})): 449 (*sh*, 302); $[\alpha]_{18}^{546}$ = 47.6° (4.42 mg mL^{-1}, CH_2Cl_2).

Λ-[Co((*S*,*S*)-dpen)$_3$]$^{3+}$ 2camphSO$_3^-$ BAr$_f^-$ (Λ-(*S*,*S*)-3^{3+} 2camphSO$_3^-$ BAr$_f^-$). A round bottom flask was charged with a solution of Λ-(*S*,*S*)-**3**$^{3+}$ 2Cl^- BAr_f^-·2H_2O (0.0520 g, 0.031 mmol) in CH_2Cl_2 (3 mL). A solution of **5** (0.0420 g, 0.128 mmol, 4.26 equiv) in H_2O (3 mL) was added and the biphasic mixture was vigorously stirred for 2 min. The aqueous layer was removed. The orange organic layer was washed with H_2O

(2 × 2 mL) and loaded onto a silica gel column. The column was washed with CH_2Cl_2 (100 mL). The orange band was eluted with 98:2 v/v CH_2Cl_2/MeOH and the solvent was removed by rotary evaporation. The residue was dried by oil pump vacuum at room temperature overnight to give Λ-(*S*,*S*)-**3**$^{3+}$ 2camphSO_3^- BAr_f^-·(1±1)H_2O as bright orange solid (0.0586 g, 0.027 mmol, 87%),[114] mp 151-155 °C dec (open capillary). Anal. Calcd. for $C_{94}H_{88}BBr_2CoF_{24}N_6O_8S_2$/$C_{94}H_{88}BBr_2CoF_{24}N_6O_8S_2$·$H_2O$ (2179.38/2197.40): C 51.80/51.38, H 4.07/4.13, N, 3.86/3.82; found C 51.52, H 4.28, N 3.78.

^{1}H NMR(500 MHz, CD_2Cl_2, δ in ppm, Figure 4.17): BAr_f^- at 7.72 (s, 8H, *o*), 7.54 (s, 4H, *p*); (*S*,*S*)-**2** ligand at 7.89 (s, 6H, **N**HH'), 7.43-7.30 (m, 30H, C_6**H**$_5$), 4.53 (s, 6H, C**H**NH_2), 3.87 (s, 6H, NH**H′**); camphorSO_3^- at 4.32 (s, 2H), 3.34 (d, $^2J_{HH}$ = 15.0 Hz, 2H), 3.07 (s, 2H), 2.99 (d, $^2J_{HH}$ = 15.0 Hz, 2H), 2.21-2.14 (m, 4H), 1.79-1.69 (m, 2H), 1.45-1.41 (m, 2H), 1.26 (s, 6H), 0.91 (s, 6H); 2.45-2.30 (br s, 3H, **H**$_2$O); $^{13}C\{^1H\}$ NMR (125 MHz, CD_2Cl_2, δ in ppm); BAr_f^- at 162.3 (q, $^1J_{BC}$ = 50.0 Hz, *i*), 135.4 (s, *o*), 129.4 (q, $^2J_{CF}$ = 32.5 Hz, *m*), 125.1 (q, $^1J_{CF}$ = 271.3 Hz, **C**F_3), 118.0 (s, *p*); (*S*,*S*)-**2** ligand at 134.6 (s, *i*), 131.0 (s, *p*), 130.4 (s, *o*), 128.4 (s, *m*), 63.2 (**C**H_2NH_2); camphSO_3^- at 213.8 (s, **C**=O), 60.5, 54.8, 48.1, 47.8, 30.8, 22.6, 18.4, 10.0 (8 × s), one carbon signal is obscured by the solvent peak.

IR (powder film, cm^{-1}): 3201 (m, ν_{NH}), 3070 (m, ν_{NH}), 1724 (m, ν_{CO}) 1609 (m, δ_{NH}), 1354 (s, $\nu_{Ar\text{-}CF_3}$), 1275 (vs, ν_{CF}), 1121 (vs, δ_{CCN}); UV-visible (nm, 1.66 × 10^{-3} M in CH_2Cl_2 (ε, M^{-1} cm^{-1})): 459 (*sh*, 172); $[\alpha]_{18}^{546}$ = 63.4° (5.05 mg mL^{-1}, CH_2Cl_2).

Λ-[Co((*S*,*S*)-*p*-OMe-dpen)$_3$]$^{3+}$ 2Cl$^-$ BAr$_f^-$ (Λ-(*S*,*S*)-11^{3+} 2Cl$^-$ BAr$_f^-$). A gas circulating flask was charged with a solution of $Co(OAc)_2$·$4H_2O$ (0.1660 g, 0.666 mmol) in MeOH (50 mL). Activated charcoal (0.1 g) and (*S*,*S*)-**7** (0.5702 g, 2.09 mmol,

3.1 equiv) were added with stirring. Air was passed through the vigorously stirred suspension for 16 h. The mixture was filtered through Celite and 12.0 M aq. HCl (2.0 mL) was added. The solvent was removed by rotary evaporation and the residue was washed with 7:3 v/v H_2O/MeOH (10 mL) onto a frit. The filter cake was washed with acetone (2 × 10 mL) and dried by oil pump vacuum at room temperature overnight. The crude trichloride salt (0.2265 g; see text) was suspended in CH_2Cl_2 (5 mL) and Na^+ BAr_f^- (0.2093 g, 0.236 mmol) was added. The mixture was sonicated for 1 min during which time the CH_2Cl_2 became bright orange and a white precipitate (NaCl) developed. The mixture was filtered and the filtrate was loaded onto a silica gel column, giving an orange band. The column was eluted with 97.5:2.5 v/v CH_2Cl_2/MeOH. The solvent was removed from the orange fraction by rotary evaporation. The residue was dried by oil pump vacuum at room temperature to give Λ-(*S*,*S*)-**11**$^{3+}$ 2Cl^- BAr_f^-·3H_2O as a bright yellow solid (0.2894 g, 0.155 mmol, 23%);[114] mp 128-132 °C dec (open capillary). Anal. Calcd. for $C_{80}H_{72}BCl_2CoF_{24}N_6O_6$·3$H_2O$ (1862.42): C 51.54, H 4.22, N 4.51, Cl 3.80; found C 51.58, H 4.12, N 4.57, Cl 3.73.

^{1}H NMR (500 MHz, CD_2Cl_2, δ in ppm, Figure 4.18): BAr_f^- at 7.71 (s, 8H, *o*), 7.54 (s, 8H, *p*); (*S*,*S*)-**7** ligand at 7.67 (br s, 6 H, N**H**H′), 7.17 (d, $^3J_{HH}$ = 9.0 Hz, 12H, *o*), 6.73 (d, $^3J_{HH}$ = 8.5 Hz, 12H, *m*), 4.34 (s, 6H, C**H**NH_2), 4.16 (br s, 6H, NH**H′**), 3.66 (s, 18H, OC**H**$_3$); 2.15 (br s, 11H, **H**$_2$O); ^{13}C{^{1}H} NMR (125 MHz, CD_2Cl_2, δ in ppm): BAr_f^- at 162.3 (q, $^1J_{BC}$ = 49.5 Hz, *i*), 135.3 (s, *o*), 129.4 (q, $^2J_{CF}$ = 34.5 Hz, *m*), 125.1 (q, $^1J_{CF}$ = 271.1 Hz, **C**F_3), 118.0 (s, *p*); (*S*,*S*)-**7** ligand at 161.2 (s, *i*), 129.8 (s, *m*), 126.8 (s, *p*), 115.6 (s, *o*), 62.9 (s, **C**HNH_2), 56.1 (s, O**C**H_3).[116]

IR (powder film, cm^{-1}): 3065 (m, ν_{NH}), 1611 (m, δ_{NH}), 1354 (s, $\nu_{Ar\text{-}CF_3}$), 1275 (vs, ν_{CF}), 1121 (vs, δ_{CCN}); UV-visible (nm, 1.61 × 10^{-3} M in CH_2Cl_2 (ε, M^{-1} cm^{-1})): featureless tail into visible, 500 (101); $[\alpha]_{18}^{546}$ = 25.0° (4.80 mg mL^{-1}, CH_2Cl_2).

Δ-[Co((*S*,*S*)-*p*-OMe-dpen)$_3$]$^{3+}$ 2Cl$^-$ BAr$_f^-$ (Δ-(*S*,*S*)-11^{3+} 2Cl$^-$ BAr$_f^-$). A gas circulating flask was charged with a solution of $Co(ClO_4)_2 \cdot 6H_2O$ (0.1360 g, 0.372 mmol) in MeOH (50 mL). Activated charcoal (0.1 g) and (*S*,*S*)-**7** (0.3346 g, 1.22 mmol, 3.3 equiv) were added with stirring. Air was passed through the vigorously stirred suspension for 16 h. The mixture was filtered through Celite and aq. $HClO_4$ (2.0 mL, 35%) was added. The solution was loaded onto a Dowex cation exchange column, giving an orange band. The column was washed with 1:1 v/v H_2O/MeOH (100 mL) and eluted with increasing gradients of aq. 12.0 M HCl in MeOH (9:1 v/v MeOH/HCl (100 mL), 8:2 v/v MeOH/HCl (100 mL), 7:3 v/v MeOH/HCl (100 mL), 6:4 v/v MeOH/HCl (100 mL)). An orange band was collected and taken to dryness by rotary evaporation (60 °C bath, base trap to scavenge HCl). The crude trichloride salt (0.1036 g; see text) was suspended in CH_2Cl_2 (5 mL) and Na$^+$ BAr$_f^-$ (0.0935 g, 0.105 mmol) was added. The mixture was sonicated for a few seconds and the CH_2Cl_2 became bright orange as a white precipitate (NaCl) developed. The mixture was filtered and the orange filtrate was loaded onto a silica gel column, giving an orange band. The column was eluted with 97.5:2.5 v/v CH_2Cl_2/MeOH. The solvent was removed from the orange fraction. The residue was dried by oil pump vacuum to give Δ-(*S*,*S*)-**11**$^{3+}$ 2Cl$^-$ BAr$_f^-$·2H$_2$O as a bright yellow solid (0.1252 g, 0.0678 mmol, 18%);[114] mp 130-135 °C dec (open capillary). Anal. Calcd. for $C_{80}H_{72}BCl_2CoF_{24}N_6O_6 \cdot 2H_2O$ (1846.11): C 52.05, H 4.15, N 4.55, Cl 3.84; found C 52.43, H 4.49, N 4.59, Cl 3.44.

^{1}H NMR (500 MHz, CD_2Cl_2/CD_3OD (0.40:0.001 mL), δ in ppm): BAr$_f^-$ at 7.73 (s, 8H, *o*), 7.57 (s, 8H, *p*); (*S*,*S*)-**7** ligand at 7.25 (d, $^3J_{HH}$ = 8.5 Hz, 12H, *o*), 6.81 (d, $^3J_{HH}$ = 8.5 Hz, *m*), 5.82 (br s, 2H, N**H**H′),[35] 5.67 (br s, 2H, NH**H′**),[35] 4.27 (s, 6H, C**H**NH$_2$), 3.74 (s, 18H, OC**H**$_3$); 1.85 (br s, 13H, **H**$_2$O);[34] ^{13}C NMR (125 MHz, CD_2Cl_2/CD_3OD (0.40:0.001 mL), δ in ppm): BAr$_f^-$ at 162.3 (q, $^1J_{BC}$ = 49.6 Hz, *i*),

135.3 (s, *o*), 129.4 (q, $^2J_{CF}$ = 34.3 Hz, *m*), 125.1 (q, $^1J_{CF}$ = 270.6 Hz, **C**F_3), 118.0 (s, *p*); (*S*,*S*)-**7** ligand at 160.8 (s, *i*), 129.3 (s, *m*), 127.6 (s, *p*), 114.9 (s, *o*), 64.9 (s, **C**HNH_2), 55.8 (s, O**C**H_3).

IR (powder film, cm^{-1}): 1572 (m, $\nu_{Ar\text{-}CC}$), 1510 (m, $\nu_{Ar\text{-}CC}$), 1354 (s, $\nu_{Ar\text{-}CF_3}$), 1275 (vs, ν_{CF}), 1119 (vs, δ_{CCN}); UV-visible (nm, 1.61 × 10^{-3} M in CH_2Cl_2 (ε, M^{-1} cm^{-1})): featureless tail into visible, 500 (144); $[\alpha]_{18}^{546}$ = –516.4° (5.50 mg mL^{-1}, CH_2Cl_2).

Λ-[Co((*S*,*S*)-*p*-Cl-dpen)$_3$]$^{3+}$ 2Cl$^-$ BAr$_f^-$ (Λ-(*S*,*S*)-12^{3+} 2Cl$^-$ BAr$_f^-$).[122] A gas circulating flask was charged with a solution of $Co(OAc)_2{\cdot}4H_2O$ (0.0712 g, 0.286 mmol) in MeOH (50 mL). Activated charcoal (0.1 g) and (*S*,*S*)-**9** (0.2743 g, 0.975 mmol, 3.4 equiv) were added with stirring. Air was passed through the vigorously stirred suspension for 16 h. The mixture was filtered through Celite and 1.5 M aq. HCl (6.0 mL) was added to the filtrate. The solvent was removed by rotary evaporation and the residue was washed with 5:1 v/v H_2O/MeOH (30 mL) onto a filter pad. The filter cake was dissolved in MeOH and the solvent was removed by rotary evaporation. The residue was dried by oil pump vacuum overnight to give the crude trichloride salt (0.2492 g; see text). A portion of the crude trichloride salt (0.1089 g) was suspended in CH_2Cl_2 (5 mL) and Na^+ BAr$_f^-$ (0.0957 g, 0.108 mmol) was added. The mixture was sonicated for 1 min during which time the CH_2Cl_2 became bright orange and a white precipitate (NaCl) developed. The mixture was filtered and the filtrate was loaded onto a silica gel column, giving an orange band. The column was eluted with 97.5:2.5 v/v CH_2Cl_2/MeOH. The solvent was removed from the orange fraction by rotary evaporation. The residue was dried by oil pump vacuum to give Λ-(*S*,*S*)-**12**$^{3+}$ 2Cl$^-$ BAr$_f^-{\cdot}3H_2O$ as an orange solid (0.0821 g, 0.045 mmol, 34%).[119]

^{1}H NMR (500 MHz, CD_2Cl_2, δ in ppm): BAr_f^- at 7.73 (s, 8H, *o*), 7.56 (s, 4H, *p*); (*S*,*S*)-**9** ligand at 7.98 (br s, 6H, N**H**H′), 7.38-7.18 (m, 24H, *o*/*m*), 4.45 (s, 6H, C**H**NH_2), 4.35 (br s, 6H, NH**H′**); 2.62 (br s, 6H, $\mathbf{H}_2O$); ^{13}C NMR (125 MHz, CD_2Cl_2, δ in ppm): BAr_f^- at 162.3 (q, $^1J_{BC}$ = 49.8 Hz, *i*), 135.4 (s, *o*), 129.4 (q, $^2J_{CF}$ = 35.5 Hz, *m*), 125.2 (q, $^1J_{CF}$ = 271.0 Hz, **C**F_3), 118.0 (s, *p*); (*S*,*S*)-**9** ligand at 137.1 (s, *i*), 133.0 (s, *p*), 130.7 (s, *o*), 129.6 (s, *m*), 62.4 (s, **C**HNH_2).[116]

Λ-[Co((*S*,*S*)-1-dnen)$_3$]$^{3+}$ 2Cl$^-$ BAr$_f^-$ (Λ-(*S*,*S*)-13^{3+} 2Cl$^-$ BAr$_f^-$). A gas circulating flask was charged with a solution of $Co(OAc)_2{\cdot}4H_2O$ (0.4002 g, 1.61 mmol) in MeOH (50 mL). Activated charcoal (0.1 g) and (*S*,*S*)-**10** (1.6360 g, 5.24 mmol, 3.25 equiv) were added with stirring. Air was passed through the vigorously stirred suspension for 16 h. The mixture was filtered through Celite and 12.0 M aq. HCl (3.0 mL) was added to the filtrate. The yellow precipitate was collected by filtration. The filtrate was concentrated to approximately 20 mL by rotary evaporation and H_2O was added (100 mL). The yellow precipitate was collected by filtration. The combined precipitates were washed with 9:1 v/v H_2O/MeOH (100 mL). The yellow filter cake was dissolved in MeOH and the solvent was removed by rotary evaporation. The residue was dried by oil pump vacuum at room temperature for 1 h. The crude trichloride salt (1.3603 g; see text) was suspended in CH_2Cl_2 (25 mL) and Na^+ BAr_f^- (1.092 g, 1.23 mmol) was added. The mixture was sonicated for 1 min during which time the CH_2Cl_2 became bright orange and a white precipitate (NaCl) developed. The mixture was filtered and the filtrate was loaded onto a silica gel column, giving an orange band. The column was eluted with CH_2Cl_2 and a bright green band separated and was collected. The column was eluted with 98:2 v/v CH_2Cl_2/MeOH and the main orange band was collected. The solvent was removed from the green and orange fractions by rotary

evaporation. Each residue was dried by oil pump vacuum at room temperature overnight to give green *trans*-[Co((*S*,*S*)-1-dnen)$_2$Cl$_2$]$^+$ BAr$_f^-$ (0.3037 g, 0.188 mmol, 12%) and orange Λ-(*S*,*S*)-**13**$^{3+}$ 2Cl$^-$ BAr$_f^-$·2H$_2$O (1.4152 g, 0.720 mmol, 45%).[114]

Data for Λ-(*S*,*S*)-**13**$^{3+}$ 2Cl$^-$ BAr$_f^-$·2H$_2$O, mp 131-135 °C dec. (open capillary). Anal. Calcd. for $C_{98}H_{72}BCl_2CoF_{24}N_6$·2H$_2$O (1966.30): C 59.86, H 3.90, N 4.27, Cl 3.61; found C 59.90, H 4.07, N 4.31, Cl 3.40.

^{1}H NMR (500 MHz, CD_2Cl_2, δ in ppm, Figure 4.20a): BAr$_f^-$ at 7.73 (s, 8H, *o*), 7.55 (s, 4H, *p*); (*S*,*S*)-**10** ligand at 9.72 (br s, 6H, N**H**H′), 8.51 (s, 6H, $C_{10}\mathbf{H}_7$), 8.02-7.95 (m, 24H, $C_{10}\mathbf{H}_7$), 7.18 (s, 12H, $C_{10}\mathbf{H}_7$), 5.61 (s, 6H, C**H**NH$_2$), 3.65 (br s, 6H, NH**H′**); 2.16 (br s, 3H, **H**$_2$O); ^{13}C{^{1}H} NMR (125 MHz, CD_2Cl_2, δ in ppm): BAr$_f^-$ at 162.3 (q, $^1J_{BC}$ = 48.9 Hz, *i*), 135.4 (s, *o*), 129.4 (q, $^2J_{CF}$ = 31.6 Hz, *m*), 125.2 (q, $^1J_{CF}$ = 271.0 Hz, **C**F$_3$), 118.0 (s, *p*); (*S*,*S*)-**10** ligand at 134.8, 131.9, 131.1 130.3, 128.8, 127.8, (125.5 × 2), 124.5, 122.8 (9 × s, **C**$_{10}$H$_7$), 59.7 (s, **C**HNH$_2$).

IR (powder film, cm^{-1}): 3053 (m, ν_{NH}), 1604 (m, δ_{NH}), 1354 (s, $\nu_{Ar\text{-}CF_3}$), 1275 (vs, ν_{CF}), 1121 (vs, δ_{CCN}); UV-visible (nm, 1.90 × 10^{-3} M in CH_2Cl_2 (ε, M^{-1} cm^{-1})): featureless tail into visible, 500 (264); $[\alpha]_{18}^{546}$ = 158.7° (5.04 mg mL^{-1}, CH_2Cl_2).

Data for *trans*-[Co((*S*,*S*)-1-dnen)$_2$Cl$_2$]$^+$ BAr$_f^-$, mp 121-128 °C dec (open capillary). Anal. Calcd. for $C_{76}H_{52}BCl_2CoF_{24}N_4$ (1617.88): C 56.42, H 3.24, N 3.46, Cl 4.38; found C 56.33, H 3.49, N 3.40, Cl 4.25.

^{1}H NMR (500 MHz, CD_2Cl_2, δ in ppm): BAr$_f^-$ at 7.72 (s, 8H, *o*), 7.56 (s, 4H, *p*); (*S*,*S*)-**10** ligand at 8.19 (s, 4H, $C_{10}\mathbf{H}_7$), 7.92 (d, $^3J_{HH}$ = 7.5 Hz, 4H, $C_{10}\mathbf{H}_7$), 7.87 (d, $^3J_{HH}$ = 8.5 Hz, 4H, $C_{10}H_7$), 7.77-7.68 (m, 4H, $C_{10}\mathbf{H}_7$), 7.62-7.52 (m, 8H, $C_{10}\mathbf{H}_7$), 7.36 (s, 4H, $C_{10}\mathbf{H}_7$), 6.15 (br s, 4H, N**H**H′), 5.09 (br s, 4H, NH**H′**), 4.78 (br s, 4H, C**H**NH$_2$); 1.56 (s, 5H, **H**$_2$O); ^{13}C NMR (125 MHz, CD_2Cl_2, δ in ppm): BAr$_f^-$ at 162.4 (q, $^1J_{BC}$ =

49.5 Hz, *i*), 135.4 (s, *o*), 129.5 (q, $^2J_{CF}$ = 31.4 Hz, *m*), 125.4 (q, $^1J_{CF}$ = 271.1 Hz, **C**F_3), 118.1 (s, *p*); (*S*,*S*)-**10** ligand at 134.9, 131.4, 131.1, 130.3, 128.8, 127.5, (126.1 × 2), 124.4, 121.4 (9 × s, **C**$_{10}H_7$), 59.1 (s, **C**HNH_2).

IR (powder film, cm^{-1}): 1572 (m, $\nu_{Ar\text{-}CC}$), 1510 (m, $\nu_{Ar\text{-}CC}$), 1354 (s, $\nu_{Ar\text{-}CF_3}$), 1275 (vs, ν_{CF}), 1118 (vs, δ_{CCN}); UV-visible (nm, 1.39 × 10^{-3} M in CH_2Cl_2 (ε, M^{-1} cm^{-1})): 597 (86); $[\alpha]_{18}^{546}$ = 233.3° (2.40 mg mL^{-1}, CH_2Cl_2).

Λ-[Co((*S*,*S*)-1-dnen)$_3$]$^{3+}$ 2BF$_4^-$ BAr$_f^-$ (Λ-(*S*,*S*)-13^{3+} 2BF$_4^-$ BAr$_f^-$). A round bottom flask was charged with a solution of Λ-(*S*,*S*)-**13**$^{3+}$ 2Cl^- BAr_f^-·2H_2O (0.4050 g, 0.206 mmol) in CH_2Cl_2 (10 mL). Then Ag^+ BF_4^- (0.0851 g, 0.44 mmol, 2.1 equiv) was added and the suspension was sonicated for 10 min. The mixture was filtered through Celite and the solvent was removed by rotary evaporation to give a red oil. The residue was dried by oil pump vacuum at room temperature for 1 h to give Λ-(*S*,*S*)-**13**$^{3+}$ 2BF_4^- BAr_f^-·(3±1)H_2O as a red solid (0.3934 g, 0.188 mmol, 91%),[31] mp 161-167 °C dec. (open capillary). Anal. Calcd. For $C_{98}H_{72}B_3CoF_{32}N_6$·3$H_2O$/$C_{98}H_{72}B_3CoF_{32}N_6$·4$H_2O$ (2087.05/2104.53): C 56.40/55.90, H 3.77/3.83, N 4.03/3.99; found C 55.97, H 3.41, N 3.85.

^{1}H NMR (500 MHz, CD_2Cl_2, δ in ppm, Figure 4.20b): BAr_f^- at 7.74 (s, 8H, *o*), 7.56 (s, 4H, *p*); (*S*,*S*)-**10** ligand at 8.07 (d, $^3J_{HH}$ = 8.0 Hz, 6H, C_{10}**H**$_7$), 7.92 (d, $^3J_{HH}$ = 8.0 Hz, 6H, C_{10}**H**$_7$), 7.71-7.64 (m, 18H, C_{10}**H**$_7$), 7.04 (t, $^3J_{HH}$ = 7.5 Hz, 6H, C_{10}**H**$_7$), 6.92 (s, 6H, C_{10}**H**$_7$), 6.32 (s, 6H, N**H**H′), 5.40 (s, 6H, C**H**NH_2), 4.04 (s, 6H, NH**H′**); 1.96 (s, 4H, **H**$_2$O). ^{13}C{^{1}H} NMR (125 MHz, CD_2Cl_2, δ in ppm): BAr_f^- at 162.2 (q, $^1J_{BC}$ = 62.5 Hz, *i*), 135.3 (s, *o*), 129.4 (q, $^2J_{CF}$ = 32.4 Hz, *m*), 125.2 (q, $^1J_{CF}$ = 271.3 Hz, **C**F_3), 118.2 (s, *p*); (*S*,*S*)-**10** ligand at 134.9, 132.5, 130.8, 130.0, 129.4, 128.6, 128.2,

125.7, 124.1, 121.3 (10 × s, $\mathbf{C}_{10}H_7$), 59.4 (s, $\mathbf{C}HNH_2$); ^{19}F NMR (470 MHz, CD_2Cl_2, δ in ppm): –62.8 (s, 24F, BAr_f^-), –141.8 (s, 8F, BF_4^-).

IR (powder film, cm^{-1}): 3251 (m, ν_{NH}), 1602 (m, δ_{NH}), 1354 (s, $\nu_{Ar\text{-}CF_3}$), 1275 (vs, ν_{CF}), 1119 (vs, δ_{CCN}); UV-visible (nm, 1.66×10^{-3} M in CH_2Cl_2 (ε, M^{-1} cm^{-1})): featureless tail into visible, 500 (1023); $[\alpha]_{18}^{546} = 604.1°$ (4.90 mg mL^{-1}, CH_2Cl_2).

4.6.2.2 Syntheses of previously unreported nitroolefins

***trans*-2-acetoxy-β-nitrostyrene (25).** A Schlenk flask was charged with *trans*-2-(2-nitrovinyl)phenol (0.5871 g, 3.54 mmol),[112a] Et_3N (0.500 mL, 3.58 mmol, 1.01 equiv), and dry CH_2Cl_2 (10 mL) under a N_2 atmosphere. The solution was cooled to 0 °C and acetyl chloride (0.375 mL, 5.28 mmol, 1.49 equiv) was added dropwise via syringe with stirring. The ice bath was removed. After 12 h, CH_2Cl_2 (50 mL) was added. The mixture was washed with H_2O (50 mL), 1.0 M HCl, (50 mL), and brine (50 mL). The organic layer was dried (Na_2SO_4) and the solvent was removed by rotary evaporation. The residue was chromatographed on silica (80:20 v/v hexanes/EtOAc). The product containing fractions were combined and the solvent was removed by rotary evaporation. The residue was dried by oil pump vacuum at room temperature to give **25** as a pale yellow solid (0.4730 g, 2.28 mmol, 65%). Compound **25** turns from a powder to a wax at 69-71 °C and then liquefies at 74-76 °C (open capillary). Anal. Calcd. for $C_{10}H_9NO_4$ (207.18): C 57.97, H 4.38, N 6.76; found C 58.13, H 4.40, N 6.73.

^1H NMR (500 MHz, $CDCl_3$, δ in ppm): 8.06 (d, $^3J_{HH}$ = 13.5 Hz, 1H, C**H**NO_2), 7.61-7.58 (m, 2H, C**H**=$CHNO_2$, $C_6\mathbf{H}_4$), 7.52 (t, $^3J_{HH}$ = 8.5 Hz, 1H, $C_6\mathbf{H}_4$), 7.32 (t, $^3J_{HH}$ = 7.5 Hz, 1H, $C_6\mathbf{H}_4$), 7.23 (d, $^3J_{HH}$ = 8.5 Hz, 1H, $C_6\mathbf{H}_4$), 2.43 (s, 3H, C**H**$_3$); $^{13}C\{^1H\}$

NMR (125 MHz, $CDCl_3$, δ in ppm): 168.8 (s, **C**(O)Me), 150.2, 138.7, 133.2, 133.1, 129.1, 126.8, 123.8, 123.0 (8 × s, $\mathbf{C}_6H_4$, **C**H=**C**HNO_2), 21.2 (s, **C**H_3).

IR (powder film, cm^{-1}): 3115 (w), 1753 (s), 1638 (m), 1510 (s), 1339 (vs), 1194 (vs), 963 (s), 758 (s).

***trans*-2-benzoyloxy-β-nitrostyrene (26).** A Schlenk flask was charged with *trans*-2-(2-nitrovinyl)phenol (0.5943 g, 3.60 mmol),[112a] Et_3N (0.630 mL, 4.52 mmol, 1.26 equiv), and dry CH_2Cl_2 (10 mL) under a N_2 atmosphere. The solution was cooled to 0 °C and benzoyl chloride (0.790 mL, 6.81 mmol, 1.89 equiv) was added dropwise via syringe with stirring. The ice bath was removed. After 12 h, CH_2Cl_2 (50 mL) was added. The mixture was washed with H_2O (50 mL), 1.0 M HCl, (50 mL), and brine (50 mL). The organic layer was dried (Na_2SO_4) and the solvent was removed by rotary evaporation. The residue was chromatographed on silica (80:20 v/v hexanes/EtOAc). The product containing fractions were combined and the solvent was removed by rotary evaporation. The residue was further dried by oil pump vacuum at room temperature to give **26** as a pale yellow solid (0.6629 g, 2.46 mmol, 69%). Compound **26** turns from a powder to a wax at 78-82 °C and then liquefies at 87-89 °C. Anal. Calcd. for $C_{15}H_{11}NO_4$ (269.25): C 66.91, H 4.12, N 5.20; found C 67.04, H 4.20, N 5.01.

^{1}H NMR (500 MHz, $CDCl_3$, δ in ppm): 8.24 (m, 2H, C**H**NO_2 and $C_6\mathbf{H}_5$/$C_6\mathbf{H}_4$), 8.13 (d, $^3J_{HH}$ = 13.5 Hz, 1H, C**H**=CHNO_2), 7.70 (t, $^3J_{HH}$ = 7.5 Hz, 1H, $C_6\mathbf{H}_5$/$C_6\mathbf{H}_4$), 7.66-7.56 (m, 5H, $C_6\mathbf{H}_5$/$C_6\mathbf{H}_4$), 7.38-7.33 (m, 2H, $C_6\mathbf{H}_5$/$C_6\mathbf{H}_4$); $^{13}C\{^1H\}$ NMR (125 MHz, $CDCl_3$, δ in ppm): 164.7 (s, **C**(O)Ph), 150.6 138.7, 134.5, 133.2, 133.2, 130.5, 129.2, 129.1, 128.5, 126.9, 124.0, 123.4 (12 × s, **C**H=**C**HNO_2, $\mathbf{C}_6H_4$, $\mathbf{C}_6H_5$).

IR (powder film, cm^{-1}): 3105 (w), 1742 (s), 1340 (s), 1209 (vs), 1057 (vs), 700 (vs).

4.6.2.3 Syntheses of previously unreported racemic Michael addition products

Dimethyl 2-(2-nitro-1-(2-acetoxyphenyl)ethyl)malonate (37) (typical procedure). A round bottom flask was charged with **25** (0.4067 g, 2.22 mmol), **15a** (0.257 mL, 2.25 mmol, 1.01 equiv), Et_3N (0.310 mL, 2.22 mmol, 1.00 equiv), and toluene (3.0 mL). The solution was stirred at 90 °C for 15 h, cooled to room temperature, and partitioned between CH_2Cl_2 (25 mL) and 1.0 M HCl (25 mL). The aqueous layer was removed and the organic layer was washed with brine (25 mL) and dried (Na_2SO_4). The solvent was removed by rotary evaporation. The residue was chromatographed on silica gel (80:20 v/v hexane/EtOAc). The product containing fractions were combined and the solvent was removed by rotary evaporation. The residue was dried by oil pump vacuum at room temperature to give **37** as a colorless oil (0.6081 g, 1.79 mmol, 81%). Anal. Calcd. for $C_{15}H_{17}NO_8$ (339.30): C 53.10, H 5.05, N 4.13; found C 53.39, H 5.11, N 4.11.

^{1}H NMR (500 MHz, $CDCl_3$, δ in ppm): 7.32 (t, $^3J_{HH}$ = 7.0 Hz, 1H, $C_6\mathbf{H}_4$), 7.27-7.25 (m, 1H, $C_6\mathbf{H}_4$), 7.20 (t, $^3J_{HH}$ = 7.5 Hz, 1H, $C_6\mathbf{H}_4$), 7.15 (d, $^3J_{HH}$ = 8.0 Hz, 1H, $C_6\mathbf{H}_4$), 4.94-4.86 (m, 2H, $C\mathbf{H}_2NO_2$), 4.50 (q, $^3J_{HH}$ = 7.0 Hz, 1H, $C\mathbf{H}{=}CH_2NO_2$), 3.92 (d, $^3J_{HH}$ = 8.5 Hz, 1H, $C\mathbf{H}(CO_2Me)_2$), 3.74 (s, 3H, $OC\mathbf{H}_3$), 3.59 (s, 3H, $OC'\mathbf{H}_3$), 2.39 (s, 3H, $C\mathbf{H}_3$); $^{13}C\{^1H\}$ NMR (125 MHz, $CDCl_3$, δ in ppm): 169.2, 168.0, 167.4 (3 × s, $\mathbf{C}O_2Me$, $\mathbf{C}'O_2Me$, $\mathbf{C}(O)Me$), 148.7, 129.4, 128.5, 128.2, 126.5, 123.5 (6 × s, $\mathbf{C}_6H_4$), 76.7 (s, $\mathbf{C}H_2NO_2$), 53.8 (s, $\mathbf{C}H(CO_2Me)_2$), 53.1 (s, $O\mathbf{C}H_3$, $O\mathbf{C}'H_3$), 36.7 (s, $\mathbf{C}H{=}CH_2NO_2$), 21.2 (s, $\mathbf{C}H_3$).[123]

IR (neat oil, cm^{-1}): 2957 (w), 1734 (vs), 1555 (s), 1192 (s), 1171 (s).

Chiral HPLC: Chiralcel OD 90:10 v/v hexanes/isopropanol, 1.0 mL/min, 220 nm; 19.1 min, 29.3 min.

Dimethyl 2-(2-nitro-1-(3,4-dichlorophenyl)ethyl)malonate (33). This compound was prepared by a procedure analogous to that given for **37** using **21** (0.5001 g, 2.29 mmol), **15a** (0.260 mL, 2.27 mmol, 0.99 equiv), Et_3N (0.260 mL, 1.89 mmol, 0.83 equiv), and toluene (3.0 mL). Obtained as a white solid (0.4906 g, 1.40 mmol, 61%), mp 78-81 °C. Anal. Calcd. for $C_{13}H_{13}Cl_2NO_6$ (350.15): C 44.59, H 3.74, N 4.00; found C 44.82, H 3.82, N 4.02.

^{1}H NMR (500 MHz, $CDCl_3$, δ in ppm): 7.40 (d, $^3J_{HH}$ = 9.0 Hz, 1H, $C_6\mathbf{H}_3$), 7.35 (s, 1H, $C_6\mathbf{H}_3$), 7.10 (d, $^3J_{HH}$ = 8.5 Hz, 1H, $C_6\mathbf{H}_3$), 4.90 (dd, $^2J_{HH}$ = 13.5 Hz, $^3J_{HH}$ = 5.0 Hz, 1H, C**H**H′NO_2), 4.85 (dd, $^2J_{HH}$ = 13.5 Hz, $^3J_{HH}$ = 9.5 Hz, 1H, CH**H′**NO_2), 4.20 (td, $^3J_{HH}$ = 9.0 Hz, $^3J_{HH}$ = 5.0 Hz, 1H, C**H**=CH_2NO_2), 3.82 (d, $^3J_{HH}$ = 9.5 Hz, 1H, C**H**$(CO_2Me)_2$), 3.77 (s, 3H, C$\mathbf{H_3}$), 3.62 (s, 3H, C′$\mathbf{H}_3$); $^{13}C\{^1H\}$ NMR (125 MHz, $CDCl_3$, δ in ppm): 167.5 (s, **C**O_2Me), 167.0 (s, **C′**O_2Me), 136.5, 133.3, 132.9, 131.1, 130.2, 127.4 (6 × s, $\mathbf{C}_6H_3$), 76.9 (s, **C**H_2NO_2), 54.4 (s, **C**H$(CO_2Me)_2$) , 53.3 (**C**H_3), 53.2 (**C′**H_3), 42.1 (**C**H=CH_2NO_2).

IR (powder film, cm^{-1}): 1744 (s), 1715 (s), 1549 (vs), 1265 (s), 1611 (s).

Chiral HPLC: Chiralpak AS-H 90:10 v/v hexanes/isopropanol, 1.0 mL/min, 220 nm; 20.3 min, 22.6 min

Dimethyl 2-(2-nitro-1-(2-trifluoromethylphenyl)ethyl)malonate (36). This compound was prepared by a procedure analogous to that given for **37** using **24** (0.1023 g, 0.472 mmol), **15a** (0.0580 mL, 0.507 mmol, 1.07 equiv), Et_3N (0.0580 mL, 0.416 mmol, 0.881 equiv), and toluene (3.0 mL). Obtained as a white solid (0.0887 g, 0.254 mmol, 55%), mp 76-79 °C. Anal. Calcd. for $C_{14}H_{14}F_3NO_6$ (349.26): C 48.14, H 4.04, N 4.01; found C 47.91, H 3.93, N 3.91.

^{1}H NMR (500 MHz, $CDCl_3$, δ in ppm): 7.72 (d, $^3J_{HH}$ = 7.5 Hz, 1H, $C_6\mathbf{H}_4$), 7.53 (t, $^3J_{HH}$ = 7.5 Hz, 1H, $C_6\mathbf{H}_4$), 7.43 (t, $^3J_{HH}$ = 8.0 Hz, 1H, $C_6\mathbf{H}_4$), 7.37 (d, $^3J_{HH}$ = 8.0 Hz, 1H, $C_6\mathbf{H}_4$), 5.16 (dd, $^2J_{HH}$ = 13.5 Hz, $^3J_{HH}$ = 7.5 Hz, 1H, C**H**H′NO_2), 4.94 (dd, $^2J_{HH}$ = 13.5 Hz, $^3J_{HH}$ = 4.5 Hz, 1H, CH**H′**NO_2), 4.65 (td, $^3J_{HH}$ = 7.5 Hz, $^3J_{HH}$ = 4.5 Hz, 1H, C**H**=CH_2NO_2), 4.11 (d, $^3J_{HH}$ = 7.5 Hz, 1H, C**H**$(CO_2Me)_2$), 3.75 (s, 3H, C**H**$_3$), 3.64 (s, 3H, C′**H**$_3$); ^{13}C NMR (125 MHz, $CDCl_3$, δ in ppm): 168.0 (s, **C**O_2Me), 167.3 (s. **C′**O_2Me), 135.1, 132.5 (2 × s, **C**$_6H_4$), 129.0 (q, $^2J_{CF}$ = 29.8 Hz, **C**CF_3), 128.6, 128.0 (2 × s, **C**$_6H_4$), 127.3 (q, $^3J_{CF}$ = 5.9 Hz, **C**$HCCF_3$), 124.2 (q, $^1J_{CF}$ = 272.6 Hz, **C**F_3), 76.6 (s, **C**H_2NO_2), 54.0 (s, **C**$H(CO_2Me)_2$), 53.2 (**C**H_3), 53.1 (**C′**H_3), 38.1 (s, **C**H=CH_2NO_2).

IR (powder film, cm^{-1}): 2957 (w), 1751 (s), 1734 (s), 1549 (s), 1126 (vs), 777 (s).

Chiral HPLC: Chiralcel OD 95:5 v/v hexanes/isopropanol, 1.0 mL/min, 220 nm; 12.6 min, 27.0 min.

Dimethyl 2-(2-nitro-1-(2-benzoyloxyphenyl)ethyl)malonate (38). This compound was prepared by a procedure analogous to that given for **37** using **26** (0.1012 g, 0.376 mmol), **15a** (0.0400 mL, 0.354 mmol, 0.94 equiv), Et_3N (0.00520 mL, 0.373 mmol, 0.99 equiv), and toluene (3.0 mL).

This gave **26a** as a pale yellow oil (0.0640 g, 0.159 mmol, 45%). Anal. Calcd. for $C_{20}H_{19}NO_8$ (401.37): C 59.85, H 4.77, N 3.49; found C 59.59, H 4.80, N 3.40.

^{1}H NMR (500 MHz, $CDCl_3$, δ in ppm): 8.27 (d, $^3J_{HH}$ = 7.0 Hz, 2H, $C_6\mathbf{H}_5$/$C_6\mathbf{H}_4$), 7.69 (t, $^3J_{HH}$ = 7.0 Hz, 1H, $C_6\mathbf{H}_5$/$C_6\mathbf{H}_4$), 7.57 (t. $^3J_{HH}$ = 8.0 Hz, 2H, $C_6\mathbf{H}_5$/$C_6\mathbf{H}_4$), 7.39-7.33 (m, 2H, $C_6\mathbf{H}_5$/$C_6\mathbf{H}_4$), 7.28-7.25 (m, 2H, $C_6\mathbf{H}_5$/$C_6\mathbf{H}_4$), 4.98 (dd, $^2J_{HH}$ = 13.5 Hz, $^3J_{HH}$ = 8.5 Hz, 1H, C**H**H′NO_2), 4.91 (dd, $^2J_{HH}$ = 13.5 Hz, $^3J_{HH}$ = 5.0 Hz, 1H, CH**H′**NO_2), 4.60 (td, $^3J_{HH}$ = 8.5 Hz, $^3J_{HH}$ = 5.0 Hz, 1H, C**H**=CH_2NO_2), 3.96

(d, $^2J_{HH}$ = 8.5 Hz, 1H, C**H**$(CO_2Me)_2$), 3.72 (s, 3H, C**H**$_3$), 3.53 (s, 3H, C′**H**$_3$); $^{13}C\{^1H\}$ NMR (125 MHz, $CDCl_3$, δ in ppm): 167.9 (s, **C**O_2Me), 167.4 (s, **C′**O_2Me), 164.9 (s, **C**(O)Ph), 149.0, 134.1, 130.5, 129.6, 129.1, 129.0, 128.7, 128.3, 126.6, 123.6 (10 × s, **C**$_6H_5$/**C**$_6H_4$), 76.6 (s, **C**H_2NO_2), 53.8 (s, **C**$H(CO_2Me)_2$), 53.1 (s, **C**O_2Me), 53.1 (s, **C′**O_2Me), 36.7 (s, **C**$H=CH_2NO_2$).

IR (neat oil, cm^{-1}): 2955 (w), 1732 (vs), 1555 (s), 1213 (s), 708 (vs).

Chiral HPLC: Chiralpak AD 90:10 v/v hexanes/isopropanol, 1.0 mL/min, 220 nm; 15.3 min, 25.9 min.

Dimethyl 2-(2-nitro-1-(2-benzyloxyphenyl)ethyl)malonate (39). This compound was prepared by a procedure analogous to that given for **37** using **27** (0.0982 g, 0.440 mmol), **15a** (0.0615 mL, 0.537 mmol, 1.22 equiv), Et_3N (0.0600 mL, 0.430 mmol, 0.98 equiv), and toluene (3.0 mL). Obtained as a colorless oil (0.1061 g, 0.274 mmol, 62%). Anal. Calcd. for $C_{20}H_{21}NO_7$ (387.38): C 62.01, H 5.46, N 3.62; found C 62.25, H 5.46, N 3.57.

^{1}H NMR (500 MHz, $CDCl_3$, δ in ppm): 7.47 (d, J = 7.5 Hz, 2H, C_6**H**$_5$/C_6**H**$_4$), 7.42 (t, 7.5 Hz, 2H, C_6**H**$_5$/C_6**H**$_4$), 7.36 (t, J = 7.5 Hz, 1H, C_6**H**$_5$/C_6**H**$_4$), 7.24 (t, J = 7.5 Hz, 1H, C_6**H**$_5$/C_6**H**$_4$), 7.17 (d, J = 7.5 Hz, 1H, C_6**H**$_5$/C_6**H**$_4$), 6.93 (d, J = 8.5 Hz, 1H, C_6**H**$_5$/C_6**H**$_4$), 6.89 (t, J = 7.5 Hz, 1H, C_6**H**$_5$/C_6**H**$_4$); 5.13 (d, $^3J_{HH}$ = 2.5 Hz, 2H, C**H**$_2$Ph), 5.05 (dd, J = 13.0 Hz, J = 4.5 Hz, 1H, C**H**H′NO_2), 4.84 (dd, J = 13.0 Hz, J = 4.5 Hz, 1H, CH**H′**NO_2), 4.44 (td, $^3J_{HH}$ = 9.5 Hz, $^3J_{HH}$ = 4.5 Hz, 1H, C**H**$=CH_2NO_2$), 4.17 (d, $^3J_{HH}$ = 9.5 Hz, 1H, C**H**$(CO_2Me)_2$), 3.72 (s, 3H, C**H**$_3$), 3.50 (s, 3H, C′**H**$_3$); ^{13}C NMR (125 MHz, $CDCl_3$, δ in ppm): 168.3, (s, **C**O_2Me), 167.7 (s, **C′**O_2Me), 156.7, 136.5, 130.9, 129.8, 128.9, 128.3, 127.7, 123.9, 121.2, 112.4 (10 × s, **C**$_6H_4$/**C**$_6H_5$), 76.0 (s, **C**H_2NO_2), 70.6 (**C**H_2Ph), 53.0 (s, **C**$H(CO_2Me)_2$), 52.7 (s, **C**H_3), 52.6 (s, **C′**H_3), 40.5 (s, **C**$H=CH_2NO_2$).

IR: 3034 (w), 2955 (w), 2886 (w), 1732 (vs), 1553 (vs), 1238 (vs), 752 (s), 696 (m).

Chiral HPLC: Chiralcel OD 90:10 v/v hexanes/isopropanol, 1.0 mL/min, 220 nm; 12.7 min, 26.9 min.

Dimethyl 2-(2-nitro-1-(3-benzyloxyphenyl)ethyl)malonate (40). This compound was prepared by a procedure analogous to that given for **37** using **28** (0.1005 g, 0.394 mmol), **15a** (0.0490 mL, 0.428 mmol, 1.08 equiv), Et_3N (0.0500 mL, 0.358 mmol, 0.91 equiv), and toluene (3.0 mL). Obtained as a colorless oil (0.1093 g, 0.282 mmol, 72%). Anal. Calcd. for $C_{20}H_{21}NO_7$ (387.38): C 62.01, H 5.46, N 3.62; found C 62.29, H 5.37, N 3.64.

^{1}H NMR (500 MHz, $CDCl_3$, δ in ppm): 7.43-7.38 (m, 4H, $C_6\mathbf{H}_5/C_6\mathbf{H}_4$), 7.33 (t, $^3J_{HH}$ = 7.0 Hz, 1H, $C_6\mathbf{H}_5/C_6\mathbf{H}_4$), 7.24 (t, $^3J_{HH}$ = 8.0 Hz, 1H, $C_6\mathbf{H}_5/C_6\mathbf{H}_4$), 6.90-6.81 (m, 3H, $C_6\mathbf{H}_5/C_6\mathbf{H}_4$), 5.03 (s, 2H, $C\mathbf{H}_2Ph$); 4.91 (dd, $^2J_{HH}$ = 13.5 Hz, $^3J_{HH}$ = 5.0 Hz, 1H, $C\mathbf{H}H'NO_2$), 4.86 (dd, $^2J_{HH}$ = 13.5 Hz, $^3J_{HH}$ = 9.5 Hz, 1H, $CH\mathbf{H}'NO_2$), 4.21 (td, $^3J_{HH}$ = 9.0 Hz, $^3J_{HH}$ = 5.0 Hz, 1H, $C\mathbf{H}{=}CH_2NO_2$), 3.85 (d, $^3J_{HH}$ = 8.5 Hz, 1H, $C\mathbf{H}(CO_2Me)_2$), 3.75 (s, 3H, $C\mathbf{H}_3$), 3.57 (s, 3H, $C'\mathbf{H}_3$); $^{13}C\{^1H\}$ NMR (125 MHz, $CDCl_3$, δ in ppm): 168.0 (s, $\mathbf{C}O_2Me$), 167.3 (s, $\mathbf{C}'O_2Me$), 159.2, 137.9, 136.8, 130.3, 128.8, 128.2, 127.7, 120.3, 115.0, 114.7 (10 × s, $\mathbf{C}_6H_4/\mathbf{C}_6H_5$), 70.2 (s, $\mathbf{C}H_2NO_2$), 54.9 (s, $\mathbf{C}H(CO_2Me)_2$), 53.2 (s, $\mathbf{C}H_3$), 52.0 (s, $\mathbf{C}'H_3$), 43.0 (s, $\mathbf{C}H{=}CH_2NO_2$).

IR: 3032 (w), 2955 (w), 2924 (w), 1732 (vs), 1553 (vs), 1258 (s), 1155 (s), 696 (vs).

Chiral HPLC: Chiralpak AS-H 90:10 v/v hexanes/isopropanol, 1.0 mL/min, 220 nm; 30.7 min, 33.7 min.

4.6.2.4 Data for previously reported racemic Michael addition products

Data for dimethyl 2-(2-nitro-1-phenylethyl)malonate (16a). ^{1}H NMR (500 MHz, $CDCl_3$, δ in ppm): 7.33-7.21 (m, 5H, $C_6\mathbf{H}_5$), 4.93 (dd, $^{2}J_{HH}$ = 13.0 Hz, $^{3}J_{HH}$ = 5.0 Hz, 1H, C**H**H′NO_2), 4.87 (dd, $^{2}J_{HH}$ = 13.0 Hz, $^{3}J_{HH}$ = 9.0 Hz, 1H, CH**H′**NO_2), 4.24 (td, $^{3}J_{HH}$ = 9.0 Hz, $^{3}J_{HH}$ = 5.0 Hz, 1H, C**H**=CH_2NO_2), 3.86 (d, $^{3}J_{HH}$ = 9.0 Hz, 1H, C**H**$(CO_2Me)_2$), 3.75 (s, 3H, C**H**$_3$), 3.54 (s, 3H, C′**H**$_3$); $^{13}C\{^{1}H\}$ (125 MHz, $CDCl_3$, δ in ppm): 167.9 (s, **C**O_2Me), 167.3 (s, **C′**O_2Me), 136.2 (s, *i*), 129.1 (s, *o*) 128.4 (s, *p*), 128.0 (s, *m*), 77.5 (s, **C**H_2NO_2), 54.8 (s, **C**H$(CO_2Me)_2$), 53.1 (s, **C**H_3), 52.9 (s, **C′**H_3), 43.0 (s, **C**H=CH_2NO_2).[123]

The NMR data agree with those in the literature.[94a]

Chiral HPLC: Chiralpak AD 98:2 v/v hexanes/isopropanol, 1.0 mL/min, 220 nm; 32.9 min, 42.5 min.

Data for diethyl 2-(2-nitro-1-phenylethyl)malonate (16b). ^{1}H NMR (500 MHz, $CDCl_3$, δ in ppm): 7.33-7.22 (m, 5H, $C_6\mathbf{H}_5$), 4.92 (dd, $^{2}J_{HH}$ = 13.5 Hz, $^{3}J_{HH}$ = 5.0 Hz, 1H, C**H**H′NO_2), 4.86 (dd, $^{2}J_{HH}$ = 13.0 Hz, $^{3}J_{HH}$ = 9.0 Hz, 1H, CH**H′**NO_2), 4.26-4.19 (m, 3H, C**H**$_2$$CH_3$ and C**H**=CH_2NO_2), 4.00 (q, $^{3}J_{HH}$ = 7.5 Hz, 2H, C′**H**$_2$C′H_3), 3.81 (d, $^{3}J_{HH}$ = 9.5 Hz, 1H, C**H**$(CO_2Et)_2$), 1.26 (t, $^{3}J_{HH}$ = 7.0 Hz, 3H, CH_2C**H**$_3$), 1.04 (t, $^{3}J_{HH}$ = 7.0 Hz, 3H, C′H_2C′**H**$_3$); $^{13}C\{^{1}H\}$ NMR (125 MHz, $CDCl_3$, δ in ppm): 167.6 (s, **C**O_2Et), 166.9 (s, **C′**O_2Et), 136.3 (s, *i*), 129.1 (s, o), 128.5 (s, *p*) 128.1 (s, *m*), 77.8 (s, **C**H_2NO_2), 62.3 (s, **C**H_2CH_3), 62.0 (s, **C′**H_2C′H_3), 55.1 (s, **C**H$(CO_2Et)_2$), 43.1 (s, **C**H=CH_2NO_2), 14.1 (s, **C**H_3), 13.9 (s, **C′**H_3).

The NMR data agree with those in the literature.[94a]

Chiral HPLC: Chiralpak AS-H 90:10 v/v hexanes/isopropanol, 1.0 mL/min, 220 nm; 12.1 min, 13.9 min.

Data for diisopropyl 2-(2-nitro-1-phenylethyl)malonate (16c). ^{1}H NMR (500 MHz, $CDCl_3$, δ in ppm): 7.32-7.22 (m, 5H, $C_6\mathbf{H}_5$), 5.08 (sept, $^{3}J_{HH}$ = 6.0 Hz, 1H, C**H**$(CH_3)_2$), 4.92 (dd, $^{2}J_{HH}$ = 13.0 Hz, $^{3}J_{HH}$ = 4.5 Hz, 1H, C**H**H′NO_2), 4.86-4.60 (m, 2H, C′**H**$(C'H_3)_2$ and CH**H′**NO_2), 4.20 (td, $^{3}J_{HH}$ = 8.5 Hz, $^{3}J_{HH}$ = 5.0 Hz, 1H, C**H**=CH_2NO_2), 3.75 (d, $^{3}J_{HH}$ = 9.5 Hz, 1H, C**H**$(CO_2i\text{Pr})_2$), 1.24 (d, $^{3}J_{HH}$ = 6.5 Hz, 6H, CH(C**H**$_3)_2$), 1.07 (d, $^{3}J_{HH}$ = 6.0 Hz, 3H, C′H((C′**H**$_3$)(C″H$_3$))), 1.01 (d, $^{3}J_{HH}$ = 6.5 Hz, 3H, C′H((C′H$_3$)(C″**H**$_3$))); $^{13}C\{^{1}H\}$ NMR (125 MHz, $CDCl_3$, δ in ppm): 167.2 (s, **C**O_2iPr), 166.5 (s, **C′**O_2iPr), 136.4 (s, *i*), 129.0 (s, *o*), 128.4 (s, *p*), 128.3 (s, *m*), 78.1 (s, **C**H_2NO_2), 70.1 (s, **C**H$(CH_3)_2$), 69.7 (s, **C′**H$(C'H_3)_2$), 55.3 (s, **C**H$(CO_2i\text{Pr})_2$), 43.1 (s, **C**H=CH_2NO_2), 21.7, 21.6, 21.41, 21.39 (4 × s, 4 × **C**H_3).

The NMR data agree with those in the literature.[94a]

Chiral HPLC: Chiralcel OD 95:5 v/v hexanes/isopropanol, 0.75 mL/min, 220 nm; 11.0 min, 13.4 min.

Data for dibenzyl 2-(2-nitro-1-phenylethyl)malonate (16d). ^{1}H NMR (500 MHz, $CDCl_3$, δ in ppm): 7.35-7.25 (m, 11H, $C_6\mathbf{H}_5$/$CH_2C_6\mathbf{H}_5$), 7.18-7.16 (m, 2H, $C_6\mathbf{H}_5$/$CH_2C_6\mathbf{H}_5$), 7.09-7.07 (m, 2H, $C_6\mathbf{H}_5$/$CH_2C_6\mathbf{H}_5$), 5.18 (d, $^{2}J_{HH}$ = 12.0 Hz, 1H, C**H**H′Ph), 5.15 (d, $^{2}J_{HH}$ = 12.5 Hz, 1H, CH**H′**Ph), 4.96 (d, $^{2}J_{HH}$ = 12.0 Hz, 1H, C′**H**H′Ph), 4.93 (d, $^{2}J_{HH}$ = 12.0 Hz, 1H, C′H**H′**Ph), 4.86-4.84 (m, 2H, C**H**$_2NO_2$), 4.26 (td, $^{3}J_{HH}$ = 8.5 Hz, $^{3}J_{HH}$ = 5.5 Hz, 1H, C**H**=CH_2NO_2), 3.94 (d, $^{3}J_{HH}$ = 9.0 Hz, 1H, C**H**$(CO_2Bn)_2$); $^{13}C\{^{1}H\}$ NMR (125 MHz, $CDCl_3$, δ in ppm): 167.3 (s, **C**O_2Bn), 166.7 (s, **C′**O_2Bn), 136.1 (s, *i* **C**$_6H_5$), 134.8 (s, *i* CH_2**C**$_6H_5$), 134.8 (s, *i* C′H$_2$**C′**$_6H_5$), 129.1,

128.8, 128.8, 128.7, 128.6, 128.5, 128.5, 128.4, 128.0 (9 × s, *o*, *m*, *p* of $\mathbf{C}_6H_5$, $CH_2\mathbf{C}_6H_5$, $C'H_2\mathbf{C}'_6H_5$), 77.5 (s, $\mathbf{C}H_2NO_2$), 67.9 (s, $\mathbf{C}H_2C_6H_5$), 67.8 (s, $\mathbf{C}'H_2C_6H_5$), 55.1 (s, $\mathbf{C}H(CO_2Bn)_2$), 43.1 (s, $\mathbf{C}H{=}CH_2NO_2$).

The NMR data are similar to those in the literature.[94a]

Chiral HPLC: Chiralcel AS-H 90:10 v/v hexanes/isopropanol, 1.0 mL/min, 220 nm; 20.3 min, 22.6 min.

Data for di-*t*-butyl 2-(2-nitro-1-phenylethyl)malonate (16e). ^{1}H NMR (500 MHz, $CDCl_3$, δ in ppm): 7.32-7.23 (m, 5H, $C_6\mathbf{H_5}$), 4.92 (dd, $^2J_{HH}$ = 13.0 Hz, $^3J_{HH}$ = 4.5 Hz, 1H, $C\mathbf{H}H'NO_2$), 4.79 (dd, $^2J_{HH}$ = 13.0 Hz, $^3J_{HH}$ = 9.5 Hz, 1H, $CH\mathbf{H}'NO_2$), 4.12 (td, $^3J_{HH}$ = 9.5 Hz, $^3J_{HH}$ = 4.0 Hz, 1H, $C\mathbf{H}{=}CH_2NO_2$), 3.61 (d, $^3J_{HH}$ = 10.0 Hz, 1H, $C\mathbf{H}(CO_2tBu)_2$), 1.46 (s, 9H, $C(C\mathbf{H}_3)_3$), 1.21 (s, 9H, $C'(C'\mathbf{H}_3)_3$); $^{13}C\{^1H\}$ NMR (125 MHz, $CDCl_3$, δ in ppm): 167.1 (s, $\mathbf{C}O_2tBu$), 166.1 (s, $\mathbf{C}'O_2tBu$), 136.7 (s, *i*), 128.9 (s, *o*), 128.4 (s, *m*), 128.3 (s, *p*), 83.1 (s, $\mathbf{C}(CH_3)_3$), 82.4 (s, $\mathbf{C}'(CH_3)_3$), 78.4 (s, $\mathbf{C}H_2NO_2$), 56.6 (s, $\mathbf{C}H(CO_2tBu)_2$), 43.2 (s, $\mathbf{C}H{=}CH_2NO_2$), 28.0 (s, $C(\mathbf{C}H_3)_3$), 27.6 (s, $C'(\mathbf{C}'H_3)_3$).

The NMR data agree with those in the literature.[94a]

Chiral HPLC: Chiralcel OD 99:1 v/v hexanes/isopropanol, 1.0 mL/min, 220 nm; 8.7 min, 10.8 min.

Data for dimethyl 2-methyl-2-(2-nitro-1-phenylethyl)malonate (16f). ^{1}H NMR (500 MHz, $CDCl_3$, δ in ppm): 7.32-7.26 (m, 3H, $C_6\mathbf{H}_5$), 7.16-7.15 (m, 2H, $C_6\mathbf{H}_5$), 5.08-5.00 (m, 2H, $C\mathbf{H}_2NO_2$), 4.18 (dd, $^3J_{HH}$ = 10.0 Hz, $^3J_{HH}$ = 4.5 Hz, 1H, $C\mathbf{H}{=}CH_2NO_2$), 3.77 (s, 3H, $OC\mathbf{H}_3$), 3.72 (s, 3H, $OC'\mathbf{H}_3$), 1.34 (s, 3H, $C(C\mathbf{H}_3)(CO_2Me)_2$); $^{13}C\{^1H\}$ NMR (125 MHz, $CDCl_3$, δ in ppm): 171.5 (s, $\mathbf{C}O_2Me$),

170.8 (s, **C′**O_2Me), 135.1 (s, *i*), 129.0 (s, *o*), 128.9 (s, *m*), 128.6 (s, *p*), 77.6 (s, **C**H_2NO_2), 56.9 (s, **C**(CH_3)(CO_2Me)$_2$), 53.2 (s, OC**H**$_3$), 53.0 (s, O**C′**H_3), 48.4 (s, **C**H=CH_2NO_2), 20.4 (s, C(**C**H_3)(CO_2Me)$_2$).

The NMR data are similar to those in the literature.[94a]

Chiral HPLC: Chiralcel AS-H 98:2 v/v hexanes/isopropanol, 1.0 mL/min, 220 nm; 16.8 min, 19.7 min.

Data for dimethyl 2-(2-nitro-1-(4-methoxyphenyl)ethyl)malonate (31). ^{1}H NMR (500 MHz, $CDCl_3$, δ in ppm): 7.14 (d, $^3J_{HH}$ = 8.5 Hz, 2H, *m* to CH), 6.83 (d, $^3J_{HH}$ = 8.5 Hz, 2H, *o* to CH), 4.89 (dd, $^2J_{HH}$ = 13.0 Hz, $^3J_{HH}$ = 5.0 Hz, 1H, C**H**H′NO_2), 4.82 (dd, $^2J_{HH}$ = 13.5 Hz, $^3J_{HH}$ = 9.5 Hz, 1H, CH**H′**NO_2), 4.19 (td, $^3J_{HH}$ = 9.0 Hz, $^3J_{HH}$ = 5.0 Hz, 1H, C**H**=CH_2NO_2), 3.82 (d, $^3J_{HH}$ = 9.5 Hz, 1H, C**H**(CO_2Me)$_2$), 3.77 (s, 3H, CO_2C**H**$_3$), 3.76 (s, 3H, C′O_2C′**H**$_3$), 3.57 (s, 3H, ArOC**H**$_3$); ^{13}C{^{1}H} NMR (125 MHz, $CDCl_3$, δ in ppm): 168.0 (s, **C**O_2Me), 167.4 (s, **C′**O_2Me), 159.6 (s, *p* to CH), 129.1 (s, *o* to CH), 128.0 (s, *i* to CH), 114.5 (s, *m* to CH), 77.8 (s, **C**H_2NO_2), 55.3 (s, ArO**C**H_3), 55.0 (**C**H(CO_2Me)$_2$), 53.1 (s, CO_2**C**H_3), 53.0 (s, C′O_2**C′**H_3), 42.4 (s, **C**H=CH_2NO_2).[124]

The NMR data are similar to those in the literature.[93b]

Chiral HPLC: Chiralpak AD 80:20 v/v hexanes/isopropanol, 1.0 mL/min, 220 nm; 11.6 min, 18.2 min.

Data for dimethyl 2-(2-nitro-1-(3,4-dioxolophenyl)ethyl)malonate (32). ^{1}H NMR (500 MHz, $CDCl_3$, δ in ppm): 6.74-6.67 (m, 3H, C_6**H**$_3$), 5.95 (s, 2H, OC**H**$_2$O), 4.87 (dd, $^2J_{HH}$ = 13.0 Hz, $^3J_{HH}$ = 8.0 Hz, 1H, C**H**H′NO_2), 4.80 (dd, $^2J_{HH}$ = 13.0 Hz, $^3J_{HH}$ = 9.5 Hz, 1H, CH**H′**NO_2), 4.16 (td, $^3J_{HH}$ = 9.0 Hz, $^3J_{HH}$ = 5.0 Hz, 1H,

C**H**=CH_2NO_2), 4.79 (dd, $^3J_{HH}$ = 9.0 Hz, 1H, C**H**($CO_2Me)_2$), 3.76 (s, 3H, C**H**$_3$), 3.61 (s, 3H, C′**H**$_3$); $^{13}C\{^1H\}$ NMR (125 MHz, $CDCl_3$, δ in ppm): 167.9 (s, **C**O_2Me), 167.3 (s, **C**′O_2Me), 148.2, 147.7, 129.7, 121.5, 108.8, 108.3, 101.5 (7 × s, **C**$_6$H$_3$, O**C**H_2O), 77.7 (s, **C**H_2NO_2), 55.0 (s, **C**H($CO_2Me)_2$), 53.2 (s, **C**H_3), 53.1 (s, **C**′H_3), 42.8 (s, **C**H=CH_2NO_2).

The NMR data are similar to those in the literature.[94b]

Chiral HPLC: Chiralcel AS-H 90:10 v/v hexanes/isopropanol, 1.0 mL/min, 220 nm; 47.9 min, 55.7 min.

Data for dimethyl 2-(2-nitro-1-α-napthylethyl)malonate (29). ^1H NMR (500 MHz, $CDCl_3$, δ in ppm): 8.18 (d, $^3J_{HH}$ = 8.5 Hz, 1H, C_{10}**H**$_7$), 7.87 (d, $^3J_{HH}$ = 8.0 Hz, 1H, C_{10}**H**$_7$), 7.80 (d, $^3J_{HH}$ = 8.0 Hz, 1H, C_{10}**H**$_7$), 7.62 (t, $^3J_{HH}$ = 8.5 Hz, 1H, C_{10}**H**$_7$), 7.53 (t, $^3J_{HH}$ = 8.0 Hz, 1H, C_{10}**H**$_7$), 7.44-7.38 (m, 2H, C_{10}**H**$_7$), 5.25-5.16 (m, 2H, C**H**H′NO_2 and C**H**=CH_2NO_2), 5.07 (dd, $^2J_{HH}$ = 13.5 Hz, $^3J_{HH}$ = 4.5 Hz, 1H, CH**H**′NO_2), 4.12 (d, $^3J_{HH}$ = 7.5 Hz, 1H, C**H**($CO_2Me)_2$), 3.72 (s, C**H**$_3$), 3.54 (s, C′**H**$_3$); $^{13}C\{^1H\}$ NMR (125 MHz, $CDCl_3$, δ in ppm): 168.1 (s, **C**O_2Me), 167.6 (s, **C**′O_2Me), 134.3, 132.3, 131.1, 129.4, 129.2, 127.2, 126.2, 125.2, 124.1, 122.3 (10 × s, **C**$_{10}$H$_7$), 76.7 (s, **C**H_2NO_2), 54.6 (s, **C**H($CO_2Me)_2$), 53.1 (s, **C**H_3), 53.0 (s, **C**′H_3), 36.9 (s, **C**H=CH_2NO_2).

The NMR data are similar to those in the literature.[93b]

Chiral HPLC: Chiralpak AD 90:10 v/v hexanes/isopropanol, 1.0 mL/min, 254 nm; 13.5 min, 18.9 min.

Data for dimethyl 2-(2-nitro-1-β-napthylethyl)malonate (30). ^1H NMR (500 MHz, $CDCl_3$, δ in ppm): 7.83-7.79 (m, 3H, C_{10}**H**$_7$), 7.70 (s, 1H, C_{10}**H**$_7$), 7.50-7.48 (m,

2H, $C_{10}\mathbf{H}_7$), 7.34 (d, $^3J_{HH}$ = 8.5 Hz, 1H, $C_{10}\mathbf{H}_7$), 5.01 (d, $^3J_{HH}$ = 8.0 Hz, 2H, $C\mathbf{H}_2NO_2$), 4.43 (q, $^3J_{HH}$ = 7.0 Hz, 1H, $C\mathbf{H}{=}CH_2NO_2$), 3.98 (d, $^3J_{HH}$ = 9.0 Hz, 1H, $C\mathbf{H}(CO_2Me)_2$), 3.77 (s, 3H, $C\mathbf{H}_3$), 3.54 (s, 3H, $C'\mathbf{H}_3$); $^{13}C\{^1H\}$ NMR (125 MHz, $CDCl_3$, δ in ppm): 166.0 (s, $\mathbf{C}O_2Me$), 167.4 (s, $\mathbf{C}'O_2Me$), 133.7, 133.4, 133.2, 129.1, 128.1, 127.8, 127.5, 126.7, 126.6, 125.3 (10 × s, $\mathbf{C}_{10}H_7$), 77.5 (s, $\mathbf{C}H_2NO_2$), 54.9 (s, $\mathbf{C}H(CO_2Me)_2$), 53.2 (s, $\mathbf{C}H_3$), 53.0 (s, $\mathbf{C}'H_3$), 43.2 ($\mathbf{C}H{=}CH_2NO_2$).

The NMR data are similar to those in the literature.[93c]

Chiral HPLC: Chiralpak OD 70:30 v/v hexanes/isopropanol, 1.0 mL/min, 254 nm; 14.2 min, 35.9 min.

Data for dimethyl 2-(2-nitro-1-(pyridine-3-yl)ethyl)malonate (34). ^1H NMR (500 MHz, $CDCl_3$, δ in ppm): 8.55-8.52 (m, 2H, $C_5\mathbf{H}_4N$), 7.59 (dt, $^3J_{HH}$ = 8.0 Hz, J_{HH} = 2.0 Hz, 1H, $C_5\mathbf{H}_4N$), 7.27-7.25 (m, 1H, $C_5\mathbf{H}_4N$), 4.94 (dd, $^2J_{HH}$ = 13.5 Hz, $^3J_{HH}$ = 8.5 Hz, $C\mathbf{H}H'NO_2$), 4.89 (dd, $^2J_{HH}$ = 13.5 Hz, $^3J_{HH}$ = 9.5 Hz, 1H, $CH\mathbf{H}'NO_2$), 4.26 (td, $^3J_{HH}$ = 8.5 Hz, $^3J_{HH}$ = 5.0 Hz, $C\mathbf{H}{=}CH_2NO_2$), 3.86 (d, $^3J_{HH}$ = 8.5 Hz, 1H, $C\mathbf{H}(CO_2Me)_2$), 3.76 (s, $C\mathbf{H}_3$), 3.58 (s, $C'\mathbf{H}_3$); $^{13}C\{^1H\}$ NMR (125 MHz, $CDCl_3$, δ in ppm): 167.6 (s, $\mathbf{C}O_2Me$), 167.0 (s, $\mathbf{C}'O_2Me$), 149.9, 149.7, 135.5, 132.1, 123.8 (5 × s, $\mathbf{C}_5H_4N$), 76.9 (s, $\mathbf{C}H_2NO_2$), 54.3 (s, $\mathbf{C}H(CO_2Me)_2$), 53.3 (s, $\mathbf{C}H_3$), 53.2 (s, $\mathbf{C}'H_3$), 40.7 (s, $\mathbf{C}H{=}CH_2NO_2$).

The NMR data are similar to those in the literature.[93b]

Chiral HPLC: Chiralpak AD 60:40 v/v hexanes/isopropanol, 1.0 mL/min, 220 nm; 6.8 min, 9.3 min.

Data for dimethyl 2-(2-nitro-1-(*o*-tolyl)ethyl)malonate (35). ^1H NMR (500 MHz, $CDCl_3$, δ in ppm): 7.19-7.11 (m, 4H, $C_6\mathbf{H_4}$), 4.91 (dd, $^2J_{HH}$ = 13.5 Hz, $^3J_{HH}$ = 5.5

Hz, 1H, C**H**H′NO_2), 4.86 (dd, $^2J_{HH}$ = 13.0 Hz, $^3J_{HH}$ = 9.0 Hz, 1H, CH**H′**NO_2), 4.57 (td, $^3J_{HH}$ = 9.0 Hz, $^3J_{HH}$ = 5.5 Hz, 1H, C**H**=CH_2NO_2), 3.83 (d, $^3J_{HH}$ = 9.0 Hz, 1H, C**H**($CO_2Me)_2$), 3.76 (s, 3H, OC**H**$_3$), 3.54 (s, OC′**H**$_3$), 2.44 (s, C**H**$_3$); $^{13}C\{^1H\}$ NMR (125 MHz, $CDCl_3$, δ in ppm): 168.1 (s, **C**O_2Me), 167.5 (s, **C′**O_2Me), 137.1, 134.6, 131.4, 128.2, 126.7, 125.9 (6 × s, **C**$_6H_4$), 77.4 (s, **C**H_2NO_2), 54.6 (s, **C**H($CO_2Me)_2$), 53.2 (s, O**C**H_3), 52.9 (s, O**C′**H_3), 37.9 (s, **C**H=CH_2NO_2), 19.6 (s, **C**H_3).

The NMR data are similar to those in the literature.[93b]

Chiral HPLC: Chiralpak AD 90:10 v/v hexanes/isopropanol, 1.0 mL/min, 220 nm; 8.9 min, 16.3 min.

Data for dimethyl 2-(2-nitro-1-furylethyl)malonate (43). ^1H NMR (500 MHz, $CDCl_3$, δ in ppm): 7.33 (m, 1H, C_4**H**$_3$O), 6.28 (m, 1H, C_4**H**$_3$O), 6.21 (d, $^3J_{HH}$ = 3.5 Hz, 1H, C_4**H**$_3$O), 4.89 (m, 2H, C**H**$_2NO_2$), 4.39 (td, $^3J_{HH}$ = 17.5 Hz, $^3J_{HH}$ = 12.5 Hz, 1H, C**H**=CH_2NO_2), 3.93 (d, $^3J_{HH}$ = 8.0 Hz, 1H, C**H**($CO_2Me)_2$), 3.75 (s, 3H, C**H**$_3$), 3.68 (s, 3H, C′**H**$_3$); $^{13}C\{^1H\}$ NMR (125 MHz, $CDCl_3$, δ in ppm): 167.6 (s, **C**O_2Me), 167.3 (s, **C′**O_2Me), 149.5, 143.0, 110.7, 106.5 (4 × s, **C**$_4H_3$O), 75.4 (s, **C**H_2NO_2), 53.2 (s, **C**H_3), 53.1 (s, **C′**H_3), 52.8 (s, **C**H($CO_2Me)_2$), 36.9 (s, **C**H=CH_2NO_2).

The NMR data are similar to those in the literature.[93b]

Chiral HPLC: Chiralpak OD 90:10 v/v hexanes/isopropanol, 1.0 mL/min, 220 nm; 11.8 min, 31.2 min.

Data for dimethyl 2-(2-nitro-1-propylethyl)malonate (44). ^1H NMR (500 MHz, $CDCl_3$, δ in ppm): 4.69 (dd, $^2J_{HH}$ = 13.5 Hz, $^3J_{HH}$ = 8.5 Hz, 1H, C**H**H′NO_2), 4.52 (dd, $^2J_{HH}$ = 13.5 Hz, $^3J_{HH}$ = 6.5 Hz, 1H, CH**H′**NO_2), 3.762 (s, 3H, OC**H**$_3$), 3.756 (s, 3H, OC′**H**$_3$), 3.66 (d, $^3J_{HH}$ = 6.0 Hz, 1H, C**H**($CO_2Me)_2$), 2.90 (sext, $^3J_{HH}$ = 6.5 Hz,

1H, C**H**=CH_2NO_2), 1.46-1.34 (m, 4H, C$\mathbf{H}_2$C$\mathbf{H}_2$), 0.92 (t, $^3J_{HH}$ = 7.5 Hz, 3H, C$\mathbf{H}_3$); $^{13}C\{^1H\}$ NMR (125 MHz, $CDCl_3$, δ in ppm): 168.5 (s, **C**O_2Me), 168.3 (s, **C′**O_2Me), 76.7 (s, **C**H_2NO_2), 53.0 (s, O**C**H_3), 52.9 (s, O**C′**H_3), 52.4 (s, **C**H($CO_2Me)_2$), 36.9 (s, **C**H=CH_2NO_2), 32.3 (s, **C**$H_2CH_2CH_3$), 20.0 (s, CH_2**C**H_2CH_3), 13.9 (s, **C**H_3).

The NMR data are similar to those in the literature.[125]

Chiral HPLC: Chiralcel OD 97.5:2.5 v/v hexanes/isopropanol, 1.0 mL/min, 220 nm; 12.9 min, 18.9 min.

Data for diphenyl (2-nitro-1-phenylethyl)phosphonate (46). ^1H NMR (500 MHz, $CDCl_3$, δ in ppm): 7.47-7.30 (m, 7H, $C_6\mathbf{H}_5$/$C_6\mathbf{H}_5$O), 7.21-7.08 (m, 6H, $C_6\mathbf{H}_5$/$C_6\mathbf{H}_5$O), 6.74 (d, $^3J_{HH}$ = 8.5 Hz, $C_6\mathbf{H}_5$/$C_6\mathbf{H}_5$O), 5.21 (ddd, $^2J_{HH}$ = 13.5 Hz, $^3J_{HH}$ = 7.0 Hz, $^4J_{HP}$ = 4.5 Hz, 1H, C**H**H′NO_2), 5.11 (ddd, $^2J_{HH}$ = 19.0 Hz, $^3J_{HH}$ = 11.0 Hz, $^4J_{HP}$ = 7.5 Hz, 1H, CH**H′**NO_2), 4.43 (ddd, $^2J_{HP}$ = 25.0 Hz, $^3J_{HH}$ = 11.0 Hz, $^3J_{HH}$ = 4.5 Hz, 1H, C**H**=CH_2NO_2); $^{13}C\{^1H\}$ NMR (125 MHz, $CDCl_3$, δ in ppm, aromatic signals unassigned): 150.1 (d, 9.6 Hz), 150.0 (d, J_{CP} = 9.8 Hz), 130.7 (d, J_{CP} = 7.8 Hz), 130.1 (d, J_{CP} = 1.1 Hz), 129.8 (d, J_{CP} = 1.0 Hz), 129.4 (d, J_{CP} = 6.5 Hz), 129.3 (d, J_{CP} = 2.4 Hz), 129.1 (d, J_{CP} = 3.3 Hz), 125.8 (s), 125.6 (s), 120.5 (d, J_{CP} = 4.4 Hz), 120.2 (d, J_{CP} = 4.4 Hz), 75.1 (d, $^2J_{CP}$ = 7.3 Hz, **C**H_2NO_2), 43.5 (d, $^1J_{CP}$ = 140.5 Hz, **C**H=CH_2NO_2).

The NMR data are similar to those in the literature.[101b]

Chiral HPLC: Chiralpak OD 90:10 v/v hexanes/isopropanol, 1.0 mL/min, 210 nm; 19.4 min, 37.7 min.

Data for 2-phenyl-1,3-dinitrobutane, *anti* isomer (*anti*-48). ^1H NMR (500 MHz, $CDCl_3$, δ in ppm): 7.34-7.33 (m, 3H, $C_6\mathbf{H}_5$), 7.20-7.19 (m, 2H, $C_6\mathbf{H}_5$), 4.89-4.78 (m, 2H, C**H**NO_2 and C**H**H′NO_2), 4.65 (dd, $^2J_{HH}$ = 13.0 Hz, $^3J_{HH}$ = 4.5 Hz, CH**H′**NO_2),

4.01 (td, $^3J_{HH}$ = 8.5 Hz, $^3J_{HH}$ = 3.5 Hz, 1H, C**H**=CH_2NO_2), 1.41 (d, $^3J_{HH}$ = 7.0 Hz, 3H, C**H**$_3$); $^{13}C\{^1H\}$ NMR (125 MHz, $CDCl_3$, δ in ppm): 133.9 (s, *i*), 129.7 (s, *o*), 129.2 (s, *p*), 128.1 (s, *m*), 84.7 (s, **C**HNO_2), 76.9 (s, **C**H_2NO_2), 47.9 (s, **C**H=CH_2NO_2), 18.0 (s, **C**H_3).

The NMR data are similar to those in the literature.[102]

Chiral HPLC: Chiralpak AS-H 90:10 v/v hexanes/isopropanol, 1.0 mL/min, 220 nm; 17.1 min, 18.7 min.

Data for 2-phenyl-1,3-dinitrobutane, *syn* isomer (*syn*-48). ^1H NMR (500 MHz, $CDCl_3$, δ in ppm): 7.38-7.33 (m, 3H, C_6**H**$_5$), 7.16-7.15 (m, 2H, C_6**H**$_5$), 4.98-4.91 (m, 2H, C**H**NO_2 and C**H**H′NO_2), 4.82 (dd, $^2J_{HH}$ = 13.5 Hz, $^3J_{HH}$ = 9.0 Hz, CH**H′**NO_2), 4.02 (q, $^3J_{HH}$ = 8.5 Hz, 1H, C**H**=CH_2NO_2), 1.58 (d, $^3J_{HH}$ = 7.0 Hz, 3H, C**H**$_3$); $^{13}C\{^1H\}$ NMR (125 MHz, $CDCl_3$, δ in ppm): 133.6 (s, *i*), 129.4 (s, *o*), 129.2 (s, *p*), 128.1 (s, *m*), 84.2 (s, **C**HNO_2), 76.2 (s, **C**H_2NO_2), 47.5 (s, **C**H=CH_2NO_2), 16.8 (s, **C**H_3).

The NMR data are similar to those in the literature.[102]

Chiral HPLC: Chiralpak AS-H 90:10 v/v hexanes/isopropanol, 1.0 mL/min, 220 nm; 24.1 min, 25.9 min.

Data for 1-methyl-3-(2-nitro-1-phenylethyl)indole (50). ^1H NMR (500 MHz, CD_2Cl_2, δ in ppm): 7.78 (d, $^3J_{HH}$ = 8.0 Hz, 1H, C_6**H**$_5$/C_8**H**$_5$N), 7.705-7.534 (m, 7H, C_6**H**$_5$/C_8**H**$_5$N), 7.38 (t, $^3J_{HH}$ = 7.0 Hz, 1H, C_6**H**$_5$/C_8**H**$_5$N), 7.26 (s, 1H, C_6**H**$_5$/C_8**H**$_5$N), 5.50 (t, $^3J_{HH}$ = 8.0 Hz, 1H, C**H**=CH_2NO_2), 5.40 (dd, $^2J_{HH}$ = 12.5 Hz, $^3J_{HH}$ = 7.5 Hz, 1H, C**H**H′NO_2), 5.29 (dd, $^2J_{HH}$ = 12.5 Hz, $^3J_{HH}$ = 8.0 Hz, 1H, CH**H′**NO_2), 4.06 (s, 3H, C**H**$_3$); $^{13}C\{^1H\}$ NMR (125 MHz, CD_2Cl_2, δ in ppm): 140.3, 137.9, 129.4, 128.3, 128.0,

127.0, 126.8, 122.6, 119.6, 119.3, 113.2, 110.1, 113.2, 110.1 (14 × s, $\mathbf{C}_6H_5/\mathbf{C}_8H_5N$), 80.1 (s, $\mathbf{C}H_2NO_2$), 42.0 (s, $\mathbf{C}H{=}CH_2NO_2$), 33.3 (s, $\mathbf{C}H_3$).

The NMR data are similar to those in the literature.[103]

Chiral HPLC: Chiralpak AS-H 90:10 v/v hexanes/isopropanol, 1.0 mL/min, 220 nm; 14.3 min, 17.9 min.

4.6.2.3 Catalysis Procedures

Michael reactions of nitroolefins and dialkylmalonates (general procedure for Tables 4.5, 4.6, 4.8, 4.9, 4.10, 4.13, 4.15, and 4.17). A 5 mm NMR tube was charged with a solution of nitroolefin (0.036 mmol), dialkyl malonate (0.039 mmol, 1.1 equiv), catalyst (0.0036 mmol, 0.10 equiv), and diphenyl dimethylsilane (0.0020 mL, internal standard) in the appropriate NMR solvent (0.40 mL). A ^{1}H NMR spectrum was recorded to measure the initial ratio of the nitroolefin to the internal standard. The mixture was adjusted to the appropriate temperature, and the base (0.036 mmol, 1.0 equiv) was added. The conversion was periodically measured by ^{1}H NMR. After the reported time, the mixture was loaded directly onto a plug of silica gel. The organic product was eluted with 1:1 v/v hexanes/EtOAc (50 mL). The solvent was removed by rotary evaporation. The product ee was assayed by chiral HPLC.[96]

Michael reaction of nitroolefin 19 and dimethyl malonate with 2 mol% catalyst (typical procedure for Table 4.12). A 5 mm NMR tube was charged with a solution of **19** (0.0180 g, 0.101 mmol), **15a** (0.0127 mL, 0.111 mmol, 1.10 equiv), Λ-(*S*,*S*)-$\mathbf{3}^{3+}$ $2Cl^-$ $BAr_f^-{\cdot}2H_2O$ (0.0032 g, 0.0019 mmol, 0.019 equiv), and diphenyl dimethylsilane (0.0020 mL, internal standard) in CD_2Cl_2 (1.0 mL). A ^{1}H NMR spectrum

was recorded to measure the initial ratio of **19** to the internal standard. Then Et_3N (0.0050 mL, 0.036 mmol, 0.36 equiv) was added and the conversion was periodically measured by ^1H NMR. After 24 h, the mixture was loaded directly onto a plug of silica gel. The organic product was eluted with 1:1 v/v hexanes/EtOAc (50 mL) and the solvent was removed by rotary evaporation. The ee of **31** was assayed by chiral HPLC.[96]

Synthesis scale reactions of nitroolefins and dimethyl malonate (typical procedure for Table 4.11, 4.14). A round bottom flask was charged with a solution of **14** (0.0529 g, 0.355 mmol), **15a** (0.0460 mL, 0.401 mmol, 1.13 equiv), and Λ-(*S*,*S*)-**3**$^{3+}$ 2Cl$^-$ BAr_f^-·2H_2O (0.0543 g, 0.0326 mmol) in acetone (3.3 mL), and cooled to 0 °C. Then Et_3N (0.0460 mL, 0.330 mmol, 0.93 equiv) was added. The reaction was monitored by TLC. After the recorded time (see table), the solvent was removed by rotary evaporation and the residue was dissolved in CH_2Cl_2 (2 mL). The orange solution was washed with 3.0 M HCl (1 mL) and H_2O (2 × 1 mL), loaded onto a silica gel column, and chromatographed with 9:1 v/v hexanes/EtOAc. The solvent was removed from the product containing fractions by rotary evaporation. The residue was dried by oil pump vacuum to give **16a** as a colorless oil (0.0940 g, 0.334 mmol, 94%). The ee was assayed by chiral HPLC, and the ^1H and $^{13}C\{^1H\}$ NMR spectra were identical to those reported for racemic **16a**.[94a]

The silica gel column was washed with CH_2Cl_2 and the orange catalyst band was eluted with 98:2 v/v CH_2Cl_2/MeOH. The solvent was removed by rotary evaporation. The residue was dried by oil pump vacuum at room temperature to recover Λ-(*S*,*S*)-**3**$^{3+}$ 2Cl$^-$ BAr_f^-·H_2O (0.0526 g, 0.0319 mmol, 98%).[114]

Data for the recovered catalyst; Anal. Calcd. for $C_{74}H_{60}BCl_2CoF_{24}N_6$·$H_2O$ (1647.94): C 53.91, H 3.79, N 5.10; found C 53.84, H 4.08, N 4.96.

Biphasic Michael reactions of nitroolefins and dimethyl malonate (typical procedure for Table 4.16). A round bottom flask was charged with a solution of **27** (0.0823 g, 0.322 mmol), **15a** (0.0460 mL, 0.401 mmol, 1.25 equiv), and Λ-(*S*,*S*)-**3**$^{3+}$ 2Cl$^-$ BAr$_f^-$·2H$_2$O (0.0541 g, 0.0325 mmol, 0.10 equiv) in CH_2Cl_2 (3.5 mL), and cooled to 0 °C. Then a solution of Na_2CO_3 (0.0350 g, 0.330 mmol, 1.02 equiv) in H_2O (0.5 mL) was added. The biphasic mixture was stirred at 600 rpm and the two phases remained visually distinct. The reaction was monitored by TLC. After 15 h, 3.0 M HCl (1 mL) was added and the aqueous phase was removed. The bright orange organic phase was washed with H_2O (2 × 1 mL) and then loaded onto a silica gel column. The column was eluted with 9:1 v/v hexanes/EtOAc. The solvent was removed from the product containing fractions by rotary evaporation. The residue was dried by oil pump vacuum to give **39** as a colorless oil (0.1045 g, 0.270 mmol, 84%). The ^{1}H and ^{13}C{^{1}H} NMR spectra were identical with those of racemic **39** given above.

The silica gel column was washed with CH_2Cl_2 and the orange catalyst band was eluted with 98:2 v/v CH_2Cl_2/MeOH. The solvent was removed by rotary evaporation. The residue was dried by oil pump vacuum at room temperature to recover Λ-(*S*,*S*)-**3**$^{3+}$ 2Cl$^-$ BAr$_f^-$ (0.0496 g, 0.0294 mmol, 90%).[126]

Michael addition of diphenyl phosphite and *trans*-β-nitrostyene (typical procedure for Table 4.18). A 5 mm NMR tube was charged with a solution of **14** (0.0102 g, 0.068 mmol), **45** (0.0154 mL, 0.080 mmol, 1.17 equiv), and diphenyl dimethylsilane (0.0020 mL, internal standard) in CD_2Cl_2 (0.67 mL). A ^{1}H NMR spectrum was recorded to measure the initial ratio of **14** to the internal standard. Then Et_3N (0.0093 mL, 0.067 mmol, 0.99 equiv) was added. The conversion was periodically measured by ^{1}H NMR. After 1 h, the mixture was loaded onto a plug of silica gel and

the organic product was eluted with 1:1 v/v hexanes/EtOAc (50 mL). The solvent was removed by rotary evaporation and the ee of **46** was assayed by chiral HPLC.[101a]

Michael addition of nitroethane and *trans*-β-nitrostyrene (typical procedure for Table 4.19). A 5 mm NMR tube was charged with a solution of **14** (0.0101 g, 0.067 mmol), **47** (0.0057 mL, 0.080 mmol, 1.2 equiv), Λ-(*S*,*S*)-$\mathbf{3}^{3+}$ $2Cl^-$ $BAr_f^-{\cdot}2H_2O$ (0.0101 g, 0.0060 mmol), and diphenyl dimethylsilane (0.0020 mL, internal standard) in acetone-d_6 (0.67 mL). A ^1H NMR spectrum was recorded to measure the initial ratio of **14** to the internal standard. The mixture was cooled to 0 °C and Et_3N (0.0093 mL, 0.067 mmol, 1.0 equiv) was added. The conversion was periodically measured by ^1H NMR. After 48 h, the mixture was loaded onto a plug of silica gel and the organic product was eluted with 1:1 v/v hexanes/EtOAc (50 mL). The solvent was removed by rotary evaporation and the ee of *anti*-**48** and *syn*-**48** were assayed by chiral HPLC.[102]

Friedel-Crafts reaction of *trans*-β-nitrostyrene and 1-methylindole (typical procedure for Table 4.20). A 5 mm NMR tube was charged with a solution of **14** (0.0043 g, 0.029 mmol), Λ-(*S*,*S*)-$\mathbf{3}^{3+}$ $2Cl^-$ $BAr_f^-{\cdot}2H_2O$ (0.0050 g, 0.003 mmol), and toluene (0.0010 mL, internal standard) in CD_2Cl_2 (0.4 mL). A ^1H NMR spectrum was recorded to measure the initial ratio of **14** to the internal standard. The mixture was cooled to 0 °C and **49** (0.0054 mL, 0.043 mmol, 1.48 equiv) was added. The conversion was periodically measured by ^1H NMR. After the recorded time (see Table 4.20), the mixture was loaded onto a plug of silica gel and the organic product was eluted with 1:1 v/v hexanes/EtOAc (50 mL). The solvent was removed by rotary evaporation and the ee of **50** was assayed by chiral HPLC.[103]

4.7 Crystallography

4.7.1 Data Collection and Structure Refinement

4.7.1.1 *The crystal structure of Λ-[Co((S,S)-dpen)$_3$]$^{3+}$ 3Cl$^-$·2H$_2$O·2MeOH* (Λ-(*S*,*S*)-3^{3+} 3Cl$^-$·*2H$_2$O·2MeOH*)

A solution of Λ-[Co((*S*,*S*)-dpen)$_3$]$^{3+}$ 3Cl$^-$ in 2:1 v/v MeOH/H$_2$O was allowed to slowly concentrate at room temperature. After 3 d, orange rods were collected. Data were obtained as outlined in Table 4.21. Cell parameters were determined from 60 data frames taken at 0.5° widths. Integrated intensity information for each reflection was obtained by reduction of the data frames with the program APEX2.[127] Data were corrected for Lorentz and polarization factors as well as crystal decay effects. The program SADABS[128] was employed to correct for absorption effects. The structure was solved by direct methods using SHELXTL (XS).[129] Two molecules of both H$_2$O and MeOH were located. Hydrogen atoms were placed in idealized positions and refined using a riding model. All non-hydrogen atoms were refined with anisotropic thermal parameters. Carbon atoms from two of the phenyl rings showed significant elongation of the thermal ellipsoids indicating disorder and were successfully modeled (C2B/C, C3B/C, C4B/C, C5B/C, C6B/C, C7B/C, 61:39 occupancy ratio; C9A/E, C10A/E, C11A/E, C12A/E, C13A/E, and C14A/E, 53:47 occupancy ratio). The parameters were refined by weighted least squares refinement on F^2 to convergence.[129,130] The absolute stereochemistry was unambiguously determined (absolute structure parameter = 0.000(12); Table 4.21).[131]

4.7.1.2 *The crystal structure of* Δ-*[Co((R,R)-dpen)$_3$]$^{3+}$ 3Cl$^-$·H$_2$O·3MeOH* (Δ-*(R,R)-**3**$^{3+}$ 2Cl$^-$ BAr$_f^-$·H$_2$O·3MeOH*

A solution of Δ-[Co((*R,R)*-dpen)$_3$]$^{3+}$ 3Cl$^-$ in MeOH was allowed to slowly concentrate at room temperature. After 5 d, orange rods were collected. Data were obtained as outlined in Table 4.22. Cell parameters were determined from 180 data frames taken at 0.5° widths. Integrated intensity information for each reflection was obtained by reduction of the data frames with the program APEX2.[127] Data were corrected for Lorentz and polarization factors as well as crystal decay effects. The program SADABS[128] was employed to correct for absorption effects. The structure was solved by direct methods using SHELXTL (XS).[129] Three molecules of MeOH and one water molecule were located. Hydrogen atoms were placed in idealized positions and refined using a riding model. All non-hydrogen atoms were refined with anisotropic thermal parameters. Unusual thermal ellipsoids on one of the phenyl groups indicated disorder, which could be refined to a 76:24 occupancy ratio (C30/30A, C31/31A, C32/32A, C33/33A, C34/34A, C35/35A). The thermal ellipsoids of the disordered atoms were constrained. The parameters were refined by weighted least squares refinement on F^2 to convergence.[129,130] The absolute stereochemistry was unambiguously determined (absolute structure parameter = 0.012(4); Table 4.22).[131]

4.7.1.3 The crystal structure of Δ-*[Co((S,S)-dpen)$_3$]$^{3+}$ 3Cl$^-$·12.5H$_2$O* (Δ-*(S,S)-**3**$^{3+}$ 3Cl$^-$ ·12.5 H$_2$O*

A solution of Δ-[Co((*S,S*)-dpen)$_3$]$^{3+}$ 3Cl$^-$ in H$_2$O was allowed to slowly concentrate at room temperature. After 7 d, orange blocks were collected. Data were

obtained as outlined in Table 4.23. Cell parameters were determined from 180 data frames taken at 0.5° widths. Integrated intensity information for each reflection was obtained by reduction of the data frames with the program APEX2.[127] Data were corrected for Lorentz and polarization factors as well as crystal decay effects. The program SADABS[128] was employed to correct for absorption effects, and the structure was solved using SHELXTL (XS).[129] The asymmetric unit contained two unique Δ-$[Co((S,S)\text{-dpen})_3]^{3+}$ moieties ($Z = 4$; $Z' = 2$) and 25 molecules of water. Hydrogen atoms were placed in idealized positions and refined using a riding model. All non-hydrogen atoms were refined with anisotropic thermal parameters. Several atoms resulted in non-positive definite matrices and some exhibited elongated thermal ellipsoids. Strong constraints (listed in the Validation Response Form of the CHECKCIF file) were placed to keep the thermal ellipsoids meaningful. The parameters were refined by weighted least squares refinement on F^2 to convergence.[129,130] The absolute stereochemistry was unambiguously determined (absolute structure parameter = 0.069(5); Table 4.23).[131]

Table 4.21. Crystallographic data for Λ-$[Co((S,S)\text{-dpen})_3]^{3+}$ $3Cl^{-}\cdot 2H_2O\cdot 2MeOH$ (Λ-(*S*,*S*)-**3**$^{3+}$ $3Cl^{-}\cdot 2H_2O\cdot 2MeOH$)

empirical formula	$C_{44}H_{60}Cl_3CoN_6O_4$
formula weight	902.26
temperature of collection [K]	110(2)
diffractometer	Bruker APEX 2
wavelength [Å]	0.71073
crystal system	tetragonal
space group	P4(3)
unit cell dimensions:	
a [Å]	13.839(4)
b [Å]	13.839(4)
c [Å]	24.216(9)
α [deg]	90
β [deg]	90
γ [deg]	90
V [Å^3]	4638(2)
Z	4
ρ_{calc} [Mg/m^3]	1.292
absorption coefficient [mm^{-1}]	0.590
F(000)	1904
crystal size [mm^3]	0.60 × 0.10 × 0.10
Θ [deg]	2.23 to 27.49
range / indices (*h*, *k*, *l*)	–17,17; –17,17; –31,31
reflections collected	70126
independent reflections	10535 [R(int) = 0.0425]
completeness to Θ = 27.49°	99.7%
absorption correction	semiempirical from equivalents
max. and min. transmission	0.9434 and 0.7187
refinement method	full-matrix least-squares on F^2
data / restraints / parameters	10535 / 7 / 525
goodness-of-fit on F^2	1.059
final R indices [I>2σ(I)]	$R1$ = 0.0442, w$R2$ = 0.1171
R indices (all data)	$R1$ = 0.0501, w$R2$ = 0.1220
absolute structure parameter	0.000(12)
largest diff. peak and hole [e Å^{-3}]	0.945 / –0.255

Table 4.22. Crystallographic data for Δ-$[Co((R,R)\text{-dpen})_3]^{3+}$ $3Cl^{-}\cdot H_2O\cdot 3MeOH$ (Δ-(*R*,*R*)-**3**$^{3+}$ $3Cl^{-}\cdot H_2O\cdot 3MeOH$)

empirical formula	$C_{44.88}H_{61.54}Cl_3CoN_6O_{3.88}$
formula weight	912.60
temperature [K]	110(2)
diffractometer	Bruker GADDS
wavelength [Å]	1.54178
crystal system	tetragonal
space group	P4(1)
unit cell dimensions:	
a [Å]	13.8725(7)
b [Å]	13.8725(7)
c [Å]	24.3173(13)
α [deg]	90
β [deg]	90
γ [deg]	90
V [Å^3]	4.679.8(4)
Z	4
ρ_{calc} [Mg/m^3]	1.295
absorption coefficient [mm^{-1}]	4.822
F(000)	1928
crystal size [mm^3]	0.12 × 0.08 × 0.04
Θ [deg]	3.19 to 60.00
range / indices (*h*, *k*, *l*)	–15,15; –15,15; –25,26
reflections collected	65183
independent reflections	6282 [R(int) = 0.0647]
completeness to Θ = 60.00°	98.5%
absorption correction	semiempirical from equivalents
max. and min. transmission	0.8305 and 0.5953
refinement method	full-matrix least-squares on F^2
data / restraints / parameters	6282 / 21 / 546
goodness-of-fit on F^2	1.071
final R indices [I>2σ(I)]	$R1$ = 0.0407, w$R2$ = 0.0841
R indices (all data)	$R1$ = 0.0510, w$R2$ = 0.0871
absolute structure parameter	0.012(4)
largest diff. peak and hole [e Å^{-3}]	0.362 / –0.622

Table 4.23. Crystallographic data for Δ-$[Co((S,S)\text{-dpen})_3]^{3+}$ $3Cl^-\cdot 12.5H_2O$ (Δ-(*S*,*S*)-**3**$^{3+}$ $3Cl^-\cdot 12.5\ H_2O$

empirical formula[a]	$C_{84}H_{146}Cl_6Co_2N_{12}O_{25}$
formula weight	2054.69
temperature [K]	110(2)
diffractometer	Bruker GADDS
wavelength [Å]	1.54178
crystal system	monoclinic
space group	P2(1)
unit cell dimensions:	
a [Å]	12.0877(6)
b [Å]	25.0985(14)
c [Å]	16.8235(8)
α [deg]	90
β [deg]	90.887(3)
γ [deg]	90
V [Å^3]	5103.4(5)
Z	2
ρ_{calc} [Mg/m^3]	1.337
absorption coefficient [mm^{-1}]	4.607
F(000)	2180
crystal size [mm^3]	0.16 × 0.15 × 0.07
Θ [deg]	2.63 to 60.00
range / indices	–13,13; –28,27; –18,18
reflections collected	112447
independent reflections	14790 [R(int) = 0.0916]
completeness to Θ = 27.49°	99.9%
absorption correction	semiempirical from equivalents
max. and min. transmission	0.7386 and 0.5260
refinement method	full-matrix least-squares on F^2
data / restraints / parameters	14790 / 265 / 1105
goodness-of-fit on F^2	1.149
final R indices [I>2σ(I)]	$R1$ = 0.0746, w$R2$ = 0.1791
R indices (all data)	$R1$ = 0.0807, w$R2$ = 0.1830
absolute structure parameter	0.069(5)
largest diff. peak and hole [e Å^{-3}]	0.972 / –0.698

[a]for the asymmetric unit; see text

CHAPTER V

SUMMARY AND CONCLUSIONS

This dissertation has, for the first time, detailed the application of chiral, $[Co(1,2\text{-diamine})_3]^{3+}$ $3X^-$ complexes, or "Werner complexes", as highly enantioselective catalysts in organic synthesis. Unlike most transition metal catalysts that require the reversible dissociation of labile ligands to provide substrate access to the metal, the catalysts described here were kinetically non-labile. Rather than direct metal activation, the Werner-type catalysts activated organic substrates *via* hydrogen bonding with the N-H units of the chelating diamine ligands. Chapter I highlighted the recent progress in hydrogen bond mediated catalysis with established organocatalysts.

Such Werner complexes possess one of the most unique forms of chirality found in chemistry. Until now, only partial treatment of the stereochemical possibilities with these systems has been reported. Because Werner complexes have had no practical applications in the past 30 years, an in depth analysis has not been necessary. However, the results discussed in this dissertation are expected to spark a renewed interest in Werner complex chemistry. Therefore, a thorough review of the stereochemical possibilities with Werner complexes was provided in Chapter II. The review taught the reader in a step-by-step manner and slowly introduced topics of increasing complexity. The most notable features of Werner complex stereochemistry include the configuration of the metal center (labeled Λ and Δ), the conformation of the chelating 1,2-diamine ligands (labeled λ and δ), and the orientation of C-C bond of the chelating ligand with the C_3 rotation axis of the complex (labeled *lel* and *ob*). The analysis featured unsubstituted, monosubstituted, and symmetrically disubstituted 1,2-diamine ligands. The chapter was not simply a review of the stereoisomers of Werner complexes that

have previously been isolated, but instead summarized all of the isomers that are possible with a particular 1,2-diamine ligand.

Chapter III offered a systematic analysis of the crystal structures reported for Werner complexes with a focus on the hydrogen bonding interactions between $[Co(1,2\text{-diamine})_3]^{3+}$ trications and counteranions or cocrystallized solvent molecules. The propensity of the Werner trications to form hydrogen bonds was clearly evident, since each structure analyzed exhibited hydrogen bonding with all 12 N-H units. Intricate and complex hydrogen bonding networks were analyzed and it was quite common to observe either two or three hydrogen bonding interactions between the Werner trication and a single counteranion. A new shorthand nomenclature was invented to classify the crystal structures. The new descriptors help the reader to quickly absorb all of the hydrogen bonding interactions in a particular crystal structure at a glance.

Chapter IV described the synthesis of new Co(III) complexes containing chiral dpen ligands. Incorporation of the lipophilic counteranion BAr_f^- rendered the complexes Λ-(*S*,*S*)-**3**$^{3+}$ $2Cl^-$ BAr_f^- and Δ-(*S*,*S*)-**3**$^{3+}$ $2Cl^-$ BAr_f^- soluble in CH_2Cl_2. Amazingly, the two diastereomers of the complexes were separated by column chromatography on silica gel with mildly polar solvents.

When applied as catalysts for Michael additions of dialkyl malonates to nitroolefins, both catalysts achieved good enantioselectivities. Depsite the presence of chiral ligands, the dominant configuration was almost entirely dependent on the configuration of the metal stereocenter. The catalysts Λ-(*S*,*S*)-**3**$^{3+}$ $2BF_4^-$ BAr_f^- and Λ-(*S*,*S*)-**3**$^{3+}$ $2PF_6^-$ BAr_f^- afforded faster reaction rates and improved enantioselectivities, consistent with less competition for substrate binding versus the counteranions. Under optimized conditions, Λ-(*S*,*S*)-**3**$^{3+}$ $2BF_4^-$ BAr_f^- achieved enantioselectivities as high as 96% ee.

Chiral Werner-type complexes are a broad platform on which to build new enantioselective catalysts. Complexes with functionalized dpen ligands or chiral counteranions have already been realized. Continued efforts are expected to further expand the scope of this catalyst system, both in terms of catalyst structure as well as applied organic transformations.

REFERENCES

(1) *Catalytic Asymmetric Synthesis*; Ojima, I. Ed.; VCH Publishers: New York, 1993; p v.

(2) (a) Trost, B. M. *Science* **1991**, *254*, 1471-1477. (b) Trost, B. M. *Angew. Chem. Int. Ed.* **1995**, *34*, 259-281; *Angew. Chem.* **1995**, *107*, 285-307.

(3) Seebach, D. *Angew. Chem. Int. Ed. Engl.* **1990**, *29*, 1320-1367; *Angew. Chem.* **1990**, *102*, 1363-1409.

(4) Nicolaou, K. C.; Chen, J. S. *Classics in Total Synthesis*; VCH Publishers: New York, 1996; p. 344.

(5) Berkessel, A.; Gröger, H. *Asymmetric Organocatalysis*; Wiley-VCH: Weinheim, 2005; p xiii.

(6) Ahrendt, K. A.; Borths, C. J.; MacMillan, D. W. C. *J. Am. Chem. Soc.* **2000**, *122*, 4243-4244.

(7) (a) Dalko, P. I.; Moisan, L. *Angew. Chem. Int. Ed.* **2001**, *40*, 3726-3748; *Angew. Chem.* **2001**, *113*, 3840-3864. (b) Dondoni, A.; Massi, A. *Angew. Chem. Int. Ed.* **2008**, *47*, 4638-4660; *Angew. Chem.* **2008**, *120*, 4716-4739. (c) MacMIllan, D. W. C. *Nature* **2008**, *455*, 304-308. (d) Thematic issue: List, B. *Chem. Rev.* **2007**, *107*, 5413-5415.

(8) (a) Ruble, J. C.; Fu, G. C. *J. Am. Chem. Soc.* **1998**, *120*, 11532-11533. (b) Hodous, B. L.; Fu, G. C. *J. Am. Chem. Soc.* **2002**, *124*, 1578-1579. (c) Schaefer, C.; Fu, G. C. *Angew. Chem. Int. Ed.* **2005**, *44*, 4606-4608; *Angew. Chem.* **2005**, *117*, 4682-4684. (d) Bappert, E.; Müller, P.; Fu, G. C. *Chem. Commun.* **2006**, 2604-2606.

(9) Taylor, M. S.; Jacobsen, E. N. *Angew. Chem. Int. Ed.* **2006**, *45*, 1520-1543; *Angew. Chem.* **2006**, *118*, 1550-1573.

(10) Etter, M. C.; Urbañczyk-Lipowska, Z.; Zia-Ebrahimi, M.; Panunto, T. W. *J. Am. Chem. Soc.* **1990**, *112*, 8415-8426.

(11) Ball and stick representation from reference 10

(12) Curran, D. P.; Kuo, L. H. *Tetrahedron Lett.* **1995**, *36*, 6647-6650.

(13) Schreiner, P. R. *Chem. Soc. Rev.* **2003**, *32*, 289-296.

(14) Hine, J.; Ahn, K.; Gallucci, J. C.; Linden, S.-M. *J. Am. Chem. Soc.* **1984**, *106*, 7980-7981.

(15) Ball and stick representation from reference 14

(16) Hine, J.; Linden, S.-M.; Kanagasabapathy, V. M. *J. Am. Chem. Soc.* **1985**, *107*, 1082-1083.

(17) Sigman, M. S.; Jacobsen, E. N. *J. Am. Chem. Soc.* **1998**, *120*, 4901-4902.

(18) Vachal, P.; Jacobsen, E. N. *J. Am. Chem. Soc.* **2002**, *124*, 10012-10014.

(19) (a) Doyle, A. G.; Jacobsen, E. N. *J. Am. Chem. Soc.* **2007**, *107*, 5713-5743. (b) Akiyama, T.; Itoh, J.; Fuchibe, K. *Adv. Synth. Catal.* **2006**, *348*, 999-1010. (c) *Hydrogen Bonding in Organic Synthesis*; Pihko, P. M., Ed.; Wiley-VCH: Weinheim, 2009.

(20) Huang, Y.; Unni, A. K.; Thadani, A. N.; Rawal, V. H. *Nature* **2003**, *424*, 146.

(21) Ooi, T.; Ohara, D.; Tamura, M.; Maruoka, K. *J. Am. Chem. Soc.* **2004**, *126*, 6844-6845.

(22) McDougal, N. T.; Schaus, S. E. *J. Am. Chem. Soc.* **2003**, *125*, 12094-12095.

(23) Uraguchi, D.; Terada, M. *J. Am. Chem. Soc.* **2004**, *126*, 5356-5357.

(24) Takenaka, N.; Chen, J.; Captain, B.; Sarangthem, R. S.; Chandrakumar, A. *J. Am. Chem. Soc.* **2010**, *132*, 4536-4537.

(25) Seebach, D.; Beck, A. K.; Heckel, A. *Angew. Chem. Int. Ed.* **2001**, *40*, 92-138; *Angew. Chem.* **2001**, *113*, 96-142.

(26) (a) Okino, T.; Hoashi, Y.; Takemoto, Y. *J. Am. Chem. Soc.* **2003**, *125*, 12672-12673; (b) Okino, T.; Hoashi, Y.; Furukawa, T.; Xu, X.; Takemoto, Y. *J. Am. Chem. Soc.* **2005**, *127*, 119-125.

(27) Zhu, Y.; Malerich, J. P.; Rawal, V. H. *Angew. Chem. Int. Ed.* **2010**, *49*, 153-156; *Angew. Chem.* **2010**, *122*, 157-160.

(28) Corey, E. J.; Grogan, M. J. *Org. Lett.* **1999**, *1*, 157-160.

(29) Terada, M.; Ube, H.; Yaguchi, Y. *J. Am. Chem. Soc.* **2006**, *128*, 1454-1455.

(30) Matsui, K.; Takizawa, S.; Sasai, H. *J. Am. Chem. Soc.* **2005**, *127*, 3680-3681.

(31) (a) Kauffman, G. B. *Coord. Chem. Rev.* **1974**, *12*, 105-149. (b) *Werner Centennial*; Kauffman, G. B. Ed.; Advances in Chemistry 62; American Chemical Society: Washington, DC, 1967.

(32) Hendry, P.; Ludi, A. *J. Chem. Soc., Chem. Commun*. **1987**, 891-892.

(33) (a) Hearson, J. A.; Mason, S. F.; Seal, R. H. *J. Chem. Soc., Dalton Trans.* **1977**, *10*, 1026-1034. (b) Searle, G. H.; Keene, F. R. *Inorg. Chim. Acta* **1989**, *155*, 125-138. (c) Serle, G. H.; Tiekink, E. R. T. *Inorg. Chim. Acta* **1989**, *156*, 57-63. (d) Atkinson, I. M.; Keene, F. R.; Searle, G. H. *J. Chem. Soc., Dalton Trans.* **1991**, *1*, 45-51.

(34) Crabtree, R. H. *The Organometallic Chemistry of the Transition Metals*, 3rd ed., John Wiley & Sons: New York, **2001**, p 2.

(35) Werner, A. *Chem. Ber.* **1912**, *45*, 121.

(36) For chromium, see ref. 37,38. For rhodium, see ref. 38,39. For iridium, see ref. 40. For platinum, see ref. 41.

(37) Werner, A. *Ber. Deut. Chem. Ges.,* **1912**, *45*, 865-869.

(38) Galsbøl, F. in *Inorganic Syntheses*; Parry, R. W. Ed.; McGraw-Hill: New York, 1970; p 269-280.

(39) Werner, A. *Chem. Ber.* **1912**, *45*, 1228-1236.

(40) (a) Werner, A.; Smirnoff, A. P. *Helv. Chim. Acta* **1920**, *3*, 472-486; (b) Galsbøl, F.; Rasmussen, B. S. *Acta Chem. Scand.* **1982**, *A36*, 83-87.

(41) Werner, A. *Vierteljahresschr. Naturforsh. Ges. Zuerich* **1917**, *62*, 553-564.

(42) Piper, T. S. *J. Am. Chem. Soc.* **1961**, *83*, 3908-3909.

(43) Friend, J. A.; Nunn, E. K. *J. Chem. Soc.* **1958**, 1567-1571.

(44) Gehman, W. G., Fernelius W. C. *J. Inorg. Nucl. Chem.* **1957**, *9*, 71-81.

(45) Douglas, B. D. *J. Am. Chem. Soc.* **1954**, *76*, 1020-1021.

(46) Corey, E. J.; Bailar, Jr., J. C. *J. Am. Chem. Soc.* **1959**, *81*, 2620-2628.

(47) Nomura, T.; Marumo, F.; Saito, Y. *Bull. Chem. Soc. Jpn.* **1969**, *42*, 1016-1020.

(48) (a) Fujita, J.; Ogino, H. *Chem. Lett.* **1974**, *1*, 57-58. (b) Sato, S.; Saito, Y.; Fujita, J.; Ogino, H. *Inorg. Nucl. Chem.* **1974**, *10*, 669-673.

(49) Harnung, S. E.; Kallesøe, S.; Sargeson, A. M.; Schäffer, C. E. *Acta Chem. Scand.* **1974**, *A28*, 385-398.

(50) (a) Kojima, M.; Funaki, H.; Yoshikawa, Y.; Yamasaki, K. *Bull. Chem. Soc. Jpn.* **1975**, *48*, 2801-2804. (b) Hilleary, C. J.; Them, T. F.; Tapscott, R. E. *Inorg. Chem.* **1980**, *19*, 102-107. (c) Gargallo, M. F.; Lechuga, L.; Puerta, M. C.; González-Vílchez, F.; Vilaplana, R. *J. Chem. Educ.* **1988**, *65*, 1018-1019.

(51) Harnung, S. E.; Sørensen, B. S.; Creaser, I.; Maegaard, H.; Pfenninger, U.; Schäffer, C. E. *Inorg. Chem.* **1976**, *15*, 2123-2126.

(52) (a) Bosnich, B.; Harrowfield, J. MacB. *J. Am. Chem. Soc.* **1972**, *94*, 3425-3437. (b) Kuroda, R.; Mason, S. F. *J. Chem. Soc., Dalton Trans.* **1977**, *10*, 1016-1020.

(c) Kojima, M.; Ishiguro, M.; Fugita, J. *Bull. Chem. Soc. Jpn.* **1978**, *51*, 3651-3652.

(53) Iwata, M.; Nakatzu, K.; Saito, Y. *Acta Cryst.* **1969**, *B25*, 2562-2571.

(54) Warren, R. M. L.; Jaller, K. J.; Tatehata, A.; Lappin, A. G. *Inorg. Chem.* **1994**, *33*, 227-232.

(55) Ball and stick representations in this chapter are adapted from the referenced crystal structures.

(56) Kuroda, R.; Shimanouchi, N.; Saito, Y. *Acta Cryst.* **1975**, *B31*, 931-932.

(57) Kuroda, R.; Saito, Y. *Acta Cryst.* **1974**, *B30*, 2126-2130.

(58) Morooka, M.; Ohba, S.; Saito, Y. *Acta Cryst.* **1991**, *B47*, 910-917.

(59) Kobayashi, A.; Marumo, F.; Saito, Y. *Acta Cryst*. **1972**, *B28*, 2709-2715.

(60) These crystal structures were in the course of this dissertation and are described in more detail in Chapter 4.

(61) Ogino, K. *Bull. Chem. Soc. Jpn.* **1969**, *42*, 447-452.

(62) Sakakibara, K.; Yoshikawa, Y.; Yamatera, H. *Bull. Chem. Soc. Jpn.* **1979**, *52*, 2725-2726.

(63) Mizuta, T.; Toshitani, K.; Miyoshi, K. *Inorg. Chem.* **1991**, *30*, 572-574.

(64) Okino, T.; Hoashi, Y.; Furukawa, T.; Xu, X.; Takemoto, Y. *J. Am. Chem. Soc.* **2005**, *127*, 119-125.

(65) Malerich, J. P.; Hagihara, K.; Rawal, V. H. *J. Am. Chem. Soc.* **2008**, *130*, 14416-14417.

(66) Witiak, D.; Clardy, J. C.; Martin Jr., D. S. *Acta Cryst.* **1972**, *B28*, 2694-2695.

(67) Brewew, G.; Butcher, R. J.; Jasinski, J. P. *Acta Cryst.* **2010**, *E66*, 1148-1149.

(68) Liebig, T. J.; Ruschewitz, U. *Cryst. Growth Des.* **2012**, *12*, 5402-5410.

(69) Duesler, E. N.; Raymond, K. N. *Inorg. Chem.* **1971**, *10*, 1486-1492.

(70) Brouty, P. C.; Spinat, P.; Whuler, A.; Herpin, P. *Acta Cryst.* **1976**, *B32*, 2153-2159.

(71) (a) Yoshikawa, Y.; Yamasaki, K. *Coord. Chem. Rev.* **1979**, *28*, 205. (b) Yoneda, H. *J. Chromatogr.* **1985**, *313*, 59.

(72) Mizuta, T.; Toshitani, K.; Miyoshi, K.; Yoneda, H. *Inorg. Chem.* **1990**, *29*, 3020-3026.

(73) Girolami, G. S.; Rauchfuss, T. B.; Angelici, R. J. *Synthesis and Technique in Inorganic Chemistry*, 3rd ed.; University Science Books: Sausalito, CA, 1999; p 143-150.

(74) Davies, J. D.; Daly, W. H.; Wang, Z. *Chem. Mater.* **1996**, *8*, 850-855.

(75) Ganzmann, C.; Gladysz, J. A. *Chem. Eur. J.* **2008**, *14*, 5397-5400.

(76) Several cobalt complexes in this chapter are isolated as hydrates, as described in the text. For readability, the abbreviated names do not include the hydrate.

(77) Ghosh, S. K.; Ojeda, A. S.; Guerrero-leal, J.; Bhuvanesh, N.; Gladysz, J. A. *Inorg. Chem.* **2013**, *52*, 9369-9378.

(78) Ganzmann, C. Doctoral Thesis, Friedrich-Alexander-Universität, Erlangen-Nürnberg, 2010.

(79) Gillard, R. D. *Prog. Inorg. Chem.* **1966**, *7*, 215-276.

(80) Lifshitz, I.; Bos, J. G. *Recl. Trav. Chim. Pays Bas* **1940**, *173*, 407-422.

(81) Gillard, R. D. *Tetrahedron* **1965**, *21*, 503- 506.

(82) Ballard, R. E.; McCaffery, A. J.; Mason, S. F. *J. Chem. Soc.* **1965**, 2883-2892.

(83) Fereday, P. L.; Mason, S. F. *Chem. Commun.* **1971***,* 1314-1315.

(84) Mason, S. F.; Seal, R. H. *J. C. S. Chem Comm.* **1973**, 422-423.

(85) Kuroda, R.; Mason, S. F. *J. Chem. Soc., Dalton Trans.* **1977**, *10*, 1016-1020.

(86) Williams, O. F.; Bailar, Jr. J. C. *J. Am. Chem. Soc.* **1959**, *81*, 4464-4469.

(87) The atom numbers have been changed from those of the original .cif file.

(88) Silverstein, R. M.; Webster, F. X.; Kiemle, D. J. *Spectrometric Identification of Organic Compounds*, 7th ed.; John Wiley & Sons: Hoboken, NJ, 2005; p 150-151.

(89) Kim, H.; Nguyen, Y.; Yen, C. P.-H.; Chagal, L.; Lough, A. J.; Kim, B. M.; Chin, J. *J. Am. Chem. Soc.* **2008**, *130*, 12184-12191.

(90) Ritchie, C. D.; Sager, W. F. in *Prog. Phys.Org. Chem*; Cohen, S. G.; Streitwieser, A.; Taft, R. W. Eds.; John Wiley & Sons, 1964; Vol. 2, p 323-400.

(91) Bailar Jr., J. C. in *Inorganic syntheses*; Fernelius, W. C. Ed.; McGraw-Hill, 1946; p 222-225.

(92) Tsukube, H.; Furuta, H.; Odani, A.; Takeda, Y.; Kudo, Y.; Inoue, Y.; Liu, Y.; Sakamoto, H.; Kimura, K. in *Comprehensive Supramolecular Chemistry*, 1st ed.; Atwood, J. L.; Davies, J. E. D.; Macnicol, D. D.; Vögtle, F., Eds.; Elsevier Science: New York, 1996; Vol. 8, p 429-430.

(93) (a) Okino, T.; Hoashi, Y.; Takemoto, Y. *J. Am. Chem. Soc.* **2003**, *125*, 12672-12673. (b) Li, H.; Wang, Y.; Tang, L.; Deng, L. *J. Am. Chem. Soc.* **2004**, *126*, 9906-9907. (c) Ye, J.; Dixon, D. J.; Hynes, P. S. *Chem. Commun.* **2005**, 481-483. (d) Andrés, J. M.; Manzano, R.; Pedrosa, R. *Chem. Eur. J.* **2008**, *14*, 5116-5119. (e) Almaşi, D.; Alfonso, D. A.; Gómez-Bengoa, E.; Nájera, C. *J. Org. Chem.* **2009**, *74*, 6163-6168.

(94) (a) Evans, D. A.; Mito, S.; Seidel, D. *J. Am. Chem. Soc.* **2007**, *129*, 11583-11952. (b) Watanabe, M.; Ikagawa, A.; Wang, H.; Murata, K.; Ikariya, T. *J. Am. Chem. Soc.* **2004**, *126*, 11148-11149.

(95) Gawley, R. E. *J. Org. Chem.* **2006**, *71*, 2411-2416.

(96) The absolute configurations (*R*/*S*) of **16a-c** were assigned by comparisons to literature HPLC data (identical compounds) under similar conditions (see references 93d,e; Appendix A). Catalysts with the Λ-(*S*,*S*) configuration gave predominantly *R* enantiomers. The configurations of other Michael products (**16d-f**, **29-40**; all Tables) were assigned analogously.

(97) (a) Hall, Jr., H. K. *J. Phys. Chem*. **1956**, *60*, 63-70. (b) Crampton, M. R.; Robotham, I. A. *J. Chem. Res. (S)* **1997**, 22-23. (c) Kolthoff, I. M.; Chantooni Jr., M. K.; Bhowmik, S. *J. Am. Chem. Soc.* **1968**, *90*, 23-28.

(98) Arnett, E. M.; Maroldo, S. G.; Schilling, S. L. Harrelson, J. A. *J. Am. Chem. Soc.* **1984**, *106*, 6759-6767.

(99) These papers each provide approximate pK_a values of ≥14. (a) Navon, G.; Panigel, R.; Meyerstein, D. *Inorg. Chim. Acta* **1972**, *6*, 299-302. (b) Pearson, R. G.; Basolo, F. *J. Am. Chem. Soc.* **1956**, *78*, 4878-4883. (c) See also Clarkson, A. J.; Buckingham, D. A.; Rogers, A. J. Blackman, A. G. Clark, C, R. *Inorg. Chem.* **2009**, *39*, 4769-4775.

(100) The dominant enantiomer is assigned an *S* configuration to maintain the same sense of chirality that was achieved with the aromatic nitroolefins.

(101) (a) Zhu, Y.; Malerich, J. P.; Rawal, V. H. *Angew. Chem. Int. Ed.* **2010**, *49*, 153-156; *Angew. Chem.* **2010**, *122*, 157-160. (b) Terada, M.; Ikehara, T.; Ube, H. *J. Am. Chem. Soc.* **2007**, *129*, 14112-14113.

(102) Yang, X.; Zhou, X.; Lin, L.; Chang, L.; Liu, X.; Feng, X. *Angew. Chem., Int. Ed.* **2008**, *47*, 7079-7081; *Angew. Chem.* **2008***, 120,* 7187-7189.

(103) Zhuang, W.; Hazell, R. G.; Jørgensen, K. A. *Org. Biomol. Chem.* **2005**, *3*, 2566-2571.

(104) Li, P.; Wen, S.; Yu, F.; Liu, Q.; Li, W.; Wang, Y.; Liang, X.; Ye, J. *Org. Lett.* **2009**, *11*, 753-756.

(105) Matthews, W. S.; Bares, J. E.; Bartmess, J. E.; Bordwell, F. G.; Cornforth, F. J.; Drucker, G. E.; Margolin, Z.; McCallum, R. J.; McCollum, G. J.; Vanier, N. R. *J. Am. Chem. Soc.* **1975**, *97*, 7006-7014.

(106) Knowles, W. S. *Acc. Chem. Res.* **1983**, *16*, 106-112.

(107) Reetz, M. T.; Guo, H.; Ma, J.-A.; Goddard, R.; Mynott, R. J. *J. Am. Chem. Soc.* **2009**, *131*, 4136-4142.

(108) Murai, K.; Matsushita, T.; Nakamura, A.; Fukushima, S.; Shimura, M.; Fujioka, H. *Angew. Chem. Int. Ed.* **2010**, *49*, 9174-9177; *Angew. Chem.* **2010**, *122*, 9360-9363.

(109) Wittkop, A.; Schreiner, P. R. *Chem. Eur. J.* **2003**, *9*, 407-414.

(110) Ooi, T.; Kameda, M.; Maruoka, K. *J. Am. Chem. Soc.* **2003**, *125*, 5139-5151.

(111) Reisman, S. E.; Doyle, A. G.; Jacobsen, E. N. *J. Am. Chem. Soc.* **2008**, *130*, 7198-7199.

(112) (a) Xia, X.-F.; Shu, X.-Z.; Ji, K.-G.; Yag, Y.-F.; Shaukat, A.; Liu, X.-Y.; Liang, Y.-M. *J. Org. Chem.* **2010**, *75*, 2893-2902. (b) Lucet, D.; Sabelle, S.; Kostelitz, O.; Gall, T. L.; Mioskowski, C. *Eur. J. Chem.* **1999**, 2583-2591.

(113) (a) Brookhart, M.; Grant, B.; Volpe, Jr., A. F. *Organometallics* **1992**, *11*, 3920-3922. (b) For hazardous aspects of this synthesis, refer to Yakelis, N. A.; Bergman, R. G. *Organometallics* **2005**, *24*, 3579-3581.

(114) The H_2O content was determined by elemental analysis and integration of the H_2O peak in the ^1H NMR spectrum.

(115) The H_2O content was not assayed.

(116) The $^{13}C\{^{1}H\}$ NMR signal with the chemical shift closest to benzene is assigned to the meta carbon: Mann, B. E. *J. Chem. Soc., Perkin Trans. 2* **1972**, 30-34.

(117) Dewey, M. A.; Gladysz, J. A. *Organometallics* **1993**, *12*, 2390-2392.

(118) Robinson, W. R. *J. Chem. Ed.* **1985**, *62*, 1001.

(119) The yield was corrected for the portion of the crude intermediate that was not carried forward.

(120) The integration of the H_2O signal may be higher than expected from the elemental analysis because the added MeOH is not dried.

(121) The integration of the NH peaks is lower than expected due to H/D exchange with CD_3OD.

(122) This compound was never isolated in pure form and only partial characterization is provided here.

(123) The NMR signals of all Michael addition products in this chapter were assigned by analogy to those of **16a** provided by Almaşi, D.; Alonso, D. A.; Gómez-Bengoa, E.; Nájera, C. *J. Org. Chem.* **2009**, *74*, 6163-6168.

(124) The aromatic NMR signals were assigned by analogy to those of $C_6H_4OCH_3$. Silverstein, R. M.; Webster, F. X.; Kiemle, D. J. *Spectrometric Identification of Organic Compounds*, 7th ed.; John Wiley & Sons: Hoboken, NJ, 2005; p 225.

(125) Li, X.-J.; Liu, K.; Ma, H.; Nie, J.; Ma, J.-A. *Synlett* **2008**, *20*, 3242-3246.

(126) The H_2O content was not assayed. The yield calculation was for Λ-(*S*,*S*)-**3**$^{3+}$ $2Cl^-$ $BAr_f^-\cdot 2H_2O$

(127) APEX2 "Program for Data Collection on Area Detectors" BRUKER AXS Inc., 5465 East Cheryl Parkway, Madison, WI 53711-5373 USA.

(128) Sheldrick, G. M. "SADABS (version 2008/1): Program for Absorption Correction of Area Detector Frames", BRUKER AXS Inc., 5465 East Cheryl Parkway, Madison, WI 53711-5373 USA.

(129) Sheldrick, G. *Acta Crystallogr.* **2008**, *A64*, 112-122.

(130) Dolomanov, O. V.; Bourhis, L. J.; Gildea, R. J.; Howard, J. A. K.; Puschmann, H. *J. Appl. Cryst.* **2009***, 42*, 339-341.

(131) Flack, H. D. *Acta Cryst.* **1983**, *A39*, 876-881.

APPENDIX A

HPLC TRACES FOR CHAPTER IV

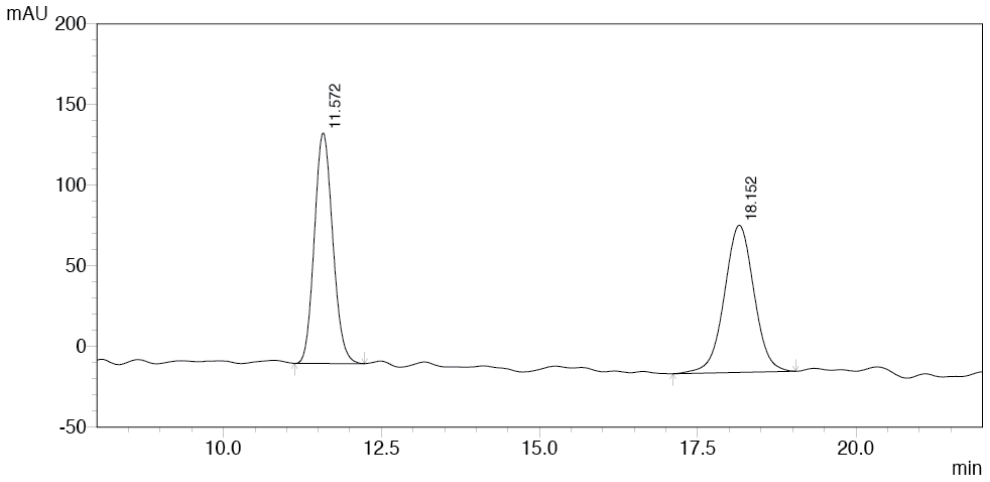

PDA 220nm

Peak#	Ret. Time	Area	Height	Area %	Height %
1	11.572	2892734	142917	49.286	61.046
2	18.152	2976564	91196	50.714	38.954
Total		5869298	234114	100.000	100.000

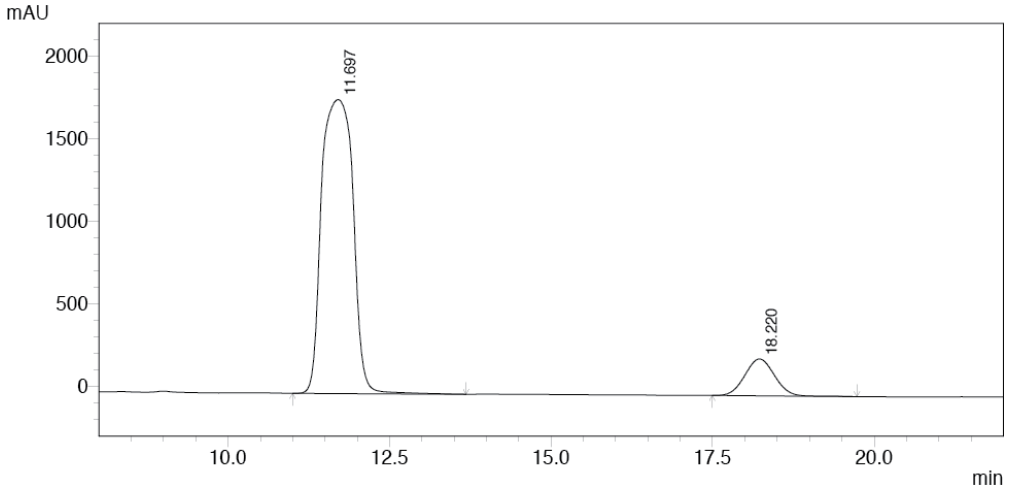

PDA 220nm

Peak#	Ret. Time	Area	Height	Area %	Height %
1	11.697	60314078	1781389	89.351	88.845
2	18.220	7188616	223672	10.649	11.155
Total		67502694	2005061	100.000	100.000

HPLC trace of racemic **31** (top) and scalemic **31** (bottom; Table 4.14, Entry 1); Chiralpak AD 80:20 v/v hexanes/isopropanol, 1.0 mL/min, 220 nm.

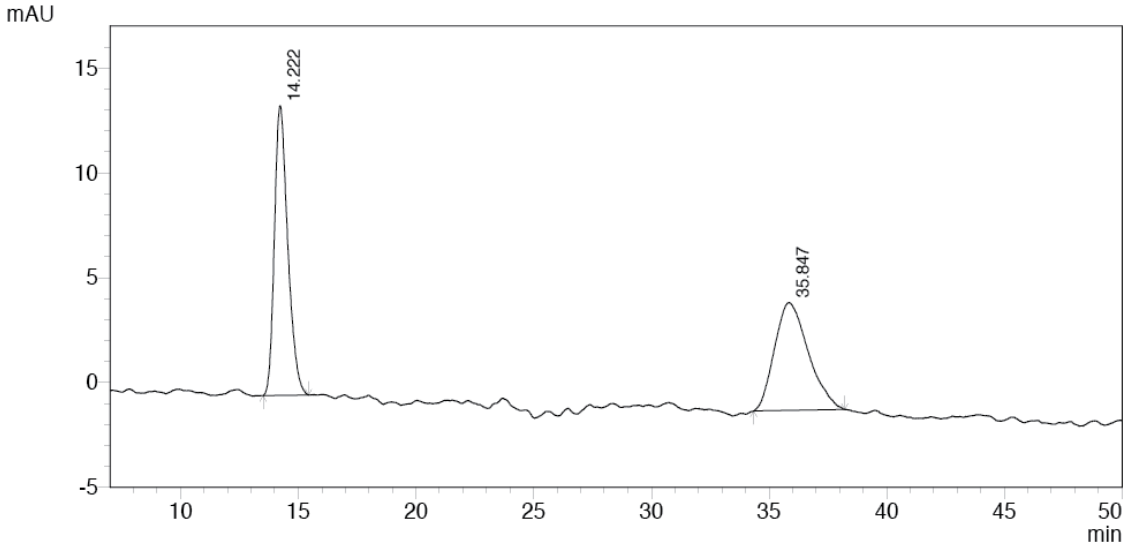

PDA 254nm

Peak#	Ret. Time	Area	Height	Area %	Height %
1	14.222	545650	13812	51.472	72.833
2	35.847	514433	5152	48.528	27.167
Total		1060083	18965	100.000	100.000

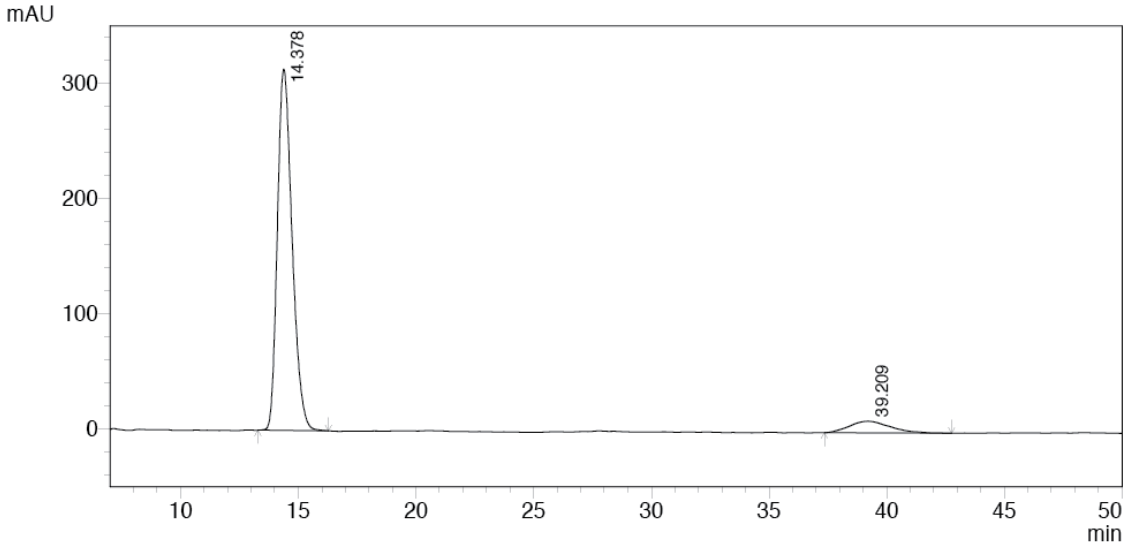

PDA 254nm

Peak#	Ret. Time	Area	Height	Area %	Height %
1	14.378	13650190	313478	91.924	96.896
2	39.209	1199200	10041	8.076	3.104
Total		14849390	323518	100.000	100.000

HPLC trace of racemic **30** (top) and scalemic **30** (bottom, Table 4.14, Entry 2); Chiralcel OD 70:30 v/v hexanes/isopropanol, 1.0 mL/min, 254 nm.

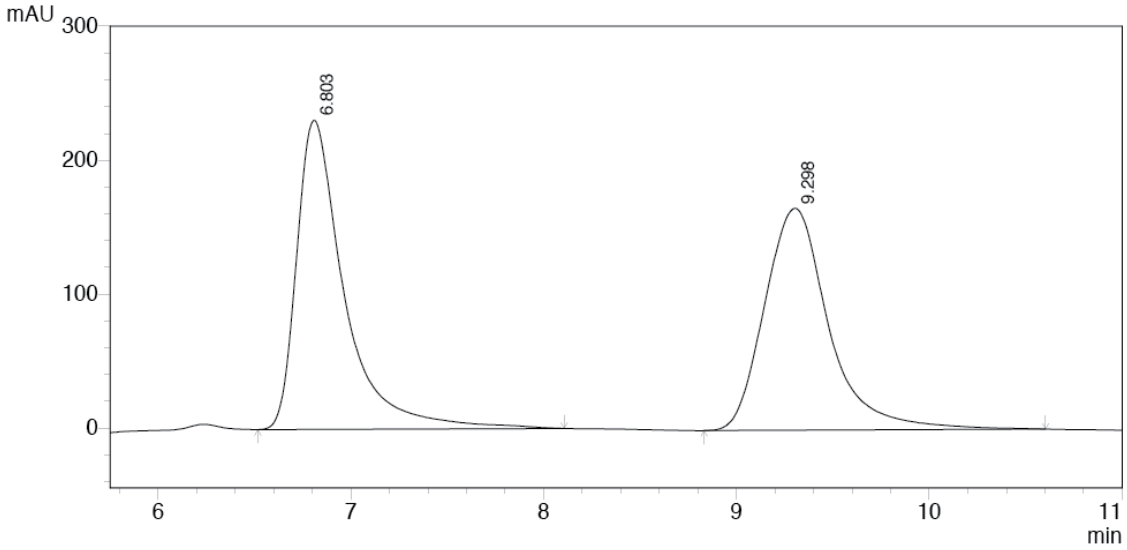

PDA 220nm

Peak#	Ret. Time	Area	Height	Area %	Height %
1	6.803	3983767	230889	50.865	58.208
2	9.298	3848303	165770	49.135	41.792
Total		7832070	396659	100.000	100.000

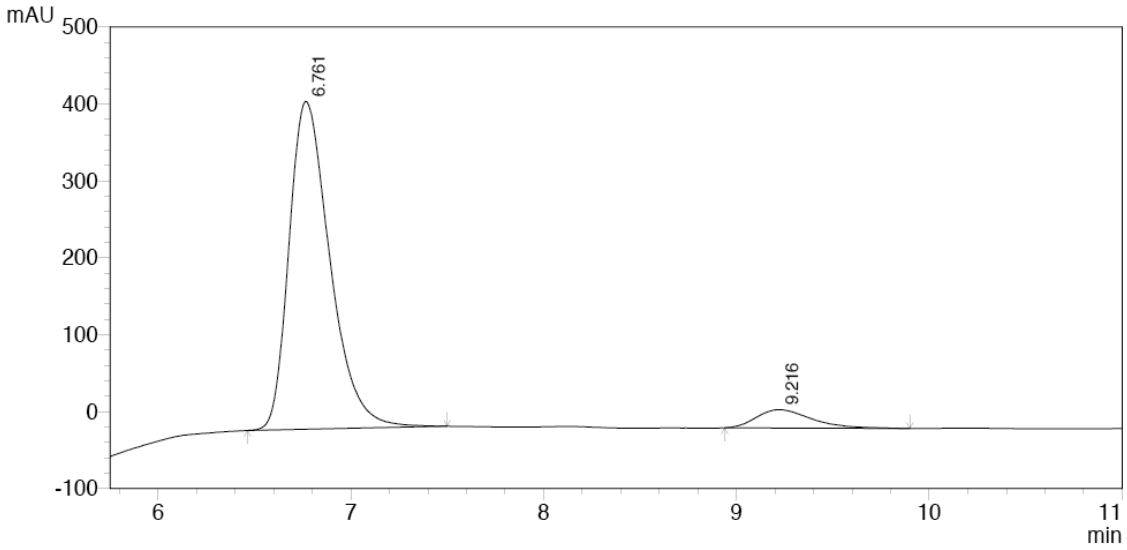

PDA 220nm

Peak#	Ret. Time	Area	Height	Area %	Height %
1	6.761	6296885	426260	93.049	94.722
2	9.216	470397	23751	6.951	5.278
Total		6767282	450011	100.000	100.000

HPLC trace of racemic **34** (top) and scalemic **34** (bottom, Table 4.14, Entry 3); Chiralpak AD 60:60 v/v hexanes/isopropanol, 1.0 mL/min, 220 nm.

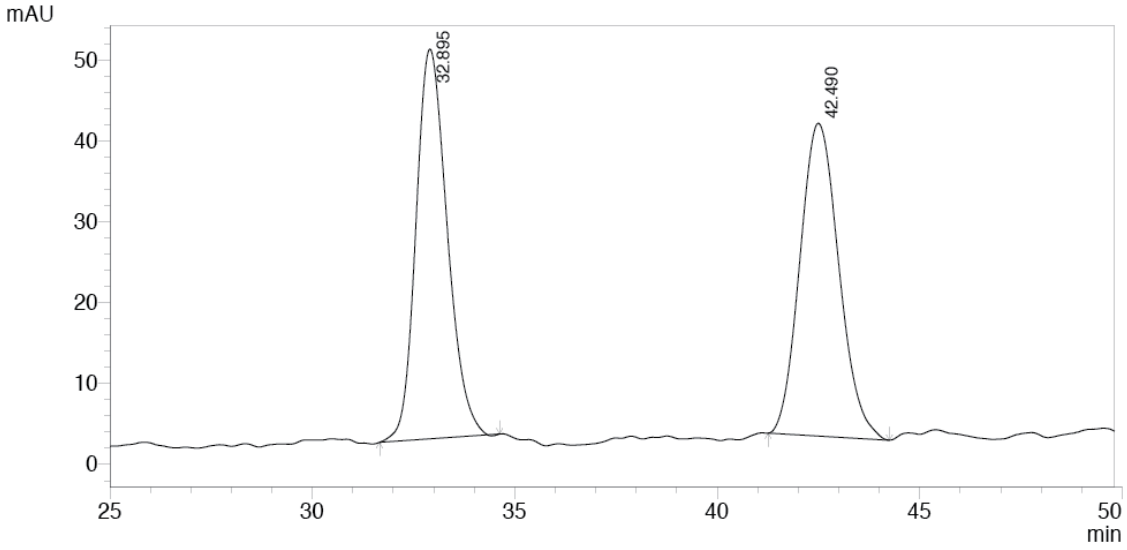

PDA 220nm

Peak#	Ret. Time	Area	Height	Area %	Height %
1	32.895	2592054	48187	49.983	55.472
2	42.490	2593793	38681	50.017	44.528
Total		5185847	86867	100.000	100.000

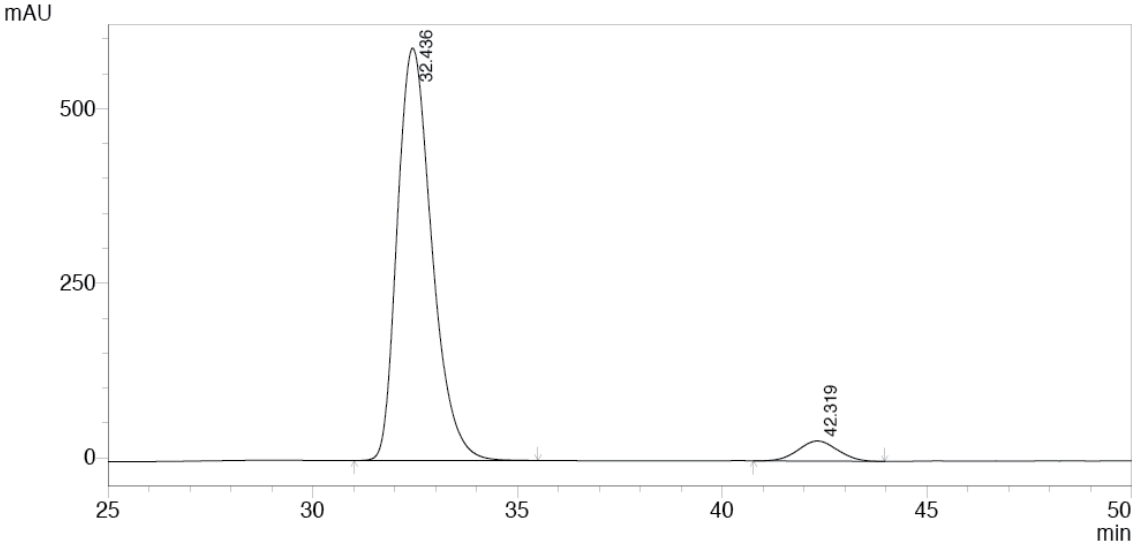

PDA 220nm

Peak#	Ret. Time	Area	Height	Area %	Height %
1	32.436	34674163	590859	94.706	95.343
2	42.319	1938180	28862	5.294	4.657
Total		36612343	619722	100.000	100.000

HPLC trace of racemic **16a** (top) and scalemic **16a** (bottom; Table 4.14, Entry 4); Chiralpak AD 98:2 v/v hexanes/isopropanol, 1.0 mL/min, 220 nm.

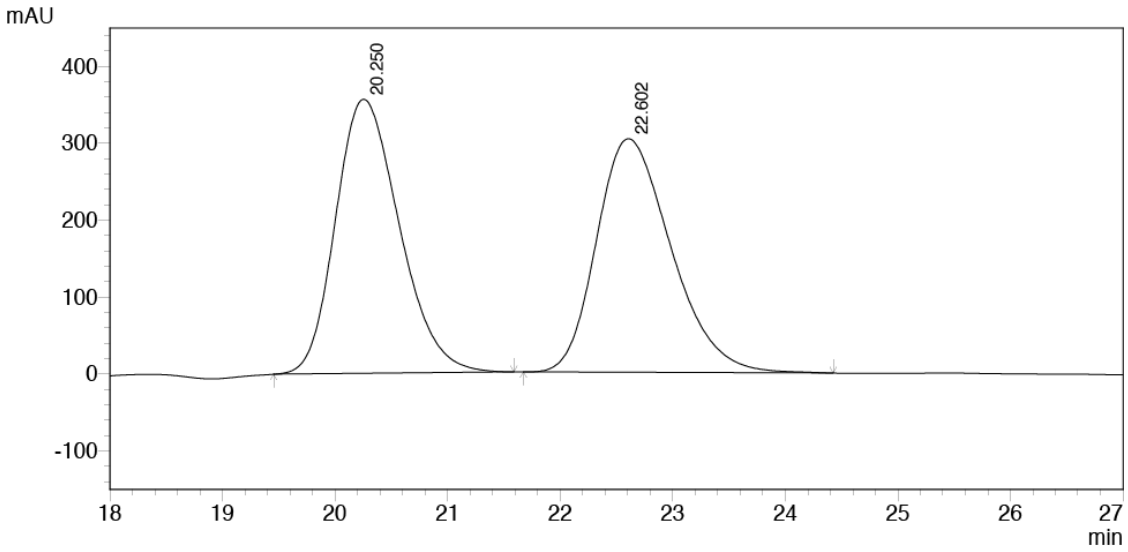

PDA 220nm

Peak#	Ret. Time	Area	Height	Area %	Height %
1	20.250	14034598	356495	50.085	53.998
2	22.602	13986920	303708	49.915	46.002
Total		28021519	660203	100.000	100.000

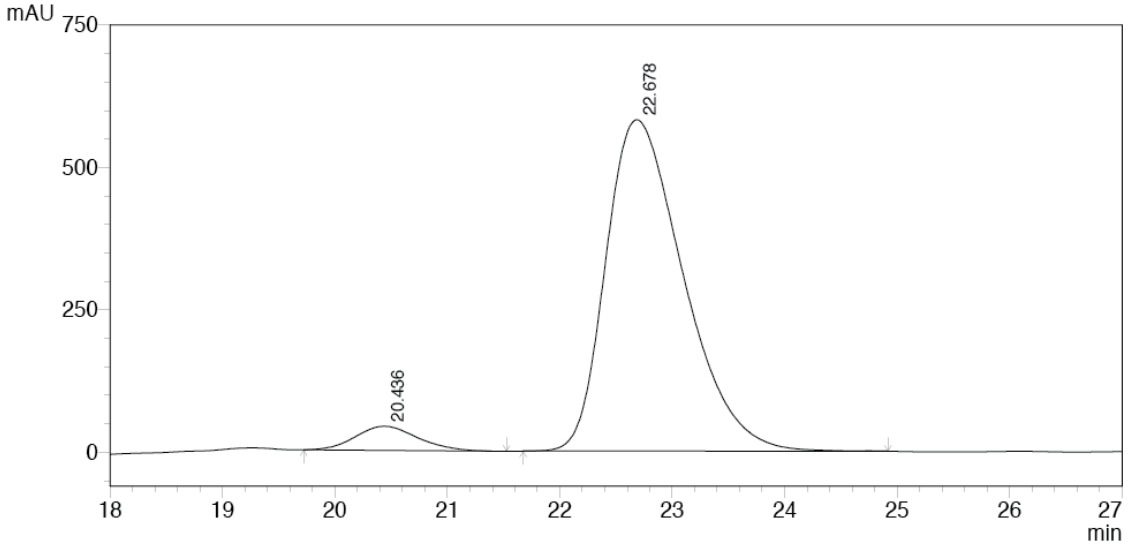

PDA 220nm

Peak#	Ret. Time	Area	Height	Area %	Height %
1	20.436	1637581	42354	5.544	6.785
2	22.678	27899733	581886	94.456	93.215
Total		29537314	624240	100.000	100.000

HPLC trace of racemic **33** (top) and scalemic **33** (bottom; Table 4.14, Entry 5); Chiralpak AS-H 90:10 v/v hexanes/isopropanol, 1.0 mL/min, 220 nm.

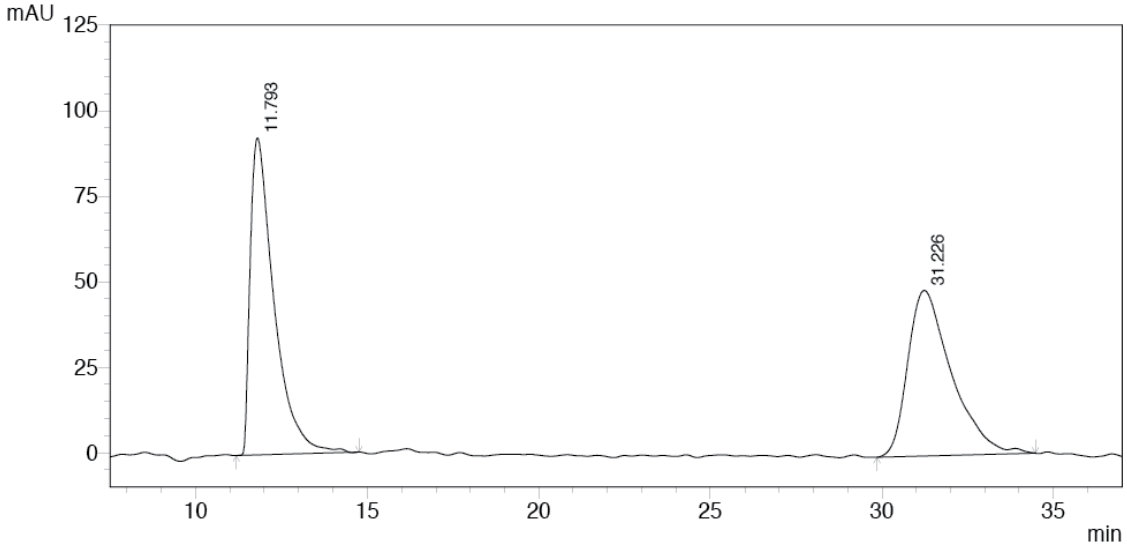

PDA 220nm

Peak#	Ret. Time	Area	Height	Area %	Height %
1	11.793	4468208	92606	51.035	65.690
2	31.226	4287008	48367	48.965	34.310
Total		8755216	140974	100.000	100.000

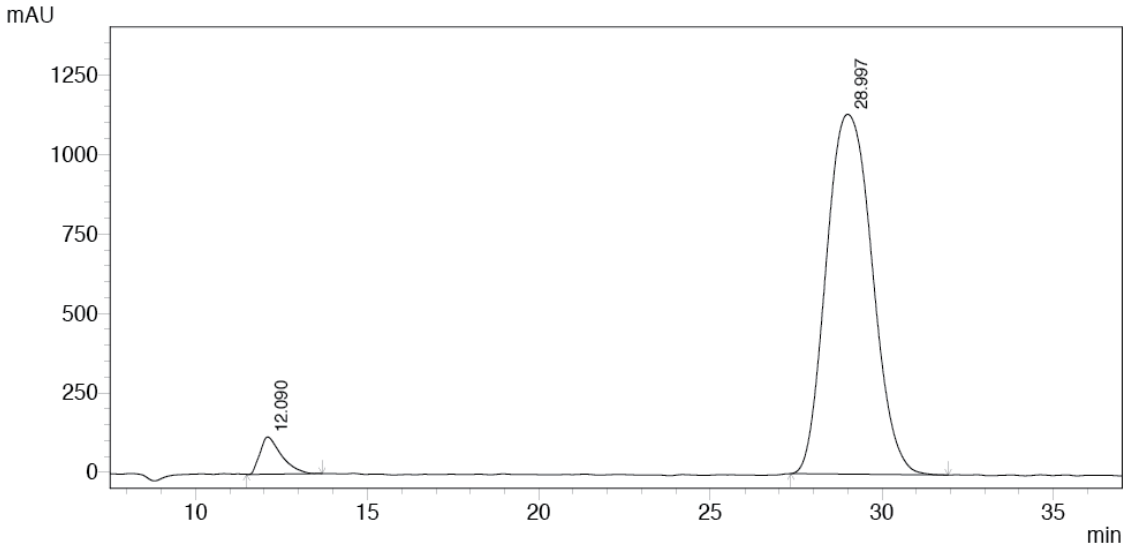

PDA 220nm

Peak#	Ret. Time	Area	Height	Area %	Height %
1	12.090	5063370	116519	4.580	9.340
2	28.997	105482048	1131049	95.420	90.660
Total		110545419	1247568	100.000	100.000

HPLC trace of racemic **43** (top) and scalemic **43** (bottom; Table 4.14, Entry 6); Chiralcel OD 90:10 v/v hexanes/isopropanol, 1.0 mL/min, 220 nm.

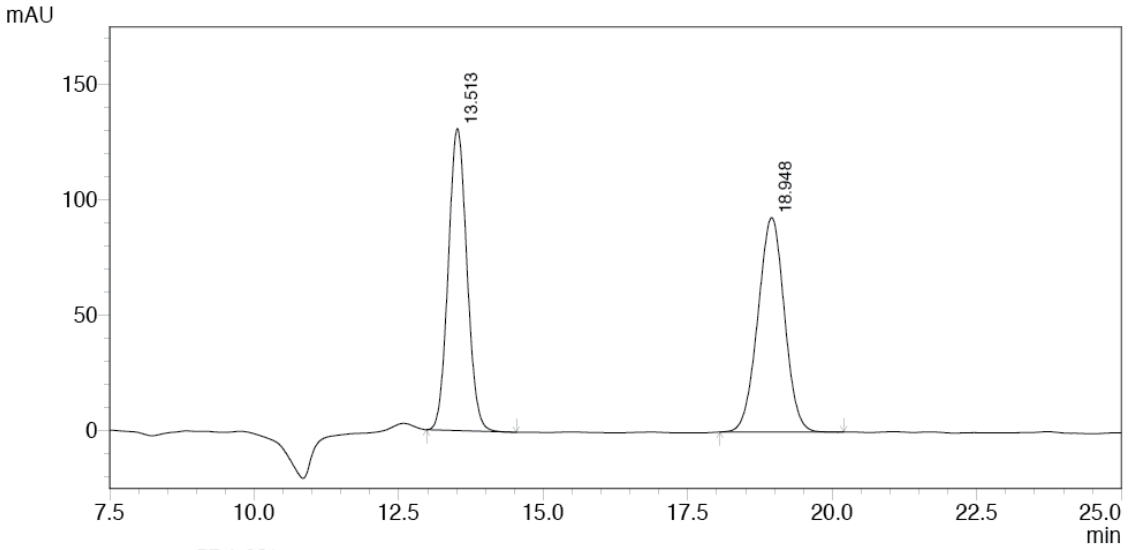

PDA 254nm

Peak#	Ret. Time	Area	Height	Area %	Height %
1	13.513	2941994	130912	49.780	58.498
2	18.948	2967956	92876	50.220	41.502
Total		5909950	223789	100.000	100.000

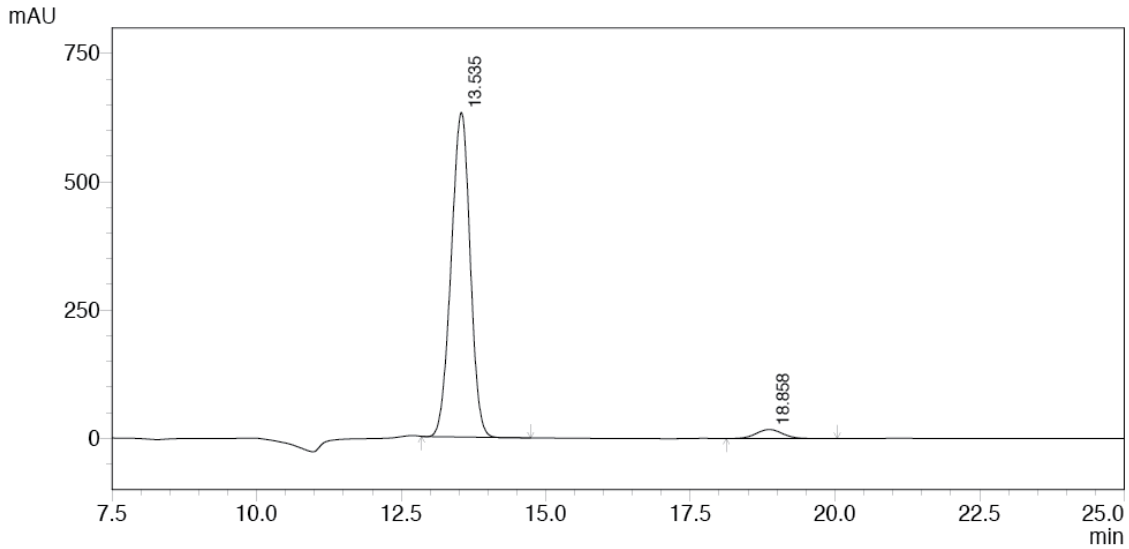

PDA 254nm

Peak#	Ret. Time	Area	Height	Area %	Height %
1	13.535	14427103	632667	96.261	97.288
2	18.858	560393	17639	3.739	2.712
Total		14987496	650305	100.000	100.000

HPLC trace of racemic **29** (top) and scalemic **29** (bottom; Table 4.14, Entry 7); Chiralpak AD 90:10 v/v hexanes/isopropanol, 1.0 mL/min, 254 nm.

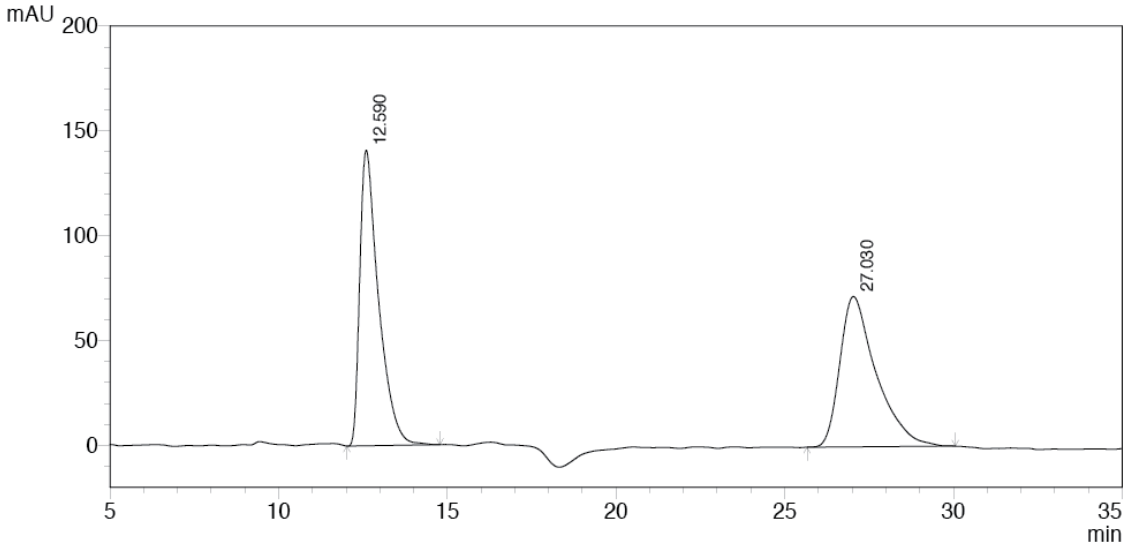

PDA 220nm

Peak#	Ret. Time	Area	Height	Area %	Height %
1	12.590	5460013	141005	50.419	66.304
2	27.030	5369188	71660	49.581	33.696
Total		10829201	212664	100.000	100.000

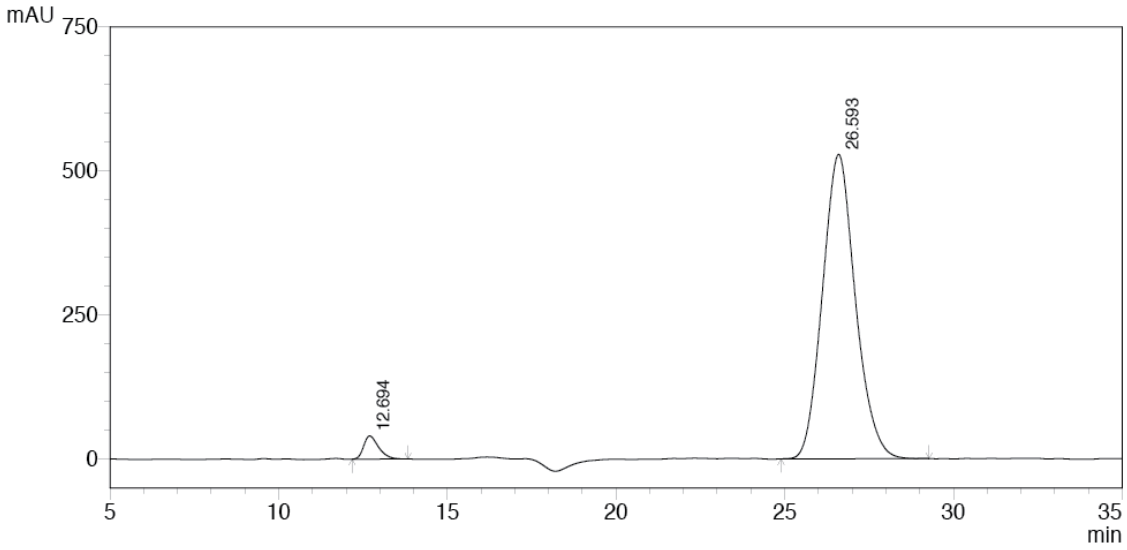

PDA 220nm

Peak#	Ret. Time	Area	Height	Area %	Height %
1	12.694	1238157	40259	3.339	7.083
2	26.593	35848703	528088	96.661	92.917
Total		37086861	568347	100.000	100.000

HPLC trace of racemic **36** (top) and scalemic **36** (bottom; Table 4.14, Entry 8); Chiralcel OD 95:5 v/v hexanes/isopropanol, 1.0 mL/min, 220 nm.

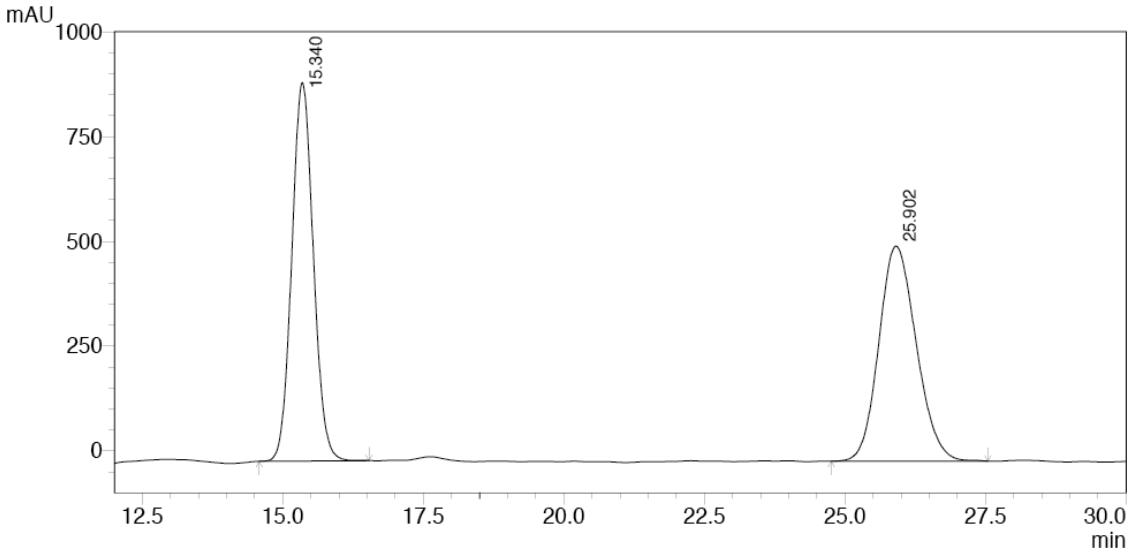

PDA220nm

Peak#	Ret. Time	Area	Height	Area %	Height %
1	15.340	24105156	903431	50.293	63.762
2	25.902	23824081	513442	49.707	36.238
Total		47929237	1416873	100.000	100.000

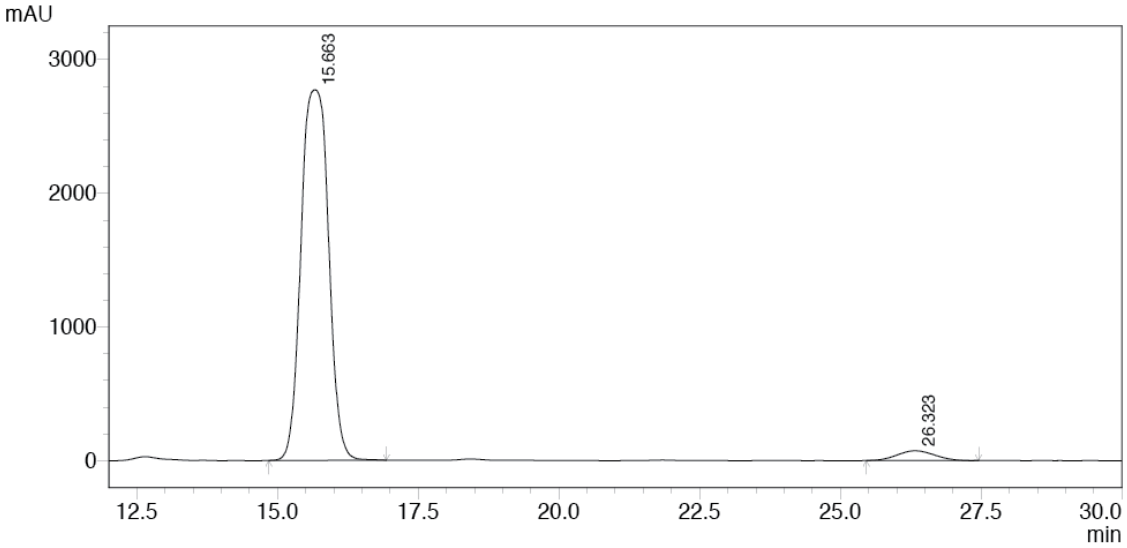

PDA 220nm

Peak#	Ret. Time	Area	Height	Area %	Height %
1	15.663	94240443	2770460	96.556	97.428
2	26.323	3360915	73149	3.444	2.572
Total		97601359	2843609	100.000	100.000

HPLC trace of racemic **38** (top) and scalemic **38** (bottom; Table 4.14, Entry 9); Chiralpak AD 90:10 v/v hexanes/isopropanol, 1.0 mL/min, 220 nm.

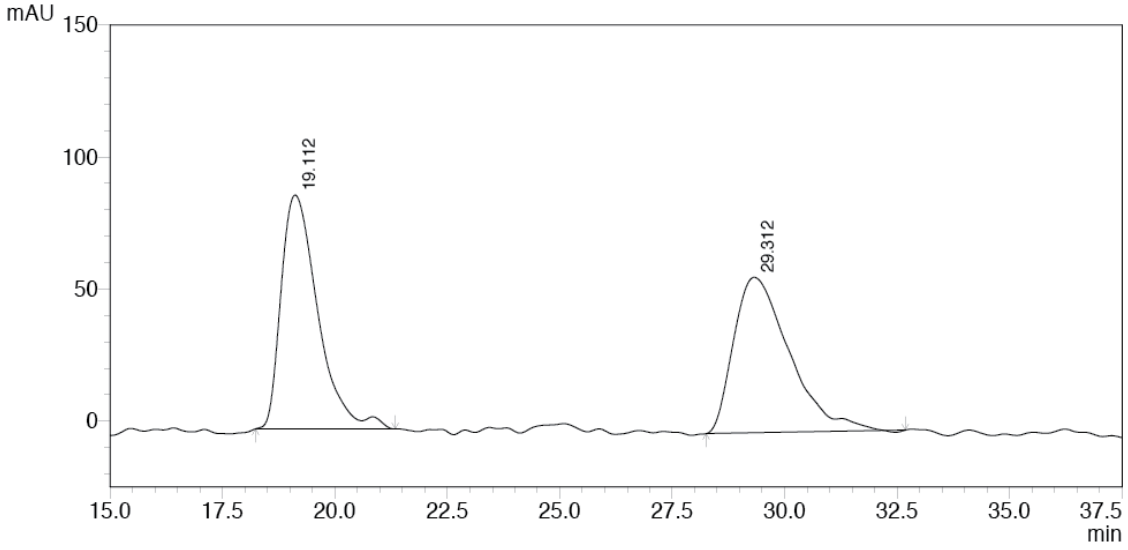

PDA 220nm

Peak#	Ret. Time	Area	Height	Area %	Height %
1	19.112	5040868	88545	49.885	60.058
2	29.312	5064198	58886	50.115	39.942
Total		10105066	147431	100.000	100.000

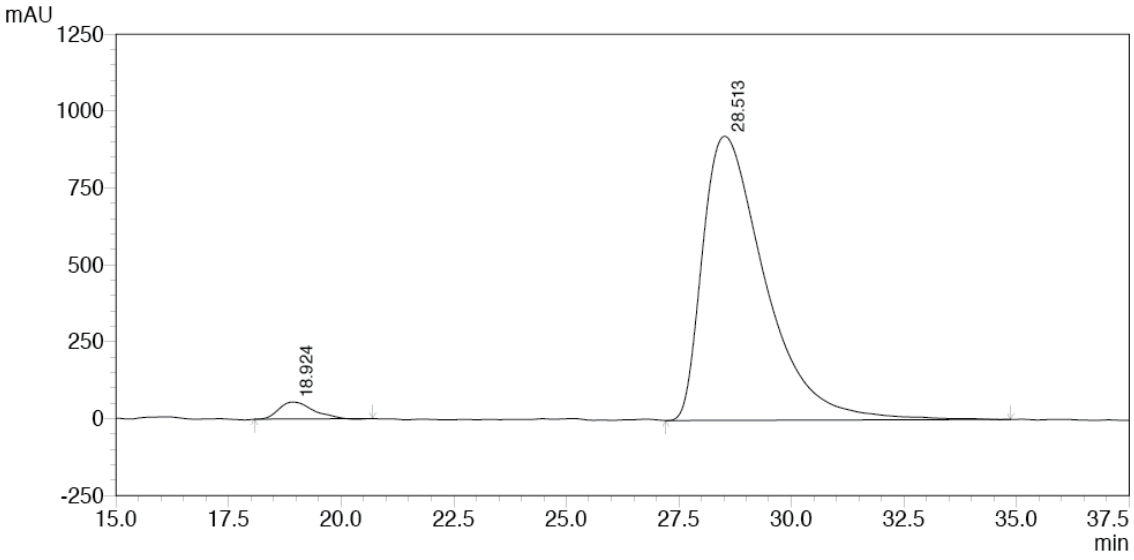

PDA 220nm

Peak#	Ret. Time	Area	Height	Area %	Height %
1	18.924	2878634	55143	3.121	5.635
2	28.513	89360381	923530	96.879	94.365
Total		92239015	978673	100.000	100.000

HPLC trace of racemic **37** (top) and scalemic **37** (bottom; Table 4.14, Entry 10); Chiralcel OD 90:10 v/v hexanes/isopropanol, 1.0 mL/min, 220 nm.

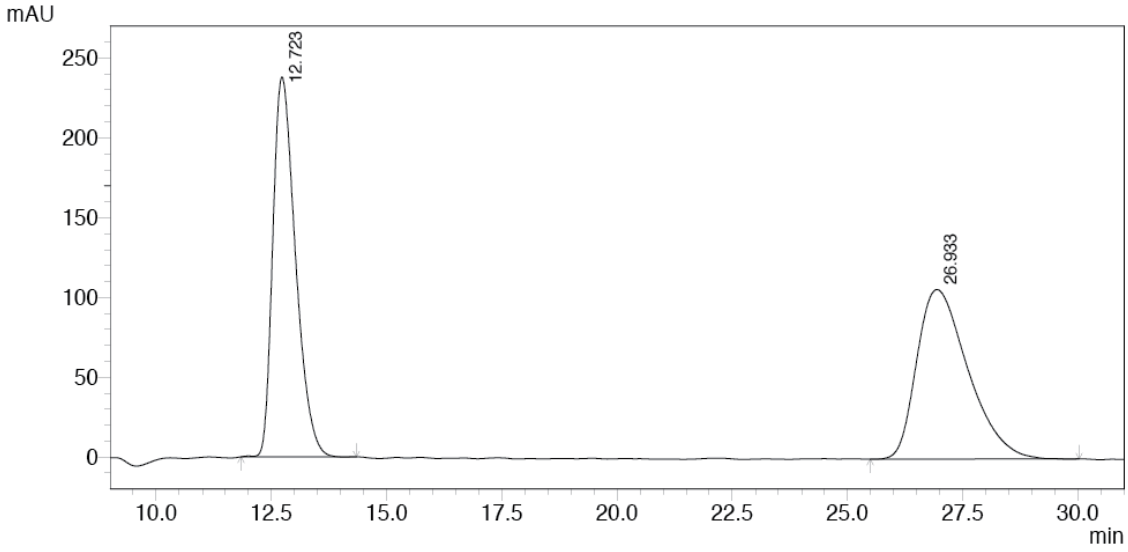

PDA 220nm

Peak#	Ret. Time	Area	Height	Area %	Height %
1	12.723	8141200	238008	49.819	69.153
2	26.933	8200292	106170	50.181	30.847
Total		16341493	344178	100.000	100.000

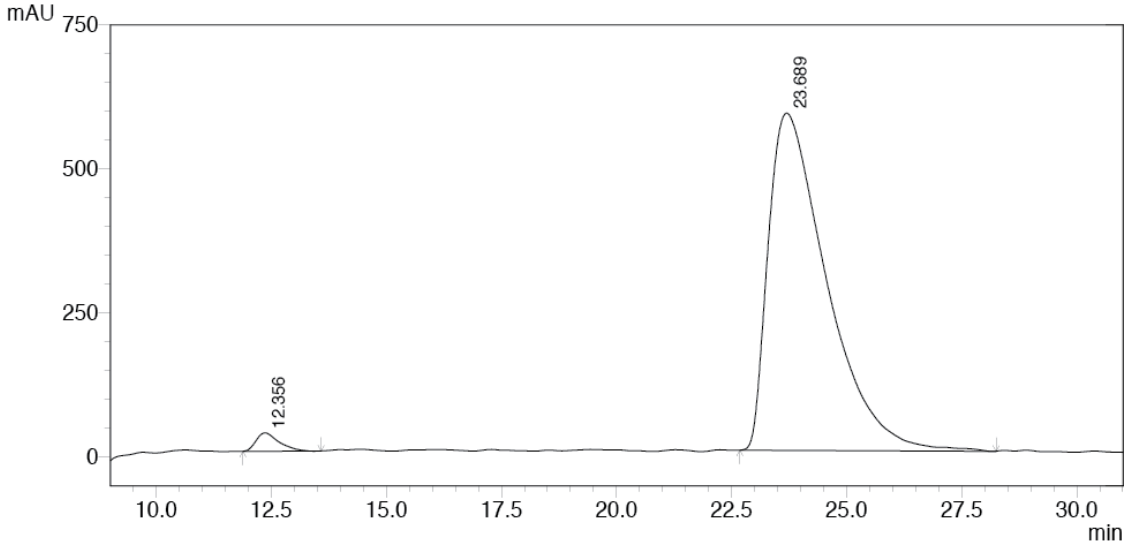

PDA 220nm

Peak#	Ret. Time	Area	Height	Area %	Height %
1	12.356	1090049	31778	2.068	5.151
2	23.689	51627061	585142	97.932	94.849
Total		52717109	616920	100.000	100.000

HPLC trace of racemic **39** (top) and scalemic **39** (bottom; Table 4.14, Entry 11); Chiralcel OD 90:10 v/v hexanes/isopropanol, 1.0 mL/min, 220 nm.

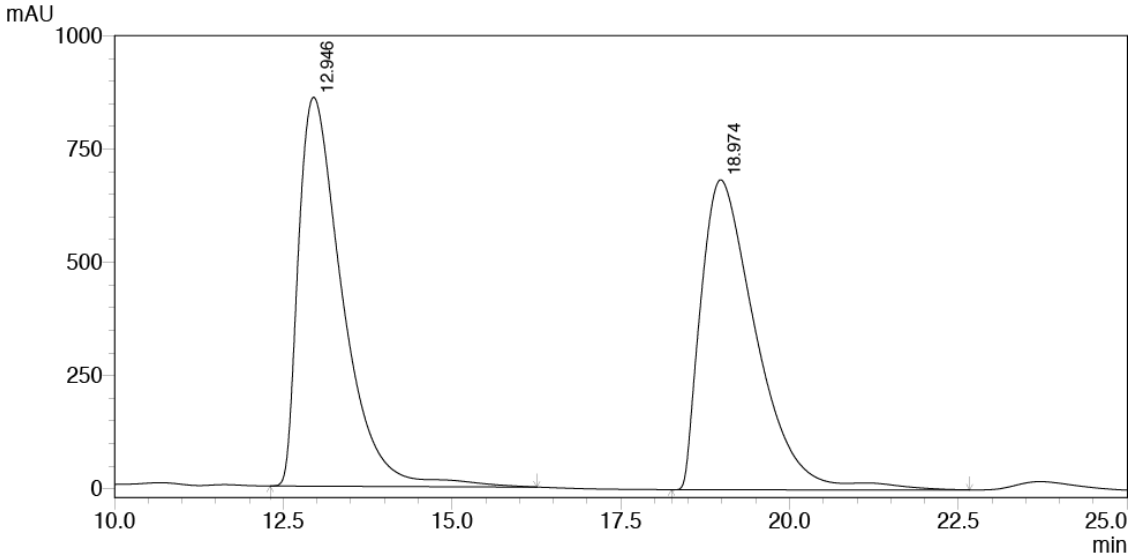

PDA 220nm

Peak#	Ret. Time	Area	Height	Area %	Height %
1	12.946	38973226	858914	49.978	55.647
2	18.974	39007602	684601	50.022	44.353
Total		77980828	1543515	100.000	100.000

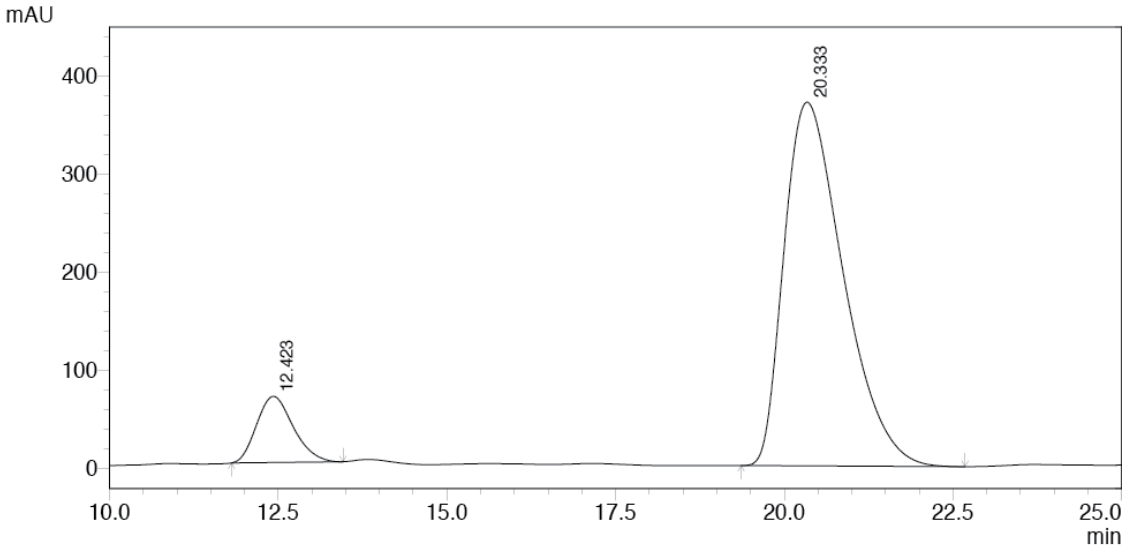

PDA 220nm

Peak#	Ret. Time	Area	Height	Area %	Height %
1	12.423	2538858	67307	10.100	15.379
2	20.333	22598513	370346	89.900	84.621
Total		25137371	437652	100.000	100.000

HPLC trace of racemic **44** (top) and scalemic **44** (bottom; Table 4.14, Entry 12); Chiralcel OD 97.5:2.5 v/v hexanes/isopropanol, 1.0 mL/min, 220 nm.

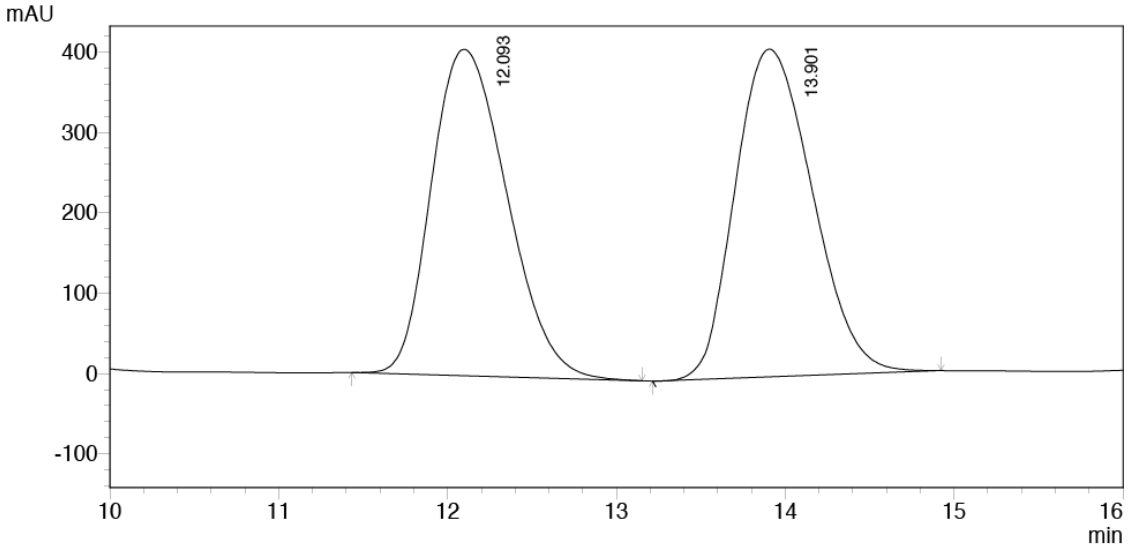

PDA 220nm

Peak#	Ret. Time	Area	Height	Area %	Height %
1	12.093	12661766	405824	49.414	49.903
2	13.901	12962212	407395	50.586	50.097
Total		25623977	813219	100.000	100.000

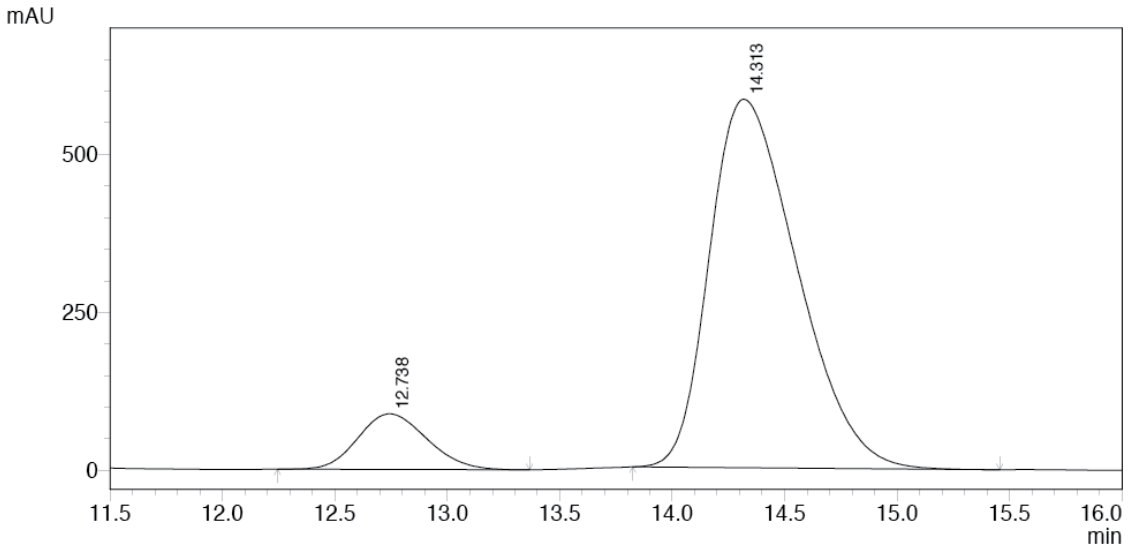

PDA 220nm

Peak#	Ret. Time	Area	Height	Area %	Height %
1	12.738	1877941	87934	10.619	13.108
2	14.313	15806284	582897	89.381	86.892
Total		17684225	670831	100.000	100.000

HPLC trace of racemic **16b** (top) and scalemic **16b** (bottom; Table 4.6, Entry 2, Λ-(*S*,*S*)-**3**$^{3+}$ 2Cl^{-} BAr$_f^{-}$); Chiralpak AS-H 90:10 v/v hexanes/isopropanol, 1.0 mL/min, 220 nm.

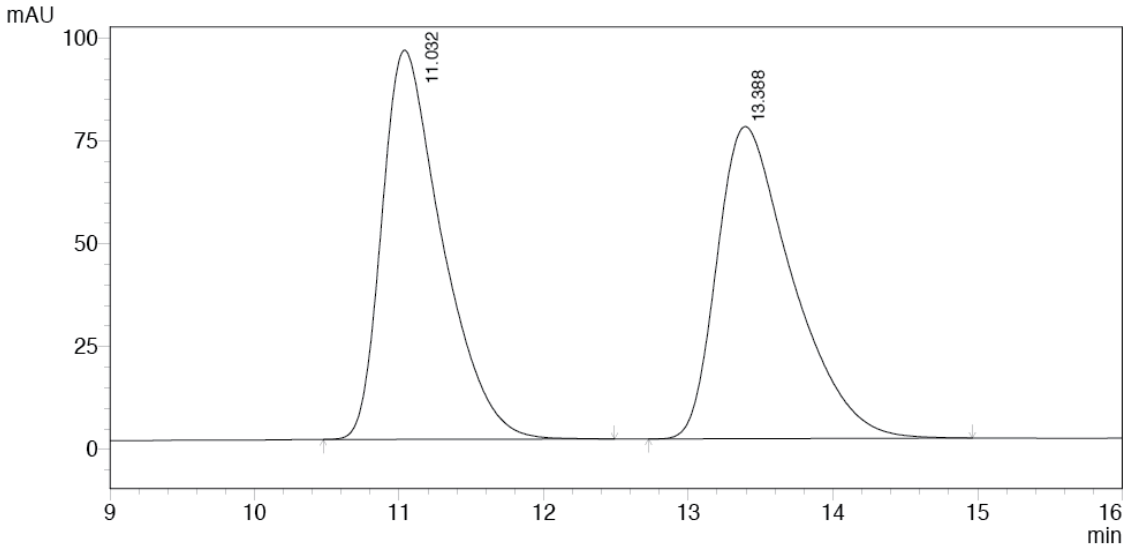

PDA 220nm

Peak#	Ret. Time	Area	Height	Area %	Height %
1	11.032	2745001	94604	49.931	55.488
2	13.388	2752610	75890	50.069	44.512
Total		5497611	170494	100.000	100.000

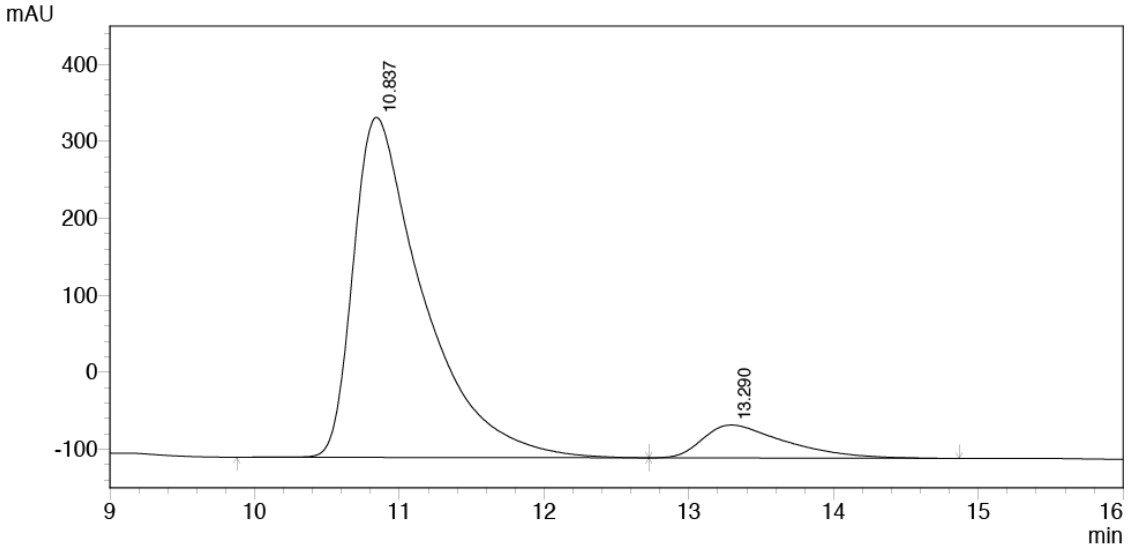

PDA 220nm

Peak#	Ret. Time	Area	Height	Area %	Height %
1	10.837	14897274	441745	89.745	91.162
2	13.290	1702201	42826	10.255	8.838
Total		16599476	484571	100.000	100.000

HPLC trace of racemic **16c** (top) and scalemic **16c** (bottom; Table 4.6, Entry 3, Λ-(*S*,*S*)-$\mathbf{3}^{3+}$ $2Cl^-$ BAr_f^-); Chiralcel OD 95:5 v/v hexanes/isopropanol, 0.75 mL/min, 220 nm.

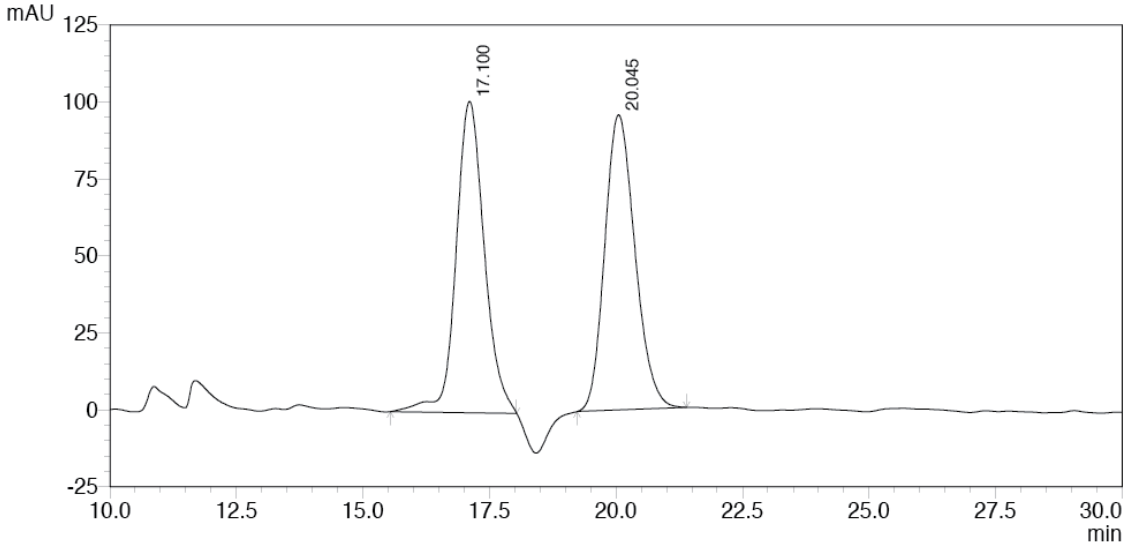

PDA 220nm

Peak#	Ret. Time	Area	Height	Area %	Height %
1	17.100	3930096	101137	49.659	51.334
2	20.045	3984017	95881	50.341	48.666
Total		7914113	197019	100.000	100.000

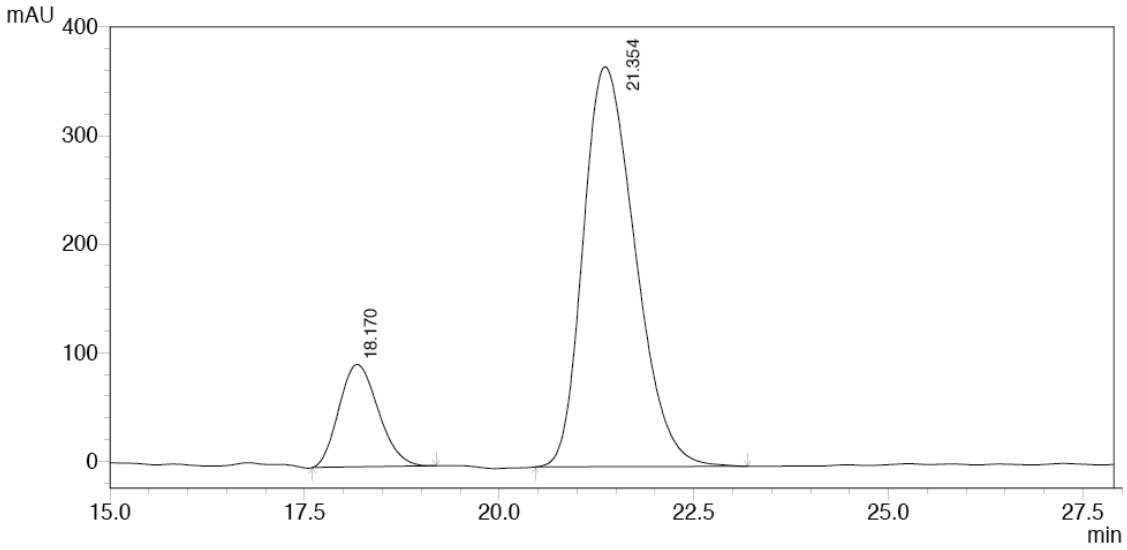

PDA 220nm

Peak#	Ret. Time	Area	Height	Area %	Height %
1	18.170	3319347	94448	16.239	20.405
2	21.354	17121171	368415	83.761	79.595
Total		20440518	462863	100.000	100.000

HPLC trace of racemic **16d** (top) and scalemic **16d** (bottom; Table 4.6, Entry 4, Λ-(*S*,*S*)-$\mathbf{3}^{3+}$ $2Cl^-$ BAr_f^-); Chiralpak AS-H 90:10 v/v hexanes/isopropanol, 1.0 mL/min, 220 nm.

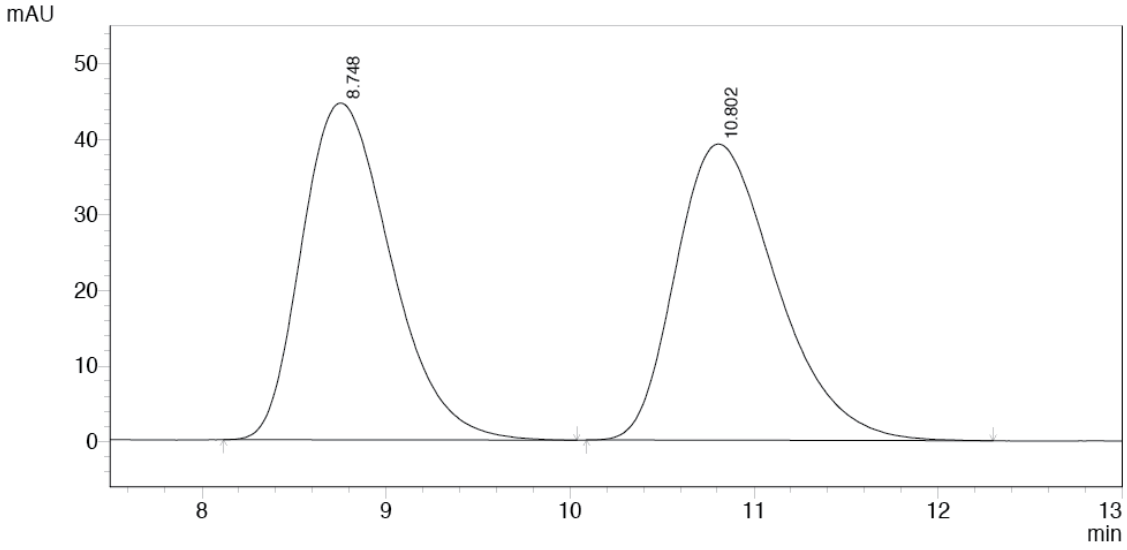

PDA 220nm

Peak#	Ret. Time	Area	Height	Area %	Height %
1	8.748	1500947	44571	50.055	53.203
2	10.802	1497676	39205	49.945	46.797
Total		2998623	83776	100.000	100.000

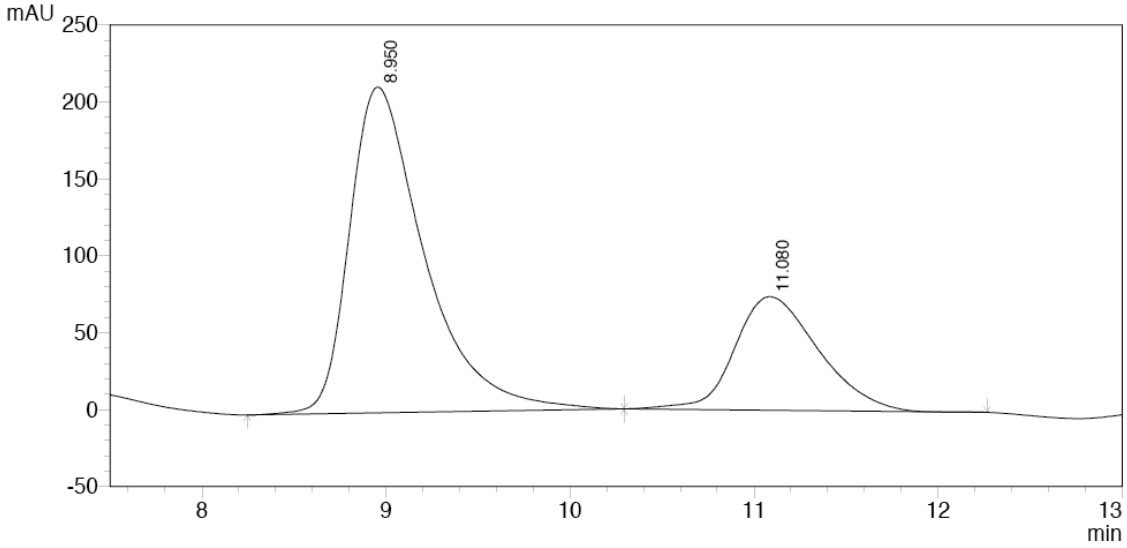

PDA 220nm

Peak#	Ret. Time	Area	Height	Area %	Height %
1	8.950	5998649	211698	71.981	74.157
2	11.080	2334985	73776	28.019	25.843
Total		8333634	285473	100.000	100.000

HPLC trace of racemic **16e** (top) and scalemic **16e** (bottom; Table 4.6, Entry 5, Λ-(*S*,*S*)-$\mathbf{3}^{3+}$ $2Cl^-$ BAr_f^-); Chiralcel OD 99:1 v/v hexanes/isopropanol, 1.0 mL/min, 220 nm.

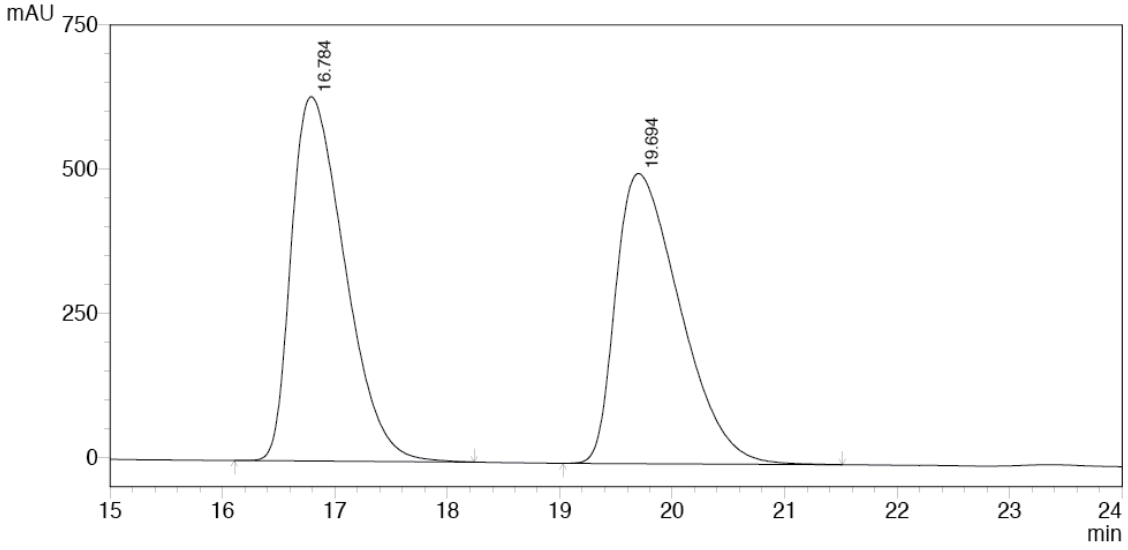

PDA 220nm

Peak#	Ret. Time	Area	Height	Area %	Height %
1	16.784	20879391	631315	51.100	55.674
2	19.694	19980317	502630	48.900	44.326
Total		40859708	1133945	100.000	100.000

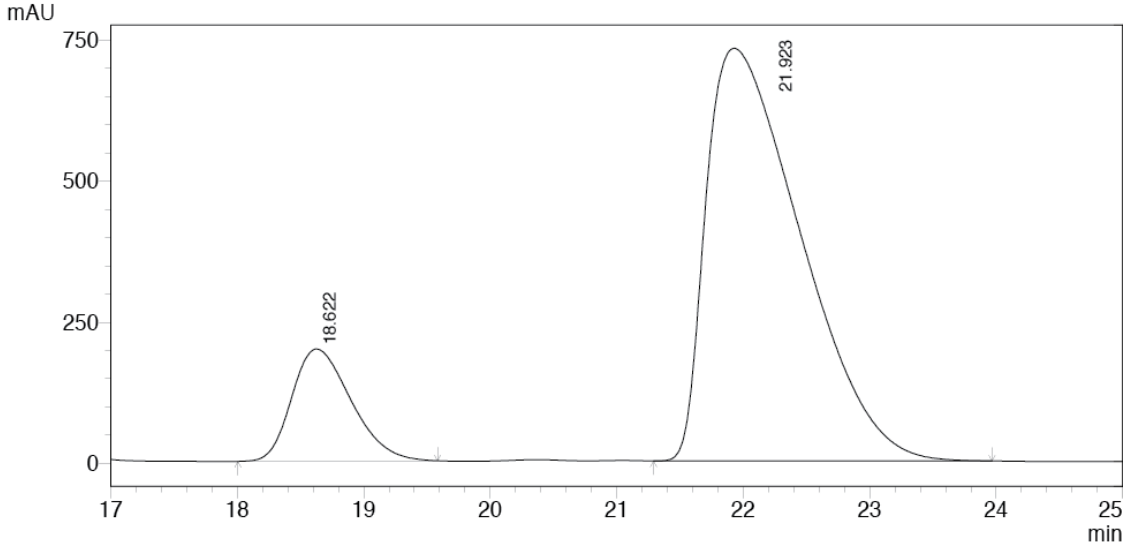

PDA 220nm

Peak#	Ret. Time	Area	Height	Area %	Height %
1	18.622	6477230	198966	14.554	21.379
2	21.923	38027036	731692	85.446	78.621
Total		44504265	930658	100.000	100.000

HPLC trace of racemic **16f** (top) and scalemic **16f** (bottom; Table 4.6, Entry 6, Λ-(*S*,*S*)-$\mathbf{3}^{3+}$ $2Cl^-$ BAr_f^-); Chiralpak AS-H 98:2 v/v hexanes/isopropanol, 1.0 mL/min, 220 nm.

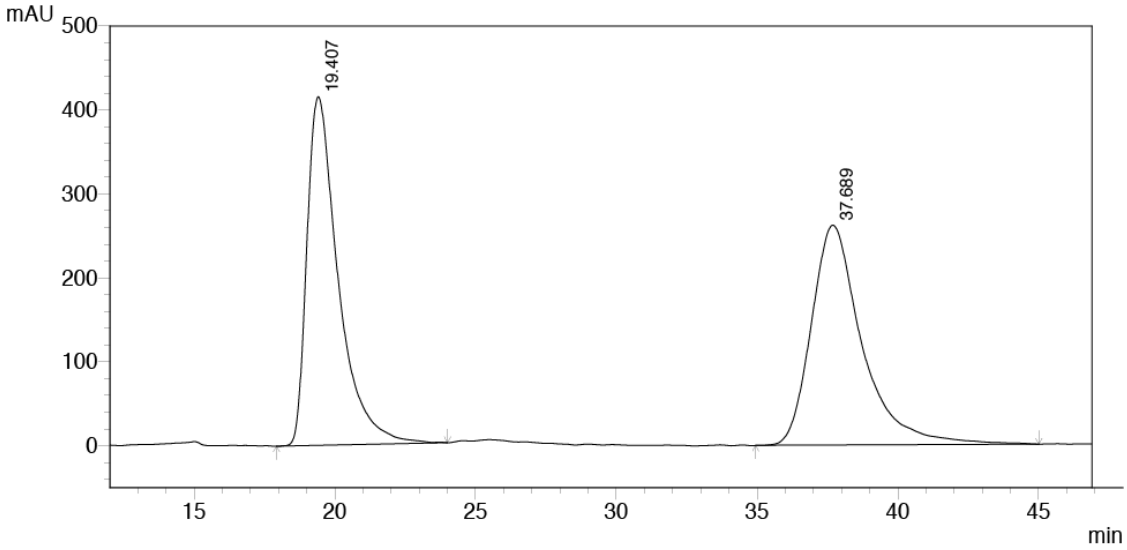

PDA 210nm

Peak#	Ret. Time	Area	Height	Area %	Height %
1	19.407	32147390	415319	49.423	61.325
2	37.689	32897644	261926	50.577	38.675
Total		65045033	677245	100.000	100.000

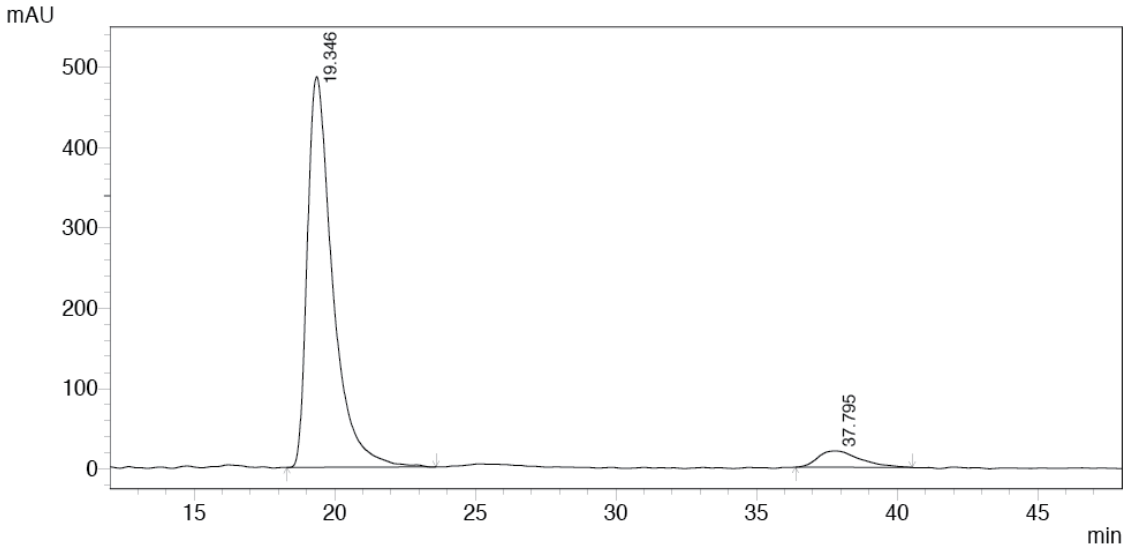

PDA 210nm

Peak#	Ret. Time	Area	Height	Area %	Height %
1	19.346	30432515	486386	93.470	96.002
2	37.795	2126237	20255	6.530	3.998
Total		32558751	506641	100.000	100.000

HPLC trace of racemic **46** (top) and scalemic **46** (bottom; Table 4.18, Entry 12); Chiralcel OD 90:10 v/v hexanes/isopropanol, 1.0 mL/min, 210 nm.

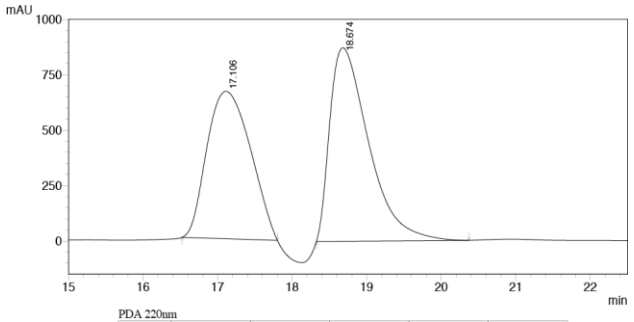

PDA 220nm

Peak#	Ret. Time	Area	Height	Area %	Height %
1	17.106	27113272	664952	46.135	43.217
2	18.674	31656310	873668	53.865	56.783
Total		58769582	1538620	100.000	100.000

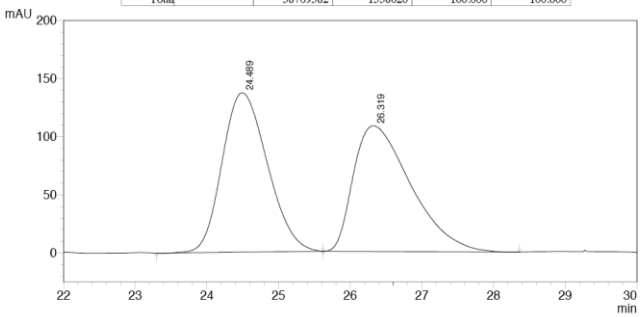

PDA 220nm

Peak#	Ret. Time	Area	Height	Area %	Height %
1	24.489	6013373	137136	49.998	55.910
2	26.319	6013821	108142	50.002	44.090
Total		12027194	245279	100.000	100.000

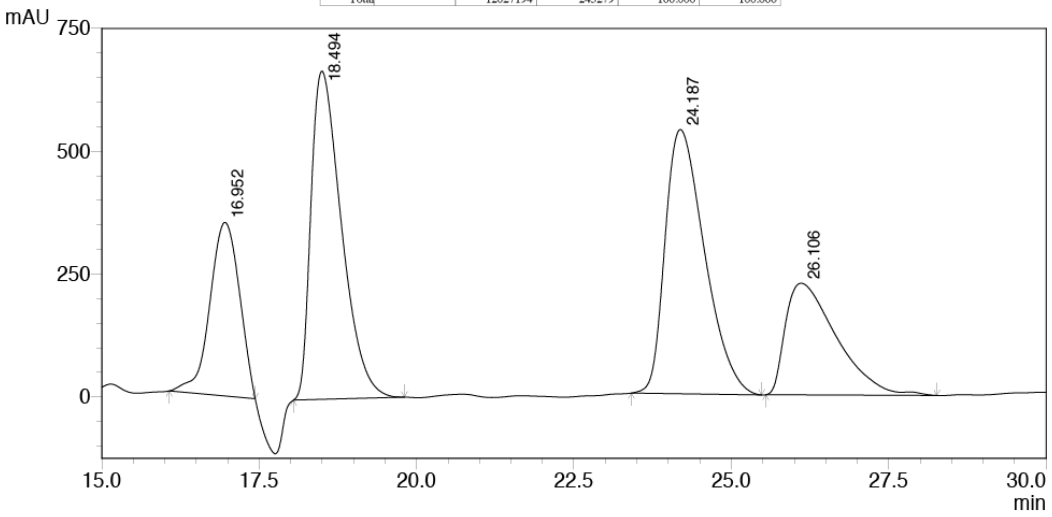

PDA 220nm

Peak#	Ret. Time	Area	Height	Area %	Height %
1	16.952	11532712	353194	16.417	19.773
2	18.494	22492469	668131	32.018	37.404
3	24.187	23425552	537679	33.346	30.100
4	26.106	12799241	227275	18.220	12.723
Total		70249973	1786278	100.000	100.000

HPLC trace of racemic *anti*-**48** (top), racemic *syn*-**48** (middle), and scalemic *anti*/*syn*-**48** (bottom; Table 4.19, Entry 4); Chiralpak AS-H 90:10 v/v hexanes/isopropanol, 1.0 mL/min, 220 nm.

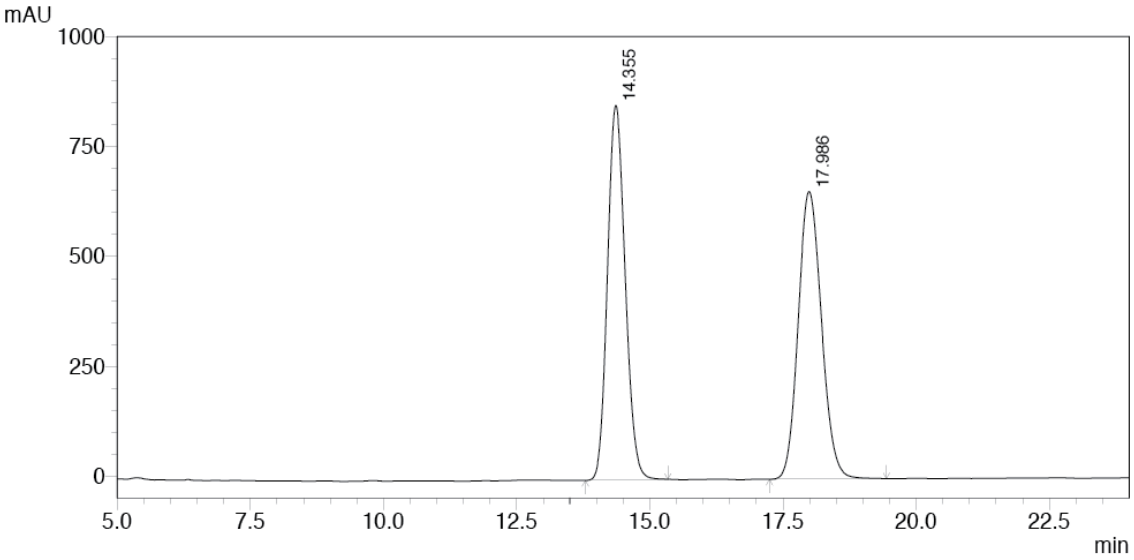

PDA 220nm

Peak#	Ret. Time	Area	Height	Area %	Height %
1	14.355	19732605	852383	49.794	56.575
2	17.986	19895478	654262	50.206	43.425
Total		39628083	1506645	100.000	100.000

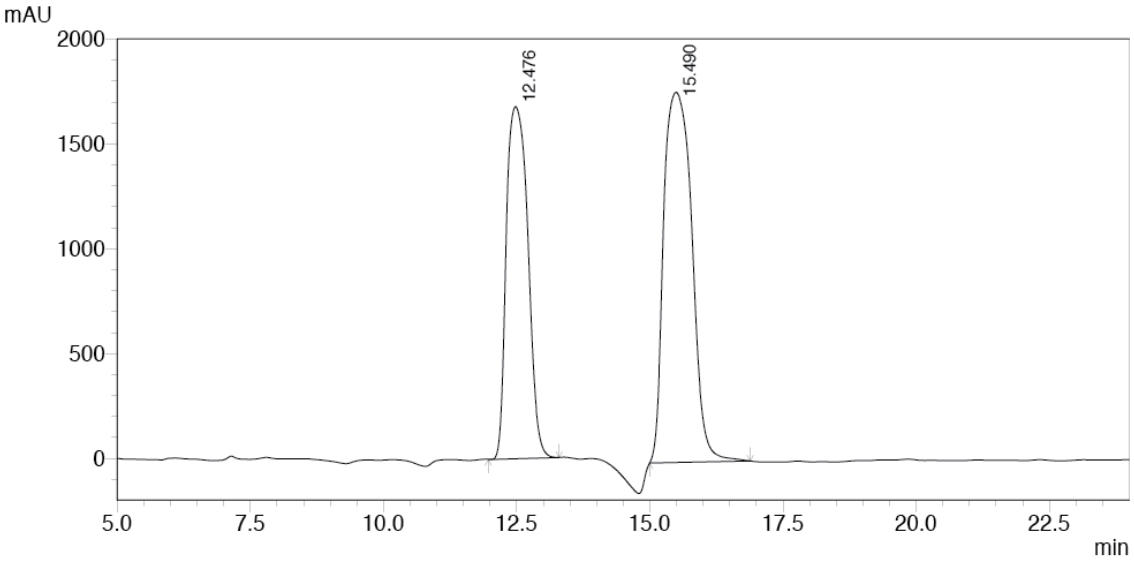

PDA 220nm

Peak#	Ret. Time	Area	Height	Area %	Height %
1	12.476	47233390	1679947	42.093	48.750
2	15.490	64978855	1766089	57.907	51.250
Total		112212245	3446035	100.000	100.000

HPLC trace of racemic **50** (top) and scalemic **50** (bottom; Table 4.20, Entry 2); Chiralpak AS-H 90:10 v/v hexanes/isopropanol, 1.0 mL/min, 220 nm.

APPENDIX B

CHECKCIF REPORTS FOR CHAPTER IV

CheckCIF report for Λ-(*S*,*S*)-**3**$^{3+}$ 3Cl^{-}·2H_2O·MeOH

Bond precision: C-C = 0.0059 Å Wavelength=0.71073

Cell: a=13.839(4) b=13.839(4) c=24.216(9)

alpha=90 beta=90 gamma=90

Temperature: 110 K

	Calculated	Reported
Volume	4638(3)	4638(2)
Space group	P 43	P4(3)
Hall group P	4cw	?
Moiety formula	$C_{42}H_{48}$ CoN_6· 2(CH_4O)·3(Cl)·2(H_2O)	?
Sum formula	$C_{44}H_{60}Cl_3Co$ N_6O_4	$C_{44}H_{60}Cl_3CoN_6O_4$
Mr	902.26	902.26
Dx,g cm^{-3}	1.292	1.292
Z	4	4
Mu (mm-1)	0.589	0.590
F000	1904.0	1904.0
F000'	1907.76	
h,k,lmax	17,17,31	17,17,31
Nref	5441[10631]	10535
Tmin,Tmax	0.932,0.943	0.719,0.943
Tmin'	0.702	

Correction method = MULTI-SCAN

Data completeness = 1.94/0.99 Theta(max) = 27.490

R(reflections) = 0.0442(9603) wR2(reflections) = 0.1220(10535)

S = 1.059 Npar= 525

The following ALERTS were generated. Each ALERT has the format test-name_ALERT_alert-type_alert-level.

Alert level B

PLAT230_ALERT_2_B Hirshfeld Test Diff for C11 -- C12 .. 7.5 su

PLAT420_ALERT_2_B D-H Without Acceptor O40 - H40A ... ?

Alert level C

PLAT048_ALERT_1_C MoietyFormula Not Given ..... ?

PLAT094_ALERT_2_C Ratio of Maximum / Minimum Residual Density 3.71

PLAT125_ALERT_4_C No '_symmetry_space_group_name_Hall' Given ..... ?

PLAT230_ALERT_2_C Hirshfeld Test Diff for N2A -- C8A .. 5.1 su

PLAT241_ALERT_2_C Check High Ueq as Compared to Neighbors for C6A

PLAT413_ALERT_2_C Short Inter XH3 .. XHn H31B .. H36C .. 2.13 Ang.

PLAT417_ALERT_2_C Short Inter D-H..H-D H1BB .. H50A .. 2.14 Ang.

Alert level G

REFLT03_ALERT_4_G Please check that the estimate of the number of Friedel pairs is correct. If it is not, please give the correct count in the _publ_section_exptl_refinement section of the submitted CIF.

From the CIF: _diffrn_reflns_theta_max 27.49

From the CIF: _reflns_number_total 10535

Count of symmetry unique reflns 5441

Completeness (_total/calc) 193.62%

TEST3: Check Friedels for noncentro structure

Estimate of Friedel pairs measured 5094

Fraction of Friedel pairs measured 0.936

Are heavy atom types Z>Si present yes

PLAT002_ALERT_2_G Number of Distance or Angle Restraints on AtSite 9

PLAT005_ALERT_5_G No _iucr_refine_instructions_details in CIF .... ?

PLAT007_ALERT_5_G Note: Number of Unrefined D-H Atoms 18

PLAT301_ALERT_3_G Note: Main Residue Disorder ..... 24 Perc.

PLAT710_ALERT_4_G Delete 1-2-3 or 2-3-4 Linear Torsion Angle ... # 32

N2A -CO1 -N1 -C1 -30.70 1.00 1.555 1.555 1.555 1.555

PLAT710_ALERT_4_G Delete 1-2-3 or 2-3-4 Linear Torsion Angle ... # 40

N2B -CO1 -N2 -C8 -38.70 0.80 1.555 1.555 1.555 1.555

PLAT710_ALERT_4_G Delete 1-2-3 or 2-3-4 Linear Torsion Angle ... # 91

N1B -CO1 -N1A -C1A -28.70 1.00 1.555 1.555 1.555 1.555

PLAT710_ALERT_4_G Delete 1-2-3 or 2-3-4 Linear Torsion Angle ... # 101

N1 -CO1 -N2A -C8A -33.30 1.00 1.555 1.555 1.555 1.555

PLAT710_ALERT_4_G Delete 1-2-3 or 2-3-4 Linear Torsion Angle ... # 140

N1A -CO1 -N1B -C1B -30.90 0.90 1.555 1.555 1.555 1.555

PLAT710_ALERT_4_G Delete 1-2-3 or 2-3-4 Linear Torsion Angle ... # 146

N2 -CO1 -N2B -C8B -24.60 0.80 1.555 1.555 1.555 1.555

PLAT720_ALERT_4_G Number of Unusual/Non-Standard Labels 10

PLAT779_ALERT_4_G Suspect or Irrelevant (Bond) Angle in CIF .... # 101

C9A -C8A -C9E 1.555 1.555 1.555 7.90 Deg.

PLAT791_ALERT_4_G Note: The Model has Chirality at C1 (Verify) S

PLAT791_ALERT_4_G Note: The Model has Chirality at C1A (Verify) S

PLAT791_ALERT_4_G Note: The Model has Chirality at C8 (Verify) S

PLAT791_ALERT_4_G Note: The Model has Chirality at C8B (Verify) S

PLAT811_ALERT_5_G No ADDSYM Analysis: Too Many Excluded Atoms .... !

PLAT850_ALERT_4_G Check Flack Parameter Exact Value 0.00 and su .. 0.01

PLAT860_ALERT_3_G Note: Number of Least-Squares Restraints 7

CheckCIF report for Δ-(*R*,*R*)-**3**$^{3+}$ 2Cl$^-$ BAr$_f^-$·H_2O·3MeOH

Bond precision: C-C = 0.0067 Å Wavelength=1.54178

Cell: a=13.8725(7) b=13.8725(7) c=24.3173(13)

alpha=90 beta=90 gamma=90

Temperature: 110 K

	Calculated	Reported
Volume	4679.8(5)	4679.8(4)
Space group	P 41	P4(1)
Hall group	P 4w	?
Moiety formula	$C_{42}H_{48}Co\ N_6$·3(CH_4O)·3(Cl)·H_2O	?
Sum formula	$C_{45}H_{62}Cl_3CoN_6O_4$	$C_{45}\ H_{62}Cl_3CoN_6O_4$
Mr	912.44	912.60
Dx,g cm^{-3}	1.295	1.295
Z	4	4
Mu (mm^{-1})	4.822	4.822
F000	1927.1	1928.0
F000’	1926.86	
h,k,lmax	15,15,27	15,15,26
Nref	3571[6952]	6282
Tmin,Tmax	0.661,0.825	0.595,0.831
Tmin’	0.534	

Correction method = MULTI-SCAN

Data completeness = 1.76/0.90 Theta(max) = 60.000

R(reflections) = 0.0407(5561) wR2(reflections) = 0.0871(6282)

S = 1.071 Npar = 546

The following ALERTS were generated. Each ALERT has the format test-name_ALERT_alert-type_alert-level.

Alert level B

THETM01_ALERT_3_B The value of sine(theta_max)/wavelength is less than 0.575

Calculated sin(theta_max)/wavelength = 0.5617

PLAT035_ALERT_1_B No _chemical_absolute_configuration info given . ?

PLAT220_ALERT_2_B Large Non-Solvent C Ueq(max)/Ueq(min) ... 4.3 Ratio

PLAT230_ALERT_2_B Hirshfeld Test Diff for C25 -- C26 .. 7.5 su

Alert level C

PLAT041_ALERT_1_C Calc. and Reported SumFormula Strings Differ ?

PLAT068_ALERT_1_C Reported F000 Differs from Calcd (or Missing)... ?

PLAT077_ALERT_4_C Unitcell contains non-integer number of atoms .. ?

PLAT213_ALERT_2_C Atom C5 has ADP max/min Ratio ..... 3.6 prola

PLAT222_ALERT_3_C Large Non-Solvent H Uiso(max)/Uiso(min) .. 4.4 Ratio

PLAT341_ALERT_3_C Low Bond Precision on C-C Bonds ..... 0.0067 Ang

PLAT413_ALERT_2_C Short Inter XH3 .. XHn H20 .. H56B .. 2.14 Ang.

Alert level G

FORMU01_ALERT_2_G There is a discrepancy between the atom counts in the chemical_formula_sum and the formula from the _atom_site* data.

Atom count from _chemical_formula_sum:C44.88 H61.54 Cl3 Co1 N6 O3.88

Atom count from the _atom_site data: C44.88 H61.52 Cl3 Co1 N6 O3.88

CELLZ01_ALERT_1_G Difference between formula and atom_site contents detected.

CELLZ01_ALERT_1_G ALERT: check formula stoichiometry or atom site occupancies.

From the CIF: _cell_formula_units_Z 4

From the CIF: _chemical_formula_sum C44.88 H61.54 Cl3 Co N6 O3.88

TEST: Compare cell contents of formula and atom_site data

atom	Z*formula	cif sites	diff
C	179.52	179.52	0.00
H	246.16	246.08	0.08
Cl	12.00	12.00	0.00
Co	4.00	4.00	0.00
N	24.00	24.00	0.00
O	15.52	15.52	0.00

REFLT03_ALERT_4_G Please check that the estimate of the number of Friedel pairs is correct. If it is not, please give the correct count in the _publ_section_exptl_refinement section of the submitted CIF.

From the CIF: _diffrn_reflns_theta_max 60.00

From the CIF: _reflns_number_total 6282

Count of symmetry unique reflns 3571

Completeness (_total/calc) 175.92%

TEST3: Check Friedels for noncentro structure

Estimate of Friedel pairs measured 2711

Fraction of Friedel pairs measured 0.759

Are heavy atom types Z>Si present yes

PLAT002_ALERT_2_G Number of Distance or Angle Restraints on AtSite 15

PLAT005_ALERT_5_G No _iucr_refine_instructions_details in CIF .... ?

PLAT007_ALERT_5_G Note: Number of Unrefined D-H Atoms 17

PLAT301_ALERT_3_G Note: Main Residue Disorder ..... 12 Perc.

PLAT302_ALERT_4_G Note: Anion/Solvent Disorder ..... 18 Perc.

PLAT710_ALERT_4_G Delete 1-2-3 or 2-3-4 Linear Torsion Angle ... # 3

N4 -CO1 -N1 -C1 29.60 1.30 1.555 1.555 1.555 1.555

PLAT710_ALERT_4_G Delete 1-2-3 or 2-3-4 Linear Torsion Angle ... # 6

N5 -CO1 -N2 -C8 32.00 1.10 1.555 1.555 1.555 1.555

PLAT710_ALERT_4_G Delete 1-2-3 or 2-3-4 Linear Torsion Angle ... # 12

N6 -CO1 -N3 -C15 39.40 1.00 1.555 1.555 1.555 1.555

PLAT710_ALERT_4_G Delete 1-2-3 or 2-3-4 Linear Torsion Angle ... # 18

N1 -CO1 -N4 -C22 34.70 1.30 1.555 1.555 1.555 1.555

PLAT710_ALERT_4_G Delete 1-2-3 or 2-3-4 Linear Torsion Angle ... # 24

N2 -CO1 -N5 -C29 28.00 1.10 1.555 1.555 1.555 1.555

PLAT710_ALERT_4_G Delete 1-2-3 or 2-3-4 Linear Torsion Angle ... # 30

N3 -CO1 -N6 -C36 24.00 1.10 1.555 1.555 1.555 1.555

PLAT790_ALERT_4_G Centre of Gravity not Within Unit Cell: Resd. # 4

C H4 O

PLAT790_ALERT_4_G Centre of Gravity not Within Unit Cell: Resd. # 7

Cl

PLAT791_ALERT_4_G Note: The Model has Chirality at C1 (Verify) R

PLAT791_ALERT_4_G Note: The Model has Chirality at C8 (Verify) R

PLAT791_ALERT_4_G Note: The Model has Chirality at C15 (Verify) R

PLAT791_ALERT_4_G Note: The Model has Chirality at C22 (Verify) R

PLAT791_ALERT_4_G Note: The Model has Chirality at C29 (Verify) R

PLAT791_ALERT_4_G Note: The Model has Chirality at C36 (Verify) R

PLAT860_ALERT_3_G Note: Number of Least-Squares Restraints 21

CheckCIF report for 2 (Δ-(*S*,*S*)-**3**$^{3+}$ 3Cl^{-})·25 H_2O

Bond precision: C-C = 0.0109 Å Wavelength=1.54178

Cell: a=12.0877(6) b=25.0985(14) c=16.8235(8)

alpha=90 beta=90.887(3) gamma=90

Temperature: 110 K

	Calculated	Reported
Volume	5103.4(5)	5103.4(5)
Space group	P 21	P2(1)
Hall group	P 2yb	?
Moiety formula	$2(C_{42}H_{48}CoN_6)\cdot 6(Cl)\cdot 25(H_2O)$	?
Sum formula	$C_{84}H_{146}Cl_6Co_2N_{12}O_{25}$	$C_{84}H_{146}Cl_6Co_2N_{12}O_{25}$
Mr	2054.69	2054.69
Dx,g cm-3	1.337	1.337
Z	2	2
Mu (mm-1)	4.607	4.607
F000	2180.0	2180.0
F000'	2180.97	
h,k,lmax	13,28,18	13,28,18
Nref	15161[7782]	14790
Tmin,Tmax	0.502,0.724	0.526,0.739
Tmin'	0.456	

Correction method = MULTI-SCAN

Data completeness = 1.90/0.98 Theta(max)= 60.000

R(reflections) = 0.0746(13847) wR2(reflections)= 0.1830(14790)

S = 1.149 Npar= 1105

The following ALERTS were generated. Each ALERT has the format test-name_ALERT_alert-type_alert-level.

Alert level A

PLAT213_ALERT_2_A Atom C1 has ADP max/min Ratio ..... 9.8 prola

Author Response: Given the complexity of the molecule with large number of water of hydration, and possibility of disorder of the peripheral phenyl groups, several atoms had NPDs. Many restraints were used to fix this and yet resulted in some of the atoms with elongated or

disc shaped thermal motions. No efforts were taken to further add any restraints.

PLAT415_ALERT_2_A Short Inter D-H..H-X H1D .. H77 .. 1.83 Ang.

Author Response: Water molecules for which the hydrogen atoms could not be located were

placed geometrically only to satisfy the stoichiometry. This results in short H - H interactions.

No efforts were made to relocate the hydrogen atoms.

PLAT415_ALERT_2_A Short Inter D-H..H-X H2C .. H50 .. 1.67 Ang.

PLAT417_ALERT_2_A Short Inter D-H..H-D H2A .. H12C .. 1.62 Ang.

Author Response: Water molecules for which the hydrogen atoms could not be located were placed geometrically only to satisfy the stoichiometry. This results in short H - H interactions.

No efforts were made to relocate the hydrogen atoms.

Alert level B

THETM01_ALERT_3_B The value of sine(theta_max)/wavelength is less than 0.575

Calculated sin(theta_max)/wavelength = 0.5617

Author Response: Data was collected on a Bruker GADDS instrument with Cu-source and

MWPC (multiwire proportional counter) detector. Under these experimental conditions the

maximum angle that can be collected is 120 degrees two-theta.

PLAT213_ALERT_2_B Atom Co1 has ADP max/min Ratio ..... 4.3 prola

Author Response: Given the complexity of the molecule with large number of water of hydration, and possibility of disorder of the peripheral phenyl groups, several atoms had NPDs.

Many restraints were used to fix this and yet resulted in some of the atoms with elongated or

disc shaped thermal motions. No efforts were taken to further add any restraints.

And 3 other PLAT213 Alerts

PLAT220_ALERT_2_B Large Non-Solvent C Ueq(max)/Ueq(min) ... 5.2 Ratio

Author Response: Given the complexity of the molecule with large number of water of hydration, and possibility of disorder of the peripheral phenyl groups, several atoms had NPDs.

Many restraints were used to fix this and yet resulted in some of the atoms with elongated or

disc shaped thermal motions. No efforts were taken to further add any restraints.

PLAT220_ALERT_2_B Large Non-Solvent C Ueq(max)/Ueq(min) ... 4.3 Ratio

PLAT415_ALERT_2_B Short Inter D-H..H-X H8C .. H14 .. 2.02 Ang.

Author Response: Water molecules for which the hydrogen atoms could not be located were

placed geometrically only to satisfy the stoichiometry. This results in short H - H interactions.

No efforts were made to relocate the hydrogen atoms.

And 2 other PLAT415 Alerts

PLAT417_ALERT_2_B Short Inter D-H..H-D H4D .. H8A .. 1.97 Ang.

Author Response: Water molecules for which the hydrogen atoms could not be located were

placed geometrically only to satisfy the stoichiometry. This results in short H - H interactions.

No efforts were made to relocate the hydrogen atoms.

And 6 other PLAT417 Alerts

PLAT420_ALERT_2_B D-H Without Acceptor O1 - H1C ... ? Check

Author Response: Water molecules for which the hydrogen atoms could not be located were

placed geometrically only to satisfy the stoichiometry. This results in short H - H interactions.

No efforts were made to relocate the hydrogen atoms.

Alert level C

PLAT089_ALERT_3_C Poor Data / Parameter Ratio (Zmax < 18) 7.04

PLAT213_ALERT_2_C Atom N2 has ADP max/min Ratio ..... 3.3 oblat

Author Response: Given the complexity of the molecule with large number of water of hydration, and possibility of disorder of the peripheral phenyl groups, several atoms had NPDs.

Many restraints were used to fix this and yet resulted in some of the atoms with elongated or

disc shaped thermal motions. No efforts were taken to further add any restraints.

And 17 other PLAT213 Alerts

PLAT222_ALERT_3_C Large Non-Solvent H Uiso(max)/Uiso(min) .. 4.5 Ratio

PLAT222_ALERT_3_C Large Non-Solvent H Uiso(max)/Uiso(min) .. 4.3 Ratio

PLAT341_ALERT_3_C Low Bond Precision on C-C Bonds ..... 0.0109 Ang.

PLAT415_ALERT_2_C Short Inter D-H..H-X H1D .. H78 .. 2.14 Ang.

Author Response: Water molecules for which the hydrogen atoms could not be located were

placed geometrically only to satisfy the stoichiometry. This results in short H - H interactions. No efforts were made to relocate the hydrogen atoms.

PLAT417_ALERT_2_C Short Inter D-H..H-D H7C .. H12D .. 2.14 Ang.

Author Response: Water molecules for which the hydrogen atoms could not be located were

placed geometrically only to satisfy the stoichiometry. This results in short H - H interactions.

No efforts were made to relocate the hydrogen atoms.

Alert level G

PLAT003_ALERT_2_G Number of Uiso or Uij Restrained non-H Atoms ... 42

PLAT005_ALERT_5_G No _iucr_refine_instructions_details in the CIF ? Do !

PLAT007_ALERT_5_G Note: Number of Unrefined Donor-H Atoms 76

PLAT033_ALERT_4_G Flack x Value Deviates > 2*sigma from Zero 0.069

PLAT083_ALERT_2_G SHELXL Second Parameter in WGHT Unusually Large. 30.89

PLAT232_ALERT_2_G Hirshfeld Test Diff (M-X) Co1 -- N5 .. 5.2 su

And 3 other PLAT232 Alerts

PLAT302_ALERT_4_G Note: Anion/Solvent Disorder ..... 3 %

PLAT710_ALERT_4_G Delete 1-2-3 or 2-3-4 Linear Torsion Angle ... # 1

N4 -CO1 -N1 -C1 78.00 3.00 1.555 1.555 1.555 1.555

And 11 other PLAT710 Alerts

PLAT779_ALERT_4_G Suspect or Irrelevant (Bond) Angle in CIF .... # 405

H14A -O14 -H14A 1.555 1.555 1.555 0.00 Deg.

And 6 other PLAT779 Alerts

PLAT791_ALERT_4_G Note: The Model has Chirality at C1 (Verify) S

And 11 other PLAT791 Alerts

PLAT860_ALERT_3_G Note: Number of Least-Squares Restraints 265

Author Response: Following restraints were used DELU C22 C15 N3 C2 C6 C31 C30 C32 C33 C7 C3 C8 C9 C10 N6 N5 DELU C51 C52 C56 C50 C66 C65 C70 C72 C77 C73 C71 C44 C49 C48 C45 SIMU 0.005 0.02 1.7 C22 C15 N3 C2 C6 C31 C30 C32 C33 C7 C3 C8 C9 C10 N6 N5 SIMU 0.005 0.02 1.7 C51 C52 C56 C50 C66 C65 C70 C72 C77 C73 C71 C44 C49 C48 C45 SIMU 0.005 0.01 1.7 C80 C79 C84 C73 C72 C77 SIMU 0.005 0.01 1.7 C56 C51 C52 SIMU 0.005 0.01 1.7 N5 C29 Co1 N6 N1 N4 N3 C15 C24 C25 C27 C2 C7 C3 C1 C8 C9 = C10 SIMU 0.005 0.01 1.7 N7 C43 C44 C51 C50 N8 ISOR 0.005 0.01 N1 N6 C15 C25 C51 C72 EADP N1 N6 C15 C25 C51 C72 N7 C58 N3 N5 N10 C22